



VCU

Virginia Commonwealth University
VCU Scholars Compass

Theses and Dissertations

Graduate School

2013

DEVELOPMENT OF ANTAGONISTS TARGETING CHEMOKINE RECEPTOR CCR5 AND THE CHEMOKINE RECEPTOR CCR5 – MU OPIOID RECEPTOR HETERODIMER

Christopher Kent Arnatt
Virginia Commonwealth University

Follow this and additional works at: <https://scholarscompass.vcu.edu/etd>



Part of the [Pharmacy and Pharmaceutical Sciences Commons](#)

© The Author

Downloaded from

<https://scholarscompass.vcu.edu/etd/517>

This Dissertation is brought to you for free and open access by the Graduate School at VCU Scholars Compass. It has been accepted for inclusion in Theses and Dissertations by an authorized administrator of VCU Scholars Compass. For more information, please contact libcompass@vcu.edu.

© Christopher Kent Arnatt 2013

All Rights Reserved

DEVELOPMENT OF ANTAGONISTS TARGETING CHEMOKINE RECEPTOR
CCR5 AND THE CHEMOKINE RECEPTOR CCR5 – MU OPIOID RECEPTOR
HETERODIMER

A dissertation submitted in partial fulfillment of the requirements for the degree of doctor
of philosophy at Virginia Commonwealth University.

by

CHRISTOPHER KENT ARNATT
Bachelors in Science, Hampden-Sydney College, 2009

Director: YAN ZHANG, PHD
ASSOCIATE PROFESSOR, DEPARTMENT OF MEDICINAL CHEMISTRY

Virginia Commonwealth University
Richmond, Virginia
May, 2013

Acknowledgement

The culmination of events in my life which have led me to graduating with a Ph.D. have revolved entirely around my family and friends. Without them in my life I would be a lesser person. Coming from a family with sixteen children there were plenty of facets of a 'normal' childhood that I was deprived from. However, it was an environment that cultivated my dedication, work ethic, and love of education which lead me to become the man I am today. My parents, Sylvia Arnatt-Nestor and Dave Nestor, instilled those characteristics into me; without them none of my achievements would have ever come to fruition. I cannot begin to encompass the acknowledgements that they deserve. My family has and will always play a central role in my life and I thank all of my brothers and sisters for being ever-present. They have helped me let my light shine on, even through the darkest of times.

While earning my Ph.D. will be a great accomplishment, it will always pale in comparison to marrying my best friend, Mary Ann Haggerty. She makes me strive to become a better person and constantly challenges my often stubborn nature. Without her, I would have never been able to make it through all of the mental and emotional challenges that have occurred during the last four years. She has kept me grounded and held me together in the best and worst of times. Too many glowing examples of her can be said, but to briefly and pitifully paraphrase them: she is the best person I know.

Beyond my family and my wife, my core group of friends has added an additional layer of support which has proved to me instrumental in my life. I would like to acknowledge my best friends Steele Parris and Sean Platt for developing my love of science and being a sounding board for all of my thoughts. Beyond them, during college, my brothers at the Beta Chi Chapter of Alpha Chi Sigma and my alma mater, Hampden-Sydney College, helped me to become a good man and a good citizen. During graduate school, my friends of the Granite Gang have provided me with comic relief and a lasting friendship that helped keep me going during the most stressful times.

My advisor Yan Zhang has always challenged my perceptions and aided in my journey to become a research scientist. He has always seen my potential and has pushed me to work harder in order to reach it. My fellow laboratory members, especially Kendra Haney and Yunyun Yuan, were indispensable in training me on all of the new chemical and biological techniques that were applied in this dissertation. From the Hauser laboratory, Seth Dever, has been instrumental in the attainment of all the biological data in the NeuroAIDS portion of my research. Also the entire Hauser and Knapp laboratories have been instrumental in the obtaining the biological data for the bivalent ligand project.

Finally, I would like to thank my committee members: Glen Kellogg, Martin Safo, Kurt Hauser, and Dana Selley. Each one of you has helped galvanize my education through either your teaching or interactions with me.

Table of Contents

	Page
Acknowledgements.....	ii
Table of Contents.....	iv
List of Tables.....	ix
List of Figures.....	xi
List of Schemes.....	xiv
List of Abbreviations.....	xv
Abstract.....	xviii
Chapter	
1 Introduction.....	1
1.1 Chemokine Receptor CCR5.....	1
1.1.1 Chemokines and Inflammatory Response.....	1
1.1.2 Chemokine Receptor CCR5 and GPCRs.....	3
1.1.3 Chemokine Receptor CCR5 Signaling.....	5
1.1.4 Chemokine Receptor CCR5 in Different Disease States.....	8
1.1.4.1 Prostate Cancer.....	9
1.1.4.2 HIV/AIDS.....	11
1.1.5 Chemokine Receptor CCR5 Ligands.....	13
1.2 Mu Opioid Receptor.....	16
1.2.1 Opioid Receptors.....	16

1.2.2 Mu Opioid Receptor Structure	18
1.2.3 Mu Opioid Receptor Signaling.....	19
1.2.4 Mu Opioid Receptor in Different Disease States	20
1.2.4.1 Addiction	20
1.2.4.2 NeuroAIDS.....	21
1.2.5 Mu Opioid Receptor Ligands	23
1.2.5.1 Agonists.....	23
1.2.5.2 Antagonists	25
1.3 GPCR Dimerization	28
1.3.1 GPCR Dimerization Involving Mu Opioid Receptor.....	33
1.3.2 Bivalent Ligands Targeting GPCR Dimerization	34
1.4 Hypotheses and Specific Aims.....	38
1.4.1 Antagonists Targeting CCR5	38
1.4.2 Bivalent Compounds Targeting the Putative CCR5 – MOR Heterodimer.....	38
2 Small Molecule Chemokine Receptor CCR5 Antagonists for Prostate Cancer Treatment.....	40
2.1 Project Design	40
2.2 Chemical Syntheses.....	44
2.2.1 Williamson Ether Synthesis	46

2.2.2 Nitro-group Reduction to Primary Amine.....	46
2.2.3 Piperazine Ring Formation.....	47
2.2.4 Aromatic Mono-Nitration.....	48
2.2.5 Final Compound Synthesis.....	51
2.3 <i>In Vitro</i> Studies.....	52
2.3.1 Calcium Mobilization Functional Assays	52
2.3.2 Prostate Cancer Anti-Proliferation Assays.....	55
2.3.3 Basal Cytotoxicity Assays.....	58
2.4 Conclusion.....	60
3 Bivalent Ligands Targeting the CCR5-MOR Heterodimer	62
3.1 Project Design	62
3.2 Chemical Syntheses.....	66
3.2.1 Buchwald-Hartwig Coupling	67
3.2.2 1,2,4-Triazole-Substituted Tropane Intermediate Synthesis	69
3.2.3 Debenzylation with Hydrogenation.....	70
3.2.4 Selective Difluorination	71
3.2.5 Linker Synthesis	72
3.2.6 6 β -Naltrexamine-Linker Intermediate Synthesis	74
3.2.7 Final Compound Synthesis.....	76
3.3 <i>In Vitro</i> Studies.....	77

3.3.1 Calcium Mobilization Functional Assays	77
3.3.2 Binding Assays.....	84
3.3.3 Cell Fusion Assays	85
3.3.4 HIV-1 Infection Assays.....	85
3.3.5 Expression Levels of CCR5 and MOR in Primary and Engineered Cells.....	90
3.4 <i>In Silico</i> Studies.....	92
3.4.1 Modeling the CCR5-MOR Heterodimer	92
3.4.2 Bivalent Ligand Docking Studies.....	95
3.4.3 CCR5-MOR Molecular Dynamics Simulations.....	97
3.5 Conclusion.....	104
4 Experimental.....	106
4.1 Chemical Syntheses.....	106
4.1.1 Small Molecule CCR5 Antagonists: Intermediates.....	106
4.1.2 Small Molecule CCR5 Antagonists: Final Compounds.....	115
4.1.3 CCR5-MOR Bivalent Ligands: Intermediates	123
4.1.4 CCR5-MOR Bivalent Ligands: Final Compounds	148
4.2 Biology Methods	151
4.2.1 Anti-Proliferation Assay.....	151
4.2.2 Basal Cytotoxicity Assay	152

4.2.3	Establishing a CCR5-hMOR-CHO Cell Line	153
4.2.4	Calcium Mobilization Assays	153
4.2.4.1	CCR5-MOLT-4 Cells.....	153
4.2.4.2	hMOR CHO Cells	154
4.2.4.3	CCR5-hMOR CHO Cells.....	155
4.2.5	Cell Fusion Assay.....	156
4.2.6	HIV-1 Infection Assay	157
4.2.7	PCR Studies.....	158
4.2	Computational Methods	159
4.2.1	Small Molecule Construction.....	159
4.2.2	Sequence Alignment and Model Building	159
4.2.3	Model Selection and Quality Assessment.....	160
4.2.4	CCR5-MOR Heterodimer Model Building.....	160
4.2.4.1	Molecular Docking.....	161
4.2.4.2	Molecular Dynamics Simulations	162
5	Conclusion	165
	References.....	167

List of Tables

	Page
Table 1: Small molecule CCR5 antagonists in clinical development.....	13
Table 2: Example MOR agonists.....	24
Table 3: Example MOR antagonists.....	26
Table 4: Selective, morphanin-based bivalent compounds targeting MOR heterodimers.....	36
Table 5: CCR5 antagonism (calcium mobilization) of compounds 42 through 48 using RANTES as the agonist.....	54
Table 6: Anti-proliferation assays for DU 145, PC-3, and M-12 prostate cancer cells Using WST-1 to measure cell proliferation.....	57
Table 7: Basal cytotoxicity assays using NRU and WST-1 to test for exogenous toxicity of compounds 27 through 48 in NIH-3T3 cells.....	59
Table 8: Antagonism of RANTES stimulated calcium mobilization in MOLT-4 cells.....	80
Table 9: Antagonism of DAMGO stimulated calcium mobilization in hMOR-CHO cells.....	81
Table 10: Results from the calcium mobilization assays using the CCR5YFP-hMOR- CHO co-expressed cell line.....	82
Table 11: CCR5 and MOR radiobinding assays.....	84

Table 12: Major amino acids in the CCR5 and MOR binding pockets, in the heterodimer, interacting with compound 49	102
---	-----

List of Figures

	Page
Figure 1: Graphical representation of the 7-TM GPCR, CCR5.....	3
Figure 2: CCR5 signaling cascade.....	6
Figure 3: β -arrestin mediated receptor internalization.....	8
Figure 4: HIV entry into host cells	11
Figure 5: Pfizer CCR5 antagonist HTS hit CCR5 antagonist which lead to maraviroc, 1	15
Figure 6: TAK-779, the first CCR5 small molecule antagonist	16
Figure 7: MOR monomer crystal structure.....	18
Figure 8: Pathophysiology and pathogenesis of neuroAIDS.....	22
Figure 9: The message-address concept for opioid receptor selectivity.....	28
Figure 10: Observed GPCR oligomers and dimers.....	31
Figure 11: Positive and negative cooperativity in GPCR dimerization.....	32
Figure 12: Example CCR5 antagonists used as the basis of the CCR5 pharmacophore ...	41
Figure 13: Molecular modeling based pharmacophore analysis, and designed CCR5 antagonist scaffold	42
Figure 14: Example pharmacophore-based compound docked into a CCR5 homology model.....	42

Figure 15: Synthesized derivatives with substituted benzyl groups based upon the CCR5 antagonist scaffold and pharmacophore in Figure 9.....	43
Figure 16: Synthesized CCR5 antagonists for elucidating the SAR of the piperazine compound library.....	44
Figure 17: Calcium assay mechanism.....	53
Figure 18: The first reported bivalent compound targeting the CCR5-MOR heterodimer.....	63
Figure 19: Bivalent compound strategy for targeting the CCR5-MOR heterodimer.....	64
Figure 20: Additional CCR5-MOR bivalent compound (50) and control compounds studying the SAR of maraviroc substitution.....	66
Figure 21: Library of compounds for the study of the CCR5-MOR heterodimer.....	78
Figure 22: Example CCR5 inhibition curve for 49	79
Figure 23: Cell fusion assay used to mimic HIV invasion without using live virus.....	86
Figure 24: Cell fusion assay based upon luminescence from expressed luciferase reporter gene.....	87
Figure 25: HIV-1 infection assay.....	90
Figure 26: Relative mRNA expression levels of MOR and CCR5.....	91
Figure 27: Sequence alignment of CCR5 and CXCR4.....	93
Figure 28: CCR5-MOR heterodimer model.....	95

Figure 29: Overview of docking procedure for docking 49 into the CCR5-MOR heterodimer	96
Figure 30: CCR5-MOR heterodimer model based on the MOR dimer crystal structure (PDB code: 4DKL) with bivalent compound 49 bound	98
Figure 31: Molecular dynamic system for the CCR5-MOR heterodimer in a membrane and water box system.....	98
Figure 32: CCR5-MOR heterodimer RMSD from dynamics study after a total of 13 ns of production	99
Figure 33: Total energy (kcal/mol) of the dynamics simulation after 13 ns.....	99
Figure 34: Trajectory of 49 in the CCR5-MOR heterodimer at 0, 2.4, 4.4, and 6 ns.....	100
Figure 35: Bivalent compound 49 RMSD from dynamics study after a total of 13 ns of production	101
Figure 36: The binding pocket for the triazole region at 0 ns and 6 ns	103

List of Schemes

	Page
Scheme 1: Synthetic route for CCR5 antagonists 42-48	45
Scheme 2: General reaction Scheme for 2,3,5,6-tetrabromo-4-methyl-4-nitrocyclohexa-2-5-dien-1-one (66)	49
Scheme 3: Mechanisms for aromatic nitration	50
Scheme 4: Alternative route for mono-nitration	51
Scheme 5: WST-1 mechanism for action for anti-proliferation assay	55
Scheme 6: Synthetic route to form the 3-amino maraviroc intermediate (80)	69
Scheme 7: Synthesis of the 1,2,4-triazole substituted tropane intermediate (86)	70
Scheme 8: Synthesis of 4,4-difluorocyclohexylcarboxylic acid (88) using Fluolead	72
Scheme 9: Synthesis of 6 β -naltrexone-linker intermediate (95) and final 3-amino bivalent compound (50)	73
Scheme 10: 6 β -Naltrexamine (98) synthesis	75
Scheme 11: Synthesis of 3-amino maraviroc monovalent control compound (52)	76

List of Abbreviations

AAH	Atypical adenomatous hyperplasia
AIDS	acquired immunodeficiency syndrome
AP2	Adapter complex protein 2
AR	Androgen receptor
ATP	Adenosine triphosphate
BBB	Blood brain barrier
β -FNA	β -funaltrexamine
BPH	benign prostate hyperplasia
BRET	Bioluminescence resonance energy transfer
cAMP	Cyclic adenosine monophosphate
CB1	cannabinoid receptor 1
C-CAM	Clocinnamox
CCK ₂	type 2 cholecystokine
CCR5	Chemokine receptor CCR5
CFP	Cyan fluorescent protein
CNS	Central nervous system
c-SRC	Proto-oncogene tyrosine-protein kinase SRC
CXCR4	chemokine CXC receptor 4
DAG	diacyl glycerol
DAST	diethylamino sulfur trifluoride
DAMGO	[D-Ala ² , N-MePhe ⁴ , Gly-ol]-enkephalin
DCM	dichloromethane
DMF	dimethylformamide
DMF	Dimethyl formamide
DOR	Delta opioid receptor
EDCI	1-ethyl-3-(3-dimethylaminopropyl)carbodiimide
EL	Extracellular loop
EL	Extracellular loop
Env	Envelope protein
ER	Endoplasmic reticulum
ERK1/2	Extracellular signal-regulated kinases 1/2
FRET	Fluorescence resonance energy transfer
GDP	guanosine diphosphate
gp	Glycoprotein
GPCR	G protein-couple receptor
GRKs	G protein-coupled receptor kinases
GTP	guanosine triphosphate

HA	influenza hemagglutinin
HAART	highly active antiretroviral therapies
HAART	highly active antiretroviral therapy
HAND	HIV-associated neurocognitive disorders
HTS	High throughput screening
HTS	high-throughput screening
IL	Intracellular loop
IP ₃	inositol triphosphate
JNK	Jun-N-terminal kinase
KOR	Kappa opioid receptor
LHMDS	lithium hexamethyldisilazide
MAPK	mitogen-activated protein kinases
MCP-2	monocyte chemoattractant protein 2
MIP-1 α	macrophage inflammatory protein-1 α
MOR	Mu opioid receptor
M-tropic	Macrophage-tropic
neuroAIDS	neurological complications of AIDS
NK1	substance P receptor
NMR	Nuclear magnetic resonance
NOR	Nociception/orphanin receptor
nRTK	Non-receptor tyrosine kinase
OPM	orientations of proteins in membranes
PBMC	peripheral blood mononuclear cells
PCa	Prostate cancer
Pd/C	Palladium on carbon
PIP ₂	phosphatidylinositol 4,5-biphosphate
PKC	Protein kinase C
PLC	Phospholipase C
PLC β	phospholipase C β isoform
PNS	Peripheral nervous system
POPC	phosphatidylcholine
PSA	Prostate specific antigen
QSAR	Quantitative structure activity relationship
RANTES	regulated upon activation normally T-cell expressed and secreted
RNS	Reactive nitrogen species
ROS	Reactive oxygen species
SAR	Structure-activity-relationship
sst _{2A}	somatostatin receptor 2A
TM	Transmembrane helix

T-tropic
YFP

T-cell-tropic
Yellow fluorescent protein

Abstract

DEVELOPMENT OF ANTAGONISTS TARGETING CHEMOKINE RECEPTOR CCR5 AND THE CHEMOKINE RECEPTOR CCR5 – MU OPIOID RECEPTOR HETERODIMER

By Christopher Kent Arnatt, Ph.D.

A dissertation submitted in partial fulfillment of the requirements for the degree of doctor of philosophy at Virginia Commonwealth University.

Virginia Commonwealth University, 2013

Major Director: Yan Zhang
Associate Professor, Department of Medicinal Chemistry

The chemokine receptor CCR5 (CCR5) plays an integral role within the inflammatory network of cells. Importantly, CCR5 is a mediator in several disease states and can be targeted using small molecule antagonists. Within this work, CCR5's role in prostate cancer and HIV/AIDS has been exploited in order to develop potential therapeutics and probes.

First, a series of novel compounds was designed by using pharmacophore-based drug design based upon known CCR5 antagonists and molecular modeling studies of the CCR5 receptor's three-dimensional conformation. Once synthesized, these compounds

were tested for their CCR5 antagonism and their anti-proliferative effects in several prostate cancer cell lines. The data from both the calcium mobilization studies and the anti-proliferation studies suggests that the compounds synthesized have activity as CCR5 antagonists and as anti-proliferative agents in certain prostate cancer cell lines.

In addition, a bivalent ligand containing both a mu opioid receptor (MOR) and a CCR5 antagonist pharmacophore was designed and synthesized in order to study the pharmacological profile of the putative CCR5-MOR heterodimer and its relation with NeuroAIDS. The structural-activity relationship between the bivalent ligand and the heterodimer was studied with radio-ligand binding assays, functional assays, HIV-1 fusion assays, cell fusion assays, and *in silico* molecular dynamics. The subsequent bivalent ligand was proven to be a potent inhibitor in both an artificial cell fusion assay mimicking HIV invasion and a native HIV-1 invasion assay using live virus.

In all, two novel sets of compounds were synthesized that targeted either CCR5 or the CCR5-MOR heterodimer. For the CCR5 antagonists, as leads for prostate cancer therapeutics, further work needs to be done to ascertain and develop their structure-activity-relationship. This library of novel compounds was shown as promising leads as CCR5 and anti-prostate cancer agents. The bivalent ligand targeting the CCR5-MOR heterodimer proved to be a potent and tissue-specific inhibitor for neuroAIDS where the known treatment, maraviroc, is less efficacious and fails to inhibit virus entry in the presence of morphine. Both projects illustrate the roles that CCR5 plays in these two unique diseases.

1. Introduction

1.1 Chemokine Receptor CCR5

1.1.1 Chemokine and Inflammatory Response

Inflammation is a key physiological process prompted by infection or injury involving trafficking of plasma and leukocytes to the site of damage. Generically, there are four sequential components to the inflammation process: inducers, sensors, mediators, and effectors.¹ Inflammatory response is first initiated by inducers, which are the factors that specifically initiated the signaling cascade. Sensors then are activated by inducers, which in turn promote the production of mediators. Mediators act as secondary messengers producing the physiological effects (effectors) of inflammation. Consequently, the effectors allow for inducer-specific inflammation conditions. Although it was developed as a protective mechanism, there are several detrimental pathological outcomes to the inflammatory process such as fibrosis, metaplasia, tumor growth, sepsis, and autoimmunity.¹

Multiple mediators aid in the different inducer-specific effects seen for inflammation. In all, the mediators can be broken into seven groups: lipid mediators, vasoactive peptides, vasoactive amines, fragments of complement components, proteolytic enzymes, cytokines, and chemokines.² Of interest, chemokines, or chemotactic cytokines, are a group of small proteins (8 to 12 kD) that induce chemotaxis

in several types of immune cells. These cells include keratinocytes, lymphocytes, fibroblasts, neutrophils, and monocytes.³ Physiologically, chemokines have several functions in inflammation, homeostasis, hematopoiesis, embryonic development, angiogenesis, and metastasis.^{3,4}

Within the inflammatory network, chemokines are secreted from the site of infection or injury as a pro-inflammatory or anti-inflammatory response.³ The secreted chemokines subsequently activate and recruit leukocytes to the site of inflammation, which guard the body against unwanted organisms.³ These biological effects are mediated through chemokines binding to cell surface chemokine receptors.

To date, approximately 47 chemokines are known and classified by the presence of conserved cysteine residues.⁵ In all, four families exist based upon the conserved cysteine residues found on the N-terminal: CC chemokine, C chemokine, CXC chemokine, and CX₃C chemokine family. The first two cysteine residues are adjacent to each other in the CC chemokine family, whereas in the CXC chemokine family they are separated by one residue. The C chemokine family lacks one of the conserved cysteine residues and the CX₃C chemokine family has three variable residues between the two conserved cysteines. Of the four families, the majority of chemokines are classified as either CC or CXC chemokines.⁵ Currently, 18 chemokine receptors are known and are classified by the profile of chemokine for which they can bind.^{3,5}

1.1.2 Chemokine Receptor CCR5 and GPCRs

All chemokine receptors are G protein-coupled receptors (GPCR), which have seven transmembrane helices (TM) and couple to heterotrimeric G proteins. Figure 1 shows a two-dimensional representation of the structure of chemokine receptor CCR5 (CCR5) and its transmembrane helices. The GPCR superfamily of proteins has approximately 791 genes encoding for the six different receptor subtypes.⁶ Chemokine receptors belong to the class A, rhodopsin-like, family and are classified into four main subclasses based upon which chemokines they bind: CC, CXC, XC, and CX₃C receptors.⁷ Many of the chemokine receptors are promiscuous and bind to several chemokines within their family and allow for tailored chemokine response and redundancy.

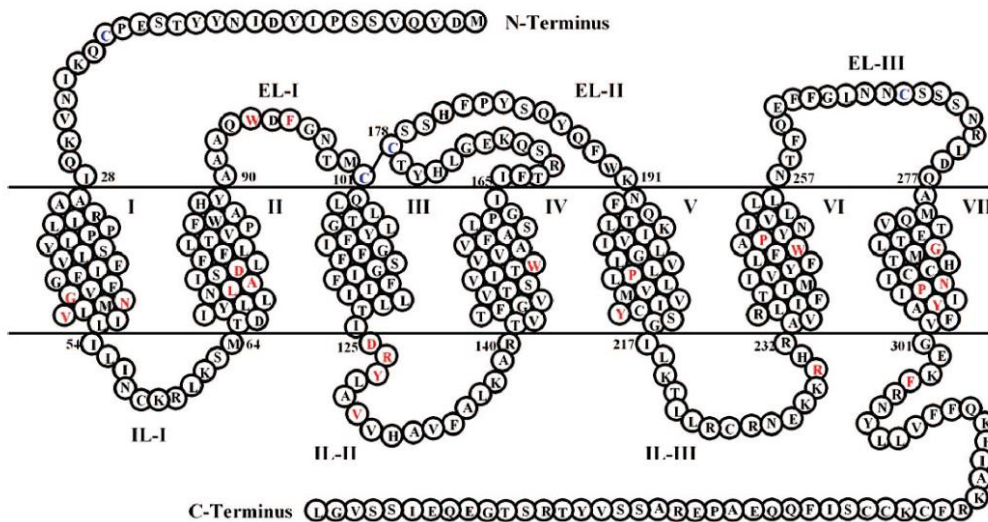


Figure 1. Graphical representation of the 7-TM GPCR, CCR5. Figure adapted from Li et al.⁸

Leukocyte activation occurs through chemokines binding to a chemokine receptor and activating it. There are several events that occur during the activation cycle for

GPCRs. First, a resting state receptor that is bound to the G protein heterotrimer, composed of a guanosine diphosphate (GDP) bound $G\alpha$ and a $G\beta\gamma$ subunit, binds an agonist. Upon binding an agonist, the receptor is converted to an active state and the GDP is exchanged for a guanosine triphosphate (GTP) and the $G\alpha$ and $G\beta\gamma$ subunits dissociate from each other. The $G\alpha$ and $G\beta\gamma$ subunits then go on to activate or inhibit several downstream signaling events through calcium channels, adenylyl cyclase, and phospholipase-C. The GTP slowly gets hydrolyzed to GDP by $G\alpha$ and then reforms the complex with $G\beta\gamma$ and the resting state GPCR.⁴

Several key observations about the active state of GPCRs have been derived from the available agonist-bound crystal structures. When comparing the inactive and active-state crystal structures of the β 2-adrenergic receptor (β 2AR, PDB codes: 2RH1 and 3SN6 respectively), upon activation, there are several movements in the transmembrane helices and changes in residue interactions.^{9,10} Notably, there is a rearrangement between TM5 and TM7, and intracellularly, an outward movement of TM6.¹¹ Concurrently, the ionic lock between D/E6.30 and R3.50 in the conserved DRY sequence is interrupted along with movement of W6.48 (“toggle switch”) from TM7 toward TM5 (amino acids represented in the Ballesteros-Weinstein nomenclature¹²).^{11,13-15} However, such observations were not commonly seen for every activated GPCR crystal structure due to a variety of factors such as varied crystallization techniques.

As a GPCR, CCR5 undergoes such conformational changes when it binds chemokines. Primarily expressed on T-cells and macrophages, CCR5 can bind and be activated through several chemokines: macrophage inflammatory protein-1 α (MIP-1 α),

MIP-1 β , monocyte chemoattractant protein 2 (MCP-2), and RANTES (regulated upon activation normally T-cell expressed and secreted).^{4,16} In all, the chemokine binding process involves two steps: first, sulfated tyrosines on CCR5's N-terminal direct the chemokine to the extracellular loop (EL) 2 of CCR5; next, the N-terminus of the chemokine interacts with the TM domains of the receptor.^{3,4} Activation of CCR5 leads to several signaling cascades and subsequent migration and inflammatory responses. CCR5 also acts as a key co-receptor for HIV-1 invasion and aids in virus invasion and infection.

1.1.3 Chemokine Receptor CCR5 Signaling

As a GPCR, CCR5 can induce several downstream signaling events including increasing intracellular Ca²⁺, activating MAP kinases, activating Jun-N-terminal kinases (JNK) and inhibiting adenylate cyclases.^{4,7,16} Upon activation, the G α subunit separates from the G $\beta\gamma$ subunit; CCR5 has been shown to couple to both G α_i and G α_q (Figure 2).¹⁷ This promiscuous binding allows for different signaling to occur through receptor activation. During signaling, G α_i inhibits adenylyl cyclase and thus decreases the production of cAMP from ATP. G α_q activates phospholipase C β (PLC β) and produces diacyl glycerol (DAG) and inositol triphosphate (IP₃) by hydrolyzing phosphatidylinositol 4,5-biphosphate (PIP₂).^{4,16} The DAG remains membrane bound and can activate protein kinase C (PKC). The cytosol soluble IP₃ then activates calcium channels on the endoplasmic reticulum (ER), which leads to an increase in cytosolic calcium concentration.

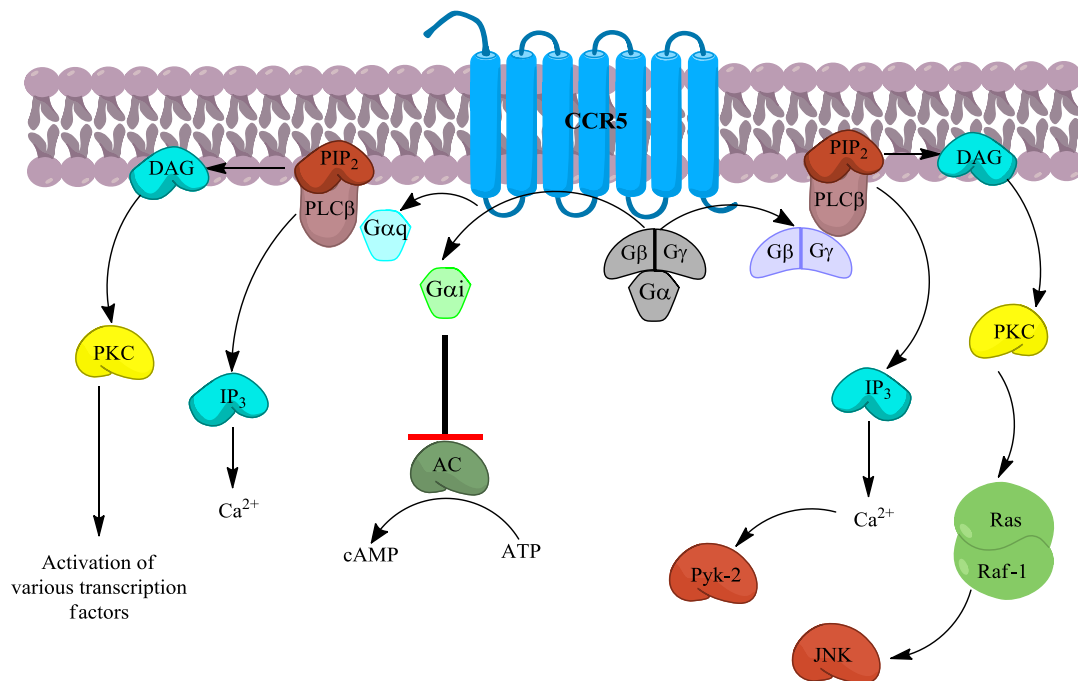


Figure 2. CCR5 signaling cascade. Upon activation, G $\beta\gamma$ unit dislodges from the G α unit. CCR5 can couple to both G α_i and G α_q which have different downstream effects. G α_i inhibits adenylyl cyclase (AC) and stops the formation of cAMP. Whereas G α_q can increase intracellular calcium through activation of phospholipase C (PLC) and production of diacyl glycerol (DAG) and inositol triphosphate (IP₃) by hydrolyzing phosphatidylinositol 4,5-biphosphate (PIP₂). DAG can then go on to activate PKC which activates various mitogen-activated protein kinases (MAPK). The G $\beta\gamma$ subunit can also affect signaling through the IP₃/DAG pathway and activation transcription factors such as Pyk-2 and JNK.

A second set of signaling arises from the G $\beta\gamma$ activating phospholipase C β isoform (PLC β). PLC β also increases calcium through the DAG/IP₃ signal transduction pathway. The G $\beta\gamma$ subunit is also important to chemokine induced chemotaxis of leucocytes.⁴ This cell motility is primarily due to activation of Pyk-2 and JNK.¹⁸

CCR5 signaling is regulated through several mechanisms including desensitization, internalization, and receptor recycling/degradation. Essentially, GPCRs can be regulated by either changing the number of receptors present or changing the

signaling efficiency of the receptors.¹⁹ An important aspect of GPCR signaling is that a GPCR will retain a 'memory' of prior activation. Prior exposure to an agonist will lead to desensitization, or a reduced capacity to be stimulated by an agonist. Homologous desensitization is an agonist specific route that starts with the phosphorylation of the C-terminus of a GPCR by G protein-coupled receptor kinases (GRKs). For CCR5, there are four main serine residues that are phosphorylated: S336, S337, S342, and S349.²⁰ In all, there are seven members of the GRK family that have specificity towards certain GPCRs;²¹ for CCR5, both GRK2 and GRK3 are essential for phosphorylation and are highly expressed in leukocytes.¹⁹

These specific phosphorylations allow for a 10 to 30 fold increase in binding affinity of CCR5 for β -arrestin.^{19,20} Once bound to CCR5, β -arrestin sterically blocks G proteins from binding to CCR5 and effectively uncouples it from the activation cycle. β -arrestin can then complex with an adaptor complex, AP2, and bind calthrin. This complex initiates receptor endocytosis of CCR5 and leads either to lysosomal degradation of the receptor or recycling it back to the cell membrane (Figure 3).¹⁹ Besides desensitization and internalization, β -arrestins can also initiate several signaling cascades by activating mitogen-activated protein kinases (MAPK) such as ERK1/2 and c-SRC and non-receptor tyrosine kinases (nRTK). CCR5 is also regulated by heterologous desensitization where one ligand can desensitize a GPCR to other ligands. For CCR5, this process is initiated by phosphorylation of its C-terminus by PKC and also leads to the desensitization and internalization through β -arrestins binding.⁴

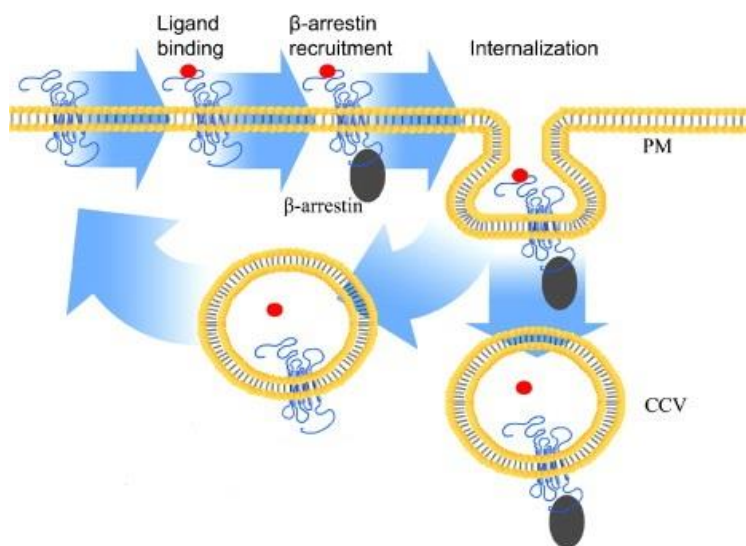


Figure 3. β -arrestin mediated receptor internalization. After ligand binding, the c-terminal of GPCR is phosphorylated which subsequently recruits β -arrestin. Once bound, β -arrestin can cause clathrin-dependent internalization from the plasma membrane (PM) and can also initiate several signaling pathways (not shown). The GPCR in the clathrin-coated vesicle (CCV) can then either undergo degradation or be recycled back to the PM. Figure adapted from Verkaar et al.²²

1.1.4 Chemokine Receptor CCR5 in Different Disease States

GPCRs are important drug targets and account for approximately 36% of all marketed drugs as of August 2011, which can serve as an indicator of their importance both in drug discovery and biological systems.²³ A large number of disease states can be attributed directly to the dysfunction of GPCRs and/or their pathways. Of those diseases, cancer has emerged as a prominent target for the development of new diagnostic techniques and therapeutics.²⁴

CCR5 has been implicated in a number of disease states including: ovarian cancer, breast cancer, prostate cancer, Alzheimer's disease, cardiovascular disease, atherosclerosis, and human immunodeficiency virus (HIV) infection. CCR5 been shown

to be a viable target in drug discovery today due to its involvement in HIV entry and cancer.²⁵⁻²⁷ In HIV pathogenesis, CCR5 acts as an essential co-receptor for HIV invasion into host cells; whereas in cancer, it provides a pro-inflammatory environment promoting cell invasion and proliferation in several cancers.²⁸⁻³⁶ The roles of CCR5 in prostate cancer and HIV are discussed in more detail below.

1.1.4.1 Prostate Cancer

Currently, prostate cancer (PCa) is the most common non-cutaneous solid cancer in men in the U.S.; in all, approximately one sixth of U.S. men will develop PCa.³⁷ Several therapies exist for PCa, but are limited to early stages of the disease due to their dependence on targeting androgen system.³⁷ Upon the onset of PCa metastasis and androgen independence, no significantly effective therapies exist.³⁷

Within the male reproductive system, the prostate gland wraps around the prostatic urethra and acts as a secretory gland.³⁸ Its primary function is to secrete proteins essential for sperm function and health.³⁸ Cell histology within the prostate consists of three main cell types: secretory luminal, basal, and endocrine-paracrine cells.³⁸ Of these three cell types, the secretory luminal cells are most pertinent in PCa due to their expression of prostate specific antigen (PSA) and androgen receptor (AR). The glycoprotein PSA is normally present in male ejaculate and in lesser quantities, in male serum. However, it is often elevated in prostate disorders and cancers, which is why it is used in early detection of PCa.³⁹ The AR is a nuclear receptor responsible for cell differentiation and growth in response to testosterone. AR based cell proliferation has

been shown in benign prostate hyperplasia (BPH), atypical adenomatous hyperplasia (AAH) and PCa.³⁸ Inflammation is key in the development of all of those conditions, especially PCa.^{40,41}

Chronic inflammation, a persistent inflammatory response over a long time course, plays a role in PCa development.²⁸⁻³⁶ While exact initiation mechanisms for prostate inflammation are not known, sexually transmitted diseases, viruses, and carcinogens have been implicated in inducing prostatic inflammation.⁴¹ However, the increase in inflammatory cells will lead to the same damaging effects. At the site of inflammation, both reactive oxygen species (ROS) and reactive nitrogen species (RNS) are produced and lead to cell damage. This inflammatory microenvironment has been shown to increase the risk of cancer formation.⁴² Prolonged cell damage then leads to an increased level of proliferating cells and somatic mutations. These mutations lead to cells that are able to thrive in an environment of chronic inflammation, which can further develop characteristics of cancer and eventually lead to cancer.⁴¹ Within the tumor microenvironment, chemokines aid in the growth, angiogenesis, and invasion of malignant cells.⁴³

Several inflammation-related proteins have been studied in PCa; of them, both CCR5 and its agonist RANTES are highly expressed in PCa compared to regular or BPH prostate cells.⁴⁰ Within the PCa microenvironment, high levels of RANTES are secreted and can serve as an autocrine survival factor. RANTES was able to promote their growth and invasiveness of the PCa cell lines DU145, PC-3, and LNCaP.³⁵ Additionally, the small molecule CCR5 antagonist, TAK-779, was able to inhibit the proliferation and

invasiveness of PCa cell lines induced by RANTES stimulation.³⁵ These results were also repeated by using a natural product CCR5 antagonist, anibamine, against PC-3, DU145, and M12 PCa cell lines.^{26,44} Anibamine and its derivatives were able to inhibit PCa proliferation both in the presence and absence of RANTES stimulation. Furthermore, in a tumor growth assay using mice injected with M12 PCa cells, anibamine and an analog were able to significantly decrease tumor volume over 16 days.⁴⁵ In all, CCR5 and its agonist, RANTES, both have been implicated in contributing to the tumor microenvironment and help contribute to proliferation.

1.1.4.2 HIV/AIDS

HIV causes the destruction of CD4+ T lymphocytes leading to the disease known as acquired immunodeficiency syndrome (AIDS).⁴⁶⁻⁴⁸ HIV/AIDS has become an epidemic and currently more than 34 million people are infected with the virus.⁴⁹ The virus itself is an enveloped single-strand RNA virus that can bind to host cells through interacting with CD4 receptors and a co-receptor. Figure 4 illustrates the mechanism for HIV entry into host cells.

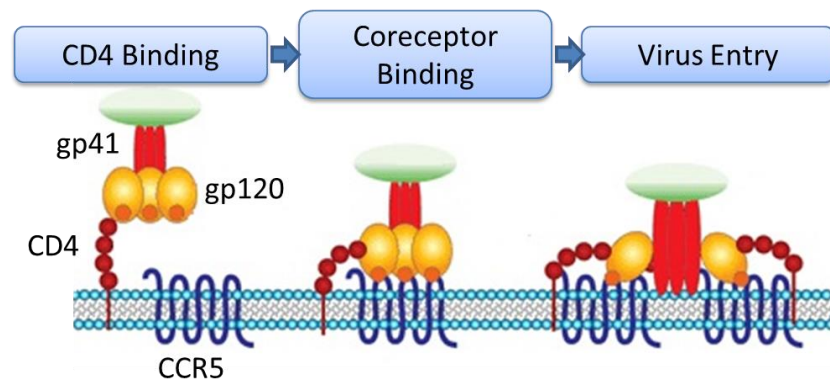


Figure 4. HIV entry into host cells.

Viral entry is first initiated by the glycoprotein (gp) 120 portion of a HIV envelope protein (Env) binding to a host cell's CD4 receptor. It is important to note that Env is a trimeric protein composed of non-covalently bound gp120-gp41 subunits. Upon binding to CD4, there is a conformational change within the Env so that the V3 loop region of gp120 becomes solvent exposed.¹⁶ The V3 loop then binds to CCR5, which acts as a co-receptor for HIV. Once the trimeric complex is formed between CD4, gp120, and CCR5, another conformational change occurs within Env, and gp41 is subsequently embedded in the host cell's membrane, which facilitates viral entry. Since Env is a trimer of gp120-gp41 subunits, there is evidence that it can act with multiple co-receptors to facilitate HIV invasion. However, only one co-receptor is needed for virus entry.¹⁶

The importance of CCR5 in HIV infection can further be seen in individuals who are homozygous for a mutant CCR5 allele. The 32 base pair deletion in CCR5, CCR5 Δ 32, is not expressed on the cell surface and therefore cannot bind to gp120. Therefore, individuals who have CCR5 Δ 32 are resistant to HIV-1 infection.⁵⁰

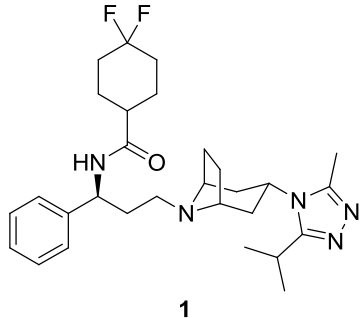
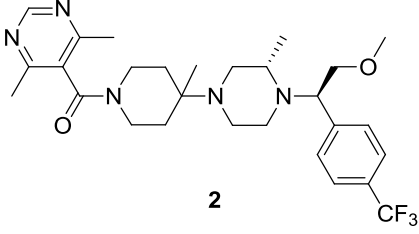
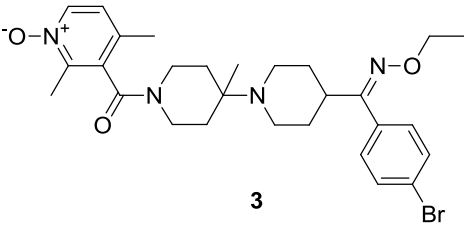
There are two main co-receptors of HIV, CCR5 (as noted above) and chemokine CXC receptor 4 (CXCR4). The difference between the two co-receptors was first noted by Cocchi et al., when they showed that CCR5 specific chemokines MIP-1 α , MIP-1 β , and RANTES only blocked macrophage-tropic (M-tropic) virus and not T-cell tropic (T-tropic).⁵¹ M-tropic viruses are the initial stage of the virus and represent asymptomatic individuals, whereas T-tropic viruses are present in individuals with accelerated disease progression and bind primarily to CXCR4.^{16,52} The ability of chemokines to inhibit virus

invasion by blocking the interaction between CCR5 and gp120 makes for an attractive target for anti-retroviral therapies.⁵³

1.1.5 Chemokine Receptor CCR5 Ligands

Due to CCR5's involvement several disease states, CCR5 antagonists have been actively perused by pharmaceutical companies.^{25,53,54} Most of the efforts have been targeted towards developing highly active antiretroviral therapies (HAART).²⁵ These efforts have produced a FDA approved CCR5 antagonist, maraviroc (**1**), and several clinical candidates, Table 1.

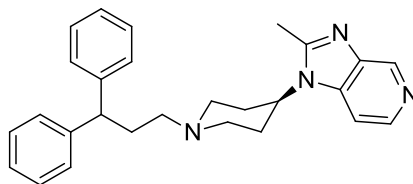
Table 1. Small molecule CCR5 antagonist in clinical development.^{25,53,54}

Name	Structure	Company	Status
Maraviroc	 1	Pfizer	FDA approved
Vicriviroc	 2	Schering-Plough	Phase III completed, withdrawn
SCH-C	 3	Schering-Plough	Phase I, withdrawn

Aplaviroc	<p>Chemical structure of Aplaviroc (4) is shown. It features a central piperidine ring substituted with a propyl group, a cyclohexane ring with a hydroxyl group, and a side chain containing a carboxylic acid group and a phenoxy group.</p> <p>4</p>	GlaxoSmith-Kline	Phase III completed, withdrawn
INCB009471	<p>Chemical structure of INCB009471 (5) is shown. It consists of two piperidine rings connected to a central carbon atom, which is also bonded to a pyridine ring and a trifluoromethyl group.</p> <p>5</p>	Incyte	Phase I/IIa completed, suspended
TBR-652	<p>Chemical structure of TBR-652 (6) is shown. It features a central piperidine ring substituted with a propyl group, a cyclohexane ring with a hydroxyl group, and a side chain containing a carboxylic acid group and a phenoxy group.</p> <p>6</p>	Torbira	Phase II completed
PF-232798	<p>Chemical structure of PF-232798 (7) is shown. It features a central piperidine ring substituted with a propyl group, a cyclohexane ring with a hydroxyl group, and a side chain containing a carboxylic acid group and a phenoxy group.</p> <p>7</p>	Pfizer	Phase II ongoing
SCH532706	Not available	Schering-Plough	Phase II ongoing

Maraviroc, **1**, was developed by Pfizer from an initial high-throughput screening (HTS) hit, **8** (Figure 5). The hit compound showed high affinity for CCR5 ($K_i = 4$ nM), but lacked any anti-HIV-1 activity.⁵⁵ Further modification and development led to maraviroc, which had an anti-HIV-1 $IC_{50} = 2$ nm in peripheral blood mononuclear cells (PBMC). Clinical studies indicated that a twice daily dose of maraviroc (25 mg) was

more effective than the HIV-1 anti-retroviral efavirenz.⁵³ In 2007 the US FDA approved maraviroc for patients with HIV-1.



8

Figure 5. Pfizer CCR5 antagonist HTS hit CCR5 antagonist which lead to maraviroc, **1**.

Developed by Schering-Plough, vicriviroc (**2**), had very high anti-HIV-1 activity in HIV-1 clinical isolates and did not display the cardiac side effects seen in its lead compound SCH-C, **3**. However, clinical trials of vicriviroc, **2**, reached Phase III and were terminated due to lack of efficacy. Another CCR5 antagonist is being developed by Schering-Plough, SCH532706 and is currently in Phase II trials; it shows high anti-HIV-1 activity and high bioavailability (no structure available).²⁵

Similarly, aplaviroc (**4**), which was developed by GlaxoSmithKline, reached Phase III trials and was terminated.⁵³ Aplaviroc showed high activity against HIV-1_{Ba-L} ($IC_{50} = 0.4 \pm 0.3$ nM), but during clinical trials severe hepatotoxicity was observed.^{25,56} INCB9471 (**5**), was developed as a ‘me-too’ drug that had structural similarities to **2** and **3** by Incyte, but was suspended after Phase II trials in 2008.⁵⁷

The first small molecule CCR5 antagonist to be reported was TAK-779 (Figure 6, **9**) in 1999 by Takeda Chemicals.⁵⁸ It was shown to be a highly potent HIV-1 entry inhibitor with an $IC_{50} = 3.7$ nM in PBMC.²⁵ This was likely due to the high CCR5 binding affinity it showed in the radioligand binding assay using [¹²⁵I]-RANTES ($K_i = 1.4$ nM).⁵⁸ However, **9** was not perused in clinical trials due to poor oral bioavailability

and general toxicity issues. Further modification to improve oral bioavailability yielded **6**, TBR-652 (anti-HIV-1 $IC_{50} = 0.061$ nM in PBMC), which is currently in phase II clinical trials.²⁵

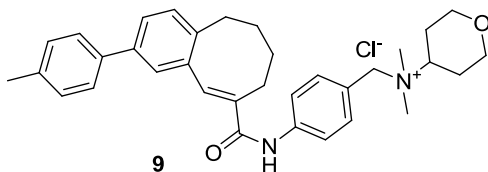


Figure 6. TAK-779, the first CCR5 small molecule antagonist.

Another Pfizer-developed CCR5 antagonist, PF-232798 (**7**), is a second generation maraviroc-based antagonist with improved anti-viral activity and pharmacokinetics. It is currently in Phase II clinical trials. Overall, there has been a large push for CCR5 antagonists by the pharmaceutical industry and there are several clinical candidates. However, maraviroc still remains the only FDA approved treatment.²⁵ Both efficacy and toxicity issues plague the development of future small-molecule CCR5 antagonists.^{25,53,57,59}

1.2 Mu Opioid Receptor

1.2.1 Opioid Receptors

To date, four GPCR opioid receptors have been identified and crystallized by various methods: δ opioid receptor (DOR), κ opioid receptor (KOR), μ opioid receptor (MOR), and nociception/orphanin receptor (NOR).⁶⁰⁻⁶⁴ Opioid receptors are most well known for being the site of action of opium and related opiates. Opiates such as morphine were isolated from opium and showed exceptional analgesic and anti-diarrheal effects.

However, morphine has a high potential for abuse due to its addictive properties.⁶⁵ Therefore, much work has done been to decrease the unwanted side effects of opiates through development of new compounds and a better understanding of opioid receptors. In addition to the exogenous ligands found to act on opioid receptors, several endogenous ligands have been discovered. These ligands are small peptides that are classified in three groups: enkephalins, dynorphins, and β -neoendorphins.⁶⁵

The pharmacological profiles of opiates in different tissues led researchers to the conclusion that multiple opioid receptors exist. Using radioligands with high specific activities and observation of neurophysiological effects of opiates, it was concluded that three opioid receptors exist.^{66,67} These three receptors, σ receptor, μ receptor, and κ receptor were thus named after the opiate they bound: SKF 10,047, morphine, and ketocyclazocine respectively. Later, evidence showed that one of the receptors in the study, σ receptor, was not an opioid receptor.⁶⁸ The δ opioid receptor was then discovered in mouse vas deferens.⁶⁹ Much later, in 1994, the nociception/orphanin receptor was cloned, but does not bind opioids and only shares homology to the other opioid receptors.⁷⁰

The opioid receptors have been shown to act in both the central and peripheral nervous system (CNS and PNS respectively) and have been linked to several pharmacological outcomes. While DOR, KOR, and MOR each exhibit analgesic effects upon stimulation they control other different neural responses. For example, DOR has been shown to produce anxiolytic and anti-depressive behaviors. KOR is linked to dysphoria and MOR is linked to euphoria/reward behavior.⁶⁵

1.2.2 Mu Opioid Receptor Structure

Recently, the MOR was co-crystallized with the morphinan antagonist β -funaltrexamine (β -FNA), Figure 7.⁶³ The mouse MOR that was crystallized shares high homology with human MOR and does not differ in the observed binding pocket for β -FNA. The overall structure of MOR is very similar to the other crystallized seven TM GPCRs. Of note, like the CXCR4 crystal structure, MOR has a β -hairpin loop in extracellular loop (EL) 2.⁷¹ In order to crystallize MOR, the intracellular loop (IL) 3 was replaced with a highly-crystallizable T4 lysozyme.

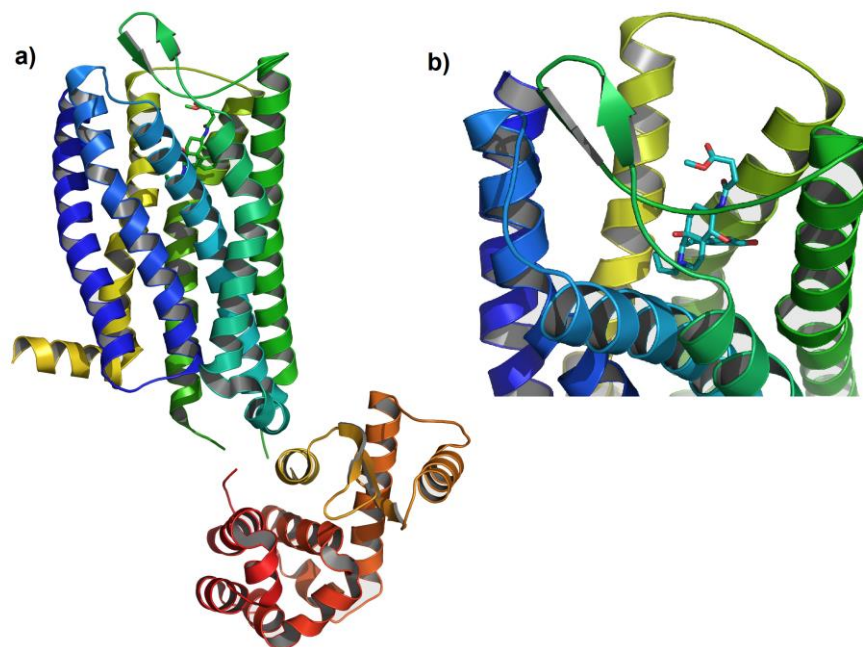


Figure 7. MOR monomer crystal structure. a) Overall all structure showing the T4-lysozyme (colored in reds) that replaced IL-3 (PDB code: 4DKL). b) Close-up of MOR binding pocket showing the β -hairpin loop in EL-2 and the bound β -FNA molecule.

While this can alter the overall conformation of the structure, it is key in the crystallization process. Interestingly, when crystallized, MOR only had a parallel

configuration within the crystal structure and formed homodimers within the crystal lattice. Two main interactions were seen: a TM5/TM6 interaction, and a TM1/TM2 interaction between receptor pairs. Overall, the TM5/TM6 dimer has a higher degree of packing interactions between the four helical bundles and may represent a possible structure of a functional MOR-MOR homodimer.⁶³

1.2.3 Mu Opioid Receptor Signaling

Since MOR is a GPCR, like CCR5, it has many of the same signaling mechanisms. Once stimulated, MOR can inhibit adenylyl cyclase activity, inhibit Ca^{+2} channels, stimulate G protein inward rectifying K^+ (GIRK) channels, and increase intracellular Ca^{+2} levels.⁷² These events occur through either $\text{G}\alpha_{i/o}$ or $\text{G}\beta\gamma$ dependent routes. For MOR, $\text{G}\alpha_i$ mediates inhibition of adenylyl cyclase and activates K^+ channels, whereas the CNS abundant $\text{G}\alpha_o$ inhibits Ca^{+2} channels and stimulates GIRK channels. However, the $\text{G}\beta\gamma$ subunit has the opposite effect; it can both activate certain subtypes of adenylyl cyclase activity and also activate PLC, which subsequently can increase intracellular Ca^{+2} concentrations. These opposing effects of inhibition and stimulation allows for fine tuning of downstream signaling events.⁷²

Due to its functions, MOR is tightly regulated; therefore, desensitization is essential in MOR activity.⁷² Unlike CCR5, phosphorylation of the C-terminus of MOR is only done by GRKs.⁷² This can be deduced from the rapid onset of phosphorylation after stimulation that PKC would not be able to facilitate. Upon phosphorylation, β -arrestin is recruited and participates in MAP kinase signaling, or in receptor internalization.⁷²

Interestingly, MOR agonists can have differential internalization effects depending on the agonist type, agonist concentration, and cell type. For example, it has been shown that both DAMGO ([D-Ala², N-MePhe⁴, Gly-ol]-enkephalin) and etorphine (MOR agonist) can induce phosphorylation and subsequent internalization, whereas morphine does not induce either effect at significant levels.⁷² Overall, when compared to CCR5, MOR desensitization is a more rapid process.

1.2.4 Mu Opioid Receptor Involvement in Different Disease States

While pain and addiction are not mutually exclusive, all opiates carry the risk of addiction and abuse for patients.⁶⁵ This use and abuse is especially dangerous for patients with compromised immune systems such as those with HIV/AIDS. Remarkably, opiates have been shown to increase the progression of HIV/AIDS and linked to the HIV-associated neurocognitive disorders (HAND) and neurological complications of AIDS (neuroAIDS).^{73–75}

1.2.4.1 Addiction

Due to its role in euphoria/reward behavior, the MOR is thought to be the main reason for the addictive properties of morphine. In MOR knockout mice, morphine's analgesic and addictive properties are abolished, which shows its central role in addiction.⁷⁶ Further studies using these mice and other addictive substances such as alcohol, nicotine, and cannabinoids also showed the addictive properties were decreased in MOR knockouts.⁷⁷ Besides analgesia and anti-diarrheal effects, MOR stimulation by

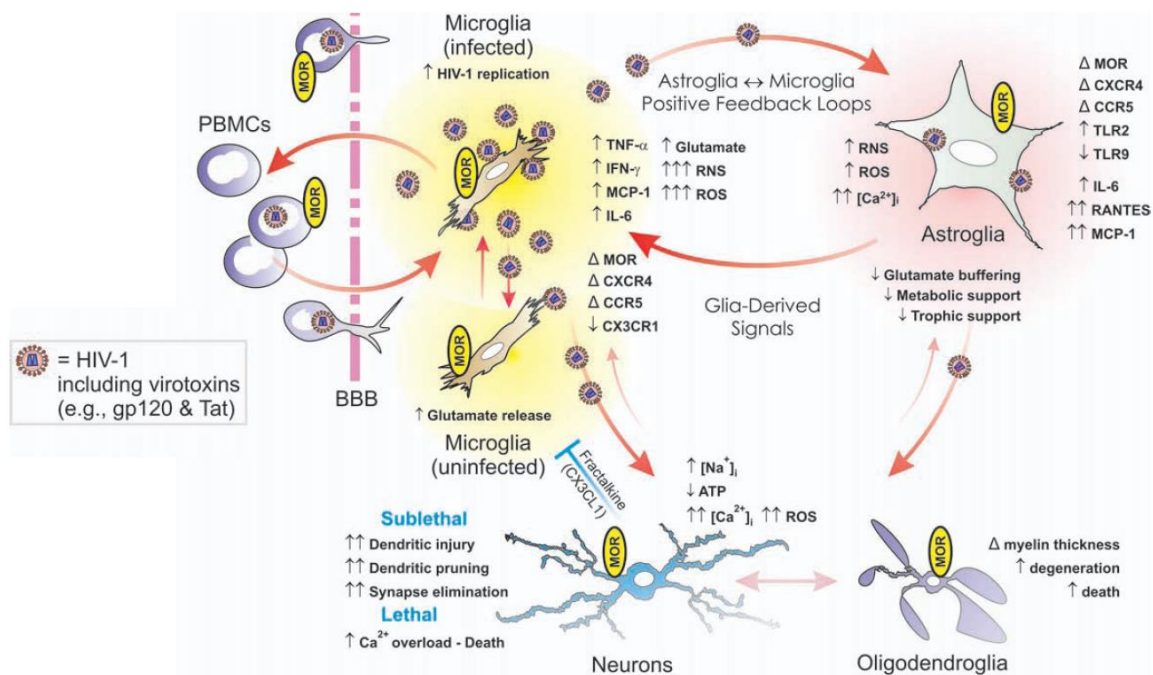
either exogenous or endogenous agonists has also been shown to depress gastrointestinal motility, respiration, immune functions, cardiovascular function, thermoregulation, and locomotor activity.⁶⁵ Despite their wide range of undesirable side effects, MOR agonists are still a frontline agent to treat moderate to severe pain. Furthermore, the use and development of classical opiates is on the rise.^{78,79} An extensive amount of work has been done to try to lessen the additive properties of MOR agonists in addition to developing more selective MOR antagonists to treat addiction.⁸⁰ However, non-medical use and abuse of opiates is still a problem in modern society.⁸¹

1.2.4.2 NeuroAIDS

Both drug abuse and HIV/AIDS are intertwined epidemics; injectable drug users are at a higher risk of being infected with HIV and developing neuroAIDS.⁷⁵ The progression of HIV/AIDS has been shown to be accelerated by abusing substances such as opioids, cocaine, and alcohol.^{75,82-84} Moreover, nearly 10% of all HIV infection has been attributed to injectable drug use with contaminated needles. Opiates negatively impact the immune system through immunomodulation regulated through the MOR, which may also effect the progression of HIV/AIDS.^{85,86} While highly active antiretroviral therapy (HAART) has improved overall health outcomes related to HIV-1 infection, other health complications involved with infection are still a significant problem in patient populations.^{75,82-84}

Opiate use and abuse has a direct influence in the progression of HIV/AIDS. Overall, the CNS is the most vulnerable to these effects.^{73,75} MOR has been known to

effect immunomodulation through acting like a chemokine and affecting chemokine receptors.^{73,75,87-89} Specifically, MOR and CCR5 have been shown to undergo heterodimerization and bidirectional cross-desensitization.⁸⁷⁻⁹⁰ Additionally, activation of the MOR has been shown to increase expression levels of CCR5, allowing for more HIV co-receptors to be present on the cell surface.⁸⁸ Figure 8 shows the complex role MOR plays in neuroAIDS.⁷³



Neurons are not directly affected by HIV-1; instead, glial cells (microglia and astroglia) are infected and initiate the neuropathogenesis of HIV.⁷⁵ Early in the progression of HIV/AIDS, HIV-1 enters the brain and collects in perivascular macrophages.⁹¹ This process is thought to occur through diapedesis of infected monocytes through the blood brain barrier (BBB).⁹² HIV-1 infects mainly microglia and infects astrocytes to a lesser extent.⁹³ Both new virions and toxic by-products of HIV-1 infection are produced at these glia sites. Toxic by-products include: viral proteins, chemokines, cytokines, ROS, and RNS.^{73,75}

Due to the proximity of glia to neurons, the excreted toxins can directly injure and damage neurons leading to neuronal inflammation. During this process, oligodendroglia are also harmed through these toxic species. Opiates potentiate this process through MORs that are present on microglia and astroglia. The positive feedback loop between microglia and astroglia helps sustain inflammation and is also potentiated by opiates.^{94,95} In order to protect themselves, neurons can release fractalkine (CX3CL1) to act on CX3CR1 receptors and limit neurotoxicity caused by infected microglia.⁹⁶

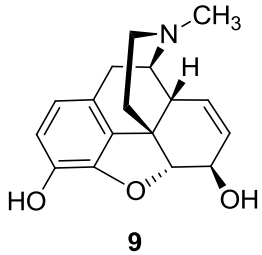
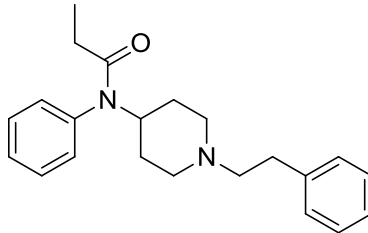
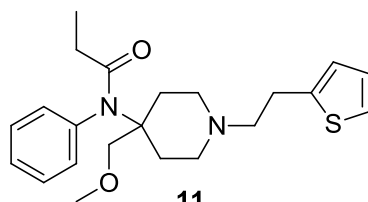
1.2.5 Mu Opioid Receptor Ligands

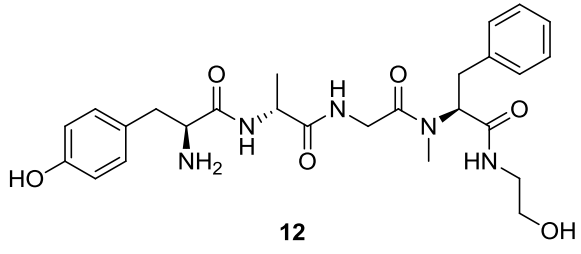
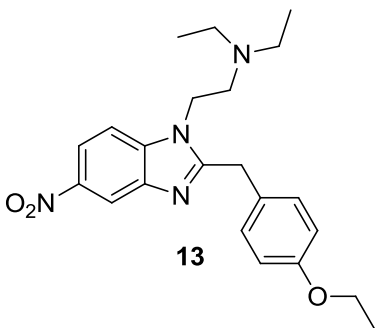
1.2.5.1 Agonists

Several peptide and non-peptide agonists and antagonists have been described for the MOR.^{65,80,97} While morphine (**9**) is a MOR agonist, its deleterious side effects have led to the development of new agonists with lesser side effects and antagonists to block MOR mediated effects. Table 2 shows some of the typical non-peptide MOR agonists

and their selectivity towards the three main opioid receptors: MOR, DOR, and KOR. Morphine is much more potent at MORs than at either KORs or DORs, while etonitazene (**13**) is highly MOR selective with a 9,000 and 12,000 fold higher selectivity for MOR compared to DOR and KOR, respectively.⁹⁸ Additionally, there are several synthetic and endogenous peptide agonists of MOR; most notable is the enkephalin derived DAMGO (**12**) with high MOR selectivity.

Table 2. Example MOR agonists. Structures are arranged in order of increasing selectivity for MOR, starting with the lowest selectivity morphine (in monkey brain membranes).⁹⁸

Name	Structure	KOR K _i (nM)	DOR K _i (nM)	MOR K _i (nM)
Morphine	 9	33.7	111	2.66
Fentanyl	 10	387	403	1.48
Sufentanil	 11	37.8	25	0.19

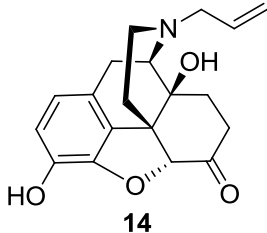
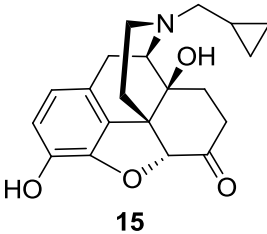
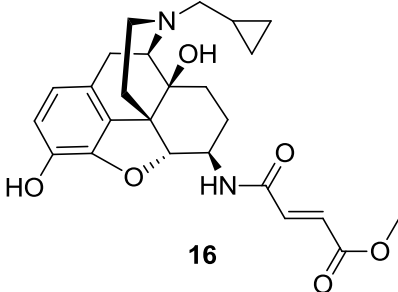
DAMGO		534	634	1.23
Etonitazene		233	176	0.02

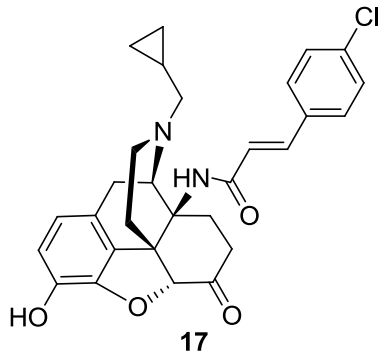
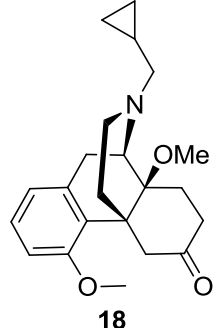
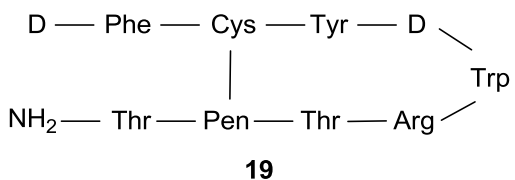
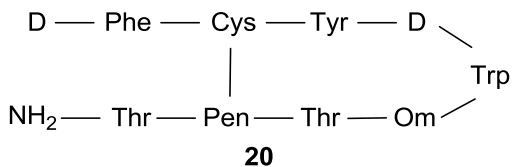
1.2.5.2 Antagonists

Several opioid antagonists have been developed in order to treat addiction, alleviate opiate induced side effects, and even alcoholism. Table 3 shows several morphinan and peptide based MOR antagonists.⁹⁸⁻¹⁰¹ Both naloxone (**14**) and naltrexone (**15**) are non-selective antagonists for the MOR. In order to overcome the lack of selectivity for MOR, β -FNA (**16**) was developed as the first selective MOR antagonist.¹⁰² The apparent binding affinity for **16** suggests that it is non-selective, but it irreversibly binds only to MOR through alkylation of K233 on TM5. The MOR crystal structure also shows this mechanism of action.⁶³ The observed interaction between **16** and MOR also supports the message-address concept originally proposed by Portoghese et al.¹⁰³ The message-address concept refers to the morphanin scaffold having two main parts: the address part is the morphanin core that is active at all of the opioid receptors; the message portion relays the receptor selectivity for the molecule and is located off of the C-ring of

the morphanin core. Figure 9 shows this concept using naltrindole (**21**, a DOR selective antagonist) docked into the MOR crystal structure and the steric clashes that arise compared to β -FNA.⁶³ Clocinnamox (**17**, C-CAM) was also designed using the message-address concept to gain MOR selectivity. Like **16**, C-CAM preferentially binds to MOR irreversibly. Cyprodime (**18**) is a modified morphanin that has the highest selectivity for MOR.⁹⁹ Removing the dihydrofuran ring dramatically decreased affinity to KOR and DOR, but affinity to MOR was maintained.⁹⁹

Table 3. Example MOR antagonists. Structures are arranged in order of increasing selectivity for MOR, starting with the lowest selectivity morphine (in monkey brain membranes).⁹⁸⁻¹⁰¹

Name	Structure	KOR K _i (nM)	DOR K _i (nM)	MOR K _i (nM)
Naloxone	 14	1.95	49	0.62
Naltrexone	 15	0.28	6.94	0.11
B-FNA	 16	3.4 ^a	78.7 ^a	1.1 ^a

Clocinnamox (C-CAM)		5.7 ^a	1.9 ^a	0.7 ^a
Cyprodime		2187	245	5.4
CTAP		5314 ^b	8452 ^b	2.1 ^b
CTOP		5598 ^b	47704 ^b	4.3 ^b

(^a)-denotes apparent K_i within mouse brain homogenates¹⁰⁰, (^b)-denotes K_d values¹⁰¹.

The most selective MOR antagonists are the CTOP and CTAP cyclic peptides (**19** and **20**, respectively).^{101,104} Both have nanomolar affinity to MOR and micromolar affinity for DOR and KOR. Using somatostatin, both CTOP and CTAP were developed to have MOR selectivity.^{101,104} Due to their cyclic nature, these peptides were stable and did not readily undergo enzymatic degradation. However, they were not membrane-

permeable and they could not pass the BBB. Therefore, they only act on MOR in the PNS and could not be used in the CNS.^{101,104}

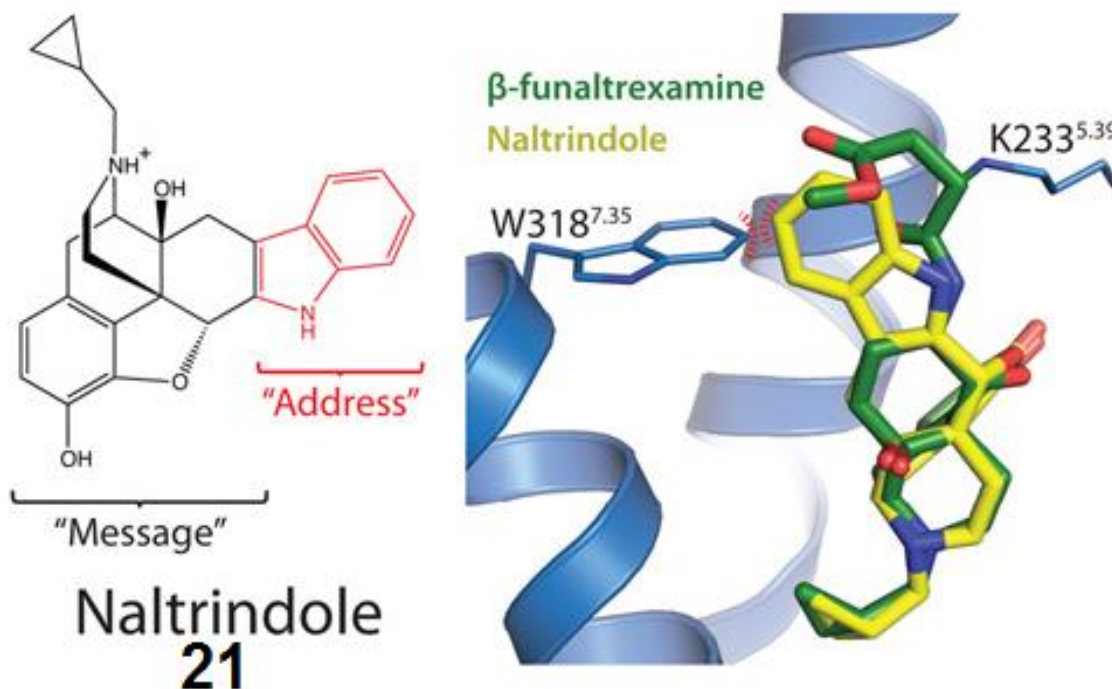


Figure 9. The message-address concept for opioid receptor selectivity. The morphanin core is the message portion, whereas the tryptophan portion is the address where DOR selectivity arises for naltrindole. When naltrindole is docked into MOR (blue helices) there are steric clashes (red lines) and does not bind as well as MOR selective β -FNA. Figure adapted from Manglik et al.⁶³

1.3 GPCR Dimerization

Originally, it was thought that GPCRs acted in a monomeric fashion and that there was a general stoichiometry of 1:1, receptor:ligand. However, increasing evidence has begun to show that they can act in dimeric or even oligomeric assemblies.^{105–107} One of the first observations of dimerization in rhodopsin-like GPCRs was seen in β -adrenergic receptors; it was seen that binding of one ligand decreased the binding of a

second one.¹⁰⁸ This type of “cross-talk”, better known as negative cooperativity, occurs when a dimer bound ligand either inhibits the binding or signaling of a second bound ligand to the dimer pair.^{106,107}

One of the earliest methods for elucidating dimer pairs was to use co-immunoprecipitation techniques. First used for the β_2 -adrenergic receptor, an influenza hemagglutinin (HA) and a myc-epitope tag were incorporated into the receptor.¹⁰⁹ These two receptor subtypes were then co-expressed, and using an anti-myc antibody, immunoprecipitation was performed. If only monomers were present, only the myc-epitope tagged β_2 -adrenergic receptor should show up on a Western blot analysis. However, using an anti-HA antibody, the HA tagged β_2 -adrenergic receptor was present. Therefore, the two subpopulations of the receptor were able to dimerize with each other.¹⁰⁸ This technique has subsequently been used as a preliminary technique to study the homo and heterodimerization of GPCRs.^{105–107}

Another important technique for GPCR dimerization/oligomerization detection is Fröster resonance energy transfer. Both bioluminescence and fluorescence (BRET and FRET respectively) have been used within this technique. For FRET detection, the two receptors of interest (either homo or hetero) are tagged with two different fluorescent proteins: i.e., a cyan fluorescent protein (CFP) and a yellow fluorescent protein (YFP). It is essential for the Fröster resonance energy transfer that the excited state of one fluorescent protein can transfer energy (donor chromophore) to an acceptor chromophore and permit it to emit its unique excitation wavelength. Essential for the observation of GPCR dimers, this interaction is very distance specific; in order for FRET to happen, the

two chromophores (and associated proteins) must be in close proximity (10 to 100 Å).¹⁰⁹ Therefore, excitation of the CFP at ~436 nm would give only one emission wavelength at ~480 nm if no dimerization was present. If the receptors do dimerize, exciting the CFP would yield both the emission wavelength at ~480 nm (for CFP) and an additional emission wavelength at ~535 nm which corresponds to the excitation/emission from the YFP on the other GPCR in close proximity. This technique can also be coupled with a bioluminescent luciferase enzyme instead of the CFP to excite the YFP through BRET.¹¹⁰ The combination of co-immunoprecipitation and FRET/BRET has led to a network of GPCR homodimers and heterodimers being discovered.¹⁰⁵

In addition to the biochemical techniques, direct observation of GPCR dimers and oligomers has been obtained through both GPCR crystallization and atomic-force microscopy.^{63,71,111} Figure 10 shows the current observed GPCR oligomers and dimers for rhodopsin, CXCR4, and MOR. Using atomic-force microscopy (Figure 10a) oligomer formations of rhodopsin were able to be seen, giving the first direct observation of GPCR oligomization.¹¹¹ Both CXCR4 and MOR were observed to form dimer formations within their crystal lattice (Figure 10b and c), and while this may be an artifact of the crystallization process, it does lend credence to GPCR dimerization.^{63,71}

Several interactions between dimers have been proposed, and two main dimerization models have subsequently been described: a contact dimer model, and a domain-swapped dimer.¹⁰⁷ Both have been supported by mutation and computational studies, but due to observations of GPCR crystal structure, the contact dimer may represent a more realistic model. The domain-swapped model proposes that TM6 and

TM7 are exchanged between monomers to form a dimer.¹¹² The contact dimer model proposes that dimerization occurs through contact between the helices of GPCRs. Both a TM5/TM6 and a TM1/TM2 interface have been postulated and observed.^{15,63,71,113}

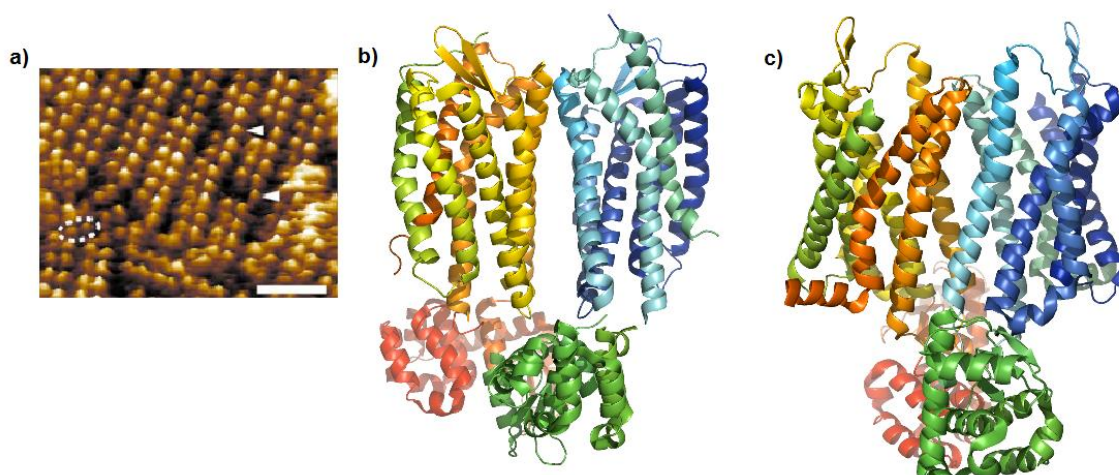


Figure 10. Observed GPCR oligomers and dimers. a) atomic-force microscopy of rhodopsin oligomers, where the dotted circle is a dimer and the arrows point to monomers [adapted from Fotiadis et al.¹¹¹]. b) Crystal structure of the CXCR4 dimer with a TM5/TM6 interface [PDB code 3ODU].⁷¹ c) Crystal structure of the MOR dimer with a TM5/TM6 interface [PDB code 4DKL].⁶³

An important aspect of GPCR dimerization is its effect on receptor function and signaling. As alluded to earlier, a possible outcome of dimerization is positive and negative cooperativity, see Figure 11.^{105,106} Positive cooperativity occurs when binding of a ligand to one receptor leads to partial, full, or enhanced activation of the second receptor. It can also occur when two ligands bind both receptors and an enhanced action is seen. Negative cooperativity can occur when one ligand bound leads to either inhibition of a ligand binding to the dimer, or inhibition of signaling from a second bound ligand.

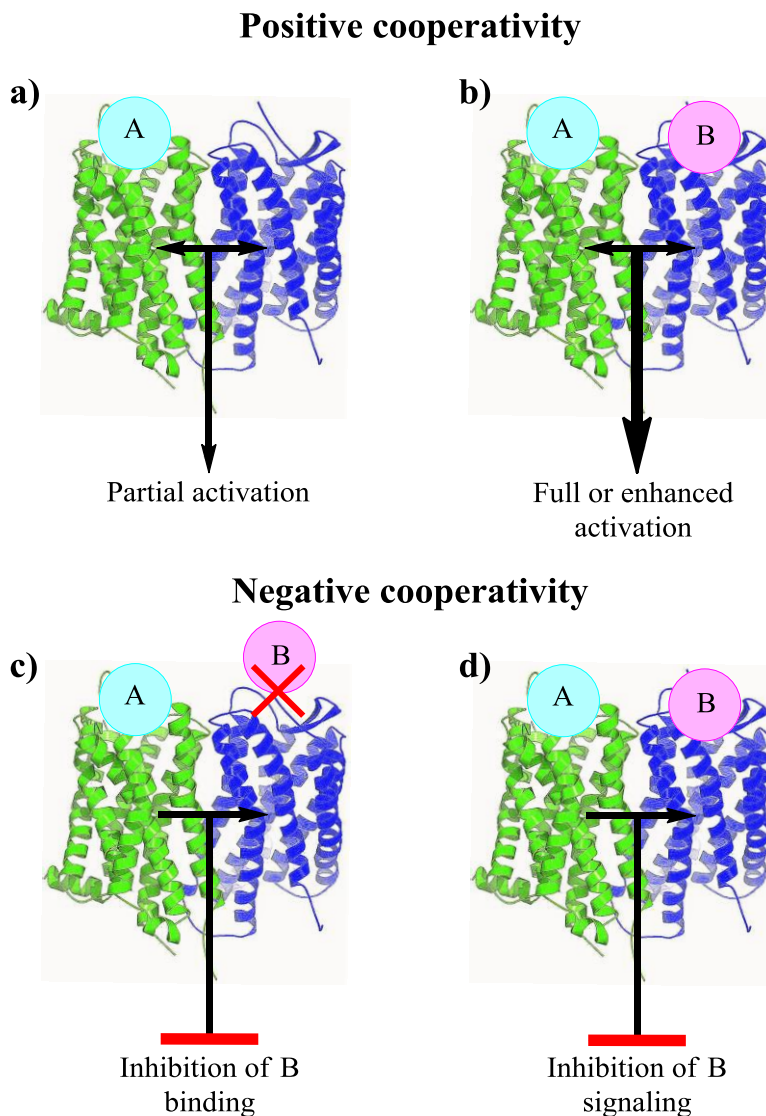


Figure 11. Positive and negative cooperativity in GPCR dimerization. a) Agonist A binding to the green GPCR results in partial activation of the blue GPCR. b) When two agonists, A and B, bind to the GPCRs there will be enhanced activation, synergism. c) In negative cooperativity binding of A to the green GPCR leads to inhibition of the binding of B to the blue GPCR, leading to suppression of B-related signaling. d) Binding of A leads to inhibition of signaling from the blue GPCR even with B bound to it.

Several reports have described homo and heterodimers for MOR. As stated above, there has been direct observation of the MOR-MOR dimer through its crystal structure.⁶³

To date, MOR has also been shown to dimerize with: DOR, KOR, NOR, CCR5,

cannabinoid receptor 1 (CB1), substance P receptor (NK1), and somatostatin receptor 2A (sst_{2A}).^{87,90,104,105,114–117} Functionally, heterodimers may allow for different mechanisms of signal regulation for MOR.¹¹⁸ For example, within the CCR2-CCR5 heterodimer, dimerization leads to the receptors being able to couple with G $\alpha_{q/11}$, which, as individuals, they normally do not couple with.¹⁸ A similar effect was seen for the MOR-DOR heterodimer; when expressed alone, pertussis toxin can inhibit agonist stimulated G α -dependent signaling from both receptors, but when expressed together pertussis toxin cannot inhibit G α -dependent signaling.¹¹⁹ These results suggest that the heterodimer can couple to different G proteins than the monomers by themselves. Dimerization may also affect receptor desensitization and internalization.^{105,106,119}

1.3.1 GPCR Dimerization Involving Mu Opioid Receptor

The effects that dimerization has on desensitization and internalization have been shown in both MOR homodimers and MOR-NK1 heterodimers. For MOR-NK1 heterodimers, it was observed that the interaction promotes DAMGO-stimulated β -arrestin internalization that is not regularly seen for MOR. Stimulation of cells expressing MOR alone leads to β -arrestin internalization to clathrin pits, while stimulation of NK1 alone leads to β -arrestin internalization into endosomes.¹¹⁶ When expressed together, stimulation of the MOR-NK1 heterodimer leads to β -arrestin internalization into endosomes. This process delays the recycling process for MOR because it is sequestered in endosomes and overall leads to greater desensitization of MOR.¹¹⁶

Differences in internalization are also seen for MOR homodimers. Under certain conditions, when stimulated by morphine, MOR does not undergo desensitization or endocytosis.¹²⁰ However, when co-administered with DAMGO, MOR becomes desensitized and internalized. The change in trafficking of MOR can be attributed to dimerization due to DAMGO and lead to reduced tolerance of morphine.¹²⁰ Overall, MOR's signaling and regulation is greatly affected by dimerization with itself or other GPCRs.

1.3.2 Bivalent Ligands Targeting GPCR Dimerization

Bivalent compounds are essential for studying the relationship between the monomers of both GPCR homodimers and heterodimers. A bivalent compound is defined as a compound that contains two distinct pharmacophores.¹²¹ By targeting dimers of GPCRs, new pharmacological profiles are obtainable because of their unique properties.¹²² Using bivalent ligands may lead to higher affinity, higher selectivity, improved physiological response, or altered physiological response. The possible synergistic effects are due to the cooperativity between the receptors and an overall drop in the entropy of the interaction by targeting two receptors at once.¹²¹

Generally, bivalent compounds can either be classified as homobivalent or heterobivalent; that is, they either have two of the same pharmacophores or two different ones. These two pharmacophores are attached to each other with a linker that will not interfere with receptor binding and is the appropriate length to allow the two pharmacophores to interact with both receptors. The average distance between dimers is

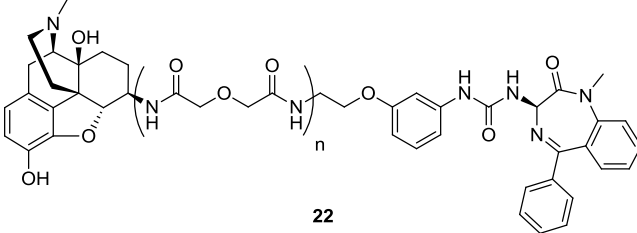
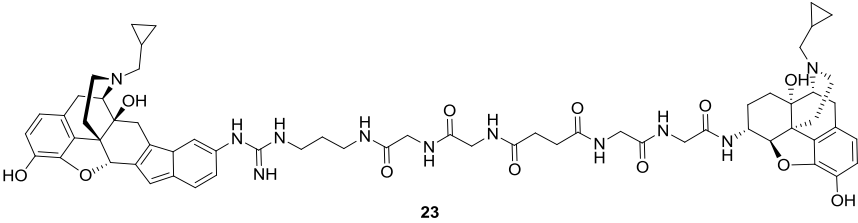
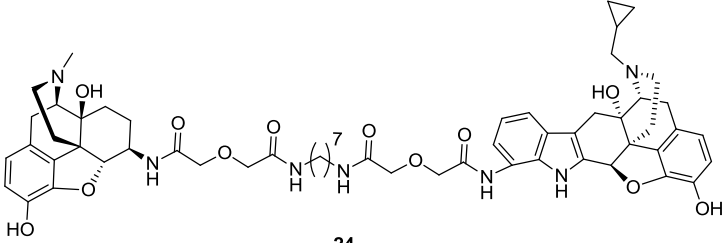
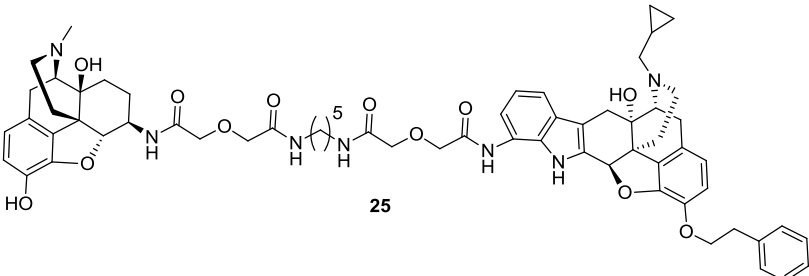
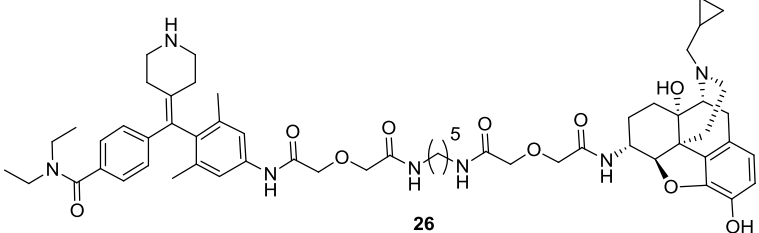
thought to be between 27 Å and 32 Å.¹²³ Therefore, the linker length should ideally be near that range. Several different linker types have been reported and range from aliphatic chains to ethers.¹²² The pharmacophores of choice usually have high affinity and selectivity for the targeted receptor(s) dimer and can tolerate added substitutions onto their structure to facilitate the addition of the linker.

To date, five selective, morphanin-based bivalent compounds targeting MOR heterodimers have been described (Table 4).^{124–127} Using a MOR agonist, oxymorphone, and a type 2 cholecystokinin (CCK₂) receptor antagonist, compound **22** was designed to determine if MOR and CCK₂ associate with each other *in vivo*. Interestingly, **22** was able to induce the heterodimerization of the two receptors that normally do not.¹²⁴ Bivalent compound **23** was designed to explore if dimerization is the probable cause of KOR subtypes.^{125,128} It is composed of the KOR antagonist 5'-GNTI and MOR antagonist naltrexone (**15**) connected together with a linker composed of glycine and succinyl units. Both the glycine and succinyl units allow for linker flexibility and a balance of the hydrophobic-hydrophilic within the molecule.

Compounds **24**, **25**, and **26** were all designed as MOR-DOR heterodimer modulators. All three have both an agonist and antagonist pharmacophore in order to evaluate the functional role of the MOR-DOR heterodimer in analgesia.^{122,126,127} Portoghese et al. had this in mind when designing MDAN-21 (**24**) as an analgesic without the deleterious side effects of morphine (**9**). The compound is comprised of a MOR agonist (oxymorphone) and a selective DOR antagonist (naltrindole) tethered together with a 21-atom spacer with a total maximum length of 25.4 Å.¹²⁶ Within *in vivo*

assays, **24** was able to cross the BBB as well as morphine and was 50-fold more potent than morphine without tolerance or dependence side effects.¹²⁶

Table 4. Selective, morphanin-based bivalent compounds targeting MOR heterodimers.^{124–127}

Heterodimer target	Structure	Ref.
MOR-CCK ₂	 <p style="text-align: center;">22</p>	124
MOR-KOR	 <p style="text-align: center;">23</p>	125
MOR-DOR	 <p style="text-align: center;">24</p>	126
MOR-DOR	 <p style="text-align: center;">25</p>	127
MOR-DOR	 <p style="text-align: center;">26</p>	127

To explore the interaction of the MOR-DOR heterodimer, Harvey et al. developed two “tuned-affinity” MOR-DOR bivalent compounds.¹²⁷ Bivalent compounds like **24** may not intrinsically be able to distinguish the MOR-DOR heterodimer from either the MOR-MOR or DOR-DOR homodimers.^{126,127} Both the pharmacophores used in **24** had high affinity for their receptors; therefore, when used to evaluate the function of MOR-DOR heterodimers, compound **24** could also interact with the homodimers and thus skew observations. To overcome this caveat, compounds **25** and **26** were designed to have high affinity MOR ligands and low affinity DOR ligands. That way the bivalent ligand should bind to the MOR-DOR heterodimer since its affinity at DOR will rise due to the change in entropy.¹²¹ This effect would not be present at either MOR or DOR homodimers, thus making **25** and **26** preferentially bind to the MOR-DOR heterodimer. Compound **25** has the MOR agonist oxymorphone and a low affinity DOR antagonist, ENTI, whereas compound **26** has a MOR antagonist, naltrexone, and a low affinity DOR agonist, DM-SNC80.¹²⁷ The composition and length of the linker connecting the pharmacophores was chosen based upon results in other studies, and its well-balanced flexibility and hydrophobic-hydrophilic characteristics.^{126,127} Both compounds were shown to preferentially bind to MOR-DOR heterodimers and synergistically raise the binding affinity for the DOR pharmacophore when binding assays were done with MOR-DOR membranes vs. DOR alone membranes. The concept of tuning the affinity of bivalent ligands by using a mixture of low and high affinity pharmacophores is a new but powerful tool.¹²⁷

1.4 Hypotheses and Specific Aims

Both prostate cancer and neuroAIDS are devastating diseases without any standout treatments; therefore, it is adventitious to develop novel ways to target these diseases in order to advance their treatment.

1.4.1 Antagonists Targeting CCR5

Targeting the underlying up-regulated inflammatory pathways in prostate cancer may help stem the proliferation of cancer cells. CCR5, a crucial receptor in the inflammation system, has been shown to play an important role in prostate cancer proliferation and therefore, it may be adventitious to target its functions. We aim to show that by targeting CCR5 with newly developed antagonists, that prostate cancer proliferation can be inhibited. The specific aims for his project are: design and synthesize CCR5 antagonists; test the compounds for their cytotoxicity, CCR5 activity, and anti-proliferative abilities; and further develop a structure-activity relationship for the antagonists.

1.4.2 Bivalent Compounds Targeting the Putative CCR5 – MOR Heterodimer

The mechanism behind the potentiation of neuroAIDS by opiates is still not fully understood. In order to elucidate the mechanism, bivalent compounds targeting the CCR5-MOR heterodimer were synthesized. The direct interaction between CCR5 and MOR may offer a potential explanation for what is seen *in vivo*. The specific aims for this project are: design and synthesize bivalent compounds targeting the CCR5-MOR heterodimer, test the compounds for their affinity and activity at both receptors, ascertain

their abilities to alter HIV-1 infection in primary human CNS cells, and postulate how the bivalent compounds directly interact with the heterodimer *in silico*.

2. Small Molecule Chemokine Receptor CCR5 Antagonists for Prostate Cancer Treatment

2.1 Project Design

Within the immune system, CCR5 primarily functions through interaction with endogenous small cytokines (chemokines) which include CCL3 (MIP-1 α), CCL4 (MIP-1 β) and CCL5 (RANTES).⁴ Of those chemokines, CCL5 expression has been correlated to the progression of several cancers.^{35,129,130} Within those cancers, prostate cancer specimens have also been shown significant overexpression of CCR5.⁴⁰ Importantly, RANTES induced prostate cancer cell invasion and proliferation can be inhibited with the CCR5 antagonist TAK-779.³⁵ This mechanism of prostate cancer progression represents a novel and targeted cancer therapy.

Currently, prostate cancer is the most common non-cutaneous solid cancer in men in the U.S.; in all, approximately one sixth of U.S. men will develop prostate cancer.³⁷ Several therapies exist for prostate cancer, but are beneficially limited to early stages of the disease. Upon the onset of prostate cancer metastasis no significantly effective therapies exist.^{26,44} Therefore, exploiting RANTES-induced cell invasion and proliferation could prove to be a useful therapy to stop the progression of prostate cancer

in later stages. In order to do so, new CCR5 antagonists targeting prostate cell proliferation and invasion need to be developed.

Several small molecule CCR5 antagonists have been developed as HIV-1 entry inhibitors and currently one has been approved by the FDA for the treatment of HIV since 2007 (Table 1).^{25,53,54} Some examples of CCR5 antagonists are maraviroc, aplaviroc, vicriviroc, and TAK-779 (Figure 12); all of which have shown high efficacy inhibiting CCR5 mediated virus entry.²⁵ However, there has been little success in getting them through clinical trials due to toxicity, cardiac side effects, lack of efficacy and bioavailability.^{25,56,58} Therefore, there is a need to continue looking for unique chemical structures and templates in order to curtail the negative side effects of those compounds.

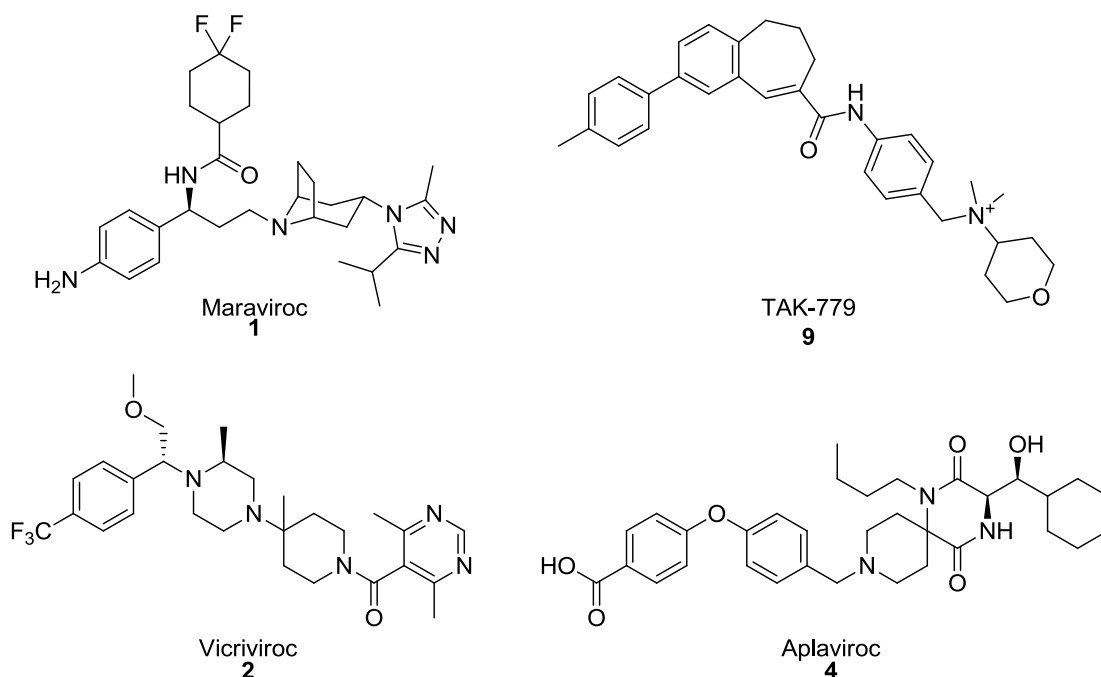


Figure 12. Example CCR5 antagonists used as the basis of CCR5-pharmacophore.

A series of novel compounds were designed by using the CCR5 antagonists in Figure 12 and a molecular modeling study of the CCR5 receptor's three-dimensional conformation analysis to create an antagonist pharmacophore. Figure 13 shows the pharmacophore found based on this fragmentation and molecular modeling study.

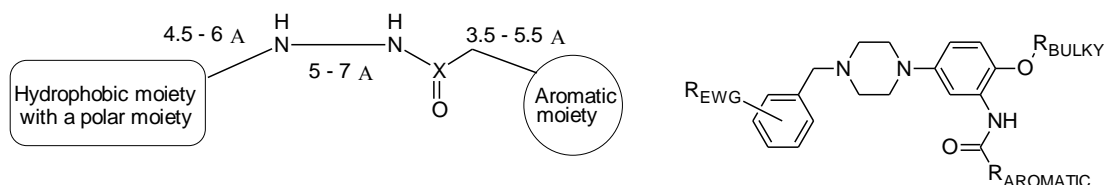


Figure 13. Molecular modeling based pharmacophore analysis, and designed CCR5 antagonist scaffold.

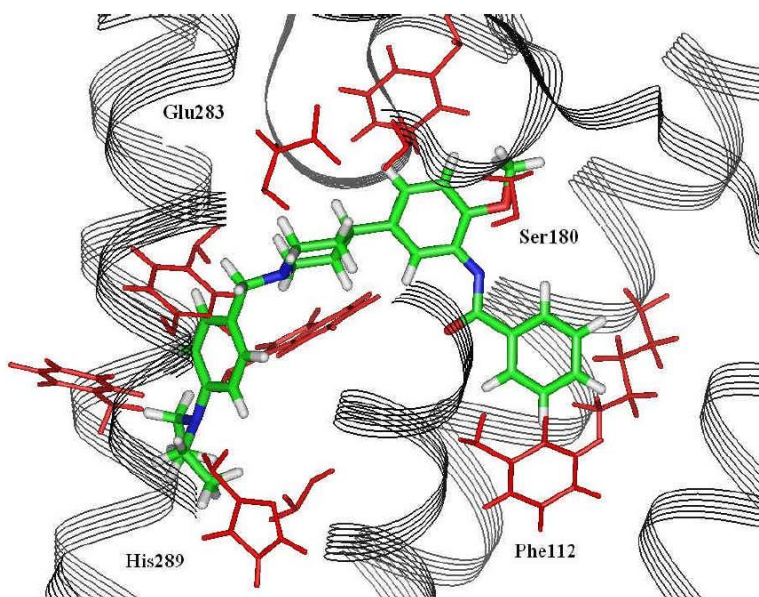


Figure 14. Example pharmacophore-based compound docked into a CCR5 homology model.

It was found that the known CCR5 antagonists shared an aromatic moiety connected with an amide bond and also contain a secondary amine with a hydrophobic group with an attached polar moiety attached. The proposed piperazine-containing CCR5

antagonists were designed based upon those pharmacophore features. Homology modeling and docking studies indicated that the piperazine-containing antagonists may bind in a similar binding pocket as maraviroc and TAK-779 (Figure 14).

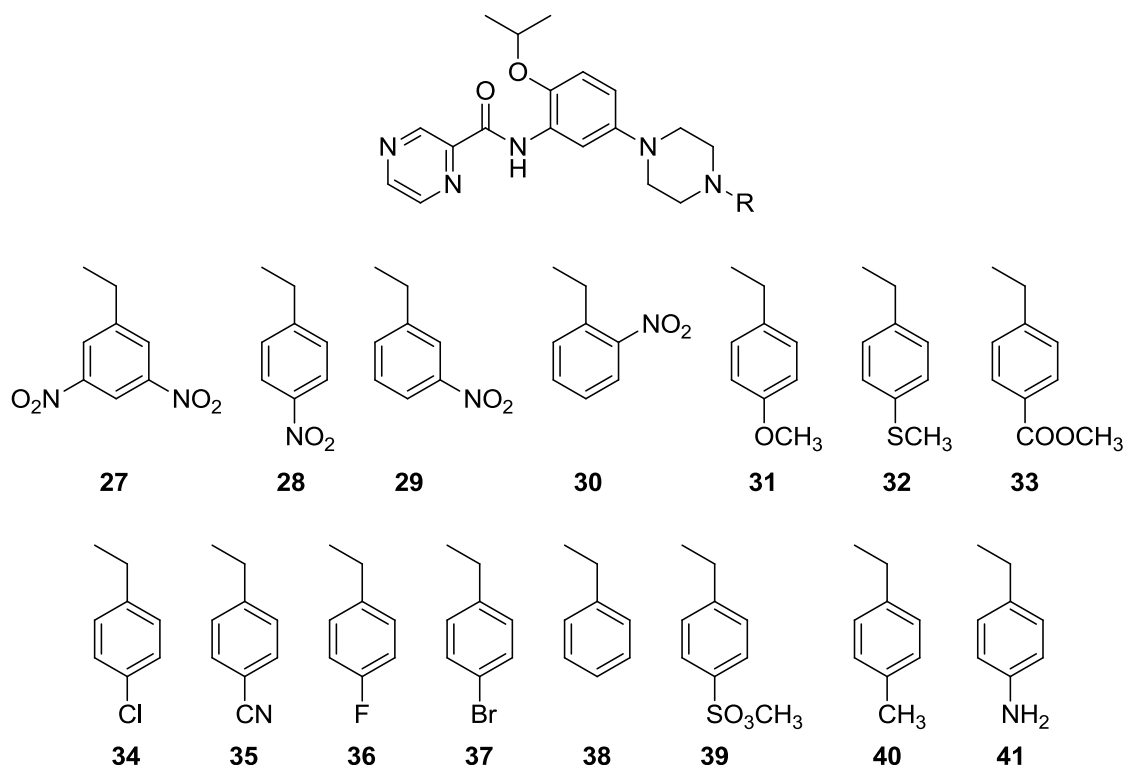


Figure 15. Synthesized derivatives with substituted benzyl groups based upon the CCR5 antagonist scaffold and pharmacophore in Figure 9.

Previously, a total of 15 compounds based on the scaffold in Figure 15 (27-41).¹³¹ As shown in Figure 11, most of the benzyl substitutions of the synthesized compounds consisted of electron withdrawing groups. Biological data for the compounds suggested that electron donating groups may enhance activity. Some additional groups were also added based upon the commercial availability of the appropriate starting materials. Figure 16 shows the compounds synthesized in this study in order to gain a better understanding of the structure-activity-relationship (SAR) of the piperazine-containing antagonists (42-

48). They were tested for their CCR5 antagonism, anti-proliferative effects in several prostate cancer cell lines, and basal cytotoxicity.

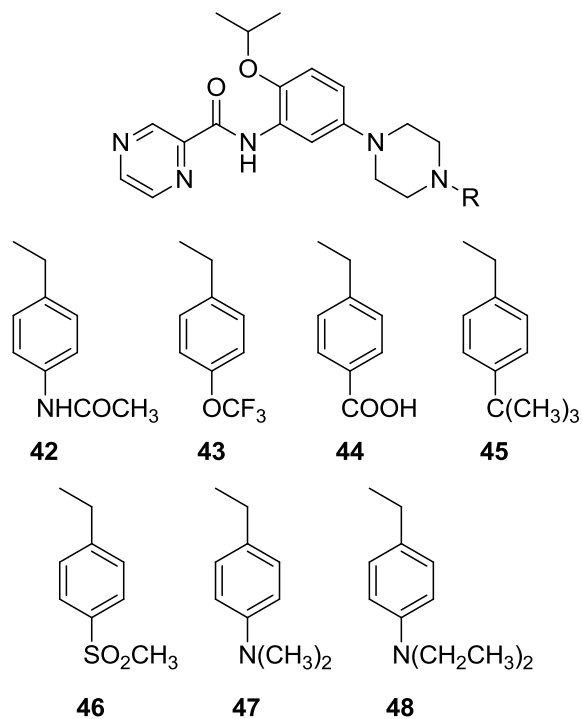
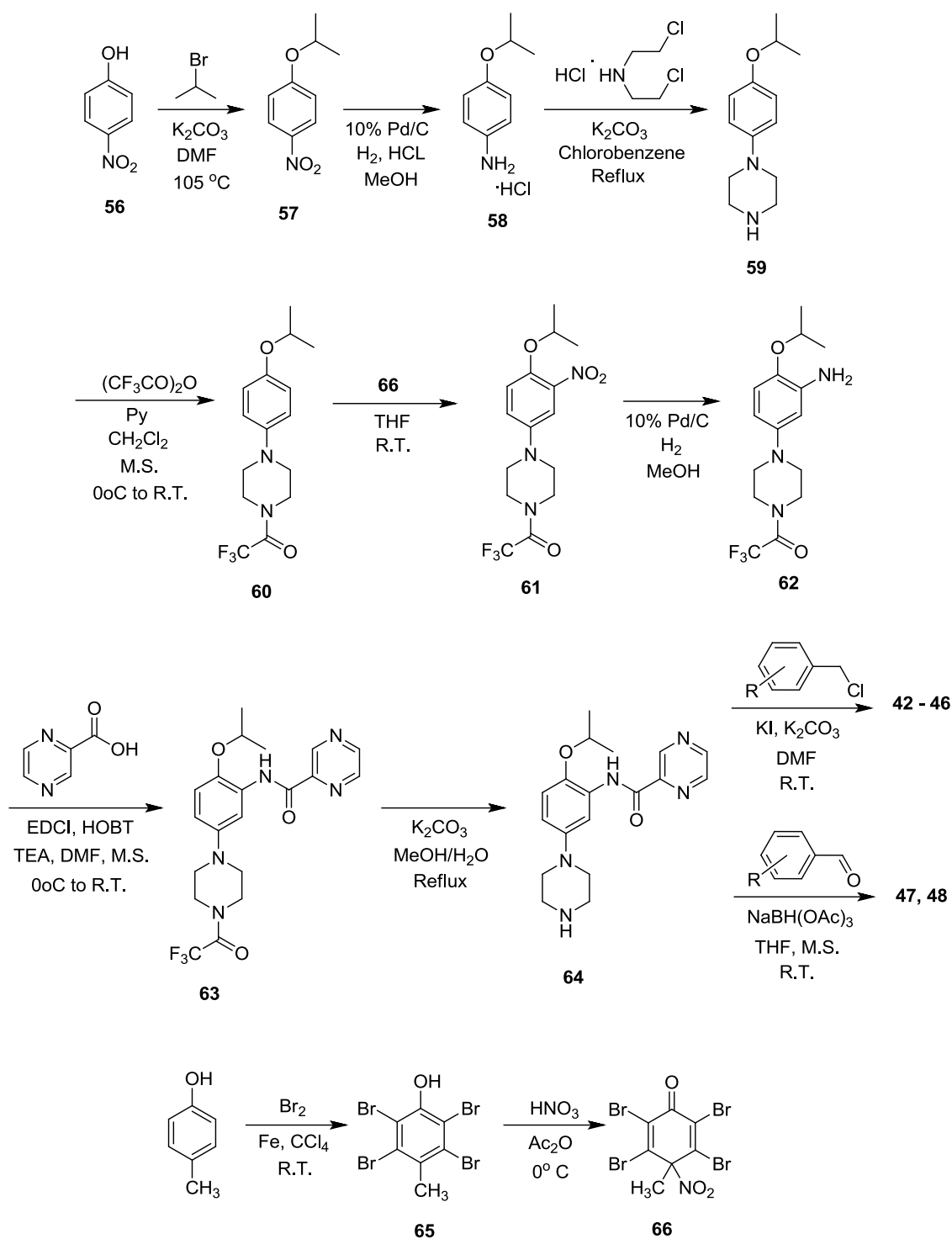


Figure 16. Synthesized CCR5 antagonists for elucidating the SAR of the piperazine-containing compound library.

2.2 Chemical Syntheses

The synthetic route for the small molecule piperazine-based antagonists had previously been elucidated by Dr. Gou Li and Ms. Joanna Adams of the Yan Zhang Group.¹³¹ However, several steps still needed to be optimized in order to receive higher yields of pure product. Scheme 1 shows the overall 11-step synthetic route used to synthesize compounds 42 through 48.



Scheme 1. Synthetic route for CCR5 antagonists **42-48**.

2.2.1 Williamson ether synthesis

A Williamson ether synthesis was used to alkylate 4-nitrophenol (**56**) with 2-bromopropane. This reaction was done in the presence of K_2CO_3 in dimethylformamide (DMF). Temperature control proved to be critical in this reaction; if the reaction was below $100\text{ }^\circ\text{C}$, no product was formed and if the temperature was raised above $110\text{ }^\circ\text{C}$ the 2-bromopropane was lost to excessive evaporation since its boiling point is around $59\text{ }^\circ\text{C}$. Therefore, the reaction was initiated in a pre-warmed oil bath at $105\text{ }^\circ\text{C}$ and kept constant at that temperature. After 1 hour of reaction 99% yields of **57** were regularly achieved.

2.2.2 Nitro-group reduction to primary amine

The hydrogenation of **57** to form the primary amine **58** was done using 10% palladium on carbon (Pd/C) with hydrogen gas and 1.3 equivalents of concentrated HCl. While yields for this reaction were previously reported to be 86%, the reaction times exceeded 24 hours.¹³¹ In order to overcome this long reaction time, we hypothesized that the starting material had to be as pure as possible and completely devoid of any chemical species that could poison the Pd/C. Therefore, before hydrogenating **57**, it was washed with activated charcoal to remove any residual salts and bromine species. After using the wash, yields were raised to 98% and reaction times ranged from 1 hour to 2 hours for up to 5 grams of starting material.

2.2.3 Piperazine ring formation

The cyclization of **58** to **59** to form the piperazine ring proved to be a very difficult and fastidious reaction. Previously, using bis(2-chloroethyl)amine hydrochloride and K_2CO_3 in chlorobenzene yields up to 71% were achieved.¹³¹ However, the reaction was not repeatable. Using the same method, **59** was synthesized with a moderate yield of 84%, but yields varied widely. The reaction is very temperature dependent and undetermined side products were readily formed if the reaction was below 130 °C for a short amount of time. Therefore, in order to improve the reproducibility of the reaction, a pre-warmed oil bath at 150 °C was used. While this raised the overall yields of the reaction, they still varied. Next, the use of a different solvent was investigated; since the boiling point of chlorobenzene is only 131 °C. Diethylene glycol monomethyl ether was tried since its boiling point is around 194 °C, and this allowed the reaction temperature to be kept constant in the reaction mixture at 150 °C. However, when used with and without K_2CO_3 at this temperature, a complex mixture was formed that could not be separated from the diethylene glycol monomethyl ether. These results suggest that the cyclization reaction required temperatures above 130 °C, but below 150 °C in order to get **59** in appreciable yields. Thus, the original reaction conditions were used, while carefully monitoring the temperatures.

The piperazine derivative formed (**59**) was found to be unstable at 0 °C after about a week's time; nuclear magnetic resonance (NMR) also showed degradation of the product. It was found that older starting material for the following protection reaction

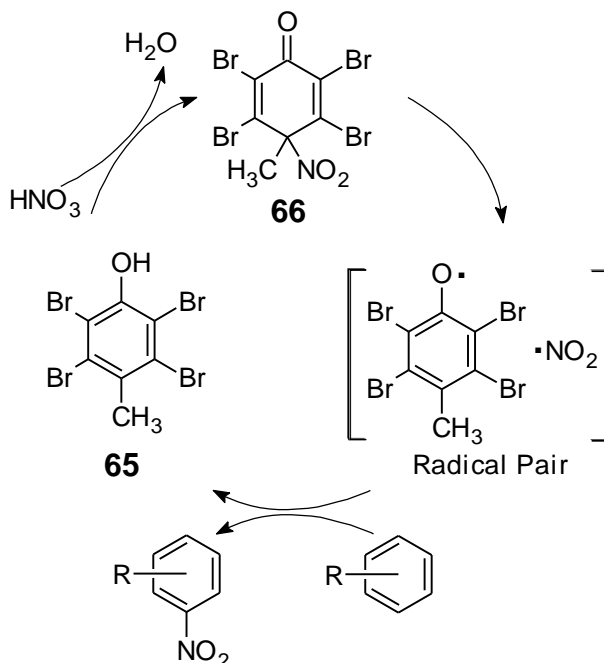
seriously diminished its yields to around 70%. Therefore, immediately after workup, **59** was protected with acetic anhydride to form **60** with consistent yields around 94%.

2.2.4 Aromatic mono-nitration

Mono-nitration of **60** to form the meta-nitro group was not obtainable through normal aromatic nitration. Using several different reaction conditions with acetic acid or acetic anhydride and nitric acid, only di-meta nitration was found to be possible. It was thought that due to the presence of both the 1-propyl-oxy group and the 4-piperazine group, that the aromatic ring was highly activated because of their electron donating capabilities. This in turn made mono-nitration unlikely with conventional synthetic routes. Therefore, a different route was devised using a nitrocyclohexadienone (**66**) as a mild nitrating reagent. This reagent has previously been shown to mono-nitrate several activated substrates without leading to the usual oxidative byproducts of normal aromatic nitration.¹³² Scheme 2 illustrates the general mechanism of nitration using **66**.

Upon hemolytic fission of the C-N bond, a radical pair is formed which can subsequently mono-nitrate the aromatic substrate. This in turn leaves the phenol byproduct, **65**, which can be regenerated using nitric acid to reform **66**.¹³² The formation of **66** was first reported using **65** in acetic acid with 100% HNO₃ at 10 °C and then consequently stirring at 5 °C for 2 hours. However, using this set of reaction conditions led to several problems. First, 100% HNO₃ must be used, which is both hard to handle and readily decomposes. Second, the reaction temperature is very crucial and difficult to maintain; it was found that above 5 °C the starting material **65** decomposed and below that

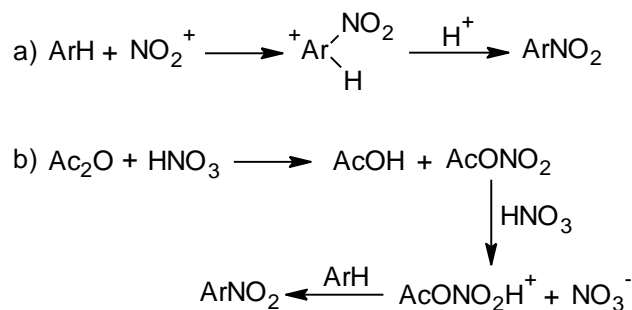
temperature the reaction would not proceed and freeze, making mechanical mixing of the reaction difficult. Lastly, **65** is sparingly soluble in acetic acid. Altogether, these factors made yields and reaction times vary widely.¹³²



Scheme 2. General reaction Scheme for 2,3,5,6-tetrabromo-4-methyl-4-nitrocyclohexa-2,5-dien-1-one (**66**). Figure adapted from Arnatt et al.¹³²

Therefore, the conditions were changed to overcome these difficulties. When 70% HNO_3 was utilized, reaction temperature still proved to be a problem to maintain and freezing of the reaction mixture was hard to overcome. Reaction times varied widely from 2 to 72 hours and yields ranged from 10% to 75%. However, replacing the acetic acid in the reaction mixture with acetic anhydride, alleviated all the above problems of the reaction. Acetic anhydride allowed for a wider range of reaction temperatures without freezing and offered a different mechanism of action than using acetic acid. When

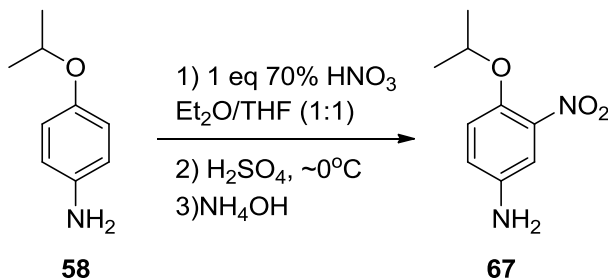
exposed to nitric acid, acetic anhydride rapidly forms acetyl nitrate and directly forms nitronium ions in solution that is milder than HNO_3 (Scheme 3).¹³²



Scheme 3. Mechanisms for aromatic nitrations. a) Nitration mechanism for HNO_3 b) Putative nitration mechanism for acetyl nitrate reaction. Adapted from Arnatt et al.¹³²

Several different reaction conditions were used with and without acetic acid present. It was found that 7 mL of acetic anhydride per gram of **65** with 4 M HNO_3 gave scalable yields up to 95%. Additionally, reaction times were drastically cut from up to 72 hours to consistently 5 to 10 minutes after the addition of nitric acid.¹³² Once synthesized, **66** had a half-life of around a month at 0 °C in a desiccator most likely due to the nature of its radical pair. Once the route to make **66** was resolved, the mono-nitration was easily facilitated. Consistent yields of 87% of the mono-nitrated product **61** were readily achieved. However, an alternative route was tried in order to eliminate the need of **66** and still get a mono-nitrated intermediate (Scheme 4). Mono-nitrating **58**, before cyclization to form the piperazine, was attempted by first making the nitric acid salt of **58**. The nitric acid salt is then stirred with concentrated H_2SO_4 to facilitate the nitration. Without excess HNO_3 in solution, there will be a stoichiometric ratio of one **58** for one nitrate and therefore only mono-nitrate products should be made. However, these conditions were

too harsh and the starting material degraded. Therefore, we returned to the original conditions using **66**.



Scheme 4. Alternative route for mono-nitration.

Subsequent reduction of the nitro group of **61** to the amine, **62**, was done using Pd/C hydrogenation with yields around 98% without any complications. The amide-coupling of **62** with pyrazine-2-carboxylic acid to form **63** was done using 1-ethyl-3-(3-dimethylaminopropyl)carbodiimide (EDCI). Originally, separation yields were reported to be 85%.¹³¹ The reaction was found to be moisture sensitive, so the starting material **62** was dried over molecular sieves overnight and yields were raised to up to 99%. Deprotection of the piperazine moiety was done by refluxing **63** under basic conditions in a methanol/water mixture (1:1). Yields of **64** for this reaction were quantitative.

2.2.5 Final compound synthesis

Compounds **42** through **48** all used the key intermediate **64**, which allowed for final compounds to be synthesized rapidly. For compounds **42** through **46** the benzyl chloride was coupled with the secondary amine of the piperazine group. This reaction was done in DMF with K_2CO_3 and a catalytic amount of KI. The KI allows for the chloride of the benzyl group to be replaced with an iodine atom via a Finkelstein reaction.

The iodine is a better leaving group than the chloride, which allows for faster reaction times for the coupling between the piperazine amine and the benzyl group. The reaction yields ranged from 35% to 94%.

Both **47** and **48** had to be coupled to **64** via a reductive amination because the benzyl chloride for dimethylamino and diethylamino was not commercially available and the synthesis of them required multiple protection and deprotection steps. Either dimethylaminobenzaldehyde or diethylaminobenzaldehyde were combined with **64** in THF and sodium triacetoxyborohydride was added to reduce the subsequent imine formed between the secondary amine of **64** and the aldehyde group. In all, **47** was recovered with a 35% yield while **48** was synthesized with a 30% yield.

All final compounds were analyzed with IR, ^1H NMR, ^{13}C NMR, MS, EA, and melting point. Before use in biological assays, all compounds were transferred into their hydrochloride salts.

2.3 In Vitro Studies

2.3.1 Calcium Mobilization Functional Assays

All of the compounds were tested for their agonism and antagonism in a calcium mobilization assay using MOLT-4 cells (human acute lymphoblastic leukemia cells) transfected with CCR5 (NIH AIDS Research and Reference Reagent Program).¹³³ Using the calcium sensing dye Fluo-4, compounds **42** through **48** were first tested for their CCR5 agonism and did not show any agonism up to 30 μM . Figure 17 shows the general Scheme for the calcium assay using Fluo-4 dye. Upon activation by an agonist, calcium

ions are released intracellularly from the endoplasmic reticulum (ER). These ions are then detected by the addition of the Fluo-4 AM (Fluo-4 acetoxymethyl ester, Invitrogen) that is hydrolyzed by esterases into its active Fluo-4 ion. When bound to a calcium ion, there is a shift in fluorescence of Fluo-4 that is proportional to the amount of calcium ions released, which is in turn proportional to receptor activation.

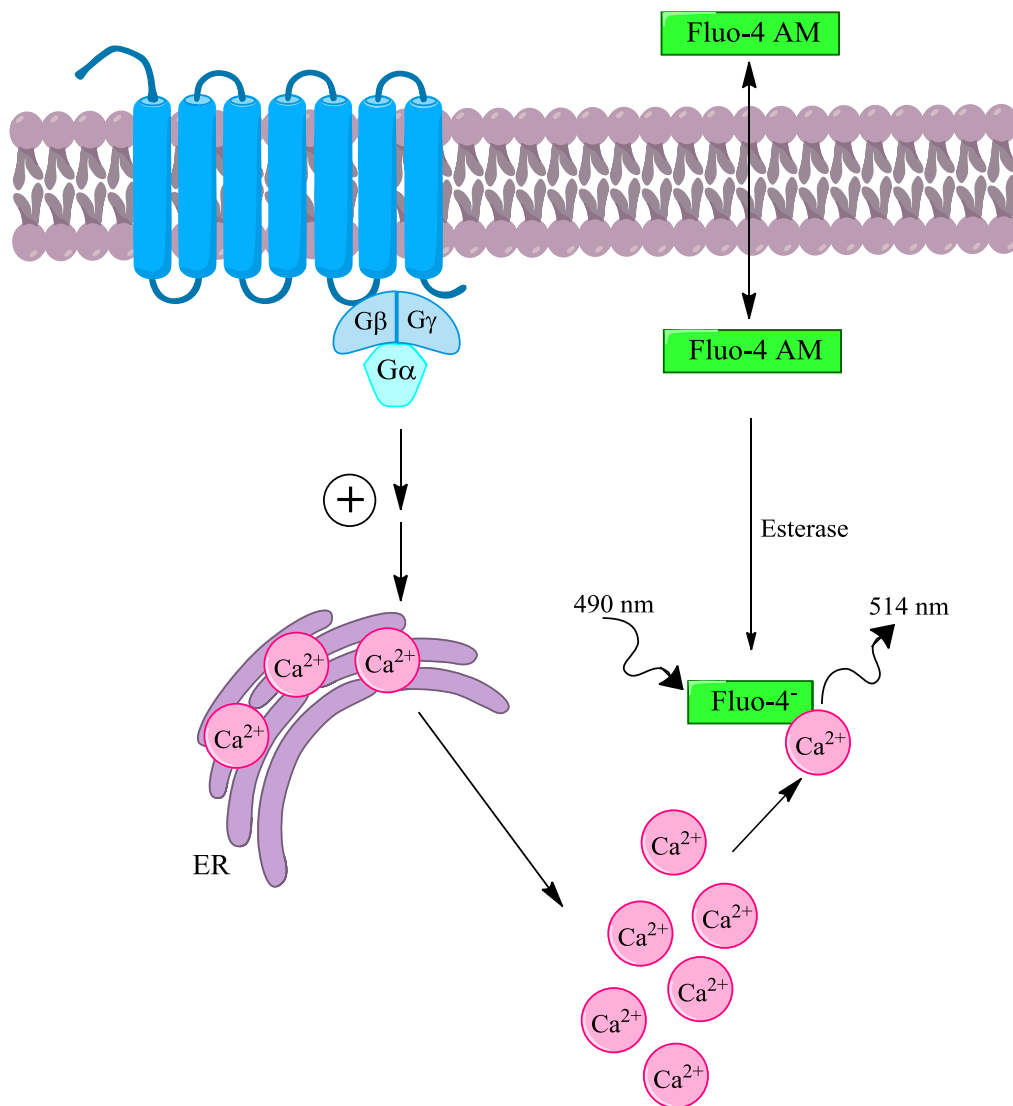


Figure 17. Calcium assay mechanism. Upon activation of a $G\alpha_q$ -coupled GPCR, there is an efflux of calcium ions from the endoplasmic reticulum (ER), which is proportional to receptor activation. Using a calcium-sensing dye such as Fluo-4 the amount of intracellular calcium mobilization can be quantified.

The compounds were tested for their antagonism of RANTES-stimulated calcium release. First, MOLT-4 cells were incubated with Fluo-4 dye and different doses of the compounds. The agonist, RANTES, was then added and the calcium mobilization was measured at 485 nm/520 nm emission/excitation wavelengths. Table 5 shows the results of three independent assays each done in triplicate.

Table 5. CCR5 antagonism (calcium mobilization) of compounds **42** through **48** using RANTES as the agonist

Compound #	R-groups	IC ₅₀ (μM)
42	-NHCOCH ₃	25.6 ± 2.1
43	-OCF ₃	43.5 ± 11.9
44	-COOH	41.2 ± 2.9
45	-C(CH ₃) ₃	-
46	-SO ₂ CH ₃	45.8 ± 9.1
47	-N(CH ₃) ₂	28.1 ± 4.0
48	-N(CH ₂ CH ₃) ₂	48.0 ± 2.9

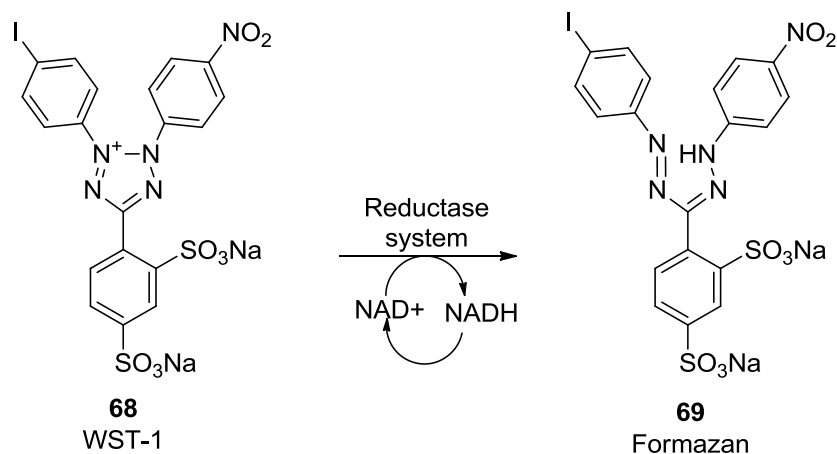
(-) Denotes that no antagonism was seen for the compound.

None of the compounds showed a high level of CCR5 antagonism since they all antagonized the receptor function at micromolar levels. Additionally, the compounds' antagonism was severely diminished compared to maraviroc (1.57 ± 0.32 nM).¹³⁴ However, they still antagonized CCR5 stimulation caused by RANTES. Compound **45** was not soluble at the concentrations tested, so no antagonism data was collected for it. Overall, the differences between substitutions could not allow for any SAR elucidation.

2.3.2 Prostate Cancer Anti-Proliferation Assays

An anti-proliferation assay using 96-well plates and the colorimetric reagent, WST-1, was used to test compound **27** through **48** against a panel of three prostate cancer cell lines. The three prostate cancer cell lines, PC-3, DU145 and M12 were chosen based upon their high expression of CCR5 and RANTES. M12 cells have been isolated from the prostate gland and selected for more metastatic cells from tumors in mice. DU145 cells are from a metastatic prostate tumor removed from a CNS lesion. PC-3 cells were obtained from a metastatic prostate tumor obtained from a lumbar vertebra.¹³⁵

After plating the respective prostate cancer cells on a 96 well plate, they were treated with up to 200 μ M of the compounds and allowed to incubate for 72 hours. After 72 hours the formazan dye WST-1 (**68**) was added and subsequently converted to the darker red formazan dye (**69**) by a mitochondrial succinate-tetrazolium-reductase system. Scheme 5 shows the general reaction for the conversion. The amount of WST-1 converted to **69** is directly related to the proliferative potential of the cells.



Scheme 5. WST-1 mechanism of action for anti-proliferation assay.

Table 6 shows the anti-proliferation data in all three prostate cancer cell lines for compounds **27** through **48**. Unfortunately, consistent data for DU-145 cells could not be obtained. These results may be due to lower expression of CCR5 and RANTES in DU-145 or corrupted cell stocks. Therefore, only M12 and PC-3 were used to evaluate all of the compounds' anti-proliferative abilities. Within PC-3 cells, compound **48** had the lowest IC₅₀ of $6.5 \pm 0.7 \mu\text{M}$, while **40** and **43** had IC₅₀s below 20 μM (19.7 ± 1.8 and $13.1 \pm 7.7 \mu\text{M}$ respectively).

These results suggest that, for PC-3 anti-proliferation, electron donating groups are more favored than electron withdrawing groups. Due to the small range between the IC₅₀ values, it is difficult to elucidate any concrete SAR for the compounds. Within M12 cells, **48** also had the lowest IC₅₀ of $11.4 \pm 0.2 \mu\text{M}$. Compound **40** again had a low IC₅₀ again of $15.8 \pm 4.4 \mu\text{M}$. However, the activity of **43** was abolished and had an IC₅₀ well above 100 μM . Overall, there was no desirable trends between the prostate cancer cell lines seen for the compounds.

These results may be explained by differences in CCR5 and RANTES expression levels between cell lines, or the compounds may be hitting off-target receptors due to their low CCR5 functional activities. Nevertheless, compound **48** did show moderate anti-proliferation activity against PC-3 and M12. TAK-779 was shown previously to have IC₅₀'s of $20.40 \pm 1.1 \mu\text{M}$ and $37.85 \pm 0.99 \mu\text{M}$ in M12 and PC-3 cells respectively.⁴⁵ However, there is a large difference in their calcium mobilization inhibition IC₅₀s: while TAK-779 has an IC₅₀ of $7.9 \pm 2.5 \text{ nM}$, **48** has an IC₅₀ of $48 \pm 2.9 \mu\text{M}$. The discrepancy in IC₅₀ but similarity in anti-proliferation may be due to **48** affecting other target sites.

That being said, TAK-779 was originally developed for HIV entry inhibition, so its prostate cancer anti-proliferation mechanism is still being elucidated.

Table 6. Anti-proliferation assays for DU-145, PC-3 and M12 prostate cancer cells using WST-1 to measure cell proliferation.

Compound #	Substitution	DU-145 IC ₅₀ (μ M)	PC-3 IC ₅₀ (μ M)	M12 IC ₅₀ (μ M)
27	3,5-NO ₂	>100	54.5 \pm 5.4	37.6 \pm 6.5
28	4-NO ₂	>100	49.1 \pm 6.6	78.7 \pm 4.0
29	2-NO ₂	83 \pm 23	62.9 \pm 9.5	183 \pm 2.5
30	3-NO ₂	>100	43.3 \pm 19	73.9 \pm 4.8
31	4-OCH ₃	>100	-	-
32	4-SCH ₃	>100	78.0 \pm 19	>100
33	4-CO ₂ CH ₃	>100	91.5 \pm 3.7	73.7 \pm 20
34	4-Cl	>100	56.1 \pm 9.6	26.3 \pm 0.8
35	4-CN	>100	68.5 \pm 12	37 \pm 11
36	4-F	>100	96.4 \pm 2.5	>100
37	4-Br	>100	31.5 \pm 1.4	48.8 \pm 25
38	H	>100	67 \pm 15	29.9 \pm 4.3
39	4-SO ₃ CH ₃	>100	119 \pm 41	198 \pm 11
40	4-CH ₃	cytotoxic	19.7 \pm 1.8	15.8 \pm 4.4
41	4-NH ₂	cytotoxic	20.1 \pm 1.3	19.7 \pm 5.3
42	4-NH ₂ COCH ₃	>100	24.3 \pm 1.6	39 \pm 12
43	4-OCF ₃	>100	13.1 \pm 7.7	104 \pm 22
44	4-COOH	>100	74 \pm 12	129 \pm 19
45	4-C(CH ₃) ₃	>100	>100	>100
46	4-SO ₂ CH ₃	>100	>100	141 \pm 26
47	4-N(CH ₃) ₂	26 \pm 17	71.2 \pm 1.6	65.9 \pm 2.9
48	4-N(CH ₂ CH ₃) ₂	8.2 \pm 2.3	6.5 \pm 0.7	11.4 \pm 0.2

Concentrations up to 200 μ M were tested. (>100) Denotes that the IC₅₀ was above 100 μ M and was not tested at higher concentrations due to solubility. (-) Denotes that the compound was not tested.

2.3.3 Basal Cytotoxicity Assays

To ensure the anti-proliferation results are not due to the toxicity of the compounds, a basal cytotoxicity assay was run. The NIH-3T3 cells used for the assay are mouse fibroblasts that have been used extensively along with neutral red uptake (NRU) to assess basal cytotoxicity levels of small molecules.^{136,137} The assay utilizes a red neutral dye that viable cells will absorb and incorporate into their lysosomes. Any alterations to the cell surface or sensitivity of the lysosomal membrane will lead to decreased uptake. Based upon the amount of dye present, NRU makes it possible to distinguish between viable and damaged cells. Therefore any toxicity caused by exogenous compounds will be seen.^{136,137}

In all, several of the compounds that showed high anti-proliferative activity in both M12 and PC-3 were also cytotoxic in NIH-3T3 cells, which indicates their observed anti-proliferative activity is related to their cytotoxicity (Table 7). For example, compound **41** has an IC_{50} of 20.1 ± 1.3 and 19.7 ± 5.3 μ M in M12 and PC-3, respectively, but it shows cytotoxicity in NIH-3T3 with a TC_{50} of 10.7 ± 1.2 μ M. Therefore, this compound is not a good lead due to its proportional effects in both cancerous and noncancerous cells.

Table 7. Basal cytotoxicity assays using NRU and WST-1 to test for exogenous toxicity of compounds **27** through **48** in NIH 3T3 cells.

Compound #	Substitution	NIH3T3 (NRU)	NIH3T3 (WST-1)
		TC ₅₀ (μM)	TC ₅₀ (μM)
27	3,5-NO ₂	204 ± 25	55.9 ± 8.4
28	4-NO ₂	29.3 ± 2.3	
29	2-NO ₂	>30	
30	3-NO ₂	16.6 ± 1.1	
31	4-OCH ₃	>30	
32	4-SCH ₃	>30	
33	4-CO ₂ CH ₃	>30	
34	4-Cl	1.6 ± 0.8	42.7 ± 4.2
35	4-CN	>30	
36	4-F	16.8 ± 3.4	
37	4-Br	>30	
38	H	46.6 ± 3.2	
39	4-SO ₃ CH ₃	>30	
40	4-CH ₃	>30	
41	4-NH ₂	10.7 ± 1.2	
42	4-NH ₂ COCH ₃	7.8 ± 1.1	15.5 ± 4.7
43	4-OCF ₃	>30	
44	4-COOH	>30	
45	4-C(CH ₃) ₃	>30	
46	4-SO ₂ CH ₃	>30	
47	4-N(CH ₃) ₂	>30	
48	4-N(CH ₂ CH ₃) ₂	31.9 ± 1.6	27.9 ± 1.2

However, two compounds in the series have both anti-proliferative activity while displaying no cytotoxicity up to 30 μM in the NRU assay. Compound **27** has an IC₅₀ of 37.6 ± 6.5 and 54.5 ± 5.4 μM for M12 and PC-3 and displayed a TC₅₀ of 204 ± 25 μM. Similar results were seen for **48**, but its TC₅₀ was found to be 31.9 ± 1.6 μM which makes for a much narrower therapeutic window when comparing its TC₅₀ to its IC₅₀'s in PC-3 and M12 cells.

In addition to using NRU to test for cytotoxicity, WST-1 was used to see the differences in measurements. Since the two assays measure different cell processes it may lead to different results relating to cytotoxicity. Only four example compounds were tested, but several discrepancies between the assays were seen. Compounds **42** and **48** were found to have similar TC_{50} 's in both assays while **27** had a lower TC_{50} and **34** had a higher TC_{50} in the latter assay. These differences for both **27** and **34** could illuminate the mechanism of anti-proliferative effects of the compounds. **27** could affect mitochondrial dehydrogenases more than the structure of its lysosomes, which leads to a lower TC_{50} in the WST-1 assay. Conversely, **34** could affect lysosome structure more than it affects mitochondrial dehydrogenase activity, which would lead to a higher apparent TC_{50} in the WST-1 assay compared to the NRU assay.

2.4 Conclusion

Accumulating evidence has shown the multiple roles that chemokine receptor CCR5 plays to promote the progression of several types of cancer. The mechanism of action of the promotion is thought to involve chronic inflammation, which creates a microenvironment that enhances tumor survival. Blocking CCR5 function with an antagonist may provide a novel treatment of cancers such as prostate cancer. Currently, several CCR5 antagonists are available, but all have been optimized for their anti-HIV entry inhibition rather than inhibition in endogenous signaling. Thus, there is need to develop antagonists focused on blocking CCR5 signaling and inhibiting CCR5 related prostate cancer proliferation. Using a combination of pharmacophore and CCR5 docking

studies a unique CCR5 antagonist skeleton was created and functionalized at multiple positions to optimize activity. A combination of calcium inhibition, anti-proliferation, and basal cytotoxicity assays were used to screen for active compounds. In CCR5 calcium mobilization inhibition assays all of the compounds acted as antagonists, but lacked the nanomolar activity of the known CCR5 antagonists they were based on. By using a combination of anti-proliferation assays and basal cytotoxicity assays, compounds having the most desirable therapeutic potential could be determined. With an IC_{50} of $11.4 \pm 0.2 \mu\text{M}$ and $6.5 \pm 0.7 \mu\text{M}$ in M12 and PC-3 prostate cancer cells, and basal cytotoxicity around $30 \mu\text{M}$, compound **48** proved to be the best lead compound. In order to increase the activity of the series of compounds, new compounds will be synthesized based upon lengthening the molecule and adding more polar substituents increase solubility.

3. Bivalent Ligands Targeting the CCR5-MOR Heterodimer

3.1 Project Design

The progression of human immunodeficiency virus (HIV)-1/acquired immunodeficiency syndrome (AIDS) has been shown to be accelerated by abused substances such as opioids, cocaine, and alcohol.^{73,75,82-84} Moreover, nearly 10% of all HIV infections have been attributed to injectable drug use with contaminated needles.¹³⁸ Both abusive and addictive behaviors are associated with the mu opioid receptor (MOR). Additionally, opiates negatively impact the immune system through immunomodulation regulated through the MOR.^{73,99} These deleterious results on the immune system may also affect the progression of HIV/AIDS.⁸⁵

CCR5 is expressed on both immune and non-immune cells, and is a major co-receptor that regulates HIV-1 invasion.^{47,48,139,140} In 2007, maraviroc, a CCR5 antagonist, was approved by the FDA as an antiretroviral therapy (ART). In combination with different ARTs, maraviroc has improved the overall health outcomes related to HIV-1 infection.¹⁴¹ However, other health complications involved with infection are still a significant problem in patient populations. In particular, the effects of HIV-associated neurocognitive disorders (HANDS) affects about half of AIDS patients and leads to abnormalities in neurocognition, behavior, and motor control.¹⁴² These neurological

complications of AIDS (neuroAIDS) are largely due to the injury of neurons by indirect effects of infected microglia and astrocytes.^{73,143}

The progression of neuroAIDS has been linked to opiate abuse that may arise from the synergistic interactions between CCR5 and MOR.^{73,75,83,84,94,95} A key example of this is that MOR agonists can up-regulate the expression of CCR5 and promote HIV-1 infection, which can be blocked by MOR antagonists.⁹⁰ Opiates can also exacerbate the amount of indirect neuronal injury in neurons and glia through HIV-1 induced CNS inflammation.^{74,144} The specific opioid dependent neuronal injury may be primarily induced by MOR expressing glia in the CNS.¹⁴⁵ Importantly, MOR and CCR5 have been shown to heterodimerize and undergo crosstalk.^{87,146} The interaction has been shown to affect immune cell function and may produce the synergistic effects seen in neuroAIDS progression.^{90,147} Previously, a bivalent compound (**49**) containing both a mu opioid receptor (MOR) and chemokine receptor CCR5 (CCR5) antagonist pharmacophore was synthesized in our laboratory in order to study the pharmacological profile of MOR–CCR5 heterodimerization and its relation with neuroAIDS (Figure 18).¹³⁴

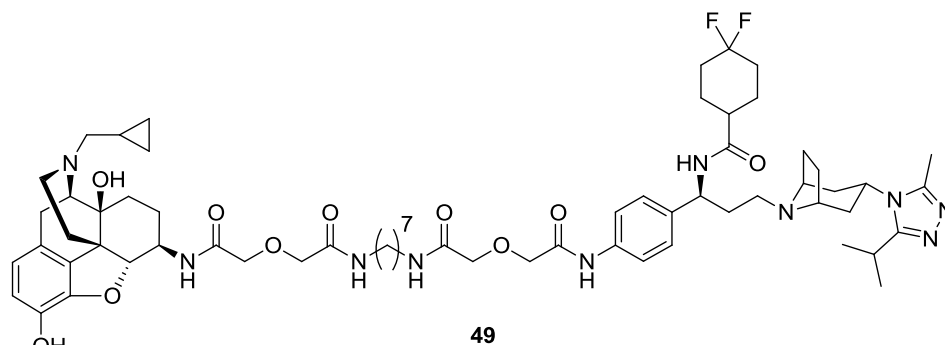


Figure 18. The first reported bivalent compound targeting the CCR5-MOR heterodimer.¹³⁴

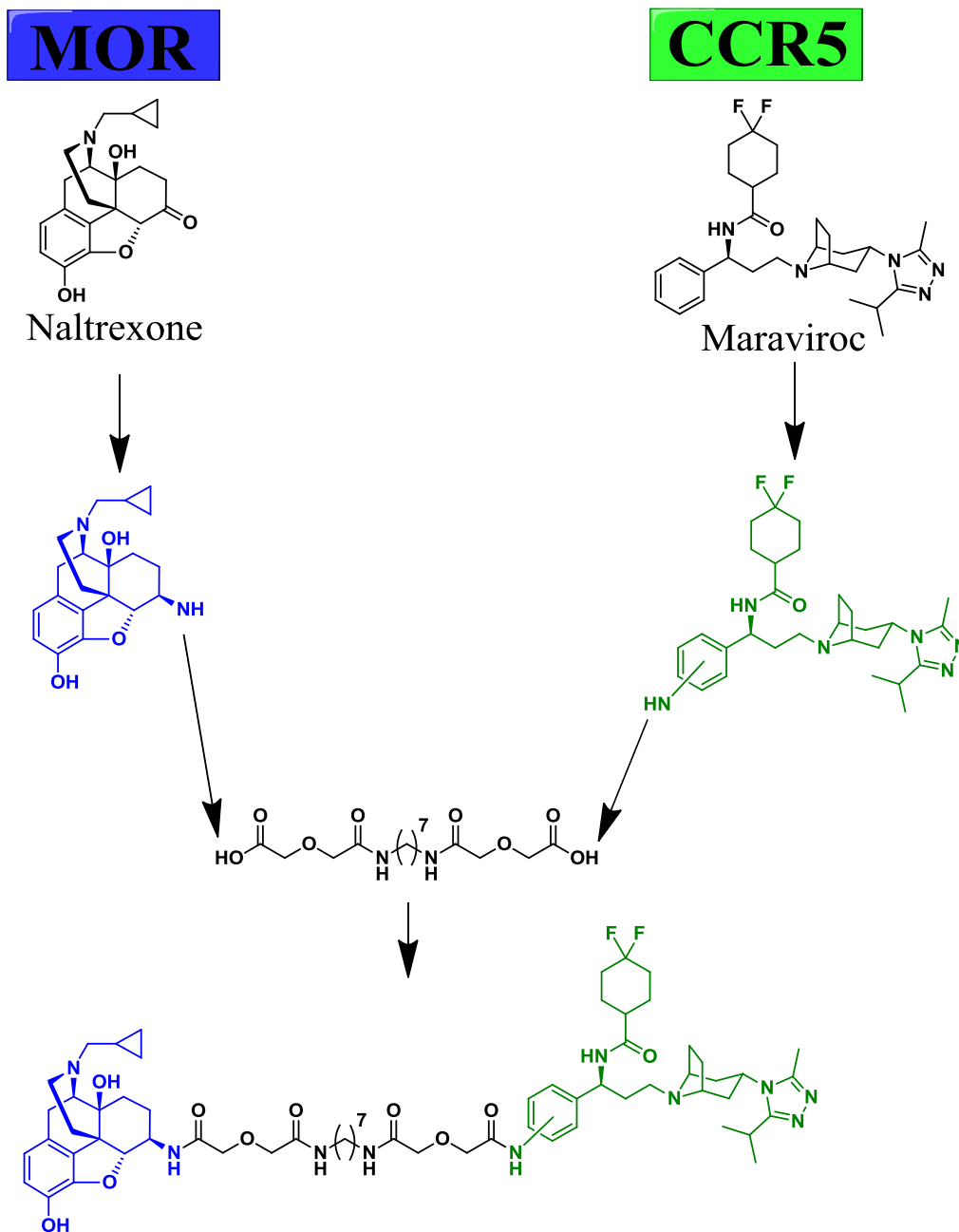


Figure 19. Bivalent compound strategy for targeting the CCR5-MOR heterodimer

The premise of the bivalent compound **49** was to use both a MOR and a CCR5 antagonist to try to block both receptors at the same time, Figure 19. Both naltrexone, **15**,

and maraviroc, **1**, were chosen for their high binding affinities and well known pharmacological profiles. Both molecules had to be functionalized with an amine group in order to allow for attachment of the linker. 6 β -Naltrexamine has been synthesized before, but 4-aminophenyl-maraviroc had never been reported, so a new synthetic route was devised.¹³⁴ The linker connecting the two pharmacophores was chosen based on the work of Daniels et al. with MOR-DOR bivalent compounds.¹²⁶ They found that a 21-atom spacer made of an aliphatic diamine flanked by two diglycolic groups was optimum for opioid receptor heterodimers.¹²⁶

In order to study the SAR of compound **49**, a new bivalent compound with the amine group at the 3-position of maraviroc was synthesized, **50** (Figure 20). The change in attachment site to maraviroc will allow for fine-tuning of the bivalent compound towards the CCR5-MOR heterodimer. Additional compounds were synthesized to study how substitutions on maraviroc affected CCR5 binding and functional activity (**51-55**, Figure 20). Calcium mobilization assays were used to determine the functional activity of the compounds to both the MOR and the CCR5. Cell fusion assays that mimic HIV-1 invasion were then carried out to assess **49** and **50** inhibition on cell fusion. Since the fusion assay may not reflect how native cells and HIV-1 interact, a HIV-1 infection assay using human astrocytes was used to assess how the compounds inhibited infection compared to maraviroc. In order to observe how the compounds interact with the CCR5-MOR heterodimer on the atomic level, computation methods such as molecular dynamics simulations were used.

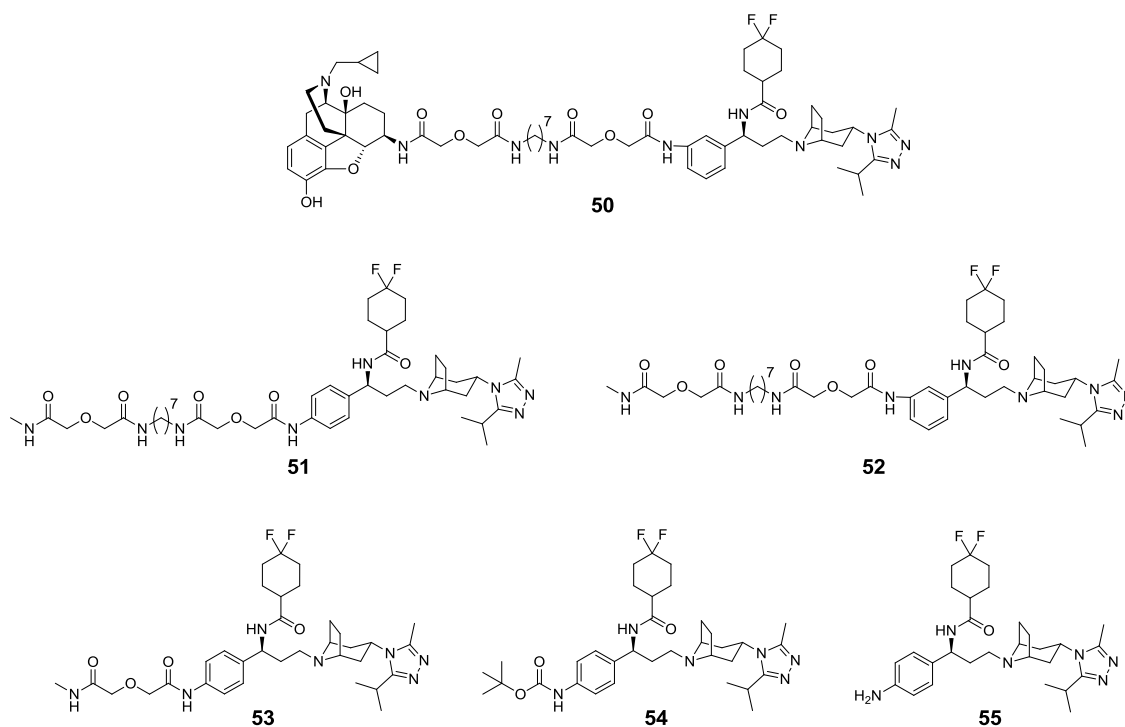
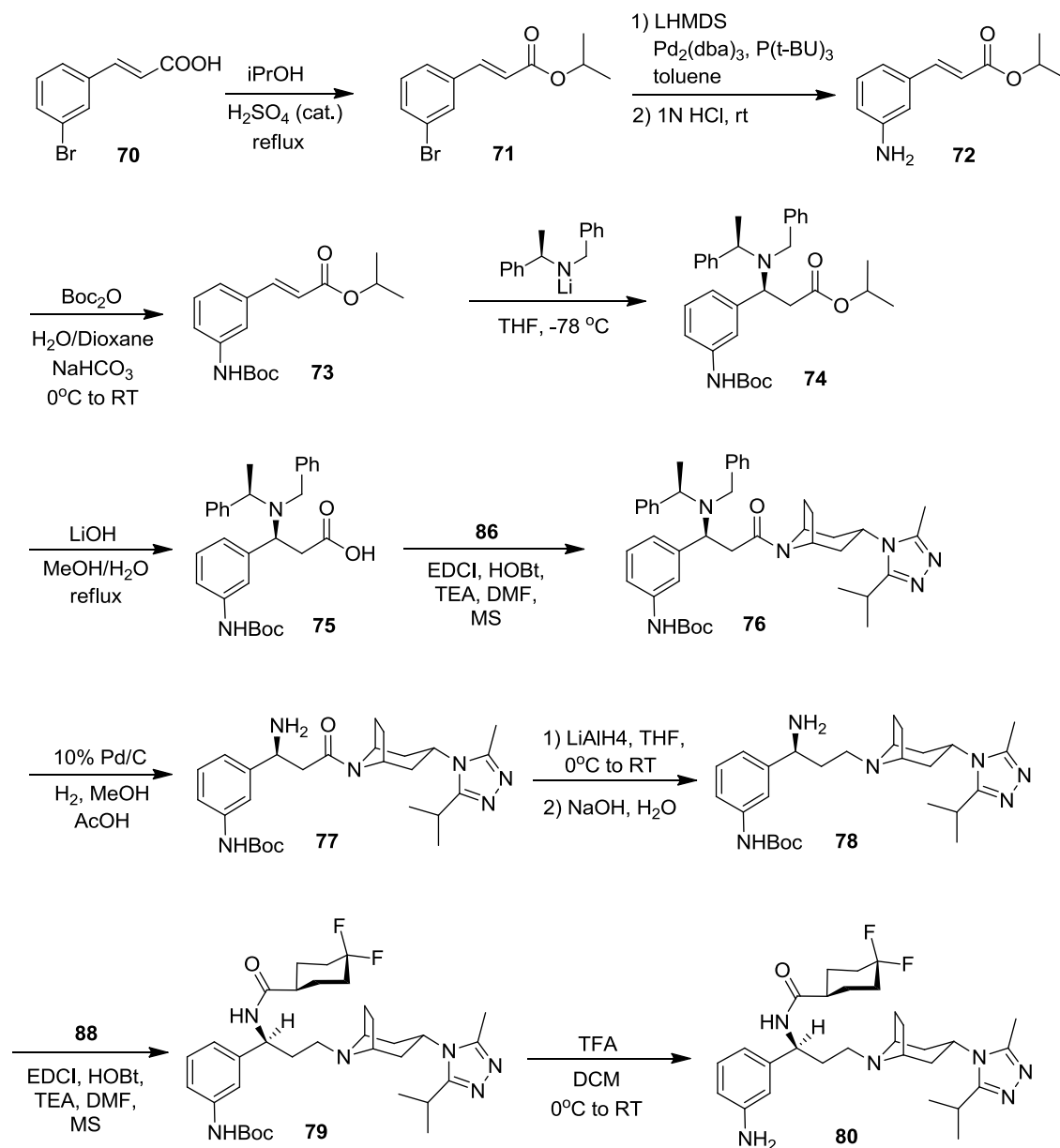


Figure 20. Additional CCR5-MOR bivalent compound (**50**) and control compounds studying the SAR of maraviroc substitution.

3.2 Chemical Syntheses

The synthetic route for the 4-amino maraviroc bivalent compound (**49**) had previously been discovered by Dr. Yunyun Yuan and Dr. Gou Li of the Yan Zhang group and compounds **49**, **51**, **53-55** were synthesized by Dr. Yunyun Yuan.¹³⁴ However, the route for the 3-amino maraviroc bivalent compound (**50**) had to be developed. Serendipitously, the same route used to make **49** could be used with minor modifications in reaction conditions and workup by using 3-bromocinnamic acid instead of 4-bromocinnamic acid. Scheme 6 shows the synthetic route used to synthesize the 3-amino maraviroc intermediate, **80**.



Scheme 6. Synthetic route to form the 3-amino maraviroc (**80**) intermediate.

3.2.1 Buchwald-Hartwig Coupling

3-Bromocinnamic acid (**70**) is first protected via an esterification reaction using isopropanol (i-PrOH) and a catalytic amount of H_2SO_4 while being refluxed. The overall yield of **71** was 79%. The bromide was then converted to the amine (**72**) using lithium

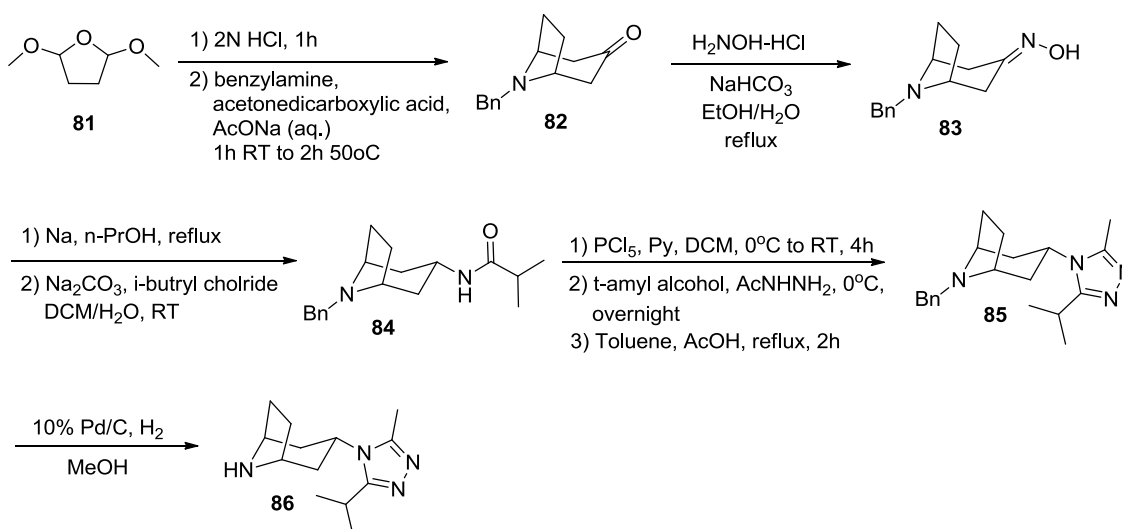
hexamethyldisilazide (LHMDS), Pd₂(dba)₃, and P(t-Bu)₃. This reaction was previously reported for the synthesis of 4-amino maraviroc and had yields around 90%. However, this reaction proved to be difficult for the 3-bromo derivative **71**. Yields of **72** were often around 50% with the highest achieved yield being 69%. The reaction can be sensitive to moisture and the catalysts can be poisoned by many chemical species, but even when extremely dry conditions were achieved and new catalyst was used, the yield failed to improve. Therefore, the starting material, **71**, may be slightly deactivated compared to the 4-bromo derivative previously reported.¹³⁴ Since the benzene is substituted at the 3-position it may lead to a different, less active, electronic configuration of the molecule that would affect subsequent reactions. Additionally, workup proved to be difficult and often required multiple rounds of column chromatography. Both dichloromethane (DCM)/MeOH and hexane/ethyl acetate eluent systems failed to effectively separate the produce from the crude reaction mixture. After a lengthy investigation on the solubility properties of **72** in different organic solvents, it was found that it could be crystallized from hot hexane with moderate separation yields.

Initially, immediately after being purified, the amine of **72** was protected with a Boc group by heating it in THF in the presence of di-tert-butyl dicarbonate. However, this reaction proved to produce an undetermined byproduct that could not be separated from the reaction mixture. New reactions conditions were used to try to produce **73** without any excess byproduct formation. Still using di-tert-butyl dicarbonate, **72** was stirred in a 1:1 mixture of H₂O/Dioxane with NaHCO₃ at room temperature which gave **73** at yields up to 76%. The stereoselective Michael addition to form **74** was achieved by

using lithium (R)-N-benzyl-N- α -methylbenzylamide. This reaction has been used previously in multiple synthetic routes to selectively form enantiomerically pure adducts.^{134,148–150} Both column chromatography and recrystallization were used to purify the product with yields up to 70%.

3.2.2 1,2,4-Triazole Substituted Tropane Intermediate Synthesis

Saponification of the isopropyl ester (**74**) to form the carboxylic acid **75** was accomplished by refluxing in MeOH/H₂O with LiOH. After reaction workup a yield of 88% was achieved. Next, an amide coupling between **75** and **86** was done by using EDCI. Compound **86** was formed using a five step synthetic route previously described in Scheme 7.^{151,152} Overall the synthetic route to form **86** proved to be straightforward except for the synthesis of **85**. Yields of only 38% could be achieved for the formation of the triazole, which were drastically lower than yields reported by literature.¹⁵¹ To form the triazole ring from **84** there are three sequential reactions that first formed the imidoyl chloride that was then trapped with acetic hydrazide and then cyclized using an acid catalyzed cyclization. The imidoyl chloride reaction intermediate could easily be decomposed, which may explain the low yields. Additionally, if excess water was present during the acetic hydrazide addition the amide could easily be hydrolyzed leading to lower yields. No optimization was attempted since large quantities could easily be synthesized through the route. Saponification of the isopropyl ester (**74**) to form the carboxylic acid **75** was accomplished by refluxing in MeOH/H₂O with LiOH. After reaction workup a yield of 88% was achieved.



Scheme 7. Synthesis of the 1,2,4-triazole substituted tropane intermediate (**86**).

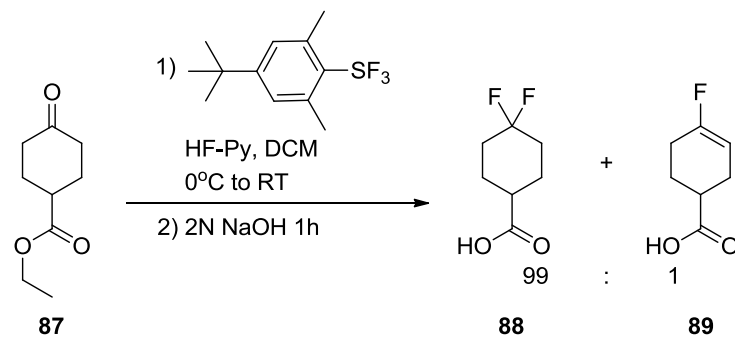
3.2.3 Debenzylation with Hydrogenation

As stated above, **76** was formed through an EDCI mediated amide coupling between **75** and **86**. The reaction yields were regularly around 74% which is close to the reported yields seen for the same reaction for the 4-amino maraviroc derivative.¹³⁴ The reduction of the (R)-N-benzyl-N- α -methylbenzylamide to form the amine **77** proved to be more difficult compared to the same reaction for the 4-amino maraviroc derivative.¹³⁴ The hydrogenation of **76** was first tried using 10% Pd/C and 60 psi H₂ in MeOH, but very little product was formed even after 168 hours. Therefore, new conditions were tried using 20% Pd(OH)₂/C, MeOH, 10% H₂O, 5% AcOH, and 1 atm H₂. This reaction successfully made **77** with a 48% yield. Reaction conditions were further modified to try to improve the yields of this reaction due to the scarcity and preciousness of the starting

material **76**. Using 10% Pd/C, 60 psi H₂, and 2 equivalents of AcOH in MeOH, a yield of 91% was achieved. Therefore, acid was essential for facilitating the reduction of **76** to **77**.

3.2.4 Selective Difluorination

Reduction of the amide, **77**, to form **78** was accomplished by using lithium aluminum hydride. This reaction was easily done, but the quenching of excess LiAlH₄ produced an inseparable reaction mixture. Therefore, using the Fieser method, an exact ratio of 1:1:2 of H₂O, 4N NaOH, and H₂O were added sequentially and the lithium salts were filtered. Using this method, **78** could easily be separated by column chromatography with a yield of 93%. Another EDCI mediated amide coupling was performed between **78** and **88** to form **79**. The 4,4-difluorocyclohexanecarboxylic acid (**88**) had previously been synthesized from ethyl-4-oxocyclohexanecarboxylate.^{134,152} Difluorination was done using diethylamino sulfur trifluoride (DAST) and only gave a 4 to 1 ratio of the difluoro product to the vinyl fluoride impurity, which is essentially inseparable. In order to overcome the difficulty and specificity of the *gem*-difluorination reaction, a different fluorination reagent was used. The reagent, 4-*tert*-butyl-2,6-dimethylphenylsulfur trifluoride (Fluolead), was more stable and selective than DAST, which leads to less vinyl fluoride impurity (**89**) formed. As shown in Scheme 8, the difluorination of **87** to form the acid, **88**, with a ratio of 99 difluoro product to 1 vinyl fluoride impurity. The overall combined yield of the difluorination and saponification reactions was 27%.

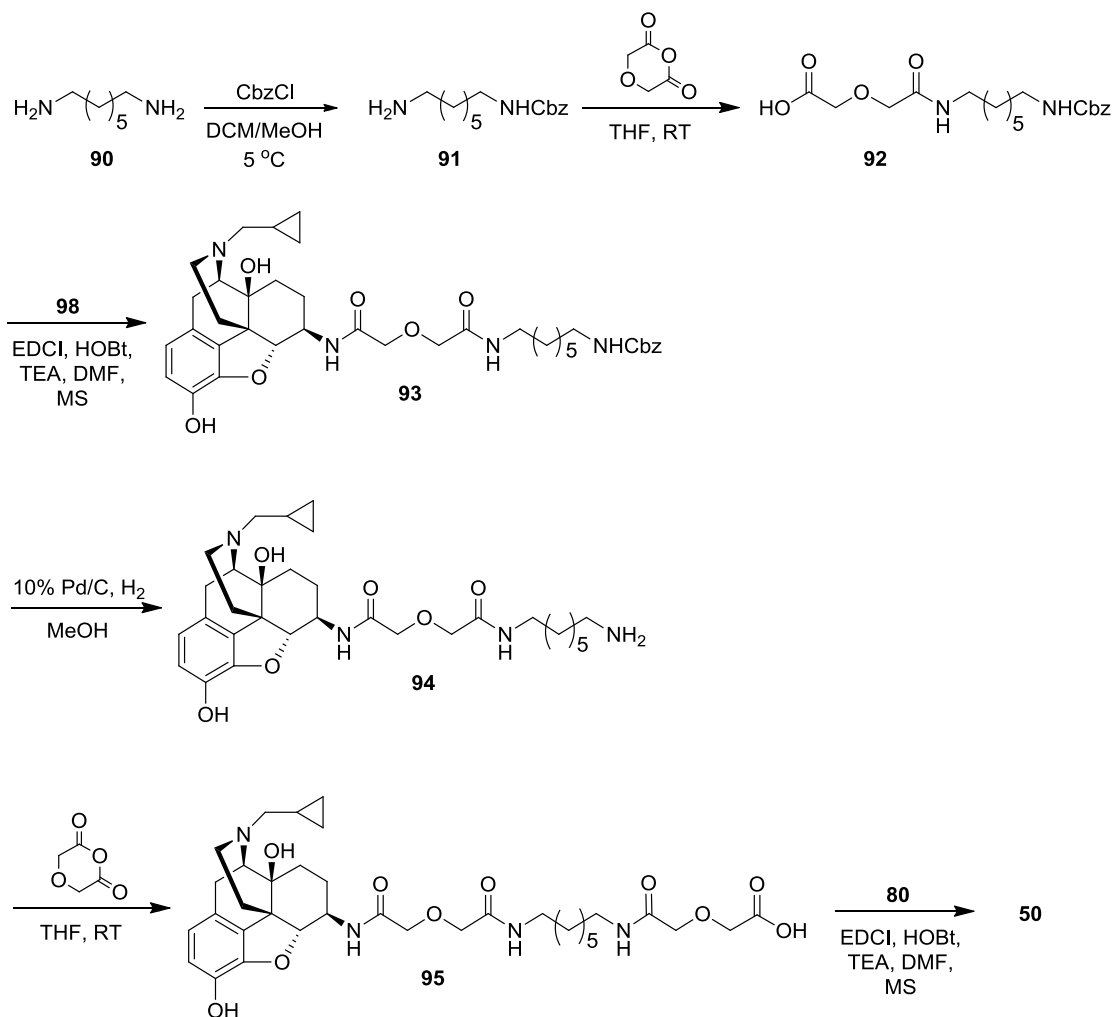


Scheme 8. Synthesis of 4,4-difluorocyclohexanecarboxylic acid (**88**) using Fluolead.

3.2.5 Linker Synthesis

The 6 β -naltrexamine-linker intermediate (**95**) was previously synthesized using the synthetic route seen in Scheme 9.¹³⁴ First diaminoheptane (**90**) was monoprotected with a carboxybenzyl group to form **91**. This product has previously been reported by several groups using various methods.^{134,153,154} The initial method consisted of adding very dilute benzyl chloroformate to an excess of very dilute 1,7 diaminoheptane over the period of a week at exactly 5 °C. Yields from this reaction did not exceed 16%, which is close to what is reported in the literature.¹³⁴ Several byproducts are present in the reaction mixture during workup, including unreacted diamine, diprotected diamine, and several other uncharacterized byproducts.

There are several drawbacks to this method: very low yields, long reaction time, hard to maintain reaction temperature, excessive solvent waste, and large amounts of byproduct formation. Separation of **91** from the reaction mixture proved to be very difficult and often required multiple rounds of column chromatography. Eventually, it was found that, after an initial column to concentrate **91** in the reaction mixture, that the product could be recrystallized using DCM.



Scheme 9. Synthesis of 6β-naltrexone-linker intermediate (**95**) and final 3-amino bivalent compound (**50**).

Due to the drawbacks of this reaction, several new reaction conditions were tested. First, the amount of benzyl chloroformate was varied from 2 equivalents to 0.5 equivalents in several reactions to see if an excess of benzyl chloroformate or an even larger excess of diamine would decrease the amount of byproducts formed in order to increase yields. However, this method failed to produce any different results. Reaction temperature was then systematically changed to 0 °C and 10 °C. At 0 °C very little

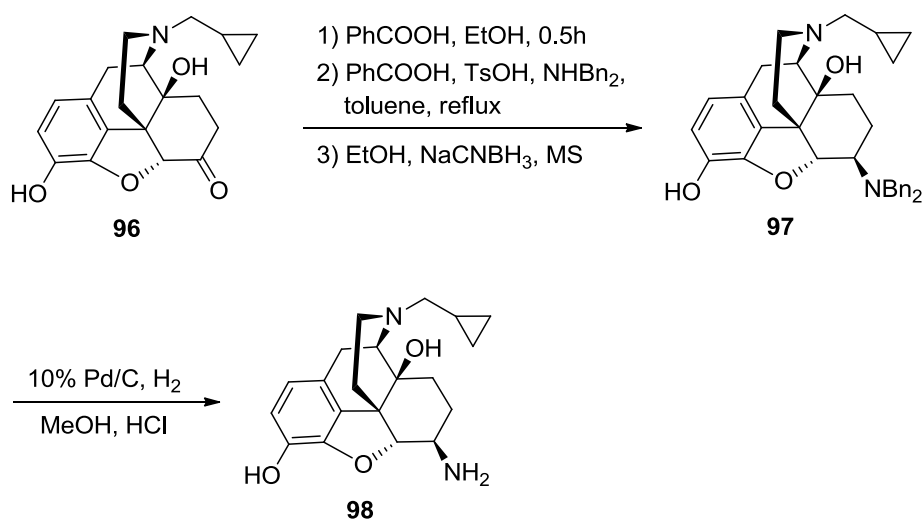
monoprotected diamine (**91**) was formed and the reaction mixture mainly consisted of unreacted diamine. At 10 °C there was more diprotected diamine and uncharacterized byproducts than **91**. Therefore, we explored a complete change in reaction conditions.

The first alternative reaction conditions consisted of reacting the diamine (**90**) with 1 equivalent of HCl to form the mono-hydrochloride salt. This effectively would only allow one of the amine groups to react with the benzyl chloroformate when added.¹⁵³ After exploring various conditions of this reaction by varying concentrations and temperatures no monoprotected diamine **91** was formed. A second set of reaction conditions was then explored that focused on controlling the pH of the reaction so that the equilibrium of the reaction would be shifted towards the formation of **91**. We hypothesized that keeping the pH around pH 4 instead of pH 14 (normal pH of reaction mixture for original conditions) may lead to more **91** being formed. An exploratory reaction was done using 1 M, pH 4 acetate buffer and MeOH to dissolve the diamine, **90**, and then benzyl chloroformate was added dropwise while the pH of the resulting solution was checked every 5 drops. No monoprotected diamine **91** was formed during the reaction and the buffer did not have enough ionic strength to keep the reaction at pH 4. Therefore, the original reaction conditions were kept, and crude product from multiple reactions was pooled together during purification to aid yields.

3.2.6 6 β -Naltrexamine-Linker Intermediate Synthesis

After monoprotection, **91** was lengthened with a diglycolic anhydride to give the corresponding carboxylic acid, **92**. Overall, this reaction was very simple and yields

around 92% were achieved after crystallization. Through an EDCI mediated amide coupling reaction, **92** and **98** were coupled to form **93** with a yield of 42%. 6 β -Naltrexamine (**98**) was previously synthesized by the Portuguese group using the synthetic route in Scheme 10.¹⁵⁵ First, naltrexone hydrochloride (**96**) was converted to 6 β -dibenzylamine intermediate **97** through a reductive amination using dibenzylamine and NaCNBH₃ with yields around 64%. The dibenzylamine intermediate **97** was then reduced using a Pd/C hydrogenation to form **98** with yields around 78%.

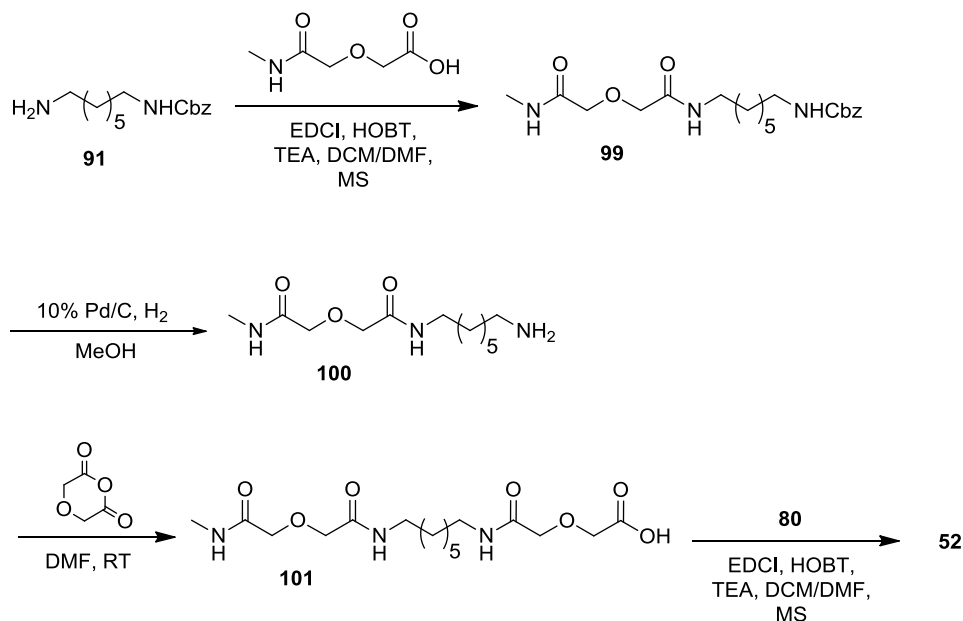


Scheme 10. 6 β -Naltrexamine (**98**) synthesis.

The 6 β -naltrexamine linker intermediate **93** is then deprotected using Pd/C hydrogenation. This reaction only had a yield of 51% of **94**, which is much lower than the reported yield of 99%.¹³⁴ The purity of the starting material may have affected this reaction, but no further investigation was done. Another diglycolic anhydride was added to **94** to bring the total linker length to 21 atoms. Compound **95** was synthesized with a final yield of 91%.

3.2.7 Final Compound Synthesis

Final compound synthesis was facilitated by coupling **95** with **80** using EDCI to form the bivalent compound **50**. This coupling reaction was done with only 1 equivalent of both **95** and **80** due to their scarcity. After 7 days, no starting material was present. Column chromatography was used and a total of 33 mg, 26% yield, of **50** was received. In addition to **50**, a 3-amino maraviroc monovalent control compound, **52**, was also synthesized using the synthetic route in Scheme 11. The monoprotected diamine **91** was coupled with methylcarbamoylmethoxy-acetic acid to form **99** with a yield of 67%. Next, **99** was deprotected using Pd/C mediated hydrogenation to form **100** (90% yield). A diglycolic anhydride group was then added to bring the total linker length to 21 atoms (**101**) with quantitative yields. Finally, **101** and **80** were coupled using EDCI to form 30 mg of the monovalent compound **52** (33% yield).



Scheme 11. Synthesis of 3-amino maraviroc monovalent control compound **52**.

All final compounds were analyzed with IR, ^1H NMR, ^{13}C NMR, MS, and melting point. Before use in biological assays all compounds were transformed into their hydrochloride salts.

3.3 In Vitro Studies

3.3.1 Calcium Mobilization Functional Assays

In all, 8 compounds were synthesized for the study of the CCR5-MOR heterodimer. Compounds **50** and **52** were synthesized by Chris Arnatt; compounds **49**, **51**, **53** through **55** and **102** were synthesized by Dr. Yunyun Yuan of the Yan Zhang laboratory. Figure 21 shows the bivalent compounds (**49**, **50**), the monovalent controls (**51**, **52**, **102**) and the 4-substituted maraviroc compounds (**53**, **54**, **55**). The compounds were tested in cells that expressed either CCR5 or MOR and cells that co-expressed both CCR5 and MOR. Calcium mobilization assays were chosen to test for the compounds functional activity due to their robustness and simplicity. During GPCR signaling, release of intracellular calcium stores is proportional and directly related to receptor activation. Ideally, the IC_{50} values of the compounds will have little deviation from the IC_{50} values of the parent compounds maraviroc and naltrexone.

Compounds were tested for both their agonism and antagonism for either CCR5 or MOR in MOLT-4 cells, hMOR-CHO cells, and a co-expressed CCR5YFP-hMOR-CHO cell line.^{133,156} For both the MOLT-4 cells and the hMOR cells, the calcium sensitive fluorescent dye Fluo-4 was used. However, a specialty red fluorescent dye had to be used in the CCR5YFP-hMOR-CHO cells (*vide infra*).

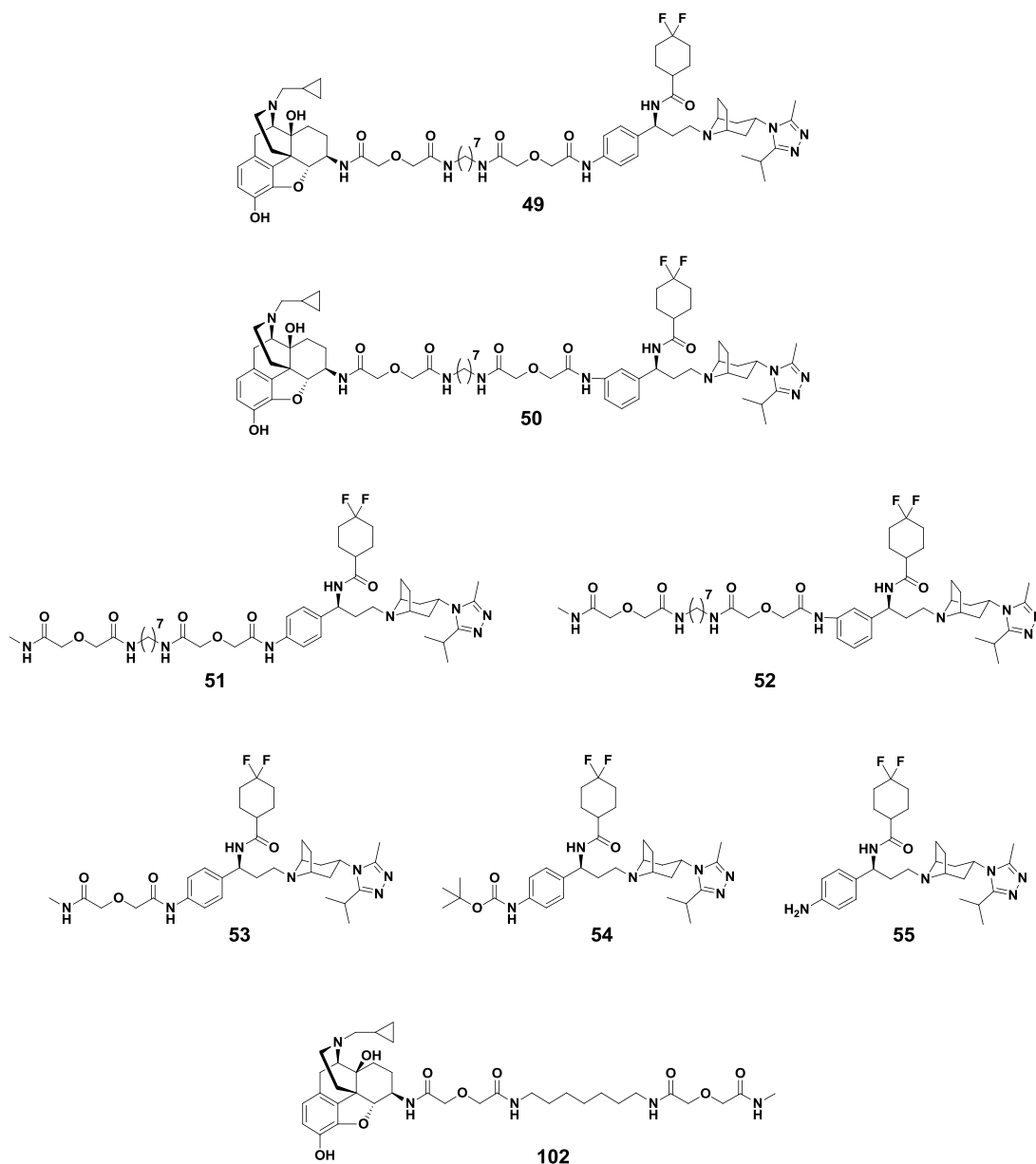


Figure 21. Library of compounds for the study of the CCR5-MOR heterodimer. The library consists of the bivalent compounds (**49**, **50**), the monovalent controls (**51**, **52**, **102**) and the 4-substituted maraviroc compounds (**53**, **54**, **55**).

First, the compounds were tested in the CCR5 expressing MOLT-4 cells for their CCR5 agonism and antagonism. Over a range of concentrations, compounds **49** through **55** showed no apparent agonism of CCR5. Antagonism assays tested for the inhibition of

RANTES stimulated calcium mobilization. Prior to use, the MOLT-4 cells were transiently transfected with a chimeric G protein, Gqi5, in order to boost their calcium signaling levels.¹⁵⁷ Gqi5 is an engineered $G\alpha_q$ protein with its last five residues on its C-terminal replaced with the last five residues from the $G\alpha_i$ protein. A range finding assay was first performed in order to find a rough IC_{50} of each compound so that a finer dose curve could be used. An example inhibition curve for compound **49** is shown in Figure 22. All measurements were run in triplicate and repeated 3 separate times.

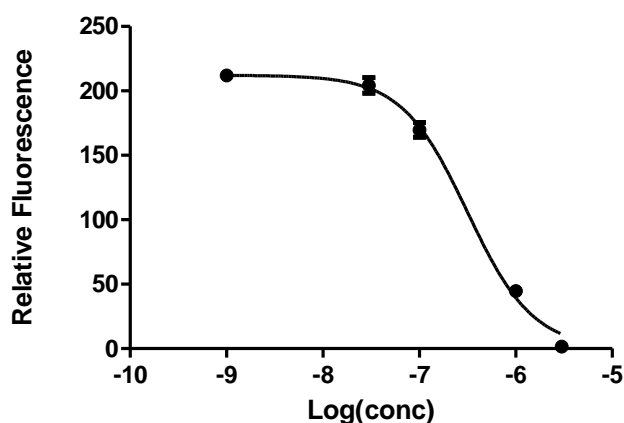


Figure 22. Example CCR5 inhibition curve for **49** MOLT-4 cells. RANTES was used to stimulate the cells.

The CCR5 antagonism results from the calcium mobilization assays (Table 8) indicate that modification of maraviroc (**1**) with phenyl substituents is not well favored and hint towards a general SAR for CCR5 antagonism for the library. When an amine is added to the 4-position (**55**), there is a close to a 7-fold loss in CCR5 inhibition. An even more drastic effect is seen for the bulkier substituents in **53** and **54** with losses in activity of 3600-fold and 700-fold respectively. Therefore, smaller substituents on the phenyl ring

of maraviroc are well tolerated compared to more sterically bulky groups. However, this observation is not seen to the same extent for the bivalent and monovalent compounds.

Table 8. Antagonism of RANTES stimulated calcium mobilization in MOLT-4 cells.

Compound	CCR5 antagonism IC ₅₀ (nM)	Fold-decrease in activity compared to 1
1 (maraviroc)	2.19 ± 0.31	-
49	126 ± 28	60
50	1340 ± 110	600
51	622 ± 36	200
52	129 ± 42	60
53	7910 ± 760	3600
54	1570 ± 180	700
55	14.2 ± 1.9	7

Both **51** and **52** have larger substituents than **53** and **54**, but they have only a 200-fold and 60-fold decrease in activity compared to **1**. These results suggest that the longer monovalent compounds may adopt a different binding mode than **53** and **54** and retain some of their CCR5 antagonism. For the bivalent compounds, **49** and **50**, there is a discrepancy between the 4- and 3-position attachments that is not seen in the monovalent compounds (**51**, **52**). While **49** has only a 60-fold decrease in activity, **50** has a large decrease in activity of 600-fold compared to **1**. Therefore, for the bivalent compounds, a 4-position attachment is favored over the 3-position attachment, which is the opposite compared to the monovalent compounds. One possible explanation for this is their ability to adopt binding modes for the different trends in activity of the 3- and 4-position attachment of the monovalent and bivalent compounds.

MOR antagonism was also tested by using calcium inhibition assays; hMOR-CHO cells were first transiently transfected with Gqi5 in order to couple MOR activation

to calcium release.¹⁵⁷ Compounds containing a morphanin group (**49**, **50**, **102**) were first tested for their MOR agonism: no apparent agonism was seen for the compounds. Using the MOR agonist DAMGO, compounds were then tested for their antagonism and compared to naltrexone (**15**). Overall, substitution of naltrexone (**15**) is much more tolerated than for maraviroc as seen in Table 9. The highest fold decrease compared to **15** was only 4.5-fold (**49**). All of the compounds had similar IC₅₀ values which means that the difference in maraviroc attachment sites and lack of maraviroc did not affect MOR antagonism.

Table 9. Antagonism of DAMGO stimulated calcium mobilization in hMOR-CHO cells.

Compound	MOR antagonism IC ₅₀ (nM)	Fold-decrease in activity compared to 15
15 (naltrexone)	8.93 ± 0.87	-
49	40.0 ± 4.8	4.5
50	17.1 ± 4.9	1.9
102	37.8 ± 4.4	4.2

Having a cell line that consistently expressed both CCR5 and MOR was essential for studying how the two receptors interact with each other using calcium mobilization assays and cell fusion assays. A previously established hMOR-CHO cell line¹⁵⁶ was transfected with a plasmid containing CCR5 tagged with a yellow fluorescent protein on its N-terminus (CCR5-YFP) by Seth Dever (Hauser Laboratory, VCU). Using fluorescence-activated cell sorting (FACS), cells containing CCR5-YFP were separated, subcultured and used in subsequent assays. Due to the YFP present in the cell line, the calcium sensitive fluorescent dye Fluo-4 could not be used due to an overlap between their excitation/emission wavelengths. Therefore, a red calcium sensitive fluorescent dye,

GFP-FluoForte was used that had a different excitation/emission spectrum compared to YFP.¹⁵⁸

Using the CCR5YFP-hMOR-CHO cell line, the activity at both receptors was studied for compounds **49** through **55** and **102**. Before the assay, cells were transfected with a chimeric G protein Gqi5 in order to boost the calcium signaling and couple to MOR signaling to calcium mobilization.¹⁵⁷ All compounds were tested for both their agonism and antagonism and none showed any agonism. Table 10 shows the IC₅₀ values for the compounds using either DAMGO (MOR agonist) or RANTES (CCR5 agonist) to stimulate calcium mobilization.

Table 10. Results from calcium mobilization assays using the CCR5YFP-hMOR-CHO co-expressed cell line.

Compound	MOR IC ₅₀ (nM) ^a	CCR5 IC ₅₀ (nM) ^b
1 (maraviroc)	-	17.8 ± 4.3
15 (naltrexone)	5.8 ± 2.5	-
49	29.9 ± 2.4	6240 ± 250
50	17.4 ± 5.7	14040 ± 350
51	-	7030 ± 400
52	-	2202 ± 8.5
53	-	8820 ± 870
54	-	6670 ± 540
55	-	54.8 ± 11.2
102	50.5 ± 4.8	-

(a) Cells were stimulated with DAMGO, (b) cells were stimulated with RANTES, (-) denotes that the compound was not tested.

The results from MOR antagonism indicate that all of the compounds maintained their ability to antagonize DAMGO signaling. However, compared to naltrexone, compounds **49** and **102** have higher IC₅₀ values, which indicate a loss in activity. The loss ranges from 5-fold to 10-fold compared to **15**. There is a less drastic decrease of 3-fold

seen for **50**. Interestingly, both **49** and **50** are more potent than the monovalent control compound **102**. The difference in activity could arise between the compounds due to **102** lacking the maraviroc portion of the full bivalent compounds. Since **49** and **50** have both antagonists present in them, they can interact with both CCR5 and MOR concurrently which could synergistically lower their IC₅₀ values and thus increase their activity. Compound **102** lacks such synergism since it can only interact with MOR.

The CCR5 antagonism results from the calcium mobilization assays indicate that modification of maraviroc through the phenyl substituents is not well favored, which agrees with the data from the mono-expressed MOLT-4 cells. Addition of an amino group at the 4-position, **55**, is the only well-tolerated change, with only a 3-fold loss in activity. However, as the substituent starts to become bulkier, as seen in **53** and **54**, there is a drastic decrease in activity of around 400-fold compared to **1**. The same trend in decreased activity is seen for bivalent compounds **49** and **50**. Overall, there is 350-fold decrease in activity for **49** compared to **1** and a 700-fold decrease for **50**. Additionally, no clear synergism is seen for bivalent compounds compared to the monovalent control compounds **51** and **52**. The lack of synergism may be due to the phenyl attachment of maraviroc not being well tolerated by CCR5. However, all of the compounds do maintain their activity at both MOR and CCR5, despite the extensive modifications.

Overall, the data from the co-expressed cell line agrees with the data from the mono-expressed cell lines for MOR and CCR5 antagonism. However, there is a decrease in the apparent CCR5 antagonism for all of the compounds when tested in the co-expressed CCR5YFP-hMOR-CHO cell line. While this may be attributed to difference

between the MOLT and CHO cell types, it is most likely from the yellow fluorescent protein tag on the C-terminal of CCR5. The YFP may alter the binding of G proteins to CCR5 enough to see a decrease in antagonism from the compounds or alter receptor conformation and thus alter its ability to signal. Additionally, these reasons may be why no synergism is seen for the bivalent compounds over the monovalent compounds.

3.3.2 Binding Assays

In addition to the CCR5 and MOR functional assays, binding assays were conducted to verify that the compounds can bind to the receptors with high affinity. Assays were run by Yunyun Yuan, Orgil Elbegdorjo, and the radioligand binding service at EMD Millipore. Table 11 shows the results of both CCR5 and MOR radiobinding assays for selected compounds. Within the MOR assay, all of the compounds bind have higher K_i values than naltrexone (**15**) and display the same trend as the functional assays. For MOR, the 3-position attachment (**50**) on maraviroc is favored compared to the 4-position (**49**).

Table 11. CCR5 and MOR radiobinding assay.

Compound	MOR K_i (nM) ^a	CCR5 K_i (nM) ^b
1 (maraviroc)	-	0.24 ± 0.06
15 (naltrexone)	0.7 ± 0.1	-
49	51.8 ± 7.9	239 ± 56
50	10.0 ± 0.6	-
51	-	151 ± 44
55	-	15.3 ± 4.8
102	9.2 ± 3.4	-

(a) [³H]naloxone was used in hMOR-CHO membranes.¹⁵⁶ (b) [¹²⁵I]MIP-1 α was used in CCR5 rhesus macaque membranes. All values are means ± S.E.M. of three independent experiments.

The data for the CCR5 radiobinding assay confirms the results seen in the functional assays that any substitution on maraviroc's phenyl ring is detrimental. There is a clear trend of decreasing affinity with increasing size of the group at the 4-position. Overall, there is a large 1000-fold loss of affinity seen for **49** compared to maraviroc. Importantly, it does still bind CCR5 at nanomolar levels, meaning that its affinity wasn't completely abolished.

3.3.3 Cell Fusion Assays

While the calcium mobilization assays can measure the activity of the compounds at the receptor level, they fail to show the compounds' anti-HIV invasion activity. Cell fusion assays provide a less dangerous alternative to working with the live virus and have been shown to mimic the HIV invasion process. Figure 23 illustrates the general process for the cell fusion assay. Two cell populations, called the target and effector cells, are used in the assay. Fundamentally, the target cells act as the host cells that HIV infects, and the effector cells act as the virus.

The CCR5YFP-hMOR-CHO cells were used as the basis for the target cells and were transiently transfected with CD4 and a luciferase reporter with the help of Seth Dever (Hauser Laboratory, VCU). Human embryonic kidney (HEK) cells were used as the effector cells and were transiently transfected with HIV-1 gp120 and a T7 polymerase. Once overlaid, CD4 and gp120 form a complex and interact with the CCR5-MOR heterodimer and initiate the fusion process. Upon cell fusion, the luciferase gene reporter is transcribed and after 18 hours luminescence is measured. Adding a CCR5

antagonist, such as maraviroc, during the overlay process inhibits the fusion process and leads to a decrease in luminescence. Therefore, addition of the bivalent compounds should also inhibit the fusion process.

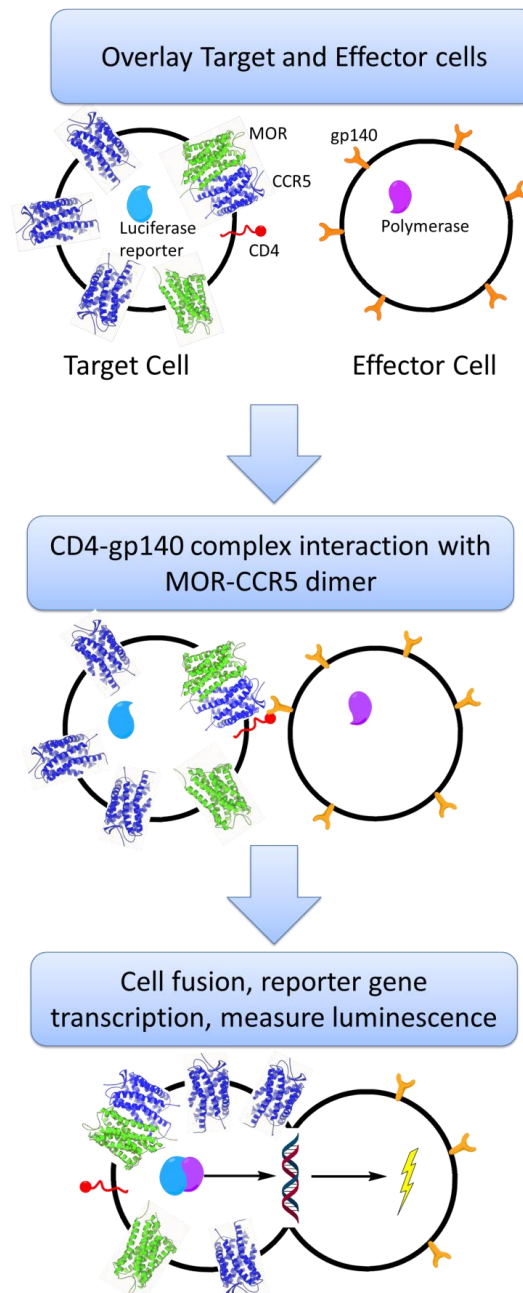


Figure 23. Cell fusion assay used to mimic HIV invasion without using live virus.

Figure 24 is a representative cell fusion assay with and without morphine (9) stimulation during the fusion process. Upon the addition of morphine and +CD4 effector cells there is a significant increase ($p < 0.05$) in fusion compared to +CD4 effector cells alone. Addition of 49, 50, and maraviroc (1) all significantly lowered cell fusion at concentrations of 3,000 nM, 10,000 nM, and 100 nM, respectively. The inhibitory effect of both 49 and 50 was amplified by 2-fold when morphine was present.

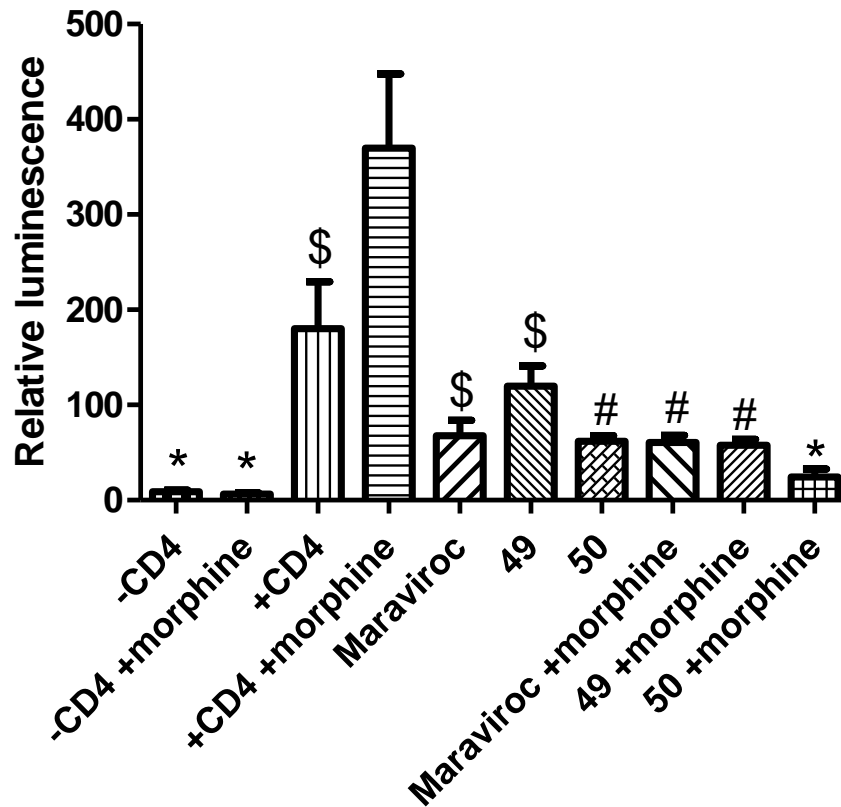


Figure 24. Cell fusion assay based upon luminescence from expressed luciferase reporter gene. For morphine stimulation, 300 nM was added. 100 nM Maraviroc, 3,000 nM 49, and 10,000 nM 50 was used. Values are representative of 4 assays run. (* $p < 0.001$ vs. +CD4 +morphine; \$ $p < 0.05$ vs. +CD4 +morphine; # $p < 0.01$ vs. +CD4 +morphine)

At the concentrations shown, 49 is less effective than 50, but it is equally effective at the higher 10,000 nM concentration that is shown for 50. Maraviroc's cell fusion

inhibition was not amplified with the addition of morphine. This trend was seen in an additional three assays. The concentrations of compounds used in the assay indicate that maraviroc is more potent than either bivalent compound.

A fundamental issue of this assay is its reproducibility. The same trends were seen in all three cell fusion assays attempted, but IC_{50} values for fusion inhibition could not be determined: IC_{50} values from plate to plate varied up to 2-fold. Assay variability may be attributed to user error, protocol setup and or transfection efficiencies. Since the fusion assay is luminescence based, errors in pipetting and protocol could severely affect the results due to the sensitivity of the measurement. The complexity and cost of the assay did not allow for optimization of all the conditions such as incubation times, cell number, and ratio of effector to target cells. Incubation time for cell fusion to occur was limited to 24 hours and no optimization was attempted. Fusion assays like this have been conducted for 8, 12 and 24 hours by various laboratories.¹⁵⁹⁻¹⁶² Both cell number and cell ratio could have been explored more in order to increase the reproducibility of the assay: only 20,000 and 15,000 cells/well were attempted and only a 1:1 and 1:2 effector to target cell ratios were attempted. Changing either parameter may lead to less variation among wells.

3.3.4 HIV-1 Infection Assays

While the cell fusion assay mimics the native system, it cannot reproduce the natural expression levels of CCR5 and MOR (and other proteins) that are seen in native systems. Therefore, an HIV-1 infection assay was conducted by the Hauser laboratory at VCU using primary human astrocytes. Primary human astrocytes were chosen because

they are one of the primary sites of infection in neuroAIDS; they are localized on the blood brain barrier and they are the sites where opioids can synergistically potentiate the pathophysiological effects of HIV-1 infection.⁷³ Figure 25 shows the effect of **49** and maraviroc have on the infection of astrocytes by HIV-1, in the presence and absence of morphine stimulation.

Upon infection with R5 HIVSF162 (with and without morphine). there was a significant increase in Tat (transactivator of transcription) expression in astrocytes that coincides with virus invasion. When maraviroc is added, virus invasion is decreased, as expected. However, when morphine is added along with maraviroc, its antiviral effects are completely abolished, which is indicated by a significant 4-fold increase in HIV Tat expression in the astrocytes. Treatment with naltrexone, or a combination of naltrexone and maraviroc, had no effect on virus invasion with and without morphine present. Addition of the bivalent compound **49** (“bivalent”) had a significant effect compared to maraviroc and maraviroc with morphine stimulation. Overall, there was a 3.3-fold decrease in virus entry compared to maraviroc alone and a 7-fold decrease when compared to maraviroc with morphine. Importantly, morphine stimulation had no effect on the bivalent compound’s activity. Cytotoxicity assays (not shown) indicate neither maraviroc nor **49** had any toxicity in the astrocytes. The results show that in a native system, the bivalent compound can act as a potent virus invasion inhibitor without deleterious effects caused by morphine stimulation.

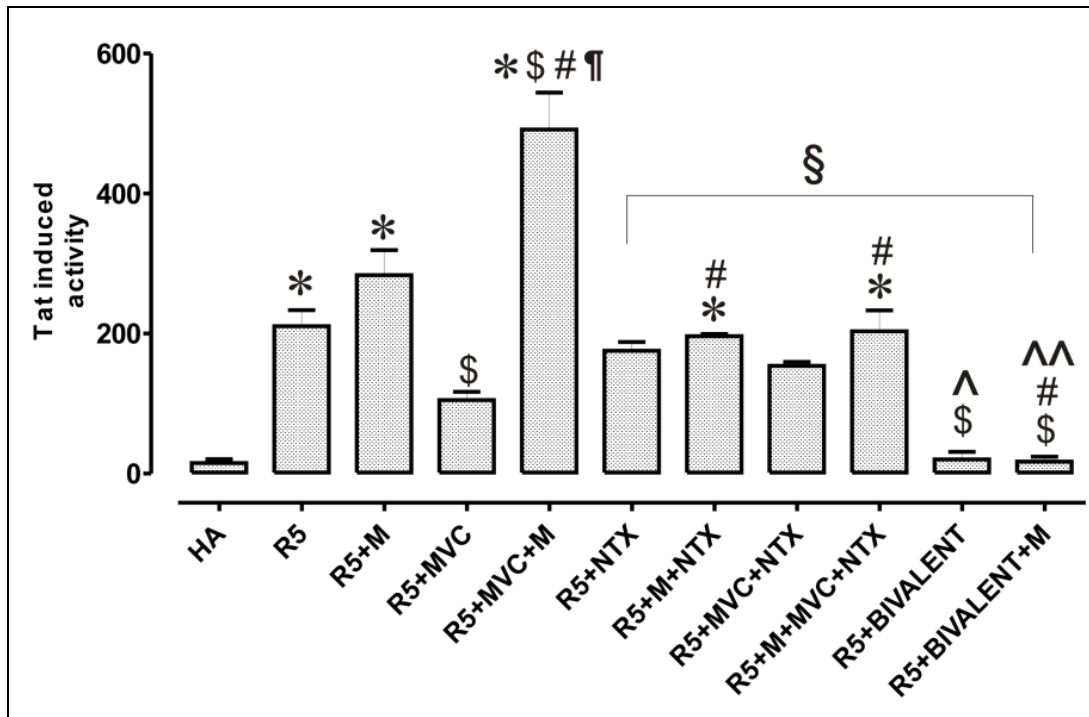


Figure 25. HIV-1 infection assay. HIV-1_{SF162} infectivity in human glial was determined based on the relative amount of Tat protein expressed by the virus using a luciferase based assay. (HA) human astrocytes, (R5) HIV-1_{SF162}, (M) morphine at 500 nM, (MVC) maraviroc at 100 nM, (bivalent) compound **49** at 100 nM, and (NTX) naltrexone at 1500 nM. Values are absorbance \pm SEM of 3 independent experiments at 18 h post-infection (* $p < 0.005$ vs. un-infected cells; \$ $p < 0.05$ vs. R5 HIV-1; # $p < 0.05$ vs. opioid; ¶ $p < 0.05$ vs. maraviroc (MVC); § $p < 0.05$ vs. morphine + MVC; ^ $p < 0.05$ vs. MVC + NTX; ^^ $p < 0.05$ vs. morphine + MVC + NTX; Ω $p < 0.05$ vs. bivalent).

3.3.5 Expression Levels of CCR5 and MOR in Primary and Engineered Cells

Overall, there is a disconnect between the cell fusion assay results and the results gained from the astrocyte HIV-1 invasion assay. The differences between the assays may be explained through the relative expression levels seen in the cells. Seth Dever (Hauser Laboratory, VCU) analyzed the mRNA expression levels, using RT-PCR, of CCR5 and MOR mRNA for both astrocytes and the CCR5YFP-hMOR-CHO cells. Figure 26 shows the results from PCR of two lots of primary human astrocytes with CCR5 being

expressed 12-fold higher than MOR. The levels of MOR and CCR5 in the CCR5-MOR CHO cell line with CCR5 mRNA being expressed 30-fold higher than MOR.

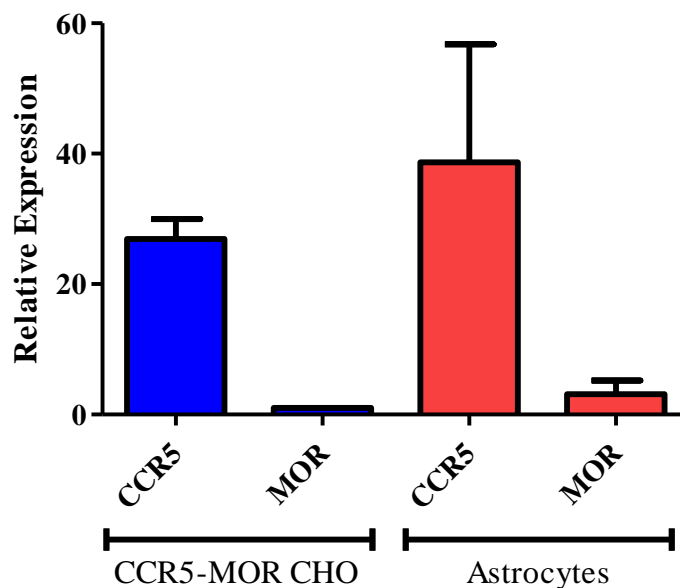


Figure 26. Relative mRNA expression levels of MOR and CCR5. mRNA levels were evaluated for both the CCR5YFP-hMOR-CHO (CCR5-MOR CHO) cell line and two lots of primary human astrocytes.

There is a 2-fold difference in the concentration of MOR and CCR5 between the two cell lines with the CCR5YFP-hMOR-CHO cell line having a much higher expression of CCR5 than MOR. With higher amounts of CCR5 than MOR, there may be less formation of heterodimers in the CCR5-MOR CHO cell line than in astrocytes. Since the bivalent compounds may preferentially bind to CCR5-MOR heterodimers, there will be fewer heterodimers available for binding in the CCR5YFP-hMOR-CHO cells than in astrocytes; therefore, its effects may be diminished in the CCR5YFP-hMOR-CHO cells.

Interestingly, when morphine was added to the cells 24 hours before being harvested for PCR, there was a downward trend in both CCR5 and MOR mRNA

compared to unstimulated cells (data not shown) for the CCR5YFP-hMOR-CHO cells. These results contradict what is seen in the native system where morphine up-regulates CCR5 expression levels.⁸⁷ One explanation for this difference is that CCR5 and MOR are both transfected into the CHO cells, and expression is driven by a non-native promoter. Therefore, there may be no significant change in expression levels of CCR5 and MOR in the CCR5YFP-hMOR-CHO cells since morphine stimulation would mainly effect endogenous expression from the natural promoter. For the CCR5YFP-hMOR-CHO cells, the differences seen with and without morphine in the cell fusion assay may be due to morphine affecting cell-surface expression of CCR5 or MOR or morphine inducing CCR5-MOR heterodimerization. A similar effect of inducing MOR dimerization has been reported with DAMGO exposure.¹²⁰

3.4 In Silico Studies

3.4.1 Modeling the CCR5-MOR Heterodimer

Computational modeling was used to further explore the relationship between the CCR5-MOR heterodimer and compound **49**. Using a homology model of CCR5 and the recently crystallized MOR homodimer, a CCR5-MOR heterodimer model was constructed.⁶³ The homology model of CCR5 was created by Saheem Zaldi using CXCR4 as the template structure:⁷¹ the two structures share 29% identity and 49% similarity to each other and are both chemokine receptors. As expected, the conserved GPCR residues: N1.5, L2.5, R3.5, W4.5, P5.5, P6.5, and P7.5 all aligned properly

between CCR5 and CXCR4; and there were no significant gaps in the transmembrane helical domains (Figure 27).

```

sp|P51681|CCR5_HUMAN      ----MDYQVSSPIYDIN----YYTSEPCQKINVKQIAARLLPPLYSLVFI
sp|P61073|CXCR4_HUMAN    MEGISITYTSDNYTEEMGSGDYDSMKEPCFREENANFNKIFLPTIYSIIFL
                          *  ..   ::      .*** : :  ::   :*:*:*:*:*:
sp|P51681|CCR5_HUMAN      FGFVGNMLVILILINCKRLKSMTDIYLLNLAISDLFFLLVVPFWAHYAAA
sp|P61073|CXCR4_HUMAN    TGIVGNGLVILVMGYQKRLRSMTDKYRLHLVADLLFVITLFWAVDAVA
                          *:*** *****:  *:*:***** * *:***:***:***:***:*** *
sp|P51681|CCR5_HUMAN      QWDFGNTMCQLLTGLYFIFGFFSGIFFIILLTIDRYLAVVHAVFALKARTV
sp|P61073|CXCR4_HUMAN    NWYFGNFLCKAVHVIYTVNLYSSVLILAFISLDRYLAVHATNSQRPRLK
                          :* *** :*: :  :*  :*:*:*:*:*:  :*:***:***. :  :*. :
sp|P51681|CCR5_HUMAN      TFGVVTSVITWVAVFASLPGIIFTRSQKEGLHYTCSSHPYSQYQFWKN
sp|P61073|CXCR4_HUMAN    LAEKVVYVGVWIPALLLTIPDFIFANVSEADDRYICDRFYPN---DLWVV
                          * . * .*: :*: :*:*:*:*. : . : * . .:*  :*:
sp|P51681|CCR5_HUMAN      FQTLKIVILGLVPLLVVICYSGILKTLRLCRNEKKRHRVRLIFTIMI
sp|P61073|CXCR4_HUMAN    VFQFHIMVGLILPGIVILSCYCIISKLSHSKGHQKRK-ALKTTVILIL
                          .  : : :*:***: **: :*. *...* :...*: **: .  :*:
sp|P51681|CCR5_HUMAN      VYFLFWAPYNIVLLLNLFQEFFGLNN-CSSSNRLDQAMQVTEITLGMTHCC
sp|P61073|CXCR4_HUMAN    AFFACWLPYYIGISIDSFILLEIIKQCEFENTVHKWISITEALAFFHCC
                          .:* * * * * : :*: *  :*: * . * : : :*:*:*. : *
sp|P51681|CCR5_HUMAN      INPIIYAFVGEKFRNYLLVFFQKHIAKRFCKCCSIFQQEAPERASSVYTR
sp|P61073|CXCR4_HUMAN    LNPILYAFLGAKFKTSAQHALTSVSRG---SSLKILSKGKRGHSSVSTE
                          :*:*:*:*: * **: .  : .  . .*: : : * * * *
sp|P51681|CCR5_HUMAN      STGEQEISVGL
sp|P61073|CXCR4_HUMAN    SESSSFHSS--
                          *  . . .  *

```

Figure 27. Sequence alignment of CCR5 and CXCR4.

Briefly, homology models of CCR5 were produced by using the homology modeling program Modeller 9v8.¹⁶³ Modeller works by using a satisfaction of spatial restraints in order to map the location of each atom based upon the template structure and the sequence alignment. A total of 100 models were generated from this process and scored with the assessment scores: molpdf, DOPE, and GA341. These scores serve as an indication of the general “native-ness” of the receptors structures made. To further analyze the individual structures, maraviroc (**1**) was docked into each model using the ligand docking program GOLD.¹⁶⁴ Analyzing the individual receptor-ligand complexes

and comparing them to known site-directed mutagenesis data guided the decision of which model to use.

Several methods have been used to model GPCR homodimers and heterodimers. Until recently, the most prominent way to model dimerization was to use protein-protein docking programs such as ZDOCK, GRAMM, or Rosetta.¹⁶⁵ Recently, several GPCR homodimer crystal structures have been characterized and offer a new way to model dimerization.^{63,71,111} These structures have either a TM4-TM5 or a TM5-TM6 interaction, which both represent feasible GPCR dimer interfaces.^{63,165,166} Current knowledge suggests that GPCRs do not undergo any significant conformational changes upon dimerization.¹⁶⁵ Therefore, GPCR dimers can now be modeled by using the experimentally observed dimer structure and overlaying the receptors being studied onto it, and aligning them based upon sequence homology. This technique has successfully been applied to model 5-HT_{1A} homodimers and has been experimentally verified.¹⁶⁶

The MOR homodimer crystal structure was chosen as the template of the CCR5-MOR heterodimer model since it may represent how MOR may potentially dimerize.⁶³ Importantly, since the crystal structure of the MOR homodimer was used as the basis for the CCR5-MOR heterodimer, the heterodimer interface will be assumed to be between TM5 and TM6. While one MOR receptor was kept in place, the other was overlaid with the CCR5 homology model, aligned based upon homology and replaced. Before docking studies, preliminary heterodimer model refinement was carried out through general energy minimization using the MMFF94 force field (Figure 28).

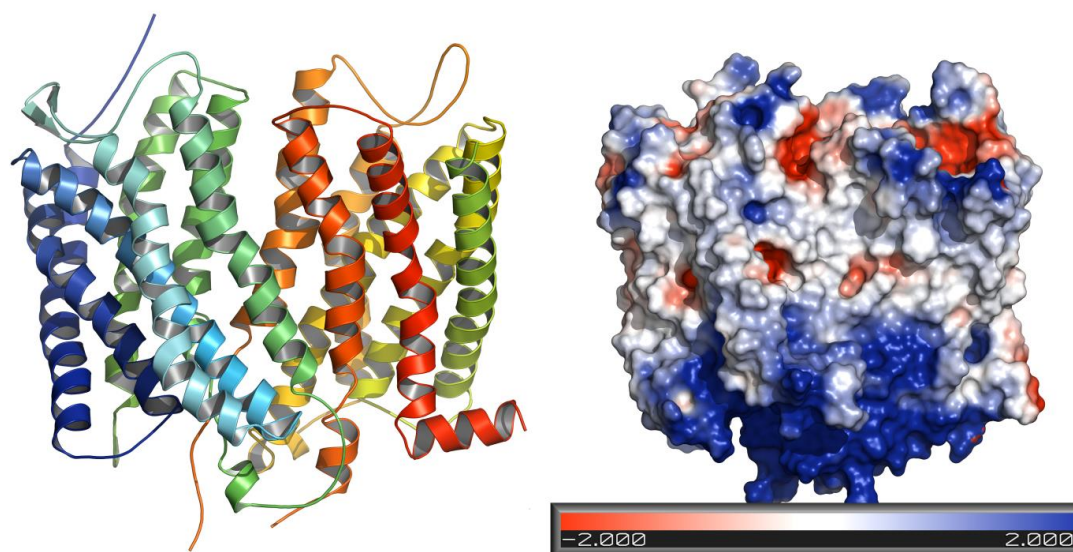


Figure 28. CCR5-MOR heterodimer model. (a) The CCR5-MOR heterodimer (MOR on the left and CCR5 on the right) model based on the MOR crystal structure (PDB id: 4DKL). (b) The electrostatic map of the heterodimer.^{167,168}

3.4.2 Bivalent Ligand Docking Studies

Docking compound **49** into both binding pockets of the heterodimer simultaneously proved to be difficult. The docking program GOLD could not simultaneously dock **49** into the CCR5-MOR heterodimer without placing a large amount of constraints on the system that may bias the docking results. Therefore, a new method had to be devised to dock **49** into the heterodimer. The two different portions of the bivalent compound were subsequently docked individually, in their respective receptors, and then, afterwards, connected to each other with the 19 atom spacer. While this is a more lengthy procedure it allows for the best binding mode of the maraviroc and naltrexone portions suited for the heterodimer to be found. Since the MOR homodimer was co-crystalized with the morphanin antagonist β -FNA, the naltrexone portion of the bivalent compound did not need to be *de novo* docked and was aligned with the bound

structure of β -FNA.⁶³ Once aligned, the 6- β position of the naltrexone portion points upward toward the TM-5/TM-6 heterodimer interface, which is the correct orientation to allow for the spacer and maraviroc to reach the CCR5 binding pocket with the assumed TM5/TM6 heterodimer interface. Next, maraviroc was docked into the CCR5 portion of the heterodimer using GOLD. The subsequent docking poses obtained were manually sifted through to find geometrically correct binding modes that allow for proper attachment between the phenyl group of maraviroc and the spacer-naltrexone portion of **49**. Of those poses, the one with the highest GOLD docking score was used. After attaching the maraviroc and naltrexone portion of compound **49** with the 19 atom spacer the system was energy minimized using the MMFF94 force field (Figure 29).

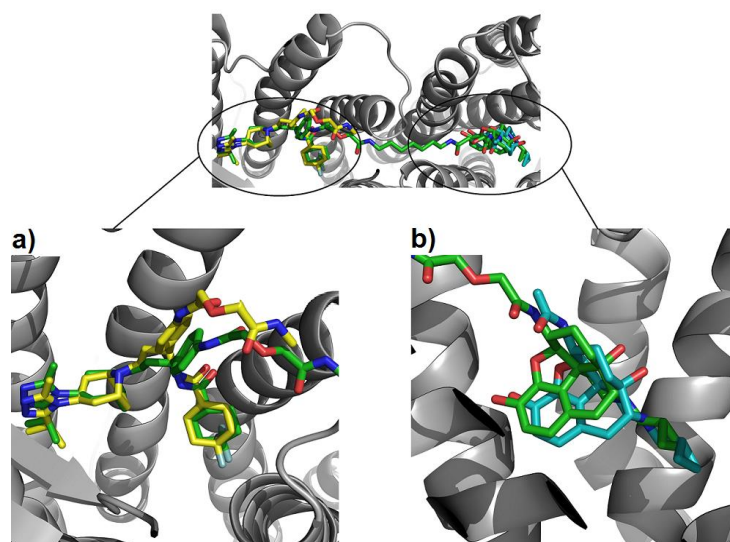


Figure 29. Overview of docking procedure for docking **49** into the CCR5-MOR heterodimer. a) maraviroc fragment before (yellow) and after linker attachment and energy minimization (green). a) naltrexone fragment before (cyan) and after linker attachment and energy minimization (green).

Using the same procedure as above, the docking of the 3-amino bivalent compound, **50**, was also attempted. When the 3-amino maraviroc fragment was docked

into the CCR5 portion of the heterodimer, the same docking mode was seen as before. However, after attempting to link the two pharmacophores together and energy minimize the resulting structure, the maraviroc portion of **50** consistently, on more than 3 attempted minimizations, lifted out of CCR5 completely. The 3-position attachment added too much strain onto the linker and did not allow for the binding mode of the maraviroc fragment portion to be maintained. Upon further analysis, we hypothesize that a longer linker may alleviate the strain on the maraviroc fragment for the 3-amino maraviroc attachment. During the energy minimization(s), the naltrexone fragment did not move from its original binding pocket. These results confirm and offer an explanation for the complete loss of activity at CCR5 that is seen for **50**, but not **49**. Since **50** cannot optimally bind CCR5 like **49**, it loses its affinity to CCR5. However, it retains its activity and affinity at MOR because the naltrexone fragment is retained in the MOR binding pocket.

3.4.3 CCR5-MOR Molecular Dynamics Simulations

The final energy minimized CCR5-MOR/**49** complex is shown in Figure 30 with the bivalent ligand spanning between the receptor's TM5/TM6 helices. While this model does give some insight into the interaction between **49** and the heterodimer, it does not indicate how favorable the interaction is or if it is even stable. Therefore, molecular dynamics using the program NAMD was used to interpret the stability of the heterodimer-bivalent compound complex.¹⁶⁹ Several steps were needed in order to prepare the heterodimer-ligand complex for dynamic simulation: the complex is first

added to a lipid bilayer and then solvated with a pre-defined water box with ions to accurately simulate its native membrane environment (Figure 31).

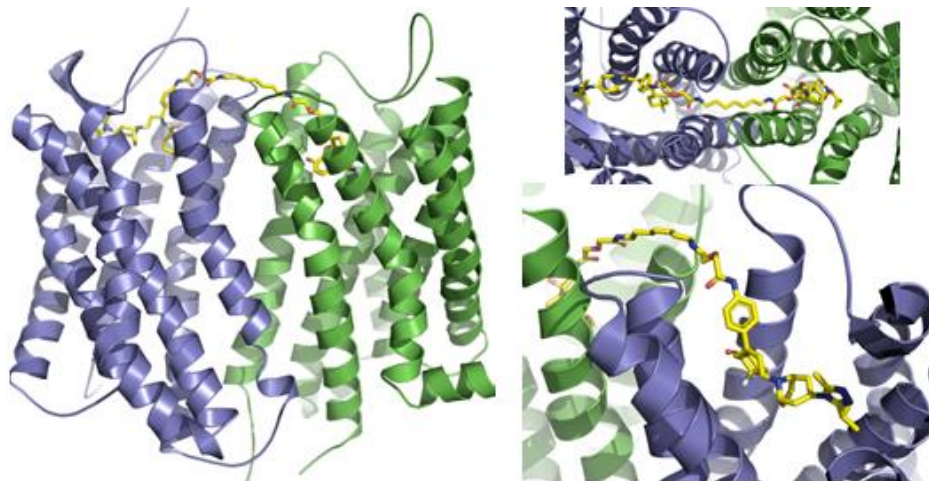


Figure 30 CCR5-MOR heterodimer model based on MOR dimer crystal structure (PDB code: 4DKL) with bivalent compound **49** bound. The blue protein represents CCR5 whereas the green protein is MOR. Compound **49** is colored in yellow.

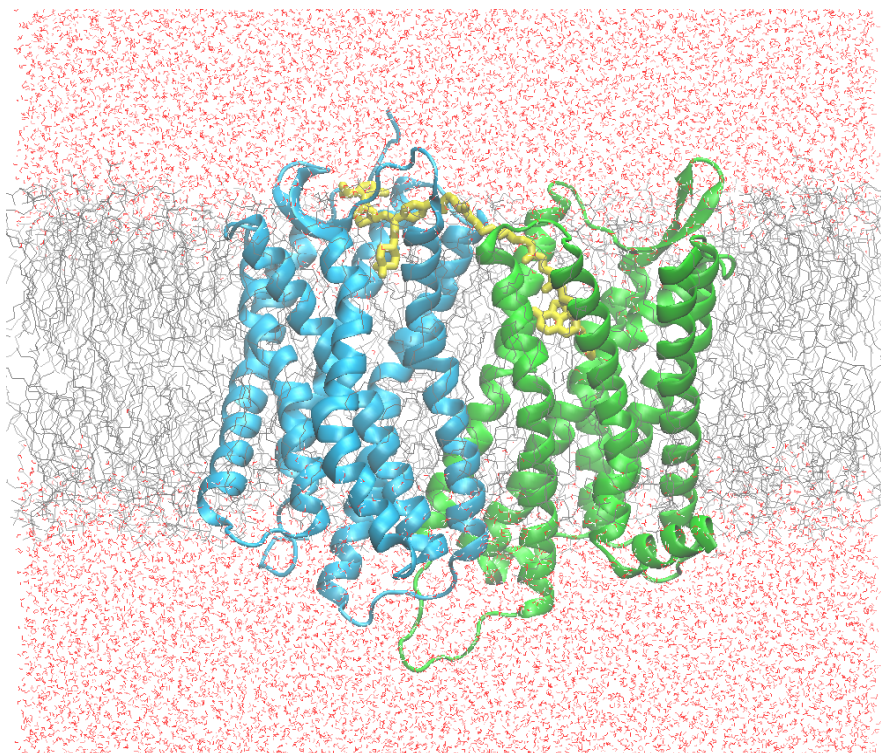


Figure 31. Molecular dynamics system for the CCR5-MOR heterodimer in a membrane (grey), and water box system (red). The green protein represents MOR while the blue protein is CCR5 and compound **49** is colored in yellow.

In all, the system built had 162385 atoms. A series of minimizations were then done in a step-wise manner to slowly equilibrate and energy minimize the components of the dimer-ligand-lipid-water-ion complex. It took a total of 13 ns for the system to equilibrate as indicated by the changes in RMSD and total energy of the heterodimer (Figure 32 and 33).

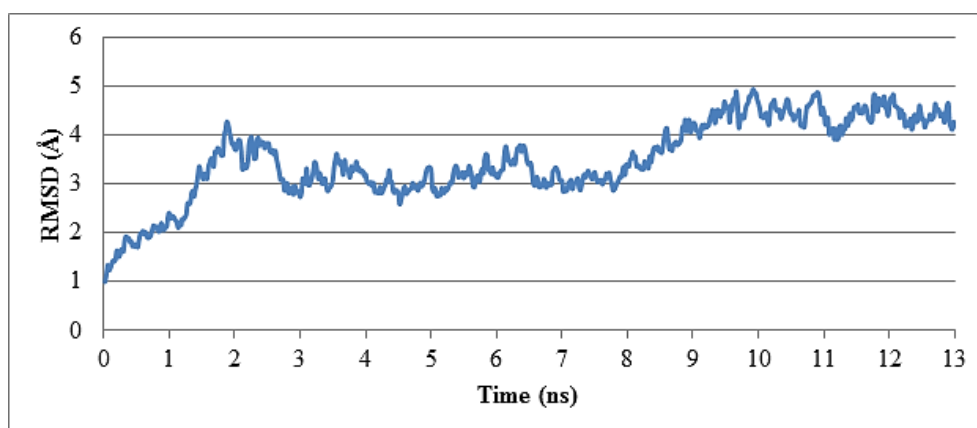


Figure 32. CCR5-MOR heterodimer RMSD from dynamics study after a total of 13 ns of production.

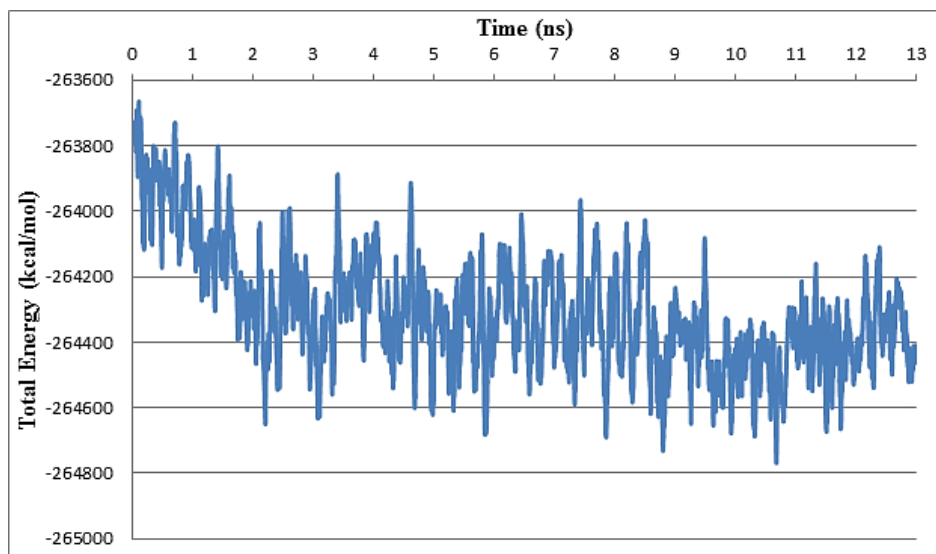


Figure 33. Total potential energy (kcal/mol) of the dynamic simulation after 13 ns.

After the 13 ns of dynamic simulation, the maraviroc portion of compound **49** partially dislodged from the CCR5 binding pocket, whereas the naltrexone portion did not move from the MOR binding pocket (Figure 34). This result indicates that for the heterodimer model, compound **49**'s initial binding mode for CCR5 was not energetically favored. However, it is important to note that the phenyl ring and the difluorocyclohexyl group of CCR5 stayed in their initial docked poses, while the rest of the molecule (triazole group and tropane ring) moved from its original, starting position. Figure 34 illustrates how after 6.0 ns of dynamic simulation, the triazole ring rotates upward out of its initial binding pocket. This shift upward is reflected in the changes in RMSD as seen in Figure 35.

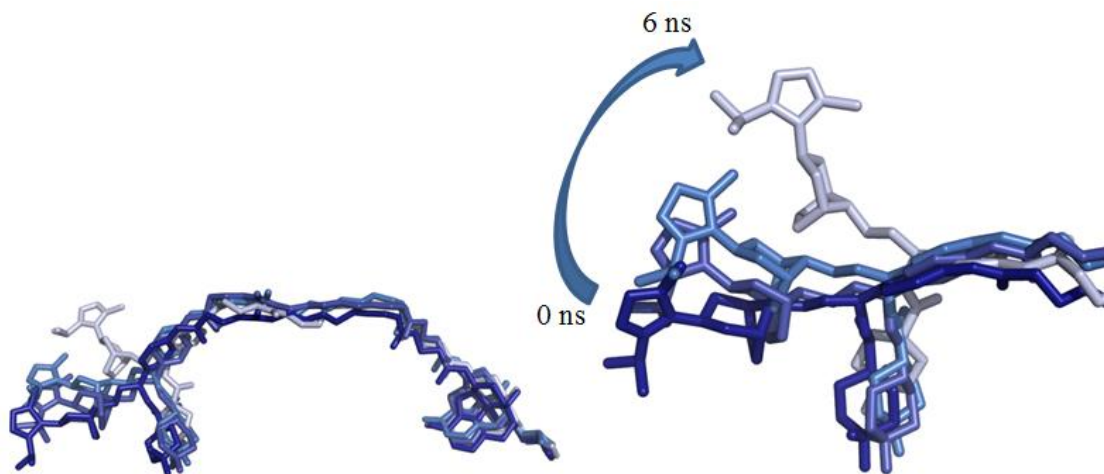


Figure 34 Trajectory of **49** in the CCR5-MOR heterodimer at 0, 2.4, 4.4, and 6.0 ns, with dark blue representing **49** at 0 ns and subsequently becoming a light blue at the 6.0 ns mark.

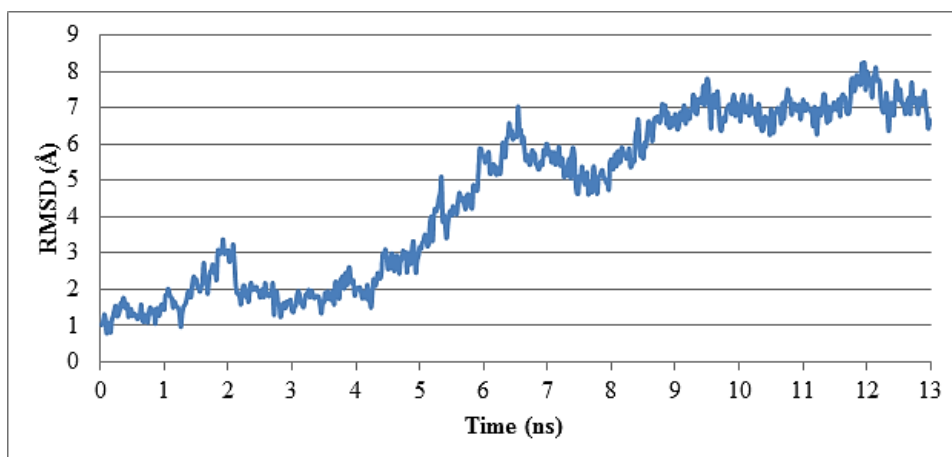


Figure 35. Bivalent compound **49** RMSD from dynamics study after a total of 13 ns of production.

Table 12 shows the major interactions between compound **49** and the CCR5-MOR heterodimer between 0 and 6.0 ns. The opiate portion of **49** does not move from its original binding pocket as indicated from the conservation of interacting residues with MOR. This binding pose matches that of β -FNA within the MOR crystal structure.⁶³ However, there are significant changes in the CCR5 interactions of **49** between 0 and 6.0 ns (after an additional 7 ns of stimulation **49** does not move from the later binding pocket). For the CCR5-maraviroc interaction several allosteric binding sites have been observed and supported by mutagenesis data, this promiscuity shows that no one binding mode is favored.¹⁷⁰⁻¹⁷⁴ At both time periods, the maraviroc portion of **49** interacts with I198, L255, N258, Q261, and M279. I198 and L255 have been deemed essential for maraviroc binding and N258 has been implicated in HIV-1 gp120 binding.^{170,171} The amino acids I198, L255, and M279 all contribute to the hydrophobic pocket surrounding the difluorocyclohexyl group. A hydrogen bond is made between the nitrogen of N258 and the carbonyl oxygen of the amide group connecting the difluorocyclohexyl group to

the rest of maraviroc. Q261 can form a carbonyl- π interaction with the phenyl group of maraviroc. Interestingly, neither binding pose for the maraviroc portion of **49** can form a salt bridge between the tertiary amine of maraviroc and E283, which site directed mutagenesis has indicated to be crucial for maraviroc binding to CCR5.^{170,173} Instead, at 0 ns, a salt bridge is formed between the tertiary amine and D276, which is two-turns before E283 on TM7. At 6.0 ns no significant interactions are observed between the tertiary amine of maraviroc and CCR5.

Table 12. Major amino acids in the CCR5 and MOR binding pockets, in the heterodimer, interacting with compound **49**.

Time Frame	CCR5 Binding Pocket ^a	MOR Binding Pocket
0 ns	W86, Y89, W94, <i>T177</i> , C178, S179, <i>I198</i> , <i>L255</i> , N258, Q261, D276, M279	D147, Y148, N150, M151, I293, H294, V297, W315, I319, Y323
6 ns	K22, E172, G173, <i>Y184</i> , K191, <i>I198</i> , <i>L255</i> , N258, Q261, S272, N273, D276, M279	D147, Y148, N150, M151, I293, V236, H294, W315, I319, Y323

^a The residues in **bold** are consistent with site-directed mutagenesis data for maraviroc binding.¹⁷⁰⁻¹⁷⁴ *Italicized* residues are important to HIV-1 gp120 binding.¹⁷⁰⁻¹⁷⁴ **Bold-italicized** residues are important to both maraviroc and gp120 binding via results of site-directed mutagenesis data.

The majority of movement between 0 and 6 ns in the CCR5 binding pocket is due to the shift of the triazole group upward out of the initial, deeper binding pocket for the maraviroc. The initial binding pocket for the triazole region at 0 ns was comprised of W86, Y89, W94, C178, and S179, whereas at 6.0 ns the binding pocket consisted of K22, G163, E172, S272, and N273 (Figure 36). The residues interacting with the triazole group at 0 ns form a hydrophobic pocket and the aromatic residues (W86, Y89, and Y94)

can form π - π interactions with it also. At 6 ns, the triazole group moves into a more polar, solvent exposed pocket and lacks the previous π - π interactions. However, after the additional 7 ns of dynamic simulation the triazole group does not move from this pocket and can form either polar or hydrogen bond interactions with K22, E172 and N273. Overall, this suggests that the shallower binding mode at 6 ns is favored over the deeper one observed at 0 ns.

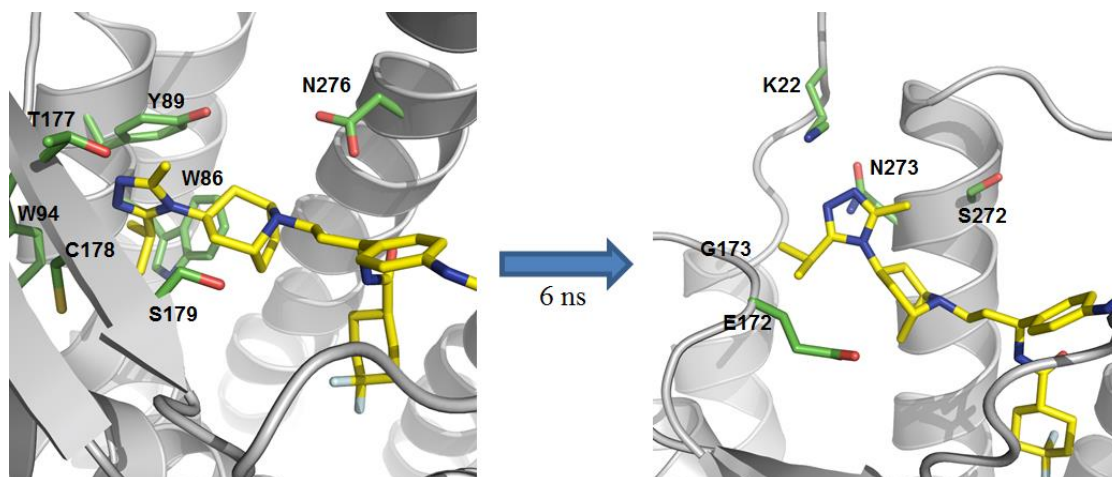


Figure 36. The binding pocket for the triazole region at 0 ns and 6.0 ns.

The dynamics simulation study can also help explain the changes in functional activities seen between maraviroc and **49**. As suggested by the simulations, addition of the linker to the *para*-phenyl portion of maraviroc leads to **49** being able to adopt only one general binding mode that may represent a lower affinity mode. Within this binding mode, there is an unstable binding pocket for the triazole portion of the molecule that led to it adopting two different conformations during the simulation. These observations are in agreement with the experimental data observed for the bivalent compounds. For the

CCR5 calcium antagonism assays, the loss in activity between maraviroc and compounds **49** through **52** can be explained by the unstable triazole binding pocket. In comparison, MOR calcium antagonism between naltrexone and compounds **49**, **50** and **102** is affected to a much lesser extent. During the simulation, the naltrexone portion of **49** does not move from its original binding pocket, which suggests that the 6 β -attachment does not affect MOR binding as greatly.

Overall, the dynamics simulations indicate that **49** can bind to the CCR5-MOR heterodimer in a stable manner. Furthermore, while the CCR5 binding mode may not be optimal for **49**, it still blocks gp120 mediated invasion/fusion. As seen in both the cell fusion assay and the HIV-1 invasion assay, **49** can block gp120 binding to CCR5. Within the HIV-1 invasion assay, **49** has even higher activity for inhibiting invasion than maraviroc or a combination of maraviroc and naltrexone. Thus, the binding mode revealed in the dynamics study may allow for greater inhibitory effects by utilizing both MOR and CCR5 to bind to.

3.5 Conclusion

Due to modern antiretroviral therapies, HIV-1 infected patients have longer lifespans and better quality of life. However, several neurological complications are now being seen due to HIV-1 associated injury of neurons by infected microglia and astrocytes. Furthermore, these effects can further be exacerbated with opiate use and abuse. A possible mechanism for the potentiation effects of opiates is the interaction of the mu-opioid receptor (MOR) with chemokine receptor CCR5 (CCR5), a known HIV-1

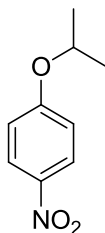
co-receptor. In order to explore this interaction and its relevance to neuroAIDS, a bivalent ligand targeting the CCR5-MOR heterodimer was previously synthesized. To understand how the bivalent ligand interacts with the heterodimer, biological studies using cell fusion, calcium inhibition and HIV-1 invasion were undertaken. These results were further confirmed using a dynamic simulation study of the CCR5-MOR heterodimer with the bivalent ligand. Overall, compound **49** was shown to have a unique pharmacological profile in HIV-1 infection assays using primary human astrocytes and morphine stimulation. Its interactions with the heterodimer were confirmed with both functional and radiobinding assays and a general SAR was elucidated for the compound series. While alteration of the naltrexone pharmacophore was well tolerated, the maraviroc pharmacophore was very sensitive to alterations. Specifically, for the other bivalent compound, **50**, MOR activity was well maintained and actually higher than **49**, but its CCR5 antagonism was essentially abolished compared to maraviroc. Molecular modeling and dynamic simulation provided evidence that **50** could not efficiently stay in the CCR5 binding pocket, while staying bound to MOR. Furthermore, molecular dynamics indicated that while not optimal, it was energetically favorable for **49** to stay bound to both MOR and CCR5 simultaneously. Within this project more optimization needs to be done with linker length and its attachment site to maraviroc. Further, studying the bivalent compound **49** in mice could also offer prove it to be a useful pharmacological tool to study the pathogenesis of neuroAIDS with and without morphine stimulation.

4. Experimental

4.1 Chemical syntheses

All chemicals and solvents were obtained from Sigma-Aldrich or another quality chemical company. Melting points were determined on a Fisher-Scientific melting point apparatus. ^1H and ^{13}C NMR were determined on a Bruker 400 MHz spectrometer with an autosampler and tetramethylsilane was used as an internal standard. Infrared spectra were obtained on a Thermo Nicolet FT-IR with a Smart iTR attachment. MS analysis was performed with a Applied Bio Systems 3200 Q trap with a turbo V source for TurbolonSpray. Column chromatography was performed on grade 230-400 mesh silica gel (Merck). Thin-layer chromatography was performed on Analtech Uniplate F254 plates. HPLC analysis of final compounds was performed on a Varian ProStar 210 system with a Microsorb-MV 100-5 C18 column (250 mm x 4.6 mm). Elemental analysis of final compounds was conducted by Atlantic Microlaboratory, Inc.

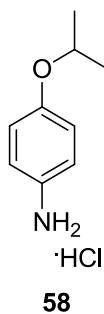
4.1.1 Small Molecule CCR5 Antagonists: Intermediates



57

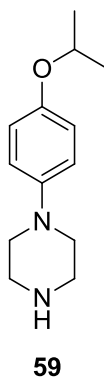
106

1-isopropoxy-4-nitrobenzene (57). In a 250 mL flask, 4-nitrophenol (10 g, 0.0719 mol) was dissolved in 25 mL of anhydrous dimethylformamide (DMF). To that potassium carbonate (1.5 equivalents, 14.9 g, 0.10785 mol) and 2-bromopropane (1.5 equivalents, 10.12 mL, 0.10785 mol) were then added to the flask while stirring. The suspension was then allowed to reflux at 120 °C for 1 h. The reaction was monitored via TLC (4:1 Hex:EA) and upon completion the reaction mixture was vacuum filtered and the DMF was evaporated under reduced pressure. The reaction mixture was then dissolved in ethyl acetate and washed once with brine, once with 1 N sodium hydroxide, and then three times with brine. The organic layer was then dried over anhydrous sodium sulfate, filtered and evaporated under reduced pressure. In all, 12.89 g of a yellow oil, 1-isopropoxy-4-nitrobenzene, was received with final yield of 99.0 %. ¹H NMR (400 MHz, CDCl₃) δ 1.379 (d, *J*=6.09 Hz, 6H), 4.667 (septet, *J*=6.08, 1H), 6.905 (d, *J*=9.28 Hz, 2H), 8.172 (d, *J*=9.28 Hz, 2H). IR (ATR, cm⁻¹) *v*_{max}: 2980, 2935, 1591, 1492, 1336, 1255, 1183, 1099, 945, 843.



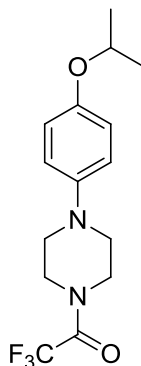
4-isopropoxybenzenamine hydrochloride salt (58). In a 500 mL hydrogenation flask, concentrated hydrochloric acid (1.3 equivalents, 2.58 mL, 0.0313 mol) was added to 60

mL MeOH. To that 1-isopropoxy-4-nitrobenzene (1) (4.349 g, 0.02403) was added to the solution along with 10 % w/w palladium on carbon (0.435 g, 10 %). The flask was placed on a hydrogenator at 60 psi H₂ gas for 16 h, and monitored via TLC (20:1:0.01 DCM:MeOH:NH₄OH). Once completed, the reaction mixture was vacuum filtered through celite, treated with activated carbon, filtered through celite, and then evaporated under reduced pressure. The obtained product was recrystallized with methanol and diethyl ether and dried. In all, 4.402 g of a purple solid, 4-isopropoxybenzenamine hydrochloride salt, was received with a final yield of 97.8 %. ¹H NMR (400 MHz, CDCl₃) δ 1.307 (d, *J*=6.0 Hz, 6H), 4.632 (septet, *J*=6.04, 1H), 7.017 (d, *J*=9.0 Hz, 2H), 7.283 (d, *J*=9.04 Hz, 2H). IR (ATR, cm⁻¹) ν_{max}: 2817, 2582, 2288, 1997, 1506, 1450, 1255, 1121, 942, 833.



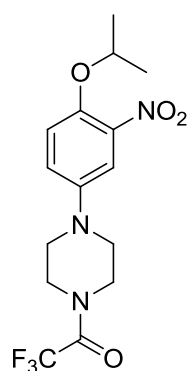
1-(4-isopropoxyphenyl)piperazine (59). In a 250 mL flask, 4-isopropoxybenzenamine hydrochloride salt (3.898 g, 0.02079 mol) was added to 100 mL of anhydrous chlorobenzene and to that suspension potassium carbonate (2 equivalents, 5.75 g, 0.04158 mol) was added over the period of an hour while being stirred under nitrogen protection. Bis(2-chloroethyl)amine hydrochloride (1.2 equivalents, 4.44 g, 0.02495 mol) was then added and stirred under nitrogen protection for an additional hour. The reaction

mixture was then refluxed at 140 °C for 24 h under nitrogen protection, and monitored via TLC (20:1:0.01 DCM:MeOH:NH₄OH). Upon completion the reaction mixture was vacuum filtered and the chlorobenzene was evaporated under reduced pressure. Column chromatography was then conducted (10:1:0.01 DCM:MeOH:NH₄OH) and a total of 3.832 g of a purple oil, 1-(4-isopropoxyphenyl)piperazine, was received with a final yield of 83.7 %. ¹H NMR (400 MHz, CDCl₃) δ 1.297 (d, *J*=8.48 Hz, 6H), 3.138 (broad s, 8H), 4.437 (septet, *J*=6.08, 1H), 6.818 (q, *J*=9.79 Hz, 4H). ¹³C NMR (400 MHz, CDCl₃) δ 22.04, 43.32, 49.02, 70.52, 117.09, 120.23.

**60**

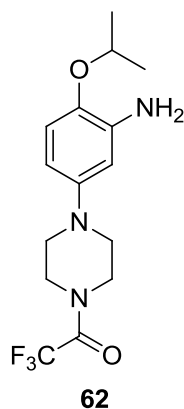
1-(trifluoromethyl)-4-(4-isopropoxyphenyl)piperazine (60). In a 250 mL flask, 1-(4-isopropoxyphenyl)piperazine (4.268 g, 0.0194 mol) was dissolved in 100 mL anhydrous dichloromethane and pyridine (3.44 mL, 0.04268 mol) was added while the reaction mixture was stirred at 0 °C for 0.5 h with 4 Å molecular sieves. Trifluoroacetic anhydride (2.2 equivalents, 2.35 mL, 0.01676 mol) was then added to the solution over a period of an hour. The reaction was allowed to proceed to room temperature over the period of 15 hours, and monitored via TLC (2:1 Hex:EA). Upon completion the reaction mixture was filtered, washed three times with 1 N hydrochloric acid, and then two times with brine.

The organic layer was dried over anhydrous sodium sulfate, filtered and evaporated under reduced pressure. Column chromatography was then conducted (6:1 Hex:EA) and a total of 5.775 g of a yellow solid, 1-(trifluoromethyl)-4-(4-isopropoxyphenyl)piperazine, was received with a final yield of 94.0 %. $^1\text{H NMR}$ (400 MHz, CDCl_3) δ 1.301 (d, $J=6.04$ Hz, 6H), 3.097 (m, 4H), 3.784 (m, 4H), 4.449 (septet, $J=6.08$, 1H), 6.851 (m, 4H).

**61**

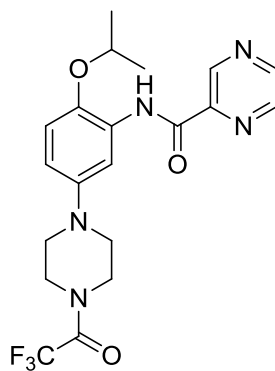
1-(trifluoromethyl)-4-(4-isopropoxy-3-nitrophenyl)piperazine (61). In a 100 mL flask, 1-(trifluoromethyl)-4-(4-isopropoxyphenyl)piperazine (1.196 g, 0.00378 mol) was dissolved in 40 mL anhydrous diethyl ether and stirred at room temperature. To the reaction mixture 1 equivalent of 2,3,5,6-tetrabromo-4-methyl-4-nitrocyclohexa-2,5-dienone (1.772 g, 0.00378) was added and stirred for 5 h. The reaction was monitored via TLC (4:1:1 Hex:EA:DCM) and upon completion the reaction mixture was vacuum filtered and the THF was evaporated under reduced pressure. The reaction mixture was then dissolved in dichloromethane and washed once with 1 N sodium hydroxide, and then once with brine. The organic layer was dried over anhydrous sodium sulfate, filtered and evaporated under reduced pressure. Column chromatography was then conducted (4:1:1

Hex:EA:DCM) and a total of 0.569 g of an orange oil, 1-(trifluoromethyl)-4-(4-isopropoxy-3-nitrophenyl)piperazine, was received with a final yield of 42%. ^1H NMR (400 MHz, CDCl_3) δ 1.340 (d, $J=6.08$ Hz, 6H), 3.036 (m, 4H), 3.748 (m, 4H), 4.529 (septet, $J=6.04$, 1H), 7.048 (m, 1H), 7.141 (d, $J=8.92$, 1H), 7.267 (s, 1H). IR (ATR, cm^{-1}) ν_{max} : 2978, 1688, 1525, 1496, 1179, 1137, 1020, 976, 828.



5-(4-(trifluoromethyl)piperazin-1-yl)-2-isopropoxybenzenamine (62). In a 250 mL hydrogenation flask, acetic acid (1.2 eq, 0.36 mL, 0.00627) was added to 60 mL MeOH. To that, 1-(trifluoromethyl)-4-(4-isopropoxy-3-nitrophenyl)piperazine (1.889 g, 0.005226 mol) was added to the solution along with 10 % w/w palladium on carbon (0.18 g, 10% w/w). The flask was placed on a hydrogenator at 60 psi H_2 gas, and monitored via TLC (20:1:0.01 DCM:MeOH: NH_4OH). Once completed (24 h), the reaction mixture was vacuum filtered through celite, and then evaporated under reduced pressure. Column chromatography was then conducted (10:1 DCM:MeOH, NH_4OH) and a total of 1.262 g of a purple oil, 5-(4-(trifluoromethyl)piperazin-1-yl)-2-isopropoxybenzenamine, was received with a final yield of 73%. ^1H NMR (400 MHz, CDCl_3) δ 1.296 (d, $J=6.08$ Hz,

6H), 2.91 (m, 4H), 3.72 (m, 4H), 4.445 (septet, $J=6.08$, 1H), 6.264 (m, 1H), 6.305 (m, 1H), 6.852 (d, $J=8.56$, 1H).

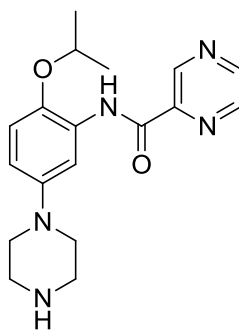


63

N-(5-(4-(trifluoromethyl)piperazin-1-yl)-2-isopropoxyphenyl)pyrazine-2-carboxamide

(63). In a 25 mL flask, pyrazine-2-carboxylic acid (2 eq, 0.061 g, 0.000489 mol) was dissolved in 1 mL anhydrous dimethylformamide (DMF). To the solution N-(3-Dimethylaminopropyl)-N'-ethylcarbodiimide hydrochloride (1.5 eq, 0.071 g, 0.0003668 mol), 1-hydroxybenzotriazole hydrate (1.5 eq, 0.05 g, 0.0003668 mol), triethylamine (3 eq, 0.1 mL, 0.000734 mol), and 4 Å molecular sieves were added and stirred under nitrogen protection at 0 °C for 0.5 h. 5-(4-(Trifluoromethyl)piperazin-1-yl)-2-isopropoxybenzenamine (1 eq, 0.081 g, 0.0002445) was then added to the reaction mixture and allowed to proceed to room temperature over the period of 24 h, and monitored via TLC (20:1 DCM:MeOH). Once completed, the reaction mixture was filtered and the DMF was evaporated under reduced pressure. The reaction mixture was then dissolved in chloroform and washed once with brine. The organic layer was dried over anhydrous sodium sulfate, filtered and evaporated under reduced pressure. Column

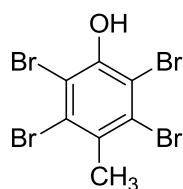
chromatography was then conducted (20:1 DCM:MeOH) and a total of 0.101 g of a yellow oil, N-(5-(4-(trifluoromethyl)piperazin-1-yl)-2-isopropoxyphenyl)pyrazine-2-carboxamide, was received with a final yield of 94%. ^1H NMR (400 MHz, CDCl_3) δ 1.357 (d, $J=6.04$ Hz, 6H), 2.974 (m, 4H), 3.852 (m, 4H), 4.612 (septet, $J=6.04$, 1H), 6.657 (m, 1H), 7.066 (d, $J=8.72$, 1H), 8.2733 (d, $J=2.89$ Hz, 1H), 8.625 (m, 1H), 8.827 (d, $J=2.48$, 1H), 9.536 (s, 1H), 10.929 (s, 1H).



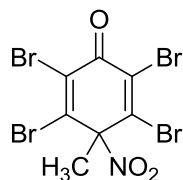
64

N-(2-isopropoxy-5-(piperazin-1-yl)phenyl)pyrazine-2-carboxamide (64). In a 25 mL flask, N-(5-(4-(trifluoromethyl)piperazin-1-yl)-2-isopropoxyphenyl)pyrazine-2-carboxamide (0.101 g, 0.000231 mol) was dissolved in 3 mL MeOH and 0.3 mL H_2O . A total of 5.2 equivalents of potassium carbonate (0.166 g, 0.00120 mol) were then added to the solution and the reaction mixture was allowed to reflux under N_2 protection for 2 h. The reaction was monitored via TLC (20:1:0.1, DCM:MeOH: NH_4OH) and upon completion the reaction mixture was filtered, evaporated down under reduced pressure, and then dissolved in DCM. The DCM solution was washed once with saturated sodium bicarbonate, brine, and then dried over sodium sulfate. The resulting solution was

filtered, evaporated down to dryness and a total of 0.0789 g of N-(2-isopropoxy-5-(piperazin-1-yl)phenyl)pyrazine-2-carboxamide was received with a total yield of 100%. ^1H NMR (400 MHz, CDCl_3) δ 1.353 (d, $J=6.04$ Hz, 6H), 2.854 (m, 4H), 3.852 (m, 4H), 3.491 (s, 1H), 4.605 (septet, $J=6.08$, 1H), 6.654 (m, 1H), 7.102 (d, $J=8.72$, 1H), 8.271 (d, $J=2.88$ Hz, 1H), 8.635 (m, 1H), 8.795 (d, $J=2.44$, 1H), 9.510 (d, $J=1.44$, 1H), 11.073 (s, 1H).

**65**

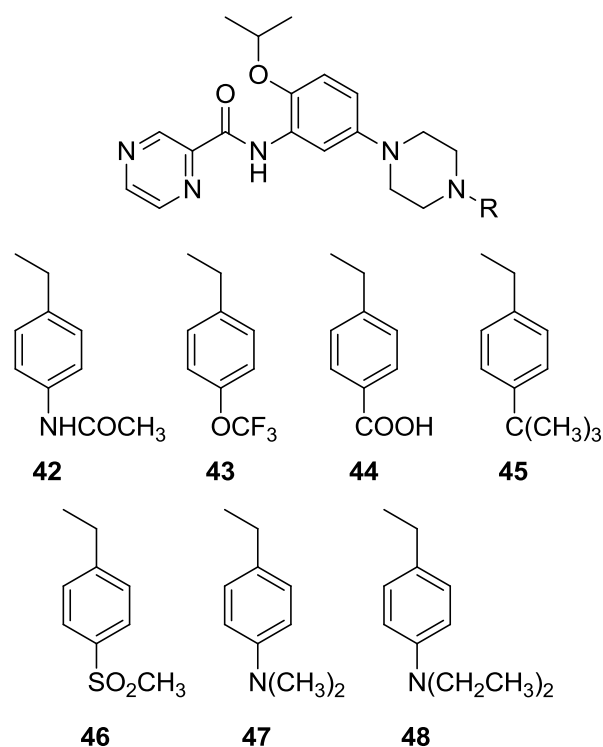
4-methyl-2,3,5,6-tetrabromophenol (65). To a solution of 1 g *p*-cresol (9.25 mmol) in 20 mL CCl_4 was added a trace amount of Fe dust and was allowed to stir at room temperature. Dropwise, 2.15 mL Br_2 (41.6 mmol) was added to the solution while carefully monitoring the reaction temperature. The reaction mixture was allowed to stir overnight and monitored via TLC (2:1 hexane:ethyl acetate). Once completed, the reaction was heated for 1 h to remove any excess Br_2 . The reaction mixture was allowed to cool to room temperature and diluted with 50 mL CHCl_3 and vacuum filtered to remove solid byproduct. The solution was then evaporated down to dryness and 4-methyl-2,3,5,6-tetrabromophenol was purified via recrystallization with CHCl_2 . ^1H NMR (400 MHz, CDCl_3) δ 2.74 (s, 3H), 6.09 (s, 1H).

**66**

2,3,5,6-tetrabromo-4-methyl-4-nitrocyclohexa-2,5-dien-1-one (66). To a solution of 4.0 g (9.35 mmol) of **2**, 4-methyl-2,3,5,6-tetrabromophenol in 28 mL of acetic anhydride was added, dropwise, 6 mL (135.2 mmol) HNO₃ (d 1.42) at 0 °C. The reaction was monitored via TLC (hexane:ethyl acetate, 2:1). The suspension was stirred at for 10 min and the product was precipitated out with the addition of 20 mL H₂O. The product was then vacuum filtered out, washed with H₂O and hexane and dried underneath vacuum giving a pale yellow powder with a yield of 4.144 g (94.6%). ¹H NMR (400 MHz, CDCl₃) δ 2.26 (s, 3H); mp: decomposed 80 °C, IR V_{max} (ATR): 1682 cm⁻¹.

4.1.2 Small Molecule CCR5 Antagonists: Final Compounds

Final compounds **42** through **46** were synthesized by reacting the unprotected piperazine derivative, **8**, with the corresponding benzyl chloride in the presence of potassium carbonate and trace potassium iodide. Compounds **47** and **48** were synthesized by reacting **64** with the corresponding substituted benzaldehyde to form the imine and then reducing it with sodium triacetoxyborohydride to form the subsequent tertiary amine. Column chromatography was then performed to afford the final product which was then converted into a hydrochloride salt.



N-(5-(4-(4-acetamidobenzyl)piperazin-1-yl)-2-isopropoxyphenyl)benzamide (42) In a 25 mL flask N-(2-isopropoxy-5-(piperazin-1-yl)phenyl)pyrazine-2-carboxamide (0.083 g, 0.000243 mol) was dissolved in 4 mL anhydrous DMF. To the solution 1.2 equivalents 4-acetamidobenzyl chloride (0.0535 g, 0.000292 mol), 1.5 equivalents potassium carbonate (0.0504 g, 0.000365 mol), and a trace amount of potassium iodide were added. The suspension was allowed to stir at room temperature overnight and the reaction was monitored via TLC (2:1 Hex:EA). Upon completion, the reaction mixture was filtered, evaporated down to dryness, dissolved in chloroform, washed once with brine, dried over sodium sulfate, and evaporated down to dryness. Column chromatography (20:1 DCM:MeOH) was performed and a total of 0.081 g N-(5-(4-(4-acetamidobenzyl)piperazin-1-yl)-2-isopropoxyphenyl)benzamide was received with a

total yield of 55%. ^1H NMR (400 MHz, DMSO) δ 1.275 (d, $J=6.04$ Hz, 6H), 2.090 (s, 3H), 3.148 (m, 4H), 3.497 (m, 4H), 4.434 (s, 2H), 4.557 (septet, $J=6.04$, 1H), 6.712 (m, 1H), 7.196 (d, $J=8.72$, 1H), 7.569 (d, $J=7.8$ Hz, 2H), 7.707 (d, $J=8.08$ Hz, 2H), 8.022 (d, $J=2.76$ Hz, 1H), 8.733 (s, 1H), 8.983 (d, $J=2.32$ Hz, 1H), 9.336 (d, $J=1.4$ Hz, 1H), 10.806 (s, 1H). ^{13}C NMR (400 MHz, DMSO) δ 21.796, 23.989, 48.554, 69.611, 106.484, 110.842, 119.001, 119.065, 133.178, 133.755, 133.859, 143.449, 143.545, 144.057, 148.089, 155.004, 155.064, 160.189, 168.635, 176.145. IR (ATR, cm^{-1}) ν_{max} : 3313, 3182, 2974, 2831, 2551, 2492, 2465, 1684, 1601. Anal. Calcd. For $\text{C}_{29}\text{H}_{34}\text{N}_4\text{O}_3\text{Cl}$: C 61.67, H 6.34, N 16.01; found: C 60.76, H 6.45, N 15.49. MS (ESI) m/z found 489 ($\text{M} + \text{H}$) $^+$. MP: 192-196 $^\circ\text{C}$.

N-(2-isopropoxy-5-(4-(4-(trifluoromethoxy)benzyl)piperazin-1-yl)phenyl)benzamide

(43) In a 25 mL flask N-(2-isopropoxy-5-(piperazin-1-yl)phenyl)pyrazine-2-carboxamide (0.048 g, 0.000141 mol) was dissolved in 4 mL anhydrous DMF. To the solution 1.2 equivalents 4-(trifluoromethoxy)benzyl chloride (0.0266 mL, 0.0356 g, 0.000169 mol), 1.5 equivalents potassium carbonate (0.0293 g, 0.000212 mol), and a trace amount of potassium iodide were added. The suspension was allowed to stir at room temperature overnight and the reaction was monitored via TLC (20:1 DCM:MeOH). Upon completion, the reaction mixture was filtered, evaporated down to dryness, dissolved in chloroform, washed once with brine, dried over sodium sulfate, and evaporated down to dryness. Column chromatography (20:1 DCM:MeOH) was performed and a total of 0.068 g N-(2-isopropoxy-5-(4-(4-(trifluoromethoxy)benzyl)piperazin-1-

yl)phenyl)benzamide was received with a total yield of 94%. ^1H NMR (400 MHz, CDCl_3) δ 1.347 (d, $J=6.04$ Hz, 6H), 2.693 (broad s, 4H), 2.9231 (m, 4H), 3.645 (s, 2H), 4.596 (septet, $J=6.04$, 1H), 6.637 (m, 1H), 7.116 (d, $J=8.72$, 1H), 7.1922 (d, $J=8$ Hz, 2H), 7.395 (d, $J=8.52$ Hz, 2H), 8.255 (d, $J=2.84$ Hz, 1H), 8.569 (m, 1H), 8.792 (d, $J=2.49$ Hz, 1H), 9.500 (d, $J=1.4$ Hz, 1H), 11.028 (s, 1H). ^{13}C NMR (400 MHz, CDCl_3) δ 22.127, 50.894, 52.614, 53.762, 62.338, 70.355, 106.643, 112.332, 120.817, 121.563, 130.431, 133.828, 135.055, 136.719, 142.597, 144.668, 145.309, 147.224, 148.394, 155.539, 160.607. IR (ATR, cm^{-1}) ν_{max} : 3296, 2980, 2941, 2845, 2538, 2496, 2469, 1688, 1247, 1159. Anal. Calcd. For $\text{C}_{28}\text{H}_{30}\text{F}_3\text{N}_3\text{O}_3\text{Cl}$: C 56.57, H 5.30, N 12.69; found: C 56.21, H 5.31, N 12.61. MS (ESI) m/z found 516 ($\text{M} + \text{H}$) $^+$. MP: 136-139 $^\circ\text{C}$.

4-((4-(3-benzamido-4-isopropoxyphenyl)piperazin-1-yl)methyl)benzoic (44) In a 25 mL flask N-(2-isopropoxy-5-(piperazin-1-yl)phenyl)pyrazine-2-carboxamide (0.086 g, 0.000252 mol) was dissolved in 4 mL anhydrous DMF. To the solution 1.2 equivalents 4-chloromethyl benzoic acid (0.0516 g, 0.0003024 mol), 1.5 equivalents potassium carbonate (0.0522 g, 0.000378 mol), and a trace amount of potassium iodide were added. The suspension was stirred, and allowed to return to room temperature overnight. The reaction was monitored via TLC (5:1:0.1 DCM:MeOH:formic acid). Upon completion, the reaction mixture was filtered, evaporated down to dryness, dissolved in chloroform, washed once with brine, dried over sodium sulfate, and evaporated down to dryness. Column chromatography (10:1:0.1, DCM:MeOH:formic acid) was performed and a total of 0.042 g 4-((4-(3-benzamido-4-isopropoxyphenyl)piperazin-1-yl)methyl)benzoic was

received with a total yield of 35%. ^1H NMR (400 MHz, DMSO) δ 1.277 (d, $J=6.0$ Hz, 6H), 3.168 (m, 6H), 3.488 (m, 2H), 4.553 (m, 3H), 6.716 (m, 1H), 7.201 (d, $J=8.84$, 1H), 7.813 (m, 2H), 8.036 (m, 3H), 8.829 (d, $J=1.52$ Hz, 1H), 9.005 (m, 1H), 9.346 (d, $J=1.32$ Hz, 1H), 11.037 (s, 1H), 13.133 (s, 1H). ^{13}C NMR (400 MHz, CDCl_3) δ 21.806, 48.555, 51.479, 69.614, 106.566, 110.865, 121.652, 129.548, 131.859, 133.109, 143.472, 143.545, 144.093, 148.105, 154.976, 160.139, 166.878. IR (ATR, cm^{-1}) ν_{max} : 3542, 3306, 2977, 2926, 2837, 2652, 2548, 2466, 1722, 1688. Anal. Calcd. For $\text{C}_{28}\text{H}_{31}\text{N}_3\text{O}_4\text{Cl} + 2\text{H}_2\text{O}$: C 57.09, H 6.00, N 12.8; found: C 57.19, H 5.85, N 12.25. MS (ESI) m/z found 476 ($\text{M} + \text{H}$) $^+$. MP: 245-250 $^\circ\text{C}$.

N-(5-(4-(4-(tert-butyl)benzyl)piperazin-1-yl)-2-isopropoxyphenyl)benzamide (45) In a 25 mL flask N-(2-isopropoxy-5-(piperazin-1-yl)phenyl)pyrazine-2-carboxamide (0.062 g, 0.000182 mol) was dissolved in 4 mL anhydrous DMF. To the solution 1.2 equivalents 4-(tert-butyl)benzyl chloride (0.0422 mL, 0.0399 g, 0.000218 mol), 1.5 equivalents potassium carbonate (0.038 g, 0.000273 mol), and a trace amount of potassium iodide were added. The suspension was allowed to stir at room temperature overnight and the reaction was monitored via TLC (10:1 DCM:MeOH). Upon completion, the reaction mixture was filtered, evaporated down to dryness, dissolved in chloroform, washed once with brine, dried over sodium sulfate, and evaporated down to dryness. Column chromatography (20:1 DCM:MeOH) was performed and a total of 0.031 g N-(5-(4-(4-(tert-butyl)benzyl)piperazin-1-yl)-2-isopropoxyphenyl)benzamide was received with a total yield of 35%. ^1H NMR (400 MHz, DMSO) δ 1.277 (d, $J=6.0$ Hz, 6H), 1.318 (s, 9H),

3.171 (m, 6H), 3.475 (m, 2H), 4.458 (m, 2H), 4.558 (septet, $J=6.04$ Hz, 1H), 6.717 (m, 1H), 7.189 (d, $J=8.76$, 1H), 7.558 (m, 4H), 8.026 (d, $J=2.76$ Hz, 1H), 8.791 (m, 1H), 9.017 (d, $J=2.12$ Hz, 1H), 9.344 (d, $J=1.36$, 1H) 11.014 (s, 1H). ^{13}C NMR (400 MHz, CDCl_3) δ 21.809, 31.026, 34.447, 48.555, 69.623, 106.539, 110.862, 121.608, 125.601, 133.085, 143.395, 143.549, 144.069, 148.118, 160.097. IR (ATR, cm^{-1}) ν_{max} : 3257, 2968, 2905, 2867, 2496, 2448, 2426, 1687. Anal. Calcd. For $\text{C}_{32}\text{H}_{39}\text{N}_3\text{O}_2\text{Cl} + \text{H}_2\text{O}$: C 64.25, H 7.44, N 12.92; found: C 65.34, H 7.30, N 13.01. MS (ESI) m/z found 488 ($\text{M} + \text{H}$)⁺. MP: 137-141 °C.

N-(2-isopropoxy-5-(4-(4-(methylsulfonyl)benzyl)piperazin-1-yl)phenyl)benzamide (46).

In a 25 mL flask N-(2-isopropoxy-5-(piperazin-1-yl)phenyl)pyrazine-2-carboxamide (0.065 g, 0.00019 mol) was dissolved in 4 mL anhydrous DMF. To the solution 1.2 equivalents 4-methylsulfonyl benzyl chloride (0.0467 g, 0.000228 mol), 1.5 equivalents potassium carbonate (0.04 g, 0.000285 mol), and a trace amount of potassium iodide were added. The suspension was allowed to stir at room temperature overnight and the reaction was monitored via TLC (10:1 DCM:MeOH). Upon completion, the reaction mixture was filtered, evaporated down to dryness, dissolved in chloroform, washed once with brine, dried over sodium sulfate, and evaporated down to dryness. Column chromatography (20:1 DCM:MeOH) was performed and a total of 0.036 g N-(2-isopropoxy-5-(4-(4-(methylsulfonyl)benzyl)piperazin-1-yl)phenyl)benzamide was received with a total yield of 37%. ^1H NMR (400 MHz, CDCl_3) δ 1.342 (d, $J=6.08$ Hz, 6H), 3.068 (m, 6H), 3.608 (m, 4H), 4.396 (m, 2H), 4.589 (septet, $J=6.08$, 1H), 6.654 (m,

1H), 7.198 (d, $J=6.6$, 1H), 8.086 (m, 4H), 8.204 (m, 1H), 8.427 (m, 1H), 8.861 (m, 1H), 9.518 (d, $J=1.32$ Hz, 1H), 13.698 (s, 1H). ^{13}C NMR (400 MHz, CDCl_3) δ 22.016, 44.291, 49.112, 50.844, 52.635, 70.38, 106.944, 112.176, 128.428, 133.489, 142.532, 144.776, 145.009, 147.825, 156.595, 160.279. IR (ATR, cm^{-1}) ν_{max} : 3282, 2982, 2919, 2844, 2534, 2410, 2324, 1682, 1524, 1304, 1147. Anal. Calcd. For $\text{C}_{28}\text{H}_{34}\text{N}_3\text{O}_4\text{SCl} + \text{H}_2\text{O}$: C 55.36, H 6.08, N 12.42; found: C 55.30, H 5.83, N 12.05. MS (ESI) m/z found 509 ($\text{M} + \text{H}$) $^+$. MP: 179-180 °C.

N-(5-(4-(4-(dimethylamino)benzyl)piperazin-1-yl)-2-isopropoxyphenyl)benzamide (47).

N-(2-isopropoxy-5-(piperazin-1-yl)phenyl)pyrazine-2-carboxamide (0.146 g, 0.000428 mol) and 1.1 equivalents of diethylaminobenzaldehyde (0.0834 g, 0.000471 mol) were dissolved in 10 mL anhydrous THF and allowed to stir for 1 hour under N_2 protection. 1.5 equivalents of sodium triacetoxyborohydride (0.136 g, 0.000672 mol) was added to the reaction mixture and allowed to stir under N_2 protection overnight. The reaction was monitored via TLC (10:1:0.1, DCM:MeOH: NH_4OH). Once completed the reaction was quenched with saturated aqueous sodium bicarbonate. The aqueous layer was extracted twice with ether and the organic layer was separated, dried over sodium sulfate and evaporated down to dryness. Column chromatography (30:1:0.1, DCM:MeOH: NH_4OH) was performed and a total of 0.075 g N-(5-(4-(4-(dimethylamino)benzyl)piperazin-1-yl)-2-isopropoxyphenyl)benzamide was received with a total yield of 35%. ^1H NMR (400 MHz, DMSO) δ 1.342 (d, $J=6.0$ Hz, 6H), 2.698 (broad s, 4H), 2.918 (s, 4H), 2.968 (s, 6H), 3.594 (m, 2H), 4.589 (septet, $J=6.04$, 1H), 6.631 (m, 1H), 6.727 (d, $J=8.48$, 2H),

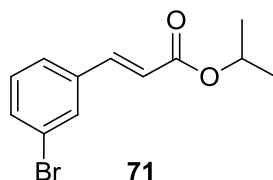
7.109 (d, $J=8.68$, 1H), 7.222 (d, $J=8.32$ Hz, 2H), 8.239 (d, $J=2.64$ Hz, 1H), 8.536 (s, 1H), 8.771 (d, $J=2.4$ Hz, 1H), 9.489 (s, 1H), 11.071 (s, 1H). ^{13}C NMR (400 MHz, CDCl_3) δ 22.139, 40.673, 52.418, 53.395, 70.379, 106.640, 112.316, 112.389, 121.688, 130.595, 133.878, 142.673, 144.612, 145.352, 147.135, 150.103, 155.578, 160.580. IR (ATR, cm^{-1}) ν_{max} : 3295, 2975, 2919, 2840, 2531, 1692. For $\text{C}_{29}\text{H}_{38}\text{N}_4\text{O}_2\text{Cl}_2$: C 59.23, H 6.63, N 15.35; found: C 58.41, H 6.48, N 15.00 MS (ESI) m/z found 475 ($\text{M} + \text{H}$) $^+$. MP: 160 °C.

N-(5-(4-(4-(diethylamino)benzyl)piperazin-1-yl)-2-isopropoxyphenyl)benzamide (48).

N-(2-isopropoxy-5-(piperazin-1-yl)phenyl)pyrazine-2-carboxamide (0.134 g, 0.0003925 mol) and 1.1 equivalents of dimethylaminobenzylaldehyde (0.0644 g, 0.000432 mol) were dissolved in 10 mL anhydrous THF and allowed to stir for 1 hour under N_2 protection. 1.5 equivalents of sodium triacetoxyborohydride (0.125 g, 0.000589 mol) was added to the reaction mixture and allowed to stir under N_2 protection overnight. The reaction was monitored via TLC (10:1:0.1, DCM:MeOH: NH_4OH). Once completed the reaction was quenched with saturated aqueous sodium bicarbonate. The aqueous layer was extracted twice with ether and the organic layer was separated, dried over sodium sulfate and evaporated down to dryness. Column chromatography (30:1:0.1, DCM:MeOH: NH_4OH) was performed and a total of 0.056 g N-(5-(4-(4-(diethylamino)benzyl)piperazin-1-yl)-2-isopropoxyphenyl)benzamide was received with a total yield of 30%. ^1H NMR (400 MHz, DMSO) δ 1.179 (t, $J=7$ Hz, 6H), 1.342 (d, $J=6.0$ Hz, 6H), 2.709 (m, 4H), 2.924 (m, 4H), 3.364 (m, 4H), 3.587 (s, 2H), 4.589 (septet, $J=6.08$, 1H), 6.646 (m, 3H), 7.112 (d, $J=8.64$, 1H), 7.182 (d, $J=8.28$, 2H), 8.237 (d,

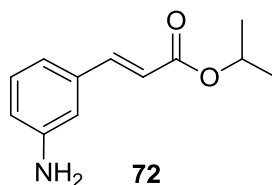
$J=2.64$ Hz, 1H), 8.513 (m, 1H), 8.762 (d, $J=2.2$ Hz, 1H), 9.485 (s, 1H), 11.082 (s, 1H). ^{13}C NMR (400 MHz, CDCl_3) δ 12.662, 22.139, 44.402, 70.380, 106.628, 1111.581, 112.307, 121.725, 133.881, 142.658, 144.599, 145.342, 147.128, 155.635, 160.558. IR (ATR, cm^{-1}) ν_{max} : 3287, 2976, 2937, 2897, 2523, 2462, 1690, 1521. For $\text{C}_{31}\text{H}_{43}\text{N}_4\text{O}_2\text{Cl}_3$: C 56.91, H 6.75, N 13.73; found: C 56.93, H 6.86, N 13.60. MS (ESI) m/z found 503 ($\text{M} + \text{H}$) $^+$. MP: 145-149 °C.

4.1.3 CCR5-MOR Bivalent Ligands: Intermediates



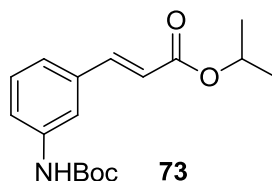
(E)-isopropyl 3-(3-bromophenyl)acrylate (71). 3-bromocinnamic acid (5 g, 0.022022 mol) was dissolved in 100 mL isopropyl alcohol in a round bottom flask. Several drops of concentrated H_2SO_4 (~100 μL) was added to the solution. The mixture was refluxed at 120 °C in an oil bath and monitored with TLC (4:1 Hex:EA). After 24 h the reaction mixture was cooled down to RT and the solvent evaporated via rotovap. Ethyl acetate was added to dissolve the residue and washed with NaHCO_3 (aq) and dried over Na_2SO_4 , filtered and purified using column chromatography (4:1 Hex:EA). A total of 4.71 g (E)-isopropyl 3-(3-bromophenyl)acrylate (**71**) was received with a yield of 79%. ^1H NMR (400 MHz, CDCl_3) δ 1.3 (d, $J=6.3$ Hz, 6H), 5.14 (septet, $J=6.28$, 1H), 6.38 (d, $J=16$ Hz, 1H), 7.23 (t, $J=7.88$ Hz, 1H), 7.46 (d, $J=1.8$ Hz, 1H), 7.48 (d, $J=1.8$ Hz, 1H), 7.55 (d,

$J=16$ Hz, 1H), 7.65 (s, 1H). IR (ATR, cm^{-1}) ν_{max} : 3061, 2978, 2935, 2874, 1705, 1638, 1144, 1105.



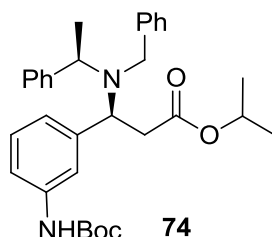
(E)-isopropyl 3-(3-aminophenyl)acrylate (72). (E)-isopropyl 3-(3-bromophenyl)acrylate (71). (4.71 g, 0.0175 mol) was dissolved in 60 mL anhydrous toluene. To it, in a stepwise manner, was added $\text{Pd}_2(\text{dba})_3$ (0.801 g, 5%), and $\text{P}(\text{t-Bu})_3$ (0.142 g, 4%) and the mixture was allowed to stir for 15 min under N_2 protection. To the suspension, LHMDS in toluene (19.25 mL, 1 M in toluene, 1.1 eq, 0.01925 mol) was added dropwise and the reaction mixture was allowed to stir overnight under N_2 protection. An additional 2.5% $\text{Pd}_2(\text{dba})_3$, 2% $\text{P}(\text{t-Bu})_3$, and 0.5 eq LHMDS was added subsequently to the reaction mixture and stirred overnight under N_2 protection. The resulting reaction mixture was quenched using 1 N HCl very slowly over ice. The mixture was stirred for an additional 2 h and filtered through celite and diluted with DCM. The organic layer was extracted and washed with saturated aq. NaCHO_3 , then brine and dried over Na_2SO_4 . The crude product was then purified using column chromatography (100:1 DCM:MeOH, NH_4OH) to give 2.461 g of (E)-isopropyl 3-(3-aminophenyl)acrylate (**72**) at a yield of 69%. ^1H NMR (400 MHz, CDCl_3) δ 1.29 (d, $J=6.3$ Hz, 6H), 3.74 (s, 2H), 5.12 (septet, $J=6.24$, 1H), 6.33 (d, $J=16$ Hz, 1H), 6.67 (dd, $J=4.28$ Hz, 1H), 6.80 (m, 1H), 6.90 (d, $J=7.6$ Hz, 1H), 7.14 (d, $J=7.8$ Hz, 1H), 7.55 (d, $J=16$, 1H). ^{13}C NMR (400 MHz, CDCl_3) δ 21.95, 67.73, 114.12,

117.00, 118.56, 118.58, 129.73, 135.55, 144.63, 146.85, 166.63. IR (ATR, cm^{-1}) ν_{max} : 3457, 3420, 3368, 2979, 2934, 1694, 1633, 1458, 1270, 1173, 1103.



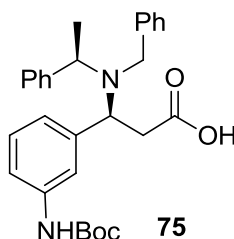
(E)-isopropyl 3-(3-((tert-butoxycarbonyl)amino)phenyl)acrylate (73). (E)-isopropyl 3-(3-aminophenyl)acrylate (**72**) (2.54 g, 0.0124 mol) was added to 30 mL H_2O , and to it NaHCO_3 (2 eq, 3.12 g, 0.0248 mol) was added and allowed to stir for 10 min. The solution was cooled to 5 °C and di-tert-butyl dicarbonate (1.5 eq, 4.06 g, 0.0186 mol) in 20 mL dioxane was added dropwise. The resultant solution was cooled to 0 °C for 1 h and allowed to stir at RT overnight. The aqueous solution was then washed with 50 mL of ethyl acetate and the organic layer was then extracted with saturated NaHCO_3 (aq). The aqueous layers were then combined and acidified with 10 % HCl to a final pH of 1. The aqueous solution was then extracted with ethyl acetate, and the organic layer was dried over Na_2SO_4 and rotovapped. The crude product was then purified with column chromatography (4:1 Hex:EA) and a total of 2.884 g (E)-isopropyl 3-(3-((tert-butoxycarbonyl)amino)phenyl)acrylate (**73**) with a yield of 76%. ^1H NMR (400 MHz, CDCl_3) δ 1.29 (d, $J=1.28$ Hz, 6H), 1.53 (s, 9H), 5.13 (septet, $J=6.24$, 1H), 6.40 (d, $J=16$ Hz, 1H), 6.55 (s, 1H), 7.19 (m, 1H), 7.28 (m, 2H), 7.60 (m, 2H). ^{13}C NMR (400 MHz, CDCl_3) δ 21.93, 28.33, 67.79, 80.81, 117.64, 119.34, 120.05, 122.79, 129.39, 135.46,

138.97, 144.03, 152.61, 166.43. IR (ATR, cm^{-1}) ν_{max} : 3307, 3057, 2979, 2936, 1702, 1484, 1439, 1229, 169, 1104.



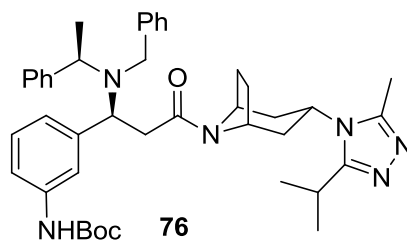
(S)-isopropyl-3-(benzyl((R)-1-phenylethyl)amino)-3-(3-((tert-butoxycarbonyl)amino)phenyl)propanoate (74). R-(+)-N-benzyl- α -methylbenzylamine (4.6 g, 0.0218 mol) was dissolved in 30 mL anhydrous THF and stirred at 0 °C under N_2 protection. To it, n-butyl-lithium (1 eq, 8.76 mL, 2.5 M in hexane, 0.0218 mol) was added dropwise and stirred for 30 minutes. During the addition, the reaction mixture went from being clear to a deep purple-drunk color. The reaction mixture was then cooled down to -78 °C and (E)-isopropyl 3-(3-((tert-butoxycarbonyl)amino)phenyl)acrylate (**73**) (2.68 g, 0.00872 mol) in 15 mL anhydrous THF was added dropwise and allowed to stir for 2 h. Saturated NH_4Cl (50 mL) was then added to the reaction mixture and it was allowed to warm up to RT over 1.5 h. Ethyl acetate was added to the reaction mixture and extracted. The organic layer was then washed twice with 1 N HCl, dried over Na_2SO_4 , filtered, and rotovapped down. MeOH was then added to the residue and then rotovapped off to get rid of any residual ethyl acetate. (S)-isopropyl-3-(benzyl((R)-1-phenylethyl)amino)-3-(3-((tert-butoxycarbonyl)amino)phenyl)propanoate (**74**) was then recrystallized from hot MeOH and a total of 1.827 g was received with a 41% yield from the first crop. ^1H NMR

(400 MHz, CDCl₃) δ 0.997 (d, $J=6.24$, 3H), 1.05 (d, $J=6.24$, 3H), 1.25 (d, $J=6.84$ Hz, 3H), 1.53 (m, 14H), 2.53 (m, 2H), 3.68 (s, 2H), 3.98 (q, $J=6.8$, 1H), 4.38 (m, 1H), 4.79 (septet, $J=6.28$, 1H), 6.43 (s, 1H), 7.07 (m, 1H), 7.15 (m, 1H), 7.21 (m, 4H), 7.28 (m, 3H), 7.31 (m, 2H), 7.35 (m, 1H), 7.41 (m, 2H). ¹³C NMR (400 MHz, CDCl₃) δ 16.27, 21.58, 21.59, 28.37, 37.82, 46.25, 50.91, 57.09, 59.55, 67.54, 80.41, 117.30, 118.27, 122.86, 126.55, 126.82, 127.88, 128.07, 128.12, 128.31, 128.39, 128.57, 128.73, 128.82, 137.50, 138.30, 141.55, 142.84, 144.07, 152.60, 171.30. IR (ATR, cm⁻¹) ν_{\max} : 3379, 2977, 2932, 2162, 1722, 1613, 1539, 1154. MS (ESI) m/z found 517 (M + H)⁺.



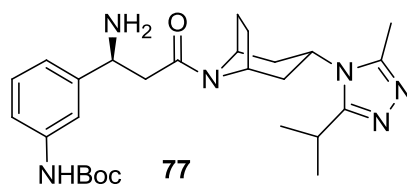
(S)-3-(benzyl((R)-1-phenylethyl)amino)-3-(3-((tert-butoxycarbonyl)amino)phenyl)propanoic acid (75). (S)-isopropyl-3-(benzyl((R)-1-phenylethyl)amino)-3-(3-((tert-butoxycarbonyl)amino)phenyl) propanoate (**74**) (1.4 g, 0.00271 mol) was dissolved in a 2:1 mixture of MeOH/H₂O (30 mL). To it LiOH (5 eq, 0.32 g, 0.01355 mol) was added will the reaction was stirring. The suspension was then refluxed (~85 °C) using a preheated oil bath under N₂ protection overnight. The reaction mixture was allowed to cool to RT and was adjusted to pH 1 using 10% HCl. The solution was then extracted with DCM three times and the resulting organic layers were dried over Na₂SO₄, filtered, and rotovapped down. No additional purification was required and a total of 1.12 g (S)-3-

(benzyl((R)-1-phenylethyl)amino)-3-(3-((tert-butoxycarbonyl) amino)phenyl)propanoic acid (**75**) was received with a 88% yield. ^1H NMR (400 MHz, CDCl_3) δ 1.28 (d, $J=6.9$, 3H), 1.54 (s, 9H), 2.43 (m, 1H), 2.88 (m, 1H), 6.64 (s, 1H), 7.04 (m, 1H), 7.28 (m, 6H), 7.34 (m, 6H), 7.47 (s, 1H). ^{13}C NMR (400 MHz, CDCl_3) δ 15.89, 27.27, 34.60, 49.88, 57.26, 58.44, 79.32, 116.97, 117.40, 118.65, 122.12, 126.61, 126.92, 127.74, 127.93, 128.04, 128.10, 128.47, 139.07, 140.60, 152.75, 161.25, 172.06. IR (ATR, cm^{-1}) ν_{max} : 3229, 2978, 2931, 2520, 1713, 1593, 1495, 1153.

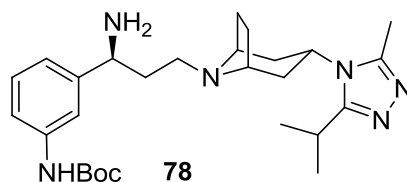


tert-butyl(3-((S)-1-(benzyl((R)-1-phenylethyl)amino)-3-((1R,3R,5S)-3-(3-isopropyl-5-methyl-4H-1,2,4-triazol-4-yl)-8-azabicyclo[3.2.1]octan-8-yl)-3-oxopropyl)phenyl) carbamate (**76**). In a 25 mL flask, (S)-3-(benzyl((R)-1-phenylethyl)amino)-3-(3-((tert-butoxycarbonyl)amino) phenyl)propanoic acid (**75**) (0.600 g, 0.0012643 mol) was dissolved in 6 mL anhydrous DCM. To the solution N-(3-Dimethylaminopropyl)-N'-ethylcarbodiimide hydrochloride (1.5 eq, 0.364 g, 0.0018965 mol), 1-hydroxybenzotriazole hydrate (1.5 eq, 0.256 g, 0.0018965 mol), triethylamine (3 eq, 0.54 mL, 0.003793 mol), and 4 Å molecular sieves were added and stirred under nitrogen protection at 0 °C for 0.5 h. (1R,3s,5S)-3-(3-isopropyl-5-methyl-4H-1,2,4-triazol-4-yl)-8-azabicyclo[3.2.1]octane (**86**) (1.2 eq, 0.314 g, 0.0015172 mol) was then added to the

reaction mixture and allowed to proceed to room temperature over the period of 96 h, and monitored via TLC (20:1 DCM:MeOH). Once completed, the reaction mixture was filtered and the DCM was evaporated under reduced pressure. The reaction mixture was then washed once with brine. The organic layer was dried over anhydrous sodium sulfate, filtered and evaporated under reduced pressure. Column chromatography was then conducted (20:1 DCM:MeOH) and a total of 0.645 g of a yellow oil, tert-butyl(3-((S)-1-(benzyl((R)-1-phenylethyl)amino)-3-((1R,3R,5S)-3-(3-isopropyl-5-methyl-4H-1,2,4-triazol-4-yl)-8-azabicyclo [3.2.1]octan-8-yl)-3-oxopropyl)phenyl)carbamate (**76**), was received with a final yield of 74%. ¹H NMR (400 MHz, CDCl₃) δ 1.31 (m, 9H), 1.51 (m, 11H), 1.71 (m, 4H), 1.87 (m, 2H), 2.06 (m, 1H), 2.12 (s, 1H), 2.26 (s, 2H), 2.56 (m, 2H), 2.83 (septet, J=6.56, 1H), 3.75 (m, 3H), 4.02 (m, 1H), 4.38 (m, 2H), 4.64 (m, 1H), 6.54 (s, 1H), 7.17 (m, 5H), 7.32 (m, 5H), 7.45 (m, 3H), 7.59 (s, 1H). ¹³C NMR (400 MHz, CDCl₃) δ 10.51, 19.46, 19.52, 19.75, 26.55, 28.28, 28.36, 28.55, 35.01, 37.29, 38.61, 39.99, 41.01, 50.63, 50.88, 51.30, 54.19, 56.49, 64.46, 80.83, 119.62, 120.95, 123.29, 126.37, 126.71, 127.31, 127.89, 127.98, 128.01, 128.14, 129.59, 142.73, 144.02, 145.35, 153.55, 166.19, 176.81. IR (ATR, cm⁻¹) ν_{max}: 3247, 2972, 2931, 2185, 2050, 1716, 1632, 1529, 1436, 1158.

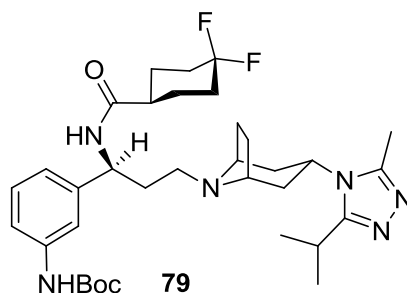


tert-butyl(3-((S)-1-amino-3-((1R,3R,5S)-3-(3-isopropyl-5-methyl-4H-1,2,4-triazol-4-yl)-8-azabicyclo[3.2.1]octan-8-yl)-3-oxopropyl)phenyl)carbamate (77). In a 250 mL hydrogenation flask, acetic acid (2 eq, 0.166 mL, 0.0029) was added to 60 mL MeOH. To that, 1-(trifluoromethyl)-4-(4-isopropoxy-3-nitrophenyl)piperazine (1.0 g, 0.00145 mol) was added to the solution along with 20 % w/w palladium on carbon (0.2 g, 10% w/w). The flask was placed on a hydrogenator at 60 psi H₂ gas for 48 h, and monitored via TLC (20:1:0.01 DCM:MeOH:NH₄OH). Once completed, the reaction mixture was vacuum filtered through celite, and then evaporated under reduced pressure. Column chromatography was then conducted (20:1 DCM:MeOH, NH₄OH) and a total of 0.66 g of a yellow oil, tert-butyl(3-((S)-1-amino-3-((1R,3R,5S)-3-(3-isopropyl-5-methyl-4H-1,2,4-triazol-4-yl)-8-azabicyclo[3.2.1]octan-8-yl)-3-oxopropyl)phenyl)carbamate, was received with a final yield of 91%. ¹H NMR (400 MHz, CDCl₃) δ 0.90 (m, 1H), 1.39 (m, 7H), 1.57 (s, 9H), 1.90 (m, 9H), 2.24 (m, 2H), 2.36 (m, 3H), 2.69 (m, 2H), 2.95 (septet, J=6.88, 1H), 4.23 (m, 1H), 4.53 (m, 2H), 4.89 (s, 1H), 5.30 (s, 2H), 6.70 (s, 1H), 7.08 (m, 1H), 7.23 (m, 2H), 7.48 (m, 1H). IR (ATR, cm⁻¹) v_{max}: 3255, 2972, 2933, 2879, 2161, 1714, 1610, 1440, 1158. MS (ESI) m/z found 497 (M + H)⁺.



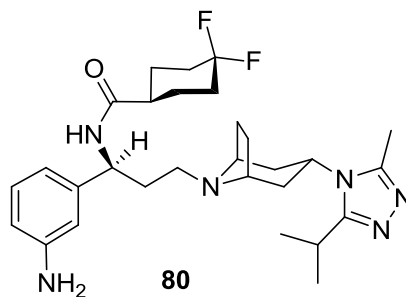
tert-butyl(3-((S)-1-amino-3-((1R,3R,5S)-3-(3-isopropyl-5-methyl-4H-1,2,4-triazol-4-yl)-8-azabicyclo[3.2.1]octan-8-yl)propyl)phenyl)carbamate (**78**). Lithium aluminum hydride (5 eq, 0.191 g, 0.005035 mol) was added to 15 mL anhydrous THF at 0 °C under N₂ protection. To the suspension tert-butyl(3-((S)-1-amino-3-((1R,3R, 5S)-3-(3-isopropyl-5-methyl-4H-1,2,4-triazol-4-yl)-8-azabicyclo[3.2.1]octan-8-yl)-3-oxopropyl)phenyl)carbamate (**77**) (0.5 g, 0.001007 mol) was dissolved in 15 mL anhydrous THF and added dropwise. The resultant mixture was stirred at 0 °C for 15 min and then allowed to reach RT over a 3 h period. The reaction mixture was then cooled to 0 °C in an ice bath and quenched with the sequential addition of 0.2 mL H₂O, 0.2 mL 4 N NaOH, and then 0.6 mL H₂O and stirred at RT for 1 h. The suspension was filtered and the filtrate was washed with THF and diethyl ether. The organic filtrates were combined, dried over Na₂SO₄, filtered, and then evaporated to dryness. After column chromatography (10:1, DCM:MeOH) a total of 0.38 g tert-butyl(3-((S)-1-amino-3-((1R,3R,5S)-3-(3-isopropyl-5-methyl-4H-1,2,4-triazol-4-yl)-8-azabicyclo[3.2.1]octan-8-yl)propyl)phenyl)carbamate (**78**), with a yield of 79%. ¹H NMR (400 MHz, CDCl₃) δ 1.254 (s, 1H), 1.386 (m, 8H), 1.508 (broad s, 10H), 1.611 (m, 6H), 1.769 (m, 2H), 1.841-2.000 (m, 7H), 2.050 (m, 3H), 2.238 (m, 3H), 2.464 (m, 5H), 2.541 (s, 1H), 2.987 (septet, *J*=6.8 Hz, 1H), 3.405 (m, 2H), 3.747 (m, 1H), 4.101 (t, *J*=6.7 Hz, 1H), 4.282 (m, 1H),

5.299 (s, 1H), 6.540 (broad s, 1H), 7.012 (d, $J=7.6$ Hz, 1H), 7.130 (m, 1H), 7.229 (m, 1H), 7.519 (s, 1H). IR (ATR, cm^{-1}) ν_{max} : 3362, 2930, 2875, 1682, 1444, 1365, 1159.



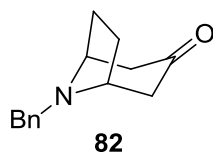
tert-butyl(3-((S)-1-(4,4-difluorocyclohexanecarboxamido)-3-((1R,3R,5S)-3-(3-isopropyl-5-methyl-4H-1,2,4-triazol-4-yl)-8-azabicyclo[3.2.1]octan-8-yl)propyl)phenyl)carbamate (79). In a 10 mL flask, 4,4-difluorocyclohexanecarboxylic acid (**88**) (1.3 eq, 0.132 g, 0.0008008 mol) was dissolved in 2 mL anhydrous DCM. To the solution N-(3-dimethylaminopropyl)-N'-ethylcarbodiimide hydrochloride (1.5 eq, 0.177 g, 0.000924 mol), 1-hydroxybenzotriazole hydrate (1.5 eq, 0.125 g, 0.000924 mol), triethylamine (3 eq, 0.26 mL, 0.001848 mol), and 4 Å molecular sieves were added and stirred under nitrogen protection at 0 °C for 0.5 hours. tert-butyl(3-((S)-1-amino-3-((1R,3R,5S)-3-(3-isopropyl-5-methyl-4H-1,2,4-triazol-4-yl)-8-azabicyclo[3.2.1]octan-8-yl)propyl)phenyl)carbamate (**78**) (0.3 g, 0.000616 mol) was then added to the reaction mixture and allowed to proceed to room temperature over the period of 48 h, and monitored via TLC (20:1 DCM:MeOH, NH_4OH). Once completed, the reaction mixture was filtered, washed with brine, dried over Na_2SO_4 and the DCM was evaporated under reduced pressure. Column chromatography was then conducted (20:1 DCM:MeOH, NH_4OH) and a total of 0.234 g of a yellow oil tert-butyl(3-((S)-1-(4,4-

difluorocyclohexanecarboxamido)-3-((1R,3R,5S)-3-(3-isopropyl-5-methyl-4H-1,2,4-triazol-4-yl)-8-azabicyclo[3.2.1]octan-8-yl)propyl)phenyl)carbamate (**79**), was received with a final yield of 60%. ¹H NMR (400 MHz, CDCl₃) δ 1.38 (d, *J*=6.12, 6H), 1.51 (s, 9H), 1.74 (m, 9H), 1.95 (m, 4H), 2.05 (m, 2H), 2.18 (m, 5H), 2.43 (m, 2H), 2.51 (s, 3H), 2.98 (septet, *J*=6.88, 1H), 3.39 (m, 2H), 4.30 (septet, *J*=6.04, 1H), 5.10 (quartet, *J*=7.24, 1H), 6.59 (m, 2H), 6.93 (d, *J*=7.64, 1H), 7.07 (m, 1H), 7.24 (m, 1H), 7.24 (t, *J*=7.8, 1H), 7.55 (s, 1H). ¹³C NMR (400 MHz, CDCl₃) δ 13.22, 21.66, 25.89, 25.92, 26.07, 26.84, 28.34, 32.55, 32.79, 33.04, 34.69, 35.12, 35.31, 42.89, 47.26, 47.66, 52.20, 53.43, 58.16, 58.79, 116.23, 117.41, 121.16, 129.29, 138.94, 142.98, 150.63, 152.67, 159.14, 173.29. IR (ATR, cm⁻¹) ν_{max}: 3257, 2968, 2936, 2875, 2227, 2161, 1980, 1717, 1655, 1527, 1443, 1367, 1236, 1158. MS (ESI) *m/z* found 529 (M + H)⁺.

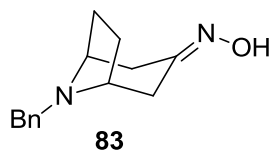


N-((S)-1-(3-aminophenyl)-3-((1R,3R,5S)-3-(3-isopropyl-5-methyl-4H-1,2,4-triazol-4-yl)-8-azabicyclo[3.2.1]octan-8-yl)propyl)-4,4-difluorocyclohexanecarboxamide (**80**). tert-butyl(3-((S)-1-(4,4-difluorocyclohexanecarboxamido)-3-((1R,3R,5S)-3-(3-isopropyl-5-methyl-4H-1,2,4-triazol-4-yl)-8-azabicyclo[3.2.1]octan-8-yl)propyl)phenyl)carbamate (**79**) (0.2 g, 0.0003181 mol) was dissolved in 5 mL anhydrous DCM and stirred at 0 °C. To the solution, 10% trifluoro acetic acid by volume (0.5 mL) was added dropwise and

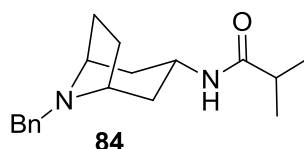
the solution was allowed to reach RT and stirred for 2 h. The solution was then cooled to 0 °C in an ice bath and saturated aqueous Na₂CO₃ was added and the aqueous layer was adjusted to pH 12 and extracted three times with DCM. The combined organic layers were then washed with brine, dried over Na₂SO₄, filtered, and evaporated to dryness. A total of 0.215 g N-((S)-1-(3-aminophenyl)-3-((1R,3R,5S)-3-(3-isopropyl-5-methyl-4H-1,2,4-triazol-4-yl)-8-azabicyclo[3.2.1]octan-8-yl)propyl)-4,4-difluorocyclohexanecarboxamide (**80**) of a yellow oil was received with quantitative yield. ¹H NMR (400 MHz, CDCl₃) δ 0.91 (m, 5H), 1.31 (m, 6 H), 1.37 (d, *J*=6.84, 6H), 1.42 (m, 1H), 1.67 (m, 7H), 1.83 (m, 4H), 1.93 (m, 5H), 2.04 (m, 2H), 2.16 (m, 4H), 2.24 (m, 1H), 2.44 (m, 2H), 2.50 (s, 3H), 2.98 (m, 1H), 3.39 (s, 2H), 3.70 (s, 2H), 4.19 (m, 2H), 4.29 (m, 1H), 5.00 (quartet, *J*=6.92, 1H), 6.38 (m, 1H), 6.59 (m, 2H), 6.65 (d, *J*=7.68, 1H), 7.13 (t, *J*=7.88, 1H), 7.52 (m, 1H), 7.69 (m, 1H). ¹³C NMR (400 MHz, CDCl₃) δ 10.96, 13.19, 14.05, 21.66, 22.99, 23.76, 25.86, 25.99, 26.10, 26.83, 28.93, 30.37, 32.60, 32.83, 33.08, 34.71, 35.16, 35.32, 38.75, 42.95, 47.25, 47.81, 52.13, 58.23, 58.76, 68.17, 113.37, 114.32, 116.26, 128.81, 129.80, 130.88, 132.47, 143.04, 146.86, 150.67, 159.13, 167.76, 173.15. IR (ATR, cm⁻¹) ν_{max}: 3318, 3224, 2957, 2932, 2873, 2257, 2177, 2035, 1979, 1724, 1651, 1519, 1455, 1345, 1165, 1105.



(1R)-8-benzyl-8-azabicyclo[3.2.1]octan-3-one (82). The synthesis of (1R)-8-benzyl-8-azabicyclo[3.2.1]octan-3-one (**82**) has been previously described elsewhere.^{149,152} Briefly, under N₂ protection 2,5-dimethyltetrahydrofuran (7.8 mL, 0.06 mol) was dissolved in 50 mL of 2 M HCl and stirred for 1 h and then cooled to 0 °C. To it, benzylamine (8 mL, 0.073 mol), acetonedicarboxylic acid (8.85 g, 0.06 mol), and aqueous AcONa (3 g in 27 mL H₂O) were added sequentially. The resulting solution was stirred at RT for 1 h and then heated to between 60-70 °C for 1.5 h. The reaction was cooled to RT and its pH was adjusted to pH 1-2 with 2 M HCl and washed with diethyl ether. The aqueous layer was then brought up to pH 6-7 with saturated aqueous NaHCO₃ and extracted 3 times with DCM. The organic layers were dried over Na₂SO₄. The crude product was purified with column chromatography (4:1, Hex:EA) and a total of 3.914 g (1R)-8-benzyl-8-azabicyclo[3.2.1]octan-3-one (**82**) was received at a yields of 30%. ¹H NMR (400 MHz, CDCl₃) δ 1.64 (m, 2H), 2.12 (m, 2H), 2.18 (d, *J*=17.2 Hz, 2H), 2.66 (m, 2H), 3.49 (m, 2H), 3.75 (s, 2H), 7.27 (t, *J*=7.16 Hz, 1H), 7.34 (t, *J*=7.12 Hz, 2H), 7.41 (d, *J*=7.2, 2H).

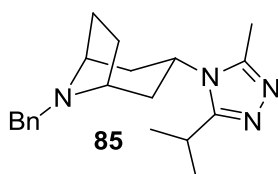


(1R,5S,Z)-8-benzyl-8-azabicyclo[3.2.1]octan-3-one oxime (83). Under N₂ protection, H₂NOH-HCl (1.125 eq, 1.423 g, 0.02049 mol), and NaHCO₃ (1.1 eq, 1.694 g, 0.020031 mol) were stirred in H₂O (50 mL) for 10 min. (1R)-8-benzyl-8-azabicyclo[3.2.1]octan-3-one (**82**) (3.914 g, 0.01821 mol) in 50 mL EtOH was added and then refluxed for 2 h. The reaction mixture was then cooled to RT and the EtOH removed through evaporation. The aqueous solution was then extracted with 50 mL five times, the combined organic layers were dried over Na₂SO₄, filtered and evaporated to dryness. A total of 4.422 g (1R,5S,Z)-8-benzyl-8-azabicyclo[3.2.1]octan-3-one oxime (**83**) was received (90% yield). ¹H NMR (400 MHz, CDCl₃) δ 1.501 (m, 1H), 1.627 (m, 1H), 2.029 (m, 2H), 2.111 (d, *J*=14.7 Hz, 1H), 2.213 (dd, *J*= 11.7, 3.8 Hz, 1H), 2.575 (dd, *J*=11.36, 3.32 Hz, 1H), 2.961 (d, *J*=15.4, 1H), 3.346 (m, 2H), 3.653 (s, 2H), 7.238 (d, *J*=7.44 Hz, 1H), 7.328 (m, 2H), 7.389 (d, *J*=7.16 Hz, 2H), 8.086 (broad s, 1H).



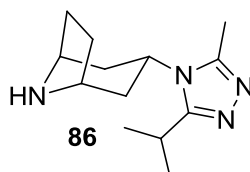
N-((1R,3s,5S)-8-benzyl-8-azabicyclo[3.2.1]octan-3-yl)isobutyramide (84). Sodium metal (7.52 g, 0.3271 mol) was added to anhydrous toluene (60 mL) at RT and then heated to reflux. (1R,5S,Z)-8-benzyl-8-azabicyclo[3.2.1]octan-3-one oxime (**83**) (4.422 g, 0.016355 mol) in a mixture of 50 mL toluene and 25 mL 1-pentanol was added dropwise

to the refluxing solution for 2 h until a thick white slurry formed. The reaction was cooled to 60 °C and isopropyl alcohol (40 mL) was added, and then the reaction mixture was cooled to RT and 60 mL H₂O was added. The pH was adjusted to 1 with concentrated HCl and the organic layer was separated out. Ethyl acetate (60 mL) was added to the aqueous layer and adjusted to pH 12. The organic layer was separated out, dried over Na₂SO₄ and evaporated to dryness. The product was then recrystallized in hot ethyl acetate and a total of 2.309 g N-((1R,3s,5S)-8-benzyl-8-azabicyclo[3.2.1]octan-3-yl)isobutyramide (**84**) was received in the first crop with a yield of 58%. ¹H NMR (400 MHz, CDCl₃) δ 1.113 (d, *J*=6.88 Hz, 6H), 1.494 (td, *J*=8.08, 1.28 Hz, 2H), 1.818 (m, 2H), 2.038 (m, 2H), 2.267 (septet, *J*=6.88, 2H), 3.221 (t, *J*=3.2 Hz, 2H), 3.535 (s, 2H), 4.151 (m, 1H), 5.170 (dd, *J*=6.88 Hz, 1H), 7.222 (d, *J*=7.24, 1H), 7.56 (t, *J*=7.56, 2H), 7.362 (d, *J*=7 Hz, 2H).



(1R,3s,5S)-8-benzyl-3-(3-isopropyl-5-methyl-4H-1,2,4-triazol-4-yl)-8-azabicyclo[3.2.1]octane (**85**). N-((1R,3s,5S)-8-benzyl-8-azabicyclo[3.2.1]octan-3-yl)isobutyramide (**84**) (2.704 g, 0.009464 mol) was dissolved in anhydrous DCM (40 mL) and stirred under N₂ at 0 °C. PCl₅ (1.5 eq, 2.96 g, 0.014215 mol) was added portion-wise and allowed to stir for 30 min. Next, pyridine (3 eq, 2.29 mL, 0.028429 mol) was added dropwise and the reaction was allowed to reach RT and stirred for 4 h. The reaction mixture was cooled to 0

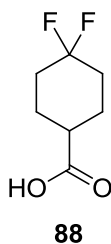
°C and t-amyl-alcohol (40 mL) was added and AcNHNH₂ (2 eq, 1.4 g, 0.018928 mol) was added portion-wise and stirred at 0 °C for 30 min and then at RT overnight. The reaction mixture was evaporated to dryness and 30 mL toluene was added along with 2.4 mL AcOH (~0.0014 mol) under N₂ protection and refluxed for 2 hours. The reaction mixture was cooled in an ice bath and then rotovapped down. DCM and H₂O were added and the pH of the aqueous layer was adjusted to pH >9 with 2 N NaOH and the organic layer was extracted, dried over Na₂SO₄, filtered, and evaporated to dryness. The crude product was recrystallized using a mixture of hexane and ethyl acetate and a total of 1.171 g (1R,3s,5S)-8-benzyl-3-(3-isopropyl-5-methyl-4H-1,2,4-triazol-4-yl)-8-azabicyclo[3.2.1]octane (**85**) at a yield of 38%. ¹H NMR (400 MHz, CDCl₃) δ 1.394 (d, *J*=8.4 Hz, 6H), 1.708-1.642 (m, 4H), 2.189 (m, 2H), 2.279 (td, *J*=9.88, 2.6 Hz, 1H), 3.359 (d, *J*=2.84, 2H), 4.318 (m, 1H), 7.270 (d, *J*=7.08 Hz, 1H), 7.361 (m, 4H).



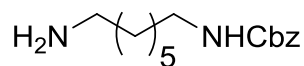
(1R,3s,5S)-3-(3-isopropyl-5-methyl-4H-1,2,4-triazol-4-yl)-8-azabicyclo[3.2.1]octane

(86). In a 250 mL hydrogenation flask, (1R,3s,5S)-8-benzyl-3-(3-isopropyl-5-methyl-4H-1,2,4-triazol-4-yl)-8-azabicyclo[3.2.1]octane (**85**) (3 g, 0.0092 mol) was dissolved in 60 mL MeOH. To that, 10% Pd/C (0.3 g, 10% w/w) was added. The flask was placed on a hydrogenator at 60 psi H₂ gas for 24 h, and monitored via TLC (5:1:0.01 DCM:MeOH:NH₄OH). Once completed, the reaction mixture was vacuum filtered

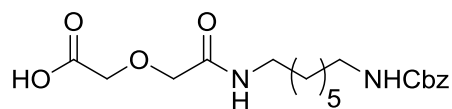
through celite, and then evaporated under reduced pressure. Hexane was added to the residue to crystallize the product and in the first crop, 2.1 g (1R,3s,5S)-3-(3-isopropyl-5-methyl-4H-1,2,4-triazol-4-yl)-8-azabicyclo[3.2.1]octane (**86**) was received with a 90% yield. ^1H NMR (400 MHz, MeOD) δ 1.065 (d, $J=6.88$ Hz, 6H), 1.437 (td, $J=10.4, 1.2$ Hz, 2H), 1.842-1.749 (m, 6H), 2.373 (septet, $J=6.84$ Hz, 1H), 3.345 (s, 2H), 3.508 (broad s, 2H), 4.067 (m, 1H).



4,4-difluorocyclohexanecarboxylic acid (**88**). Ethyl 4-oxycyclohexanecarboxylate (1.13 g, 0.00667 mol) was dissolved in anhydrous DCM (10 mL) in an HDPE container. To it, Fluolead (1.5 eq, 2.5 g, 0.00999 mol) was added and stirred under N_2 at 0 °C. HF-pyridine (0.4 eq, 0.64 mL, 0.00264 mol) was added to the vessel and the reaction was allowed to reach RT. After 5 hours, the reaction mixture was quenched with saturated aqueous NaHCO_3 . The organic layer was allowed to stir at RT and 2 N NaOH for 1 h and washed with DCM and the aqueous layer was acidified to pH 1 and extracted with DCM. A total of 0.435 g 4,4-difluorocyclohexanecarboxylic acid (**88**) (99:1, difluoro:monofluoro-vinyl byproduct) at a 27% yield. ^1H NMR (400 MHz, CDCl_3) δ 1.872-1.753 (m, 4H), 1.984-1.881 (m, 4H), 2.498-2.278 (m, 1H).

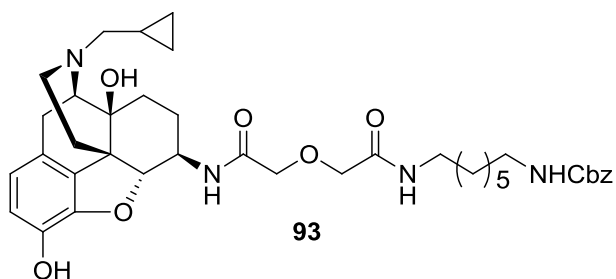
**91**

(7-amino-heptyl)-carbamic acid benzyl ester (91). The synthesis of **91** was previously described.¹³⁴ 1,7-Diaminoheptane (1.1 eq, 1.5 g, 0.01152 mol) was dissolved in 250 mL DCM/MeOH (1:1) and stirred in an ice-water bath at 5 °C. To it, benzylchloroformate (1 eq 1.787 g, 0.010473 mol) in 250 mL DCM was added dropwise over a period of 48 h while keeping the temperature at 5 °C. After the addition, the reaction mixture was allowed to stir for an additional 24 h. The reaction mixture was evaporated down to ~50 mL and the H₂O was added and the pH was adjusted to pH 2 with 6 N HCl. The layers were separated and the aqueous layer was washed with DCM and then adjusted to pH 12 with 10 N NaOH. The aqueous layer was then extracted with DCM, dried over Na₂SO₄. The crude product was then purified with column chromatography (10:1 DCM:MeOH, NH₄OH) and recrystallized with hot DCM. A total of 0.482 g (7-amino-heptyl)-carbamic acid benzyl ester (**91**) was received with a 16% yield. ¹H NMR (400 MHz, CDCl₃) δ 1.314 (broad s, 6H), 1.469 (broad s, 4H), 1.820 (s, 1H), 2.007 (s, 1H), 2.339 (broad s, 2H), 2.708 (t, *J*=7.08 Hz, 1H), 3.172 (q, *J*=6.4 Hz, 2H), 5.092 (s, 2H), 7.315 (m, 5H).

**92**

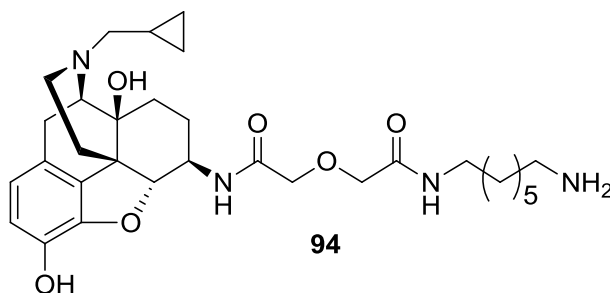
[(7-benzyloxycarbonylamino-heptylcarbamoyl)-methoxy]-acetic acid (92). (7-amino-heptyl)-carbamic acid benzyl ester (**91**) (0.55 g, 0.0021 mol) was dissolved in 10 mL

THF, stirred at RT, and to it, diglycolic anhydride (1.05 eq, 0.254 g, 0.002205 mol) was added. The solution was stirred overnight and then evaporated to dryness. The crude product was recrystallized with ethyl acetate and hexane giving 0.734 g of [(7-benzyloxycarbonylamino-heptylcarbamoyl)-methoxy]-acetic acid (**92**) at a yield of 92%. ^1H NMR (400 MHz, CDCl_3) δ 1.235 (s, 6H), 1.368 (m, 4H), 2.963 (q, $J=6.6$ Hz, 2H), 3.071 (q, $J=6.6$ Hz, 2H), 3.323 (s, 4H), 3.939 (s, 2H), 4.089 (d, $J=4.2$ Hz, 3H), 4.998 (s, 2H), 7.214 (t, $J=5.5$ Hz, 1H), 7.379-7.286 (m, 5H), 7.814 (t, $J=5.5$ Hz, 1H), 12.779 (s, 1H).



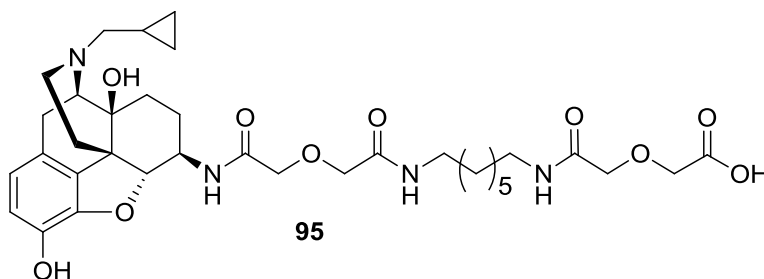
benzyl(7-(2-(2-(((4R,4aS,7R,7aR,12bS)-3-(cyclopropylmethyl)-4a,9-dihydroxy-2,3,4,4a,5,6,7,7a-octahydro-1H-4,12-methanobenzofuro[3,2-e]isoquinolin-7-yl)amino)-2-oxoethoxy)acetamido)heptyl)carbamate (**93**). In a 10 mL flask, [(7-benzyloxycarbonylamino-heptylcarbamoyl)-methoxy]-acetic acid (**92**) (0.9 eq, 0.414 g, 0.0010872 mol) was dissolved in 3 mL anhydrous DMF. To the solution N-(3-Dimethylaminopropyl)-N'-ethylcarbodiimide hydrochloride (1.5 eq, 0.347 g, 0.001812 mol), 1-hydroxybenzotriazole hydrate (1.5 eq, 0.245 g, 0.001812 mol), triethylamine (6 eq, 1.01 mL, 0.007248 mol), and 4 Å molecular sieves were added and stirred under nitrogen protection at 0 °C for 0.5 h. 6β-naltrexamine hydrochloride salt (**98**) (0.5 g,

0.001208 mol) was then added to the reaction mixture and allowed to proceed to room temperature over the period of 96 h, and monitored via TLC (20:1 DCM:MeOH, NH₄OH). Once completed, the reaction mixture was filtered, washed with brine, dried over Na₂SO₄ and the DCM was evaporated under reduced pressure. Column chromatography was then conducted (20:1 DCM:MeOH, NH₄OH) and a total of 0.33 g of benzyl(7-(2-(2-(((4R,4aS,7R,7aR,12bS)-3-(cyclopropylmethyl)-4a,9-dihydroxy-2,3,4,4a,5,6,7,7a-octahydro-1H-4,12-methanobenzofuro[3,2-e]isoquinolin-7-yl)amino)-2-oxoethoxy)acetamido)heptyl)carbamate (**93**), was received with a final yield of 42%. ¹H NMR (400 MHz, DMSO) δ 0.116 (m, 2H), 0.454 (d, *J*=7.6 Hz, 2H), 0.836 (1H), 1.256 (broad s, 8H), 1.434 (m, 6H), 1.773 (m, 1H), 1.977 (m, 1H), 2.153 (m, 1H), 2.330 (m, 2H), 2.576 (m, 2H), 2.981 (m, 4H), 3.159 (m, 3H), 3.930 (m, 4H), 4.579 (d, *J*=7.6 Hz, 1H), 4.883 (s, 1H), 4.995 (s, 2H), 5.745 (s, 2H), 6.529 (dd, *J*=15.6, 8.04 Hz), 7.191 (broad s, 1H), 7.336 (m, 5H), 8.007 (t, *J*=5.52 Hz, 1H), 8.200 (d, *J*=8.4 Hz, 1H), 9.008 (s, 1H).



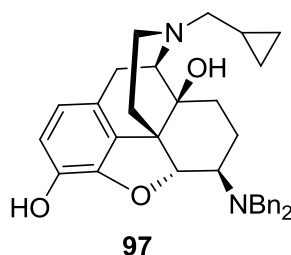
N-(7-aminoheptyl)-2-(2-(((4R,4aS,7R,7aR,12bS)-3-(cyclopropylmethyl)-4a,9-dihydroxy-2,3,4,4a,5,6,7,7a-octahydro-1H-4,12-methanobenzofuro[3,2-e]isoquinolin-7-yl)amino)-2-oxoethoxy)acetamide (**94**). In a 250 mL hydrogenation flask, **93** (0.2 g, 0.0002837 mol)

was dissolved in 60 mL MeOH. To that, 10% Pd/C (0.2 g, 10% w/w) was added. The flask was placed on a hydrogenator at 60 psi H₂ gas for 24 h, and monitored via TLC (5:1:0.01 DCM:MeOH:NH₄OH). Once completed, the reaction mixture was vacuum filtered through celite, and then evaporated under reduced pressure. In total, 0.082 g **94** was received with a crude yield of 51% and used without further purification. ¹H NMR (400 MHz, DMSO) δ 0.1096 (m, 2H), 0.458 (d, *J*=7.56 Hz, 2H), 0.839 (m, 1H), 1.269 (broad s, 9H), 1.448 (m, 6H), 1.776 (m, 1H), 1.848 (s, 3H), 1.972 (td, *J*=3.5, 8.7 Hz, 1H), 2.140 (td, *J*=4.9, 7.3 Hz, 1H), 2.333 (m, 3H), 2.577-2.64 (m, 3H), 2.945-3.015 (m, 3H), 3.269-3.339 (m, 8H), 3.508-3.600 (m, 2H), 3.859-3.893 (m, 1H), 3.933 (d, *J*=3.6 Hz, 4H), 4.000-4.300 (m, 5H), 4.577 (d, *J*=7.8 Hz, 1H), 6.508 (d, *J*=8.1 Hz, 1H), 6.569 (d, *J*=8.0 Hz, 1H), 8.037 (m, 1H), 8.221 (m, 1H).



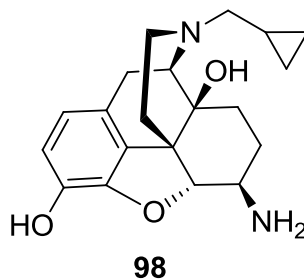
19-(((4R,4aS,7R,7aR,12bS)-3-(cyclopropylmethyl)-4a,9-dihydroxy-2,3,4,4a,5,6,7,7a-octahydro-1H-4,12-methanobenzofuro[3,2-e]isoquinolin-7-yl)amino)-5,15,19-trioxo-3,17-dioxo-6,14-diazanonadecan-1-oic acid (**95**). **94** (0.082 g, 0.00014367 mol) was dissolved in 1 mL DMF, stirred at RT, and to it, diglycolic anhydride (1.0 eq, 0.0179 g, 0.00014367 mol) were added. The solution was stirred overnight and then evaporated to dryness. The crude product was recrystallized with ethyl acetate and hexane giving 0.1 g

of **95** at quantitative yield. ^1H NMR (400 MHz, DMSO) δ 0.185 (m, 2H), 0.507 (m, 2H), 0.894 (m, 1H), 1.304 (m, 8H), 1.445 (m, 6H), 1.800 (m, 1H), 2.015-2.452 (m, 2H), 2.539-2.890 (m, 4H), 3.043-3.167 (m, 6H), 3.243-3.682 (m, 11H), 3.820-3.900 (m, 2H), 3.928 (m, 6H), 4.004 (m, 2H), 4.083-4.273 (m, 1H), 4.443-4.527 (m, 1H), 4.646-4.751 (m, 1H), 6.542-6.627 (m, 1H), 6.756-6.939 (m, 1H), 7.953-8.351 (m, 4 H).



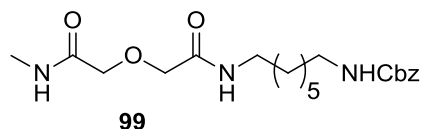
(4R,4aS,7R,7aR,12bS)-3-(cyclopropylmethyl)-7-(dibenzylamino)-2,3,4,4a,5,6,7,7a-octahydro-1H-4,12-methanobenzofuro[3,2-e]isoquinoline-4a,9-diol (**97**). Naltrexone, free base, (2.0 g, 0.00586 mol) was dissolved in 75 mL absolute EtOH and to it benzoic acid (1.2 eq, 0.859 g, 0.007032 mol) was added and allowed to stir for 30 minutes under N_0 protection. The EtOH was rotovapped off and toluene was added to remove any leftover H_2O . Anhydrous toluene (200 mL) was added, and to it benzoic acid (1.2 eq, 0.859 g, 0.007032 mol), dibenzylamine (1.2 eq, 1.34 mL, 0.007032), and a trace amount of p-toluenesulfonic acid were added. The reaction was refluxed under N_0 for 20 h with a Dean-Stark trap to remove produced H_2O . The reaction mixture was then concentrated to 50 mL. Absolute EtOH (200 mL), molecular sieves, and NaCNBH_4 (0.8 eq, 0.295 g, 0.004688 mol) were added and allowed to stir under N_0 protection overnight. The reaction mixture was then filtered, rotovapped, and then re-dissolved in chloroform and

3% aqueous NH_4OH was added. The chloroform layer was extracted and rotovapped down. **97** was then recrystallized from 9:1 MeOH/ H_2O to give 1.942 g at a 64% yield. ^1H NMR (400 MHz, CDCl_3) δ 0.094 (m, 2H), 0.495 (m, 2H), 0.815 (m, 1H), 1.230 (td, $J=10.4, 2.8$ Hz, 1H), 1.409 (dd, $J=10.3, 2.4$ Hz, 1H), 1.575 (m, 1H), 1.681 (m, 1H), 1.955-2.119 (m, 2H), 2.170-2.244 (m, 1H), 2.327 (m, 2H), 2.475 (dd, $J=12.6, 5.8$ Hz, 1H), 2.547-2.62 (m, 2H), 2.971 (m, 1H), 3.593 (d, $J=14.2$ Hz, 1H), 3.874 (m, 2H), 4.693 (d, $J=7.8$ Hz, 1H), 6.420 (d, $J=8$ Hz, 1H), 6.551 (d, $J=8$ Hz, 1H), 7.189 (m, 2H), 7.279 (m, 5H), 4.222 (d, $J=7.2$, 4H).



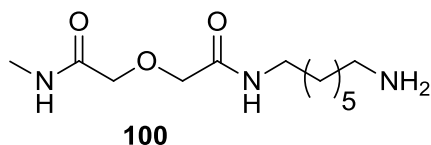
6 β -naltrexamine (98). In a 250 mL hydrogenation flask, **97** (1.0 g, 0.0019194 mol) was dissolved in 50 mL anhydrous MeOH. To that, 20% Pd/C (0.2 g, 10% w/w) and concentrated HCl (2.5 eq, 0.4 mL, 0.0047985 mol) were added. The flask was placed on a hydrogenator at 60 psi H_2 gas for 24 hours, and monitored via TLC (10:1:0.01 DCM:MeOH: NH_4OH). Once completed, the reaction mixture was vacuum filtered through celite, and then evaporated under reduced pressure. After crystallization with MeOH/ Et_2O , a total of 0.622 g **98** x 2 hydrochloride salt was received with yield of 78% in the first crop. ^1H NMR (400 MHz, DMSO) δ 0.387-0.521 (m, 2H), 0.533-0.6812 (m, 2H), 1.081 (m, 1H), 1.295 (m, 1H), 1.434 (m, 1H), 1.769 (m, 1H), 1.855 (m, 1H), 2.013

(m, 1H), 2.444 (m, 2H), 2.751 (m, 1H), 2.906 (m, 1H), 3.042 (m, 2H), 3.363 (m, 5H), 3.956 (m, 1H), 4.707 (d, $J=7.4$ Hz, 1H), 6.505 (s, 1H), 6.657 (d, $J=8.2$ Hz, 1H), 6.837 (d, $J=8.2$ Hz, 1H), 8.594 (broad s, 3H), 8.967 (broad s, 1H), 9.662 (s, 1H).

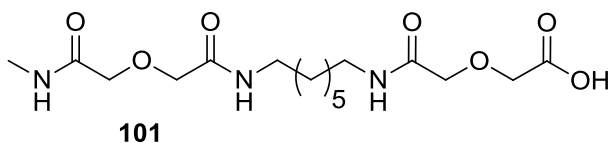


Benzyl (7-(2-(2-(methylamino)-2-oxoethoxy)acetamido)heptyl)carbamate (99). In a 10 mL flask, methylcarbamoylethoxy acetic acid (1.2 eq, 0.179 g, 0.0012168 mol) was dissolved in 2 mL anhydrous DMF. To the solution, N-(3-Dimethylaminopropyl)-N'-ethylcarbodiimide hydrochloride (1.5 eq, 0.292 g, 0.001521 mol), 1-hydroxybenzotriazole hydrate (1.5 eq, 0.206 g, 0.001521 mol), triethylamine (3 eq, 0.43 mL, 0.003042 mol), and 4 Å molecular sieves were added and stirred under nitrogen protection at 0 °C for 1 h. (7-Amino-heptyl)-carbamic acid benzyl ester (**91**) (0.268 g, 0.001014 mol) was then added to the reaction mixture and allowed to proceed to room temperature over the period of 96 h, and monitored via TLC (20:1 DCM:MeOH, NH₄OH). Once completed, the reaction mixture was filtered, washed with brine, dried over Na₂SO₄ and the DCM was evaporated under reduced pressure. Column chromatography was then conducted (30:1 DCM:MeOH, NH₄OH) and a total of 0.266 g of benzyl (7-(2-(2-(methylamino)-2-oxoethoxy)acetamido)heptyl)carbamate (**99**), was received with a final yield of 67%. ¹H NMR (400 MHz, CDCl₃) δ 1.325 (s, 6H), 1.511 (m, 6H), 2.869 (d, $J=4.9$ Hz, 3H), 3.175 (m, 2H), 3.288 (m, 2H), 4.032 (d, $J=4.3$ Hz, 4H), 4.796 (broad s, 1H), 5.092 (s, 2H), 6.448 (m, 2H), 7.324 (m, 1H), 7.349 (m, 4H). IR

(ATR, cm^{-1}) ν_{max} : 3330, 3096, 2931, 2855, 2284, 1685, 1652, 1533, 1391, 1377, 1269, 1128, 1107.



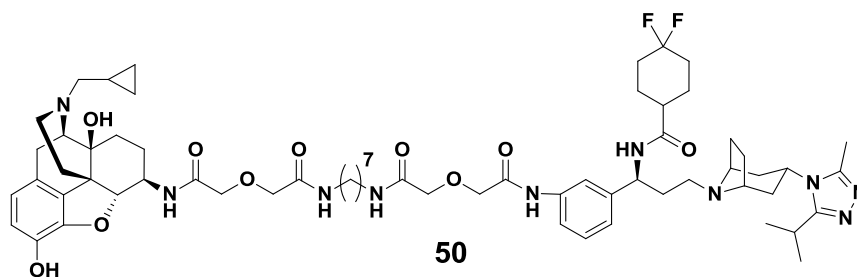
N-(7-aminoheptyl)-2-(2-(methylamino)-2-oxoethoxy)acetamide (100). In a 50 mL hydrogenation flask, benzyl (7-(2-(2-(methylamino)-2-oxoethoxy)acetamido)heptyl)carbamate (**99**) (0.252 g, 0.00064 mol) was dissolved in 30 mL MeOH. To that, 10% Pd/C (0.025 g, 10% w/w) was added. The flask was placed on a hydrogenator at 60 psi H_2 gas for 24 h, and monitored via TLC (10:1:0.01 DCM:MeOH: NH_4OH). Once completed, the reaction mixture was vacuum filtered through celite, and then evaporated under reduced pressure to give 0.15 g N-(7-aminoheptyl)-2-(2-(methylamino)-2-oxoethoxy)acetamide (**100**) at a yield of 90%. IR (ATR, cm^{-1}) ν_{max} : 3234, 3058, 2928, 2857, 2161, 1725, 1651, 1552, 1448, 1382, 1266, 1122, 1098. ^1H NMR (400 MHz, CDCl_3) δ 0.836 (m, 2H), 1.236 (broad s, 6H), 1.456 (m, 2H), 1.989 (m, 2H), 3.168 (s, 3H), 5.510 (m, 2H), 4.070 (broad s, 1H).



3,7,17-trioxo-5,19-dioxa-2,8,16-triazahenicosan-21-oic acid (101). N-(7-aminoheptyl)-2-(2-(methylamino)-2-oxoethoxy)acetamide (**100**) (0.142 g, 0.000548 mol) was dissolved

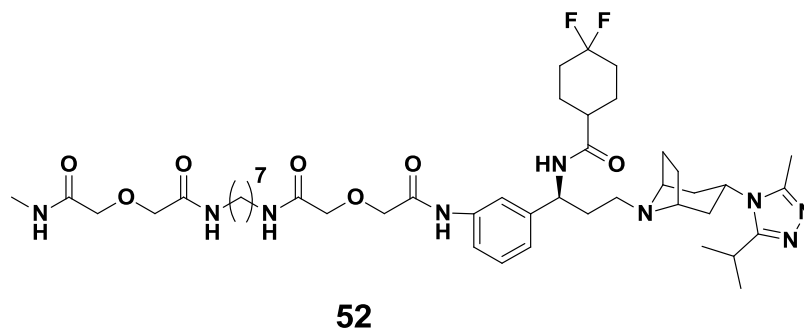
in 3 mL DMF, stirred at RT, and to it, diglycolic anhydride (1.0 eq, 0.064 g, 0.000548 mol) was added. The solution was stirred for 3 hours and then evaporated to dryness. A total of 0.212 g of 3,7,17-trioxo-5,19-dioxa-2,8,16-triazahenicosan-21-oic acid (**101**) was obtained at quantitative yield and used without further purification. IR (ATR, cm^{-1}) ν_{max} : 3306, 3090, 2929, 2857, 2532, 2161, 1735, 1633, 1551, 1436, 1220, 1130, 1047. ^1H NMR (400 MHz, CDCl_3) δ 0.836 (m, 2H), 1.259 (m, 12H), 1.429 (m, 4H), 1.989 (m, 2H), 2.632 (m, 2H), 3.111 (s, 3H).

4.1.4 CCR5-MOR Bivalent Ligands: Final Compounds



3-amino bivalent compound 50. In a 10 mL flask, **95** (1.0 eq, 0.073 g, 0.00010592 mol) was dissolved in 2 mL anhydrous DMF. To the solution N-(3-Dimethylaminopropyl)-N'-ethylcarbodiimide hydrochloride (1.5 eq, 0.031 g, 0.0015888 mol), 1-hydroxybenzotriazole hydrate (1.5 eq, 0.022 g, 0.00015888 mol), triethylamine (3 eq, 0.05 mL, 0.00031776 mol), and 4 Å molecular sieves were added and stirred under nitrogen protection at 0 °C for 1 h. **80** (0.056 g, 0.00010592 mol) was then added to the reaction mixture and allowed to proceed to room temperature over the period of 24 h, and monitored via TLC (20:1 DCM:MeOH, NH_4OH). After 24 h, more N-(3-dimethylaminopropyl)-N'-ethylcarbodiimide hydrochloride (1.5 eq, 0.031 g, 0.0015888

mol), 1-hydroxybenzotriazole hydrate (1.5 eq, 0.022 g, 0.00015888 mol), triethylamine (3 eq, 0.05 mL, 0.00031776 mol) were added. Once completed (5 days), the reaction mixture was filtered, washed with brine, dried over Na_2SO_4 and the DCM was evaporated under reduced pressure. Column chromatography was then conducted (30:1 DCM:MeOH, NH_4OH) and a total of 0.033 g of **50** was received with a final yield of 26%. ^1H NMR (400 MHz, DMSO) δ 0.099 (m, 2H), 0.45 (m, 2H), 0.83 (1H), 1.25 (m, 17H), 1.43 (m, 7H), 1.56 (m, 1H), 1.65 (m, 7H), 1.80 (m, 8H), 1.93 (m, 3H), 2.07 (m, 6H), 2.33 (m, 6H), 2.39 (s, 4H), 2.99 (m, 2H), 3.11 (m, 6H), 3.50 (m, 1H), 3.93 (d, $J=3.48$, 4H), 4.03 (s, 2H), 4.13 (s, 2H), 4.22 (m, 1H), 4.58 (d, $J=8.08$, 1H), 6.57 (d, $J=7.88$, 1H), 7.03 (d, $J=7.52$, 1H), 7.27 (t, $J=7.8$, 1H), 7.44 (d, $J=9.04$, 1H), 7.61 (s, 1H), 8.02 (t, $J=5.8$, 1H), 8.08 (t, $J=6.04$, 1H), 8.20 (d, $J=8.32$, 1H), 8.26 (d, $J=8.68$, 1H), 9.03 (s, 1H), 9.99 (s, 1H). ^{13}C NMR (400 MHz, CDCl_3) δ 3.74, 4.08, 9.26, 13.04, 21.59, 22.69, 23.53, 25.79, 25.92, 25.99, 26.28, 26.66, 28.25, 28.99, 29.31, 32.57, 32.82, 33.06, 35.00, 35.14, 38.77, 38.99, 42.66, 47.25, 47.84, 50.31, 51.89, 58.33, 58.46, 58.97, 59.26, 62.34, 70.07, 70.95, 71.38, 71.63, 91.65, 118.09, 118.24, 119.19, 119.31, 122.62, 129.23, 130.68, 137.87, 143.11, 150.79, 159.16, 167.75, 168.62, 168.86, 169.11, 173.88. IR (ATR, cm^{-1}) ν_{max} : 3271, 3078, 2931, 2858, 2161, 2036, 1979, 1655, 1536, 1447, 1323, 1251, 1106, 1034. MS (Tof-MS) m/z found 599.365 ($[\text{M} + 2]/2$)⁺.



3-amino monovalent compound 52. In a 10 mL flask, **100** (1.0 eq, 0.04 g, 0.000102 mol) was dissolved in 2 mL anhydrous DMF. To the solution N-(3-Dimethylaminopropyl)-N'-ethylcarbodiimide hydrochloride (1.5 eq, 0.03 g, 0.000153 mol), 1-hydroxybenzotriazole hydrate (1.5 eq, 0.021 g, 0.000153 mol), triethylamine (3 eq, 0.043 mL, 0.000306 mol), and 4 Å molecular sieves were added and stirred under nitrogen protection at 0 °C for 1 h. **80** (0.070 g, 0.0001053 mol) was then added to the reaction mixture and allowed to proceed to room temperature over the period of 7 days, and monitored via TLC (20:1 DCM:MeOH, NH₄OH). Once completed (7 days), the reaction mixture was filtered, washed with brine, dried over Na₂SO₄ and the DCM was evaporated under reduced pressure. Column chromatography was then conducted (30:1 DCM:MeOH, NH₄OH) and a total of 0.030 g of **50** was received with a final yield of 33%. ¹H NMR (400 MHz, MeOD) δ 1.175 (t, *J*=7 Hz, 3H), 1.366 (m, 7H), 1.416 (d, *J*=6.7 Hz, 6H), 1.558 (m, 4H), 1.808 (m, 5H), 1.957 (m, 1H), 2.103 (m, 2H), 2.252-2.443 (m, 10H), 2.787 (m, 8H), 3.129 (m, 1H), 3.477 (q, *J*=7 Hz, 2H), 3.668 (m, 1H), 4.031 (s, 4H), 4.143 (s, 2H), 4.226 (s, 3H), 4.337 (1H), 4.709 (m, 1H), 4.998 (m, 1H), 7.224 (d, *J*=7.4 Hz, 1H), 7.378 (t, *J*=7.9 Hz, 1H), 7.475 (d, *J*=8 Hz, 1H), 7.789 (s, 1H). ¹³C NMR (400 MHz, MeOD) δ 15.428, 21.724, 21.778, 26.698, 27.805, 29.916, 30.323, 33.873, 34.973, 36.455, 40.011,

40.068, 43.488, 63.77, 66.888, 71.428, 71.699, 71.982, 120.366, 121.413, 130.513, 139.581, 158.673, 165.968, 168.864, 171.961. IR (ATR, cm^{-1}) ν_{max} : 3256, 3054, 2933, 2857, 2531, 2161, 1979, 1651, 1544, 1444, 1108. MS (Tof-MS) m/z found: 443.788, 886.556 ($[M + 2]/2$ and $[M + H]$ respectively)⁺.

4.2 Biology Methods

4.2.1 Anti-Proliferation Assay

All cell lines, PC-3 and M12, were incubated at 37 °C in the presence of 5% CO₂. RPMI 1640 serum free media (GIBCO Invitrogen) containing 1 % L-glutamine, 0.1% ITS (insulin, 5 $\mu\text{g}/\text{mL}$; transferrin, 5 $\mu\text{g}/\text{mL}$; and selenium, 5 $\mu\text{g}/\text{mL}$; Collaborative Research, Bedford) and 0.1% gentamicin was used to cultivate all cells. M12 cells were first incubated in media with 5% fetal bovine serum (FBS); after 24 h serum free media was added with 0.01% epidermal growth factor (EGF). DU-145 and PC-3 cell lines were incubated in media containing 10% FBS at all times.

Prostate cancer tumor cells (PC-3, and M12) were plated into 96 well plates (BD Falcon, VWR) at a concentration of 1000 cells per well. Each cell line was plated in its respective serum containing media for a total concentration of 100 μL per well. After 24 hours, various concentrations of drugs in a 50 μL PBS solution were added to the cells. Control cells were given 50 μL of PBS. Seventy-two hours after incubation with drug, the serum containing media was replaced with 100 μL of a 9:1 solution of serum free media and WST-1 (Roche). After 3 h of incubation with WST-1, the absorbance of each well was measured by a microplate reader (FlexStation3, Molecular Devices). Absorbance

values were obtained using SoftMaxPro software (Molecular Devices) and non-linear regression curves were generated using Prism (GraphPad) to calculate IC₅₀ values.

4.2.2 Basal Cytotoxicity Assay

NIH-3T3 cells were routinely maintained in Dulbecco's Modified Eagle's Medium (DMEM, with high-glucose, L-glutamate, and sodium pyruvate; Invitrogen) supplemented with 10% new born calf serum (NBCS, Invitrogen) and 1% penicillin:streptomycin. Mouse embryonic fibroblast cells (NIH-3T3) were plated into 96 well plates (Costar, Corning) at a concentration of 2000 cells/well/100 μ L. Plates were incubated at 37.5 °C, 5% CO₂ for 24 h. At that point, media was discarded from the plates and 50 μ L of fresh culture media was added to the wells. Plates were then treated with 50 μ L of compounds at various concentrations in a dilution media made up of DMEM with 1% penicillin:streptomycin. Control wells were given 50 μ L of the dilution media. After 48 h of incubation, media was removed from the plates, each well was washed with 200 μ L of Hank's Buffered Salt Solution (HBSS, with calcium and magnesium, Invitrogen) and the rinsing solution was removed from the plates. To each well, 200 μ L of 25 μ g/mL of neutral red (NR, 0.33% solution in DPBS; Sigma) in DMEM containing 5% NBCS and 1% penicillin:streptomycin was added and plates were incubated for 3.0 \pm 0.1 h. After incubation, NR media was removed from the plates and each well was washed with 200 μ L of HBSS. The washing solution was decanted from the plates and 100 μ L of a solution containing 50% ethanol, 49% H₂O, and 1% glacial acetic acid was added. Plates were shaken rapidly for 20 min while being protected from

light. Once removed from the shaker, plates were allowed to sit for 5 min and absorbance at 540 nM was measured by a microplate reader (FlexStation3, Molecular Devices). Absorbance values were obtained using SoftMaxPro software (Molecular Devices) and TC50 values were calculated using non-linear regression curves on Prism (GraphPad).

4.2.3 Establishing a CCR5-hMOR-CHO Cell Line

Initially, hMOR-CHO cells¹⁵⁶ were cultured in DMEM/F12 (1:1) (Gibco) supplemented with 5% FBS, 1% penicillin-streptomycin, and 0.25 mg/mL Hygromycin B (Invitrogen). For stable selection of hMOR/hCCR5-CHO cells, hMOR-CHO cells were transfected with a plasmid encoding human CCR5-eYFP (GeneCopoeia, Inc.; Rockville, MD, USA; catalog number EX-Z0659-M16) using Lipofectamine 2000 (Invitrogen) and selected with 800 µg/mL Geneticin (Gibco) using the manufacturers' protocol. To further enrich the population of stably transfected CCR5 cells under selection, YFP-positive cells were sorted from non-fluorescent cells using the 530/30 filter of a BD FACSAria II cell sorter (BD Biosciences; San Jose, CA, USA) at the VCU Massey Cancer Center Flow Cytometry Shared Resource Core.

4.2.4 Calcium Mobilization Assays

4.2.4.1 CCR5-MOLT-4 Cells

CCR5-MOLT-4 cells (Obtained through the AIDS Research and Reference Reagent Program, NIAID, NIH, from Dr. Masanori Baba, Dr. Hiroshi Miyake, Dr. Yuji Iizawa¹³³) were transfected with Gqi5 pcDNA1¹⁵⁷ using Lipofectamine 2000 (Invitrogen)

according to the manufacturer's recommended procedure and maintained in RPMI 1640 supplemented with 10% fetal bovine serum, 100 µg/mL penicillin, 100 µg/mL streptomycin, and 1 mg/mL G418 at 37 °C and 5% CO₂. 48 h after transfection, a total of 2,500,000 cells were spun down and brought back up in 8 mL of 50:1 HBSS:HEPES assay buffer. Cells were then plated at 25,000 cells per well into a clear bottom, black 96-well plate (Greiner Bio-one) and 50 µL of Fluo-4 loading buffer (40 µL 2 µM Fluo-4-AM (Invitrogen), 100 µL 2.5 mM probenacid, in 5 mL assay buffer) was added to bring the volume up to 130 µL. After incubating for 45 min, 50 µL of varying concentrations of ligands and controls were added and the plate was incubated for an additional 15 min. Plates were then read on a FlexStation3 microplate reader (Molecular Devices) at 494/516 ex/em for a total of 120 seconds. After 16 s of reading, 20 µL of 200 nM RANTES (Biosource) in assay buffer, or assay buffer alone, was added to the wells to bring the total volume up to 200 µL. The changes in Ca²⁺ mobilization were monitored and peak height values were obtained using SoftMaxPro software (Molecular Devices). Non-linear regression curves and IC₅₀ values were generated using GraphPad Prism. All experiments were repeated a total of three times.

4.2.4.2 hMOR-CHO Cells

HMOR-CHO (established previously¹⁵⁶) cells were transfected with Gqi5 pcDNA1¹⁵⁷ using Lipofectamine 2000 (Invitrogen) according to the manufacturer's recommended procedure. Cells were incubated for 6 hours at 37 °C and 5% CO₂ and then trypsinized and transferred to a clear bottom, black 96-well plate (Greiner Bio-one) at

20,000 cells per well in DMEM/F-12 supplemented with 5% fetal bovine serum, 100 µg/mL penicillin, 100 µg/mL streptomycin, and 250 µg/mL hygromycin B. 48 h after transfection the growth media was decanted and wells were washed with 100 µL of 50:1 HBSS:HEPES assay buffer. Cells were then incubated with 55 µL of Fluo-4 loading buffer [30 µL 2 µM Fluo4-AM (Invitrogen), 84 µL 2.5 mM probenacid, in 5.5 mL assay buffer] for 30 minutes. Varying concentrations of ligands and controls were added to the wells to bring the total volume up to 80 µL in each well and the plates were subsequently incubated for 15 min. Plates were then read on a FlexStation3 microplate reader (Molecular Devices) at 494/516 ex/em for a total of 90 s. After 15 s of reading, 20 µL of 1.25 µM DAMGO in assay buffer, or assay buffer alone, was added to the wells to bring the total volume up to 100 µL. The changes in Ca²⁺ mobilization were monitored and peak height values were obtained using SoftMaxPro software (Molecular Devices). Non-linear regression curves and IC₅₀ values were generated using GraphPad Prism. All experiments were repeated a total of three times.

4.2.4.3 CCR5-hMOR CHO Cells

CCR5-hMOR-CHO cells were transfected with Gqi5 pcDNA1 using Lipofectamine 2000 (Invitrogen) according to the manufacturer's recommended procedure.¹⁵⁷ Cells were incubated for 6 hours at 37 °C and 5% CO₂ and then trypsinized and transferred to a clear bottom, black 96-well plate (Greiner Bio-one) at 20,000 cells per well in DMEM/F-12 supplemented with 5% fetal bovine serum, 100 µg/mL penicillin, 100 µg/mL streptomycin, 250 µg/mL hygromycin B and 800 µg/mL geneticin.

48 h after transfection the growth media was decanted and wells were washed with 100 μL of 50:1 HBSS:HEPES assay buffer. Cells were then incubated with 55 μL of GFP-fluoforte loading buffer [10 μL 1 μM GFP-fluoforte (Enzo Life Sciences), 84 μL 2.5 mM probenacid, in 5.5 mL assay buffer] for 30 min. Varying concentrations of ligands and controls were added to the wells to bring the total volume up to 80 μL in each well and the plates were subsequently incubated for 15 min. Plates were then read on a FlexStation3 microplate reader (Molecular Devices) at 530/555 ex/em for a total of 90 s. After 15 s of reading, 20 μL of 1.25 μM DAMGO in assay buffer, or assay buffer alone, was added to the wells to bring the total volume up to 100 μL . The same procedure was done for CCR5 antagonism, but 50 nM RANTES was used instead of DAMGO for stimulation. The changes in Ca^{2+} mobilization were monitored and peak height values were obtained using SoftMaxPro software (Molecular Devices). Non-linear regression curves and IC_{50} values were generated using GraphPad Prism. All experiments were repeated a total of three times.

4.2.5 Cell Fusion Assay

For the cell fusion assay two cell populations were constructed: target cells containing CCR5, MOR, CD4, and pT7EMCLuc; and effector cells containing pCAGGS-SF162gp160 and pCAGT7pol. The established CCR5-MOR cells (target cells) were transfected with the plasmids pcDNA3.1 CD4 (PMID: 17722977) and pT7EMCLuc (PMIDs: 9770428, 9349488, and 14625051) using Lipofectamine 2000 (Invitrogen) according to the manufacturer's recommended procedure. HEK-293T (GenHunter

Corporation; Nashville, TN, USA; catalog number Q401) cells (effector cells) were also transfected with plasmids pCAGGS-SF162gp160 (PMIDs: 10890360, 9737584, and 8995695) and pCAGT7pol using polyethylenimine (Polysciences, Inc.; Warrington, PA, USA; catalog number 23966). Prior to being overlaid, compound dilutions were added to a 96-well, white, clear bottom plate at 25 μ L of 5 times concentration stock. For morphine stimulation assays, morphine stock was added to the 5 times concentrated stocks to give a final concentration of 500 nM in test wells. 24 h post transfection, the target and effectors cells were detached and overlaid onto each other at a 1:1 mixture in the 96-well white, clear bottom plate at a final concentration of 15,000 cells/well and incubated at 37 °C and 5% CO₂. After an additional 24 h, 96 well plates are allowed to reach room temperature in darkness. Once equilibrated, 100 μ L of a luciferin-lysis buffer solution was added (Bright-Glo Luciferase Assay System, Promega). Plates were allowed to incubate for 2 min and read luminescence for each well with a FlexStation3 plate reader (Molecular Devices). IC₅₀s were obtained using GraphPad Prism. All experiments repeated a total of three independent times.

4.2.6 HIV-1 Infection Assay

In a 24-well plate, primary human astroglia cells (Sciencell catalog #1901) were infected by incubation with the neurotropic HIV-1 strain SF162 and obtained through the NIH AIDS Research and Reference Reagent Program. A concentration of HIV-1 p24 50 pg /106 cells was used and a no virus condition served as a negative control. Cells were treated with and without morphine (500 nM) along with naltrexone (1.5 μ M), maraviroc

(increasing concentrations of 10, 50, 100, 500 nM), and bivalent compound **49** (increasing concentrations of 10, 50, 100, 500 nM) 60 minutes before HIV-1 infection. After approximately 18 to 20 h the supernatant was removed and stored at -80 °C, cells were rinsed twice with PBS and lysed. The lysate was subsequently tested for the relative Tat protein expression by using the Luciferase assay system (Promega) by measuring luciferase activity. Luciferase activity was measured using a PHERAstar FS plate reader (BMG Laboratorytech) and

4.2.7 PCR Studies

Total RNA was isolated from the CCR5-MOR CHO cell line and two lots of primary human astrocytes from two different individuals (ScienCell Research Laboratories; Carlsbad, CA, USA; catalog number 1800) using the miRNeasy Mini Kit (Qiagen, Inc.; Valencia, CA, USA) and used to generate cDNA templates by reverse transcription using the High Capacity cDNA Reverse Transcription Kit (Applied Biosystems; Carlsbad, CA, USA) according to the manufacturer's instructions. PCR reactions were performed in a total volume of 20 µL containing SensiMix SYBR qPCR reagents (Bioline USA, Inc.; Tauton, MA, USA) using a Corbett Rotor-Gene 6000 real-time PCR system (Qiagen, Inc.). PCR conditions consisted of an initial hold step at 95 °C for 10 min followed by 35 amplification cycles of 95 °C for 5 s, 55 °C for 10 s, and 72 °C for 20 s. Sequences of the primer sets used were forward: 5'-CCCAACCTCTTCCAACATTGAGCAA -3' and reverse: 5'-AACGGAGCAGTTTCTGCTTCCAGAT -3' for MOR-1; forward: 5'-

CTGCTCAACCTGGCCATCTCT -3' and reverse: 5'-
 CTTTAAAGCAAACACAGCAT GGAC -3' for CCR5; forward: 5'-
 CATGGCACCGTCAAGGCTGAGAA -3' and reverse: 5'-
 CAGTGGACTCCACGACGTACTCA -3' for human GAPDH; and forward: 5'-
 CTGGAGAAACCTGCCAAGTA -3' and reverse: 5'- ACCACTCTGTTGCTGTAGCC -
 3' for hamster GAPDH. The specificity of the amplified products was verified by melting
 curve analysis and agarose gel electrophoresis. qRT-PCR data were calculated as relative
 expression levels by normalization against GAPDH mRNA using the $2^{-\Delta\Delta C_t}$ method
 (reference PMID: 11846609).

4.2 Computational Methods

4.2.1 Small Molecule Construction

All ligands used in the docking studies were built with standard bond lengths and angles using the molecular modeling package SYBYL-X 2.0. The small molecules were assigned Gasteiger-Hückel charges and energy minimized with the Tripos Force Field.

4.2.2 Sequence Alignment and Model Building

All molecular modeling was collected using the SYBYL-X 2.0 molecular modeling package (Tripos LP, St. Louis, MO) on dual-core AMD Opteron(tm) 2.4 GHz processors. The amino acid sequence of chemokine receptor CCR5 was obtained from UniProtKB/Swiss-Prot (P51681). Within ClustalX a multiple alignment was performed with a gap opening penalty of 15 using the BLOSUM protein weight matrix series.¹⁷⁵

Sequence alignment between CCR5 and CXCR4 was further optimized based on the most conserved residues among most GPCRs and used for model construction for both the inactive and active models. The comparative modeling software, MODELLER 9v8, was used to generate 100 homology models for each state using the default parameters.¹⁶³

4.2.3 Model Selection and Quality Assessment

Model screening was performed by using the genetic-algorithm docking program GOLD 5.1 (Cambridge Crystallographic Data Centre, Cambridge, UK) to dock maraviroc into the CCR5 homology models using GOLD score as the fitness function.¹⁶⁴ Once receptor model was chosen based upon the discrete optimized protein energy (DOPE) scores, fitness function values, and the electronic and steric interactions between the ligands and receptor. Further model refinement was done by using molecular mechanics based energy minimization in Sybyl-X 2.0. Briefly, the model was minimized using a Tripos Force Field with Gasteiger-Hückel charges, a non-bonded interaction cutoff of 8 Å with a distance-dependent dielectric constant of $\epsilon = 4$ being terminated at 0.05 kcal/(mol Å). The minimized models were then analyzed using PROCHECK and ProTable within SYBYL-X 2.0 to ensure the overall quality of the models (i.e., acceptable torsion angles, steric clashes, bond lengths, etc.).

4.2.4 CCR5-MOR Heterodimer Model Building

The heterodimer was built within SYBYL-X 2.0 using the above described CCR5 homology model and the mu opioid receptor crystal structure functional dimer (PDB

code: 4DKL).⁶³ MOR was crystallized as both a dimer and both a TM5/TM6 and a TM1/TM2 dimer interface were observed.⁶³ The TM5/TM6 has more extensive packing and network of interactions, which make it a more plausible dimer interface. In order to construct the heterodimer, one of the MOR units was aligned with the CCR5 homology model according to their homology levels. The subsequent MOR was removed and a MOR-CCR5 heterodimer was left. Initial heterodimer refinement was done by using molecular mechanics based energy minimization in Sybyl-X 2.0. Briefly, the model was minimized using a MMFF94 force field with Gasteiger-Hückel charges, a non-bonded interaction cutoff of 8 Å, with a distance-dependent dielectric constant of $\epsilon = 4$, and terminated at 0.05 kcal/(mol Å). The minimized heterodimer was then analyzed using PROCHECK and ProTable within SYBYL-X 2.0 to ensure the overall quality of the models (i.e. acceptable torsion angles, steric clashes, bond lengths, etc.).

The heterodimer interface had extensive hydrophobic and polar interactions similar to the ones seen in the MOR homodimer.⁶³ Using APBS, the electrostatic interfaces between MOR and CCR5 were mapped (Figure 17).^{167,168}

4.2.4.1 Molecular Docking

The optimized heterodimer model was then subjected to another round of docking of the agonists and antagonists. Using GOLD 5.1, the ligands were docked into both the heterodimer. The putative binding area was restricted to a 15 Å radius around E283 and compound **53** was docked into the receptor a total of 100 iterations using the generic GOLD docking parameters.^{170,173} Concurrently, naltrexone was aligned/overlapped with

the morphinan antagonist β -FNA within the MOR binding pocket of the heterodimer model. The attachment site of the linker to naltrexone allows for the linker to span into the CCR5 binding pocket through the TM5/TM6 interface (Figure 18). Therefore, of the 100 docked poses of maraviroc, the poses with the linker portion pointed towards the TM5/TM6 interface were sorted out for further analysis. The pose with the highest GOLD score and that was within the proper 21-atom distance to naltrexone (linker length: 21 atoms long) was chosen. Once both the naltrexone and **53** binding modes were chosen, they were connected to each other using SYBYL X 2.0 with the 21-atom linker to yield compound **49**. The subsequent bivalent compound was then merged with the heterodimer and the whole system was energy minimized using a MMFF94 force field.

The same procedure was attempted for the 3-position attachment (compound **50**). While the same binding mode as the 4-position compound **53** was seen, the distance between it and naltrexone was too great. During minimization of compound **50** bound to the heterodimer, the maraviroc portion came out of the CCR5 binding pocket due to the strain the 3-position attachment put on the linker.

4.2.4.2 Molecular Dynamics Simulations

All molecular dynamics simulations were run using the Teal cluster housed at the Virginia Commonwealth University Center for High Performance Computing. The cluster consists of ~2480 64 bit AMD computer cores, each with 2-4 GB RAM/core.

The heterodimer-**49** complex was further analyzed using molecular dynamics with the CHARMM force field using NAMD.^{169,176,177} Using the program VMD (Visual

Molecular Dynamics), a solvated 150 Å x 150 Å phosphatidylcholine (POPC) was constructed on the x-y plane.¹⁷⁸ The CCR5-MOR bound **49** complex was then properly orientated for insertion into the lipid bilayer using the orientations of proteins in membranes (OPM) database.¹⁷⁹ After inserting the protein into the middle of the membrane, lipids within 0.8 Å of the protein were removed. Next the system was solvated with TIP3 water and equilibrated with 0.15 M NaCl ions. In the completed system there were a total of 162385 atoms. A modified CHARMM27 force field was constructed with the parameters for compound **49**; the online server SwissParam was used to calculate the CHARMM force field for the ligand.¹⁸⁰

Using NAMD, the system was equilibrated in a three step process. First, 500 ps of molecular dynamic simulation was run (with a time step of 2 fs) on only the lipid tails of the POPC bilayer while keeping the protein, water, ions, ligand, and lipid-head groups fixed. During the second round of equilibration, the protein and ligand were harmonically constrained while the rest of the system was allowed to move. The simulation was run for 500 ps (2 fs time step) while keeping water out of the lipid bilayer. The third step was run completely without constraints for 500 ps while keeping a constant area for the water box.

Molecular dynamics stimulation was then run on the equilibrated system for 13 ns with a time step of 2 fs with the area of the membrane kept constant. Langevin dynamics helped maintained a constant temperature of 310 K and a hybrid Nosé-Hoover Langevin piston method was used to keep a constant pressure of 1 atm with an oscillation period of 200 fs. Electrostatics were maintained using periodic boundary conditions and the

particle mesh ewalds method. A 12 Å non-bonded cutoff and a grid spacing of 1 Å per point in each dimension while calculating van der Waals energies using a switching radius of 10 Å and a cutoff radius of 12 Å. Trajectory analyses were carried out using VMD focusing on the heterodimer and **49** interactions.

5. Conclusion

The role of CCR5 in both prostate cancer and neuroAIDS was explored by developing antagonists either targeting CCR5 or the CCR5 – MOR heterodimer. CCR5 plays a major role in the pro-inflammatory environment that aids in the proliferation of prostate cancer cells. First, using molecular modeling and a homology model of CCR5, a series of compounds were designed based upon the proposed CCR5 antagonist pharmacophore. The developed CCR5 antagonists were able to antagonize CCR5 at μM levels and inhibit the proliferation of metastatic prostate cancer cell lines. However, the compounds' cytotoxicity and solubility will limit their use. From the series of compounds, compound **48** showed the most promising activity with an IC_{50} of $11.4 \pm 0.2 \mu\text{M}$ and $6.5 \pm 0.7 \mu\text{M}$ in M12 and PC-3 prostate cancer cells, and basal cytotoxicity around $30 \mu\text{M}$. Based upon the available data, the structure-activity relationship suggests that the pharmacophore needs to be lengthened and additional polar groups need to be adding to increase solubility.

Morphine potentiates neuroAIDS and viral invasion, and the putative CCR5 – MOR heterodimer may help explain its effects on AIDS pathogenesis and neuroAIDS development. Based upon previous bivalent ligand strategies, a bivalent ligand targeting the CCR5 – MOR heterodimer was synthesized to contain both a CCR5 and MOR antagonist pharmacophore. Several compounds were made, including two bivalent

compounds, in order to elucidate the structure-activity relationship of the bivalent ligand. In all, bivalent compound **49** proved to have a more balanced pharmacological profile between its CCR5 and MOR activity compared to bivalent compound **50**. This difference can be explained by the difference in linker attachment between the two compounds; the 4-position attachment is more tolerated, **49**, than the 3-position attachment, **50**. Interestingly, under morphine stimulation, the CCR5 antagonist, maraviroc, fails to inhibit HIV-1 infection of astrocytes, while bivalent compound **49** shows full inhibition. When the interaction between **49** and the heterodimer was investigated using molecular modeling, the results closely matched the experimental data; they suggested that the bivalent compound **49** could favorably bind the heterodimer and block viral gp120 from binding to CCR5. Overall, compound **49** may be an invaluable tool to help elucidate the role of the CCR5 – MOR heterodimer in neuroAIDS.

In all, the CCR5 antagonists developed in this study may be useful leads for prostate cancer therapies for the later, metastatic stages of the disease; while the bivalent compounds may be useful as diagnostic tools and molecular probes for determining the underlying mechanisms of neuroAIDS development. Using the two different strategies to target CCR5 function has shown its usefulness in therapeutics and the multiple roles it plays *in vivo*.

References

References

- (1) Medzhitov, R. Origin and physiological roles of inflammation. *Nature* **2008**, *454*, 428–435.
- (2) Laskin, D. L.; Pendino, K. J. Macrophages and inflammatory mediators in tissue injury. *Annu. Rev. Pharmacol. Toxicol.* **1995**, *35*, 655–677.
- (3) Borish, L. C.; Steinke, J. W. 2. Cytokines and chemokines. *J. Allergy Clin. Immunol.* **2003**, *111*, S460–S475.
- (4) Oppermann, M. Chemokine receptor CCR5: Insights into structure, function and regulation. *Cell. Signalling* **2004**, *16*, 1201–1210.
- (5) Zlotnik, A.; Yoshie, O. Chemokines: a new classification system and their role in immunity. *Immunity* **2000**, *12*, 121–127.
- (6) Bjarnadottir, T. K.; Gloriam, D. E.; Hellstrand, S. H.; Kristiansson, H.; Fredriksson, R.; Schioth, H. B. Comprehensive repertoire and phylogenetic analysis of the G protein-coupled receptors in human and mouse. *Genomics* **2006**, *88*, 263–273.
- (7) Horuk, R. Chemokine receptors. *Cytokine Growth Factor Rev.* **2001**, *12*, 315–335.
- (8) Li, G.; Haney, K. M.; Kellogg, G. E.; Zhang, Y. Comparative docking study of anibamine as the first natural product CCR5 antagonist in CCR5 homology models. *J. Chem. Inf. Model.* **2009**, *49*, 120–132.
- (9) Cherezov, V.; Rosenbaum, D. M.; Hanson, M. A.; Rasmussen, S. G.; Thian, F. S.; Kobilka, T. S.; Choi, H. J.; Kuhn, P.; Weis, W. I.; Kobilka, B. K.; Stevens, R. C. High-resolution crystal structure of an engineered human β -2-adrenergic G protein-coupled receptor. *Science* **2007**, *318*, 1258–1265.
- (10) Rasmussen, S. G. F.; DeVree, B. T.; Zou, Y.; Kruse, A. C.; Chung, K. Y.; Kobilka, T. S.; Thian, F. S.; Chae, P. S.; Pardon, E.; Calinski, D.; Mathiesen, J. M.; Shah, S. T. A.; Lyons, J. A.; Caffrey, M.; Gellman, S. H.; Steyaert, J.; Skiniotis, G.; Weis, W. I.; Sunahara, R. K.; Kobilka, B. K. Crystal structure of the β 2 adrenergic receptor-Gs protein complex. *Nature* **2011**, *477*, 549–557.
- (11) Kontoyianni, M.; Liu, Z. Structure-based design in the GPCR target space. *Curr. Med. Chem.* **2012**, *19*, 544–556.

- (12) Ballesteros, J. A. W. H. Integrated methods for the construction of three dimensional models and computation probing of structure function relations in G protein-coupled receptors. *Methods Neurosci.* **1995**, *25*, 366–428.
- (13) Congreve, M.; Langmead, C. J.; Mason, J. S.; Marshall, F. H. Progress in structure based drug design for G protein-coupled receptors. *J. Med. Chem.* **2011**, *54*, 4283–4311.
- (14) Park, P. S.-H. Ensemble of G protein-couple receptor active states. *Curr. Med. Chem.* **2012**, *19*, 1146–1154.
- (15) Fanelli, F.; Benedetti, P. G. D. Update 1 of: Computational modeling approaches to structure – function analysis of G protein-coupled receptors. *Chem. Rev.* **2011**, *111*, PR438–PR535.
- (16) Lederman, M. M.; Penn-Nicholson, A.; Cho, M.; Mosier, D. Biology of CCR5 and its role in HIV infection and treatment. *J. Am. Med. Assoc.* **2006**, *296*, 815–826.
- (17) Lin, Y. L.; Mettling, C.; Portales, P.; Reant, B.; Robert-Hebmann, V.; Reynes, J.; Clot, J.; Corbeau, P. The efficacy of R5 HIV-1 infection is determined by CD4 T-cell surface CCR5 density through G alpha i-protein signalling. *AIDS* **2006**, *20*, 1369–1377.
- (18) Mellado, M.; Rodriguez-Frade, J. M.; Manes, S.; Martinez, A. C. Chemokine signaling and functional responses: the role of receptor dimerization and TK pathway activation. *Annu. Rev. Immunol.* **2001**, *19*, 397–421.
- (19) Gainetdinov, R. R.; Premont, R. T.; Bohn, L. M.; Lefkowitz, R. J.; Caron, M. G. Desensitization of G protein-coupled receptors and neuronal functions. *Annu. Rev. Neurosci.* **2004**, *27*, 107–144.
- (20) Oppermann, M.; Mack, M.; Proudfoot, A. E. I.; Olbrich, H. Differential effects of CC chemokines on CC chemokine receptor 5 (CCR5) phosphorylation and identification of phosphorylation sites on the CCR5 carboxyl terminus. *J. Biol. Chem.* **1999**, *274*, 8875–8885.
- (21) Krupnick, J. G.; Benovic, J. L. The role of receptor kinases and arrestins in G protein-coupled receptor regulation. *Annu. Rev. Pharmacol. Toxicol.* **1998**, *38*, 289–319.
- (22) Verkaar, F.; Van Rosmalen, J. W. G.; Blomenrohr, M.; Van Koppen, C. J.; Blankesteyn, W. M.; Smits, J. F. M.; Zaman, G. J. R. G protein-independent cell-based assays for drug discovery on seven-transmembrane receptors. *Biotech. Annu. Rev.* **2008**, *14*, 253–274.
- (23) Rask-Andersen, M.; Almen, M. S.; Schioth, H. B. Trends in the exploitation of novel drug targets. *Nat. Rev. Drug Disc.* **2011**, *10*, 47–60.

- (24) Lappano, R.; Maggiolini, M. G protein-coupled receptors: novel targets for drug discovery in cancer. *Nat. Rev. Drug Disc.* **2011**, *10*, 47–60.
- (25) Chen, W.; Zhan, P.; DeClercq, E.; Liu, X. Recent progress in small molecule CCR5 antagonists as potential HIV-1 Entry Inhibitors. *Curr. Pharm. Des.* **2012**, *18*, 100–112.
- (26) Zhang, X.; Haney, K. M.; Richardson, A. C.; Wilson, E.; Gewirtz, D. A.; Ware, J. L.; Zehner, Z. E.; Zhang, Y. Anibamine, a natural product CCR5 antagonist, as a novel lead for the development of anti-prostate cancer agents. *Bioorg. Med. Chem. Lett.* **2010**, *20*, 4627–4630.
- (27) Zhang, Y.; Arnatt, C. K.; Zhang, F.; Wang, J.; Haney, K. M.; Fang, X. The potential role of anibamine, a natural product CCR5 antagonist, and its analogues as leads toward development of anti-ovarian cancer agents. *Bioorg. Med. Chem. Lett.* **2012**, *22*, 5093–5097.
- (28) Kedzierska, K.; Corwe, S. M.; Turville, S.; Cunningham, A. L. The influence of cytokines, chemokines and their receptors on HIV-1 replication in monocytes and macrophages. *Rev. Med. Virol.* **2003**, *13*, 39–56.
- (29) Chinen, J.; Shearer, W. T. Molecular virology and immunology of HIV infection. *Allergy Clin. Immunol.* **2002**, *110*, 189–198.
- (30) Samson, M.; Libert, F.; Doranz, B. J.; Rucker, J.; Liesnard, C.; Farber, C. M.; Saragosti, S.; Lapoumeroulie, C.; Cognaux, J.; Forceille, C.; Muyldermans, G.; Verhofstede, C.; Burton, G.; Georges, M.; Imai, T.; Rana, S.; Yi, Y.; Smyth, R. J.; Collman, R. J.; Doms, R. W.; Vassart, G.; Parmentier, M. Resistance to HIV-1 infection in caucasian individuals bearing mutant alleles of the CCR-5 chemokine receptor gene. *Nature* **1996**, *382*, 722–725.
- (31) Opdenakker, G.; Van Damme, J. Cytokines and proteases in invasion processes: Molecular similarities between inflammation and cancer. *Cytokine* **1992**, *4*, 251–258.
- (32) Mantovani, A.; Bottazzi, B.; Colotta, F.; Sozzani, S.; Luigi, R. The origin and function of tumor-associated macrophages. *Immunol. Today* **1992**, *13*, 265–270.
- (33) Opdenakker, G.; Van Damme, J. Chemotactic factors, passive invasion and metastasis of cancer cells. *Immunol. Today* **1992**, *13*, 463–464.
- (34) Frederick, M. J.; Clayman, G. L. Chemokines in Cancer. *Expert Rev. Mol. Med.* **2001**, *3*, 1–18.
- (35) Vaday, G. G.; Peehl, D. M.; Kadam, P. A.; Lawrence, D. M. Expression of CCL5 (RANTES) and CCR5 in prostate cancer. *Prostate* **2005**, *66*, 124–134.

- (36) Haung, J.; Chen, K.; Gong, W.; Dunlop, N. M.; Wang, J. M. G-protein coupled chemoattractant receptors and cancer. *Front. Biosci.* **2008**, *13*, 3352–3363.
- (37) American Cancer Society *Cancer Facts and Figures 2012*; Atlanta, GA, 2012.
- (38) Bonkhoff, H.; Remberger, K. Differentiation pathways and histogenic aspects of normal and abnormal prostatic growth: a stem cell model. *The Prostate* **1996**, *28*, 98–106.
- (39) Catalona, W. J.; Richie, J. P.; Abmann, F. R.; Hudson, M. A.; Scardino, P. T.; Flanigan, R. C.; DeKernion, J. B.; Ratliff, T. L.; Kavoussi, L. R.; Dalkin, B. L. Comparison of digital rectal examination and serum prostate specific antigen in the early detection of prostate cancer: results of a multicenter clinical trial of 6,630 men. *J. Urol.* **1994**, *151*, 1283–1290.
- (40) Konig, J. E.; Senge, T.; Allhoff, E. P.; Konig, W. Analysis of the inflammatory network in benign prostate hyperplasia and prostate cancer. *Prostate* **2004**, *58*, 121–129.
- (41) Maitland, N. J.; Collins, A. Inflammation as the primary aetiological agent of human prostate cancer: a stem cell connection? *J. Cell. Biochem.* **2008**, *105*, 931–939.
- (42) Lucia, M. S.; Torkko, K. C. Inflammation as a target for prostate cancer chemoprevention: pathological and laboratory rationale. *J. Urol.* **2004**, *171*, S30–S35.
- (43) O'Hayre, M.; Salanga, C. L.; Handel, C. L.; Allen, S. J. Chemokines and cancer: migration intracellular signalling and intercellular communication in the microenvironment. *Biochem. J.* **2008**, *409*, 635–649.
- (44) Zhang, F.; Arnatt, C. K.; Haney, K. M.; Fang, H. C.; Bajacon, J. E.; Richardson, A. C.; Ware, J. L.; Zhang, Y. Structure activity relationship studies of natural product chemokine receptor CCR5 antagonist anibamine toward the development of novel anti prostate cancer agents. *Eur. J. Med. Chem.* **2012**, *55*, 395–408.
- (45) Haney, K. M.; Zhang, F.; Arnatt, C. K.; Yuan, Y.; Li, G.; Ware, J. L.; Gewirtz, D. A.; Zhang, Y. The natural product CCR5 antagonist anibamine and its analogs as anti-prostate cancer agents. *Bioorg. Med. Chem. Lett.* **2011**, *21*, 5159–5163.
- (46) Barre-Sinoussi, F.; Chermann, J. C.; Rey, F.; Nugeyre, M. T.; Chamaret, S.; Gruest, J.; Dauguet, C.; Axler-Blin, C.; Vezinet-Brun, F.; Rouzioux, C.; Rozenbaum, W.; Montagnier, L. Isolation of a T-lymphotropic retrovirus from a patient at risk for acquired immune deficiency syndrome (AIDS). *Science* **1983**, *220*, 868–871.

- (47) Alkhatib, G.; Comadiere, C.; Broder, C. C.; Feng, Y.; Kennedy, P. E.; Murphy, P. M.; Berger, E. A. CC CKR5: a RANTES, MIP-1alpha, MIP-1beta receptor as a fusion cofactor for macrophage-tropic HIV-1. *Science* **1996**, *272*, 1955–1958.
- (48) Deng, H.; Liu, R.; Ellmeier, W.; Choe, S.; Unutmaz, D.; Burkhart, M.; Di Marzio, P.; Marmon, S.; Sutton, R. E.; Hill, C. M.; Davis, C. B.; Peiper, S. C.; Shall, T. J.; Littman, D. R.; Landau, N. R. Identification of a major co-receptor for primary isolates of HIV-1. *Nature* **1996**, *381*, 661–666.
- (49) Organization, W. H. Global summary of the HIV/AIDS epidemic, December 2011 <http://www.who.int/hiv/data/en/> (accessed Jan 2, 2013).
- (50) Liu, R.; Paxton, W. A.; Choe, S.; Ceradini, D.; Martin, S. R.; Horuk, R.; MacDonald, M. E.; Stuhlmann, H.; Koup, R. A.; Landau, N. R. Homozygous defect in HIV-1 coreceptor accounts for resistance of some multiply-exposed individuals to HIV-1 infection. *Cell* **1996**, *86*, 367–377.
- (51) Cocchi, F.; DeVico, A. L.; Garzino-Demo, A.; Arya, S. K.; Gallo, R. C.; Lusso, P. Identification of RANTES, MIP-1alpha, and MIP-1beta as the major HIV-suppressive factors produced by CD8+ T cells. *Science* **1995**, *270*, 1811–1815.
- (52) Tersmette, M.; Gruters, R.; De Wolf, F.; De Goede, R. E.; Lange, J. M. A.; Schellekens, P. T. A.; Goudsmit, J.; Huisman, H. G.; Miedema, F. Evidence for a role of virulent human immunodeficiency virus (HIV) variants in the pathogenesis of acquired immunodeficiency virus syndrome: study on sequential isolates. *J. Virol.* **1989**, *63*, 2118–2125.
- (53) Wilkin, T. J.; Gulick, R. M. CCR5 antagonism in HIV infection: current concepts and future opportunities. *Ann. Rev. Med.* **2012**, *63*, 81–93.
- (54) Allegretti, M.; Cesta, M. C.; Garin, A.; Proudfoot, A. E. I. Current status of chemokine receptor inhibitors in development. *Immunol. Lett.* **2012**, *145*, 68–78.
- (55) Palani, A.; Tagat, J. Discovery and development of small-molecule chemokine coreceptor CCR5 antagonists. *J. Med. Chem.* **2006**, *49*, 2851–2855.
- (56) Nichols, W. G.; Steel, H. M.; Bonny, T.; Adkison, K.; Curtis, L.; Millard, J.; Kabeya, K.; Clumeck, N. Hepatotoxicity observed in clinical trials of aplaviroc (GW873140). *Antimicrob. Agents Chemother.* **2008**, *52*, 858–865.
- (57) Lemoine, R. C.; Wanner, J. Small molecule antagonists of the chemokine receptor CCR5. *Curr. Top. Med. Chem.* **2010**, *10*, 1299–1338.
- (58) Baba, M.; Nishimura, O.; Kanzaki, N.; Okamoto, M.; Sawada, H.; Iizawa, Y.; Shiraiishi, M.; Aramaki, Y.; Okonogi, K.; Ogawa, Y.; Meguro, K.; Fujino, M. A small-molecule, nonpeptide CCR5 antagonist with highly potent and selective anti-HIV-1 activity. *Proc. Natl. Acad. Sci. USA* **1999**, *96*, 5698–5703.

- (59) Gilliam, B. L.; Riedel, D. J.; Redfield, R. R. Clinical use of CCR5 inhibitors in HIV and beyond. *J. Transl. Med.* **2010**, *9*, S9–S23.
- (60) Waldhoer, M.; Bartlett, S. E.; Whistler, J. L. Opioid receptors. *Annu. Rev. Biochem.* **2004**, *73*, 953–990.
- (61) Wu, H.; Wacker, D.; Mileni, M.; Katritch, V.; Han, G. W.; Vardy, E.; Liu, W.; Thompson, A. A.; Huang, X.-H.; Carroll, F. I.; Mascarella, S. W.; Westkaemper, R. B.; Mosier, P. D.; Roth, B. L.; Cherezov, V.; Stevens, R. C. Structure of the human κ -opioid receptor in complex with JDTic. *Nature* **2012**, *485*, 327–332.
- (62) Thompson, A. A.; Liu, W.; Chun, E.; Katritch, V.; Wu, H.; Vardy, E.; Huang, X.-P.; Trapella, C.; Guerrini, R.; Calo, G.; Roth, B. L.; Cherezov, V.; Stevens, R. C. Structure of the nociception/orphanin FQ receptor in complex with a peptide mimetic. *Nature* **2012**, *485*, 395–399.
- (63) Manglik, A.; Kruse, A. C.; Kobilka, T. S.; Thian, F. S.; Mathiesen, J. M.; Sunahara, R. K.; Pardo, L.; Weis, W. I.; Kobilka, B. K.; Granier, S. Crystal structure of the μ -opioid receptor bound to a morphinan antagonist. *Nature* **2012**, *485*, 321–326.
- (64) Granier, S.; Manglik, A.; Kruse, A. C.; Kobilka, T. S.; Thian, F. S.; Weis, W. I.; Kobilka, B. K. Structure of the δ -opioid receptor bound to naltrindole. *Nature* **2012**, *485*, 400–404.
- (65) Dhawan, B. N.; Cesselin, F.; Raghbir, R.; Reisine, T.; Bradley, P. B.; Portoghese, P. S.; Hamon, M. International union of pharmacology. XII. Classification of opioid receptors. *Pharmacol. Rev.* **1996**, *48*, 567–592.
- (66) Martin, W. R.; Eades, C. G.; Thompson, J. A.; Huppler, R. E.; Gilbert, P. E. The effects of morphine- and nalorphine-like drugs in the nondependent and morphine dependent chronic spinal dog. *J. Pharmacol. Exp. Ther.* **1976**, *197*, 517–532.
- (67) Pert, C. B.; Snyder, S. H. Opiate receptor: demonstration in nervous tissue. *Science* **1973**, *179*, 1011–1014.
- (68) Mannalack, D. T.; Beart, P. M.; Gundlach, A. L. Psychotomimetic sigma-opiates and PCP. *Trends Pharm. Sci.* **1986**, *7*, 448–451.
- (69) Lord, J. A. H.; Waterfeild, A. A.; Hughes, J.; Kosterlitz, H. W. Endogenous opioid peptides: multiple agonists and receptors. *Nature* **1977**, *267*, 495–499.
- (70) Henderson, G. The orphan opioid receptor and its endogenous ligand - nociceptin/orphanin FQ. *Trends Pharm. Sci.* **1997**, *18*, 293–300.
- (71) Wu, B.; Chien, E. Y.; Mol, C. D.; Fenalti, G.; Liu, W.; Katritch, V.; Abagyan, R.; Brooun, A.; Wells, P.; Bi, F. C.; Hamel, D. J.; Kuhn, P.; Handel, T. M.; Cherezov,

- V.; Stevens, R. C. Structures of the CXCR4 chemokine GPCR with small-molecule and cyclic peptide antagonists. *Science* **2010**, *330*, 1066–1071.
- (72) Law, P.-Y.; Wong, Y. H.; Loh, H. H. Molecular mechanisms and regulation of opioid receptor signaling. *Annu. Rev. Pharmacol. Toxicol.* **2000**, *40*, 389–430.
- (73) Hauser, K. F.; Fitting, S.; Dever, S. M.; Podhaizer, E. M.; Knapp, P. E. Opiate drug use and the pathophysiology of neuroAIDS. *Curr. HIV Res.* **2012**, *10*, 435–452.
- (74) Turchan-Cholewo, J.; Liu, Y.; Gartner, S.; Reid, R.; Jie, C.; Peng, X.; Chen, K. C.; Chauhan, A.; Haughey, N.; Cutler, R.; Mattson, M. P.; Pardo, C.; Conant, K.; Sacktor, N.; McArthur, J. C.; Hauser, K. F.; Gairola, C.; Nath, A. Increased vulnerability of ApoE4 neurons to HIV proteins and opiates: protection by diosgenin and L-deprenyl. *Neurobiol. Dis.* **2006**, *23*, 109–119.
- (75) Hauser, K. F.; El-Hage, N.; Buch, S.; Berger, J. R.; Tyor, W. R.; Nath, A.; Bruce-Keller, A. J.; Knapp, P. E. Molecular targets of opiate drug abuse in neuroAIDS. *Neurotoxic. Res.* **2005**, *8*, 63–80.
- (76) Matthes, H. W. D.; Maldonado, R.; Simonin, F.; Valverde, O.; Slowe, S.; Kitchen, I.; Befort, K.; Dierich, A.; LeMeur, M.; Dolle, P.; Tzavara, E.; Hanoune, J.; Roques, B. P.; Kieffer, B. L. Loss of morphine-induced analgesia, reward effect and withdrawal symptoms in mice lacking the mu-opioid receptor gene. *Nature* **1996**, *383*, 819–823.
- (77) Kieffer, B. L.; Gaveriaux-Ruff, C. Exploring the opioid system by gene knockout. *Prog. Neurobiol.* **2002**, *66*, 285–306.
- (78) Stromer, W.; Michaeli, K.; Sandner-Kiesling, A. Perioperative pain therapy in opioid abuse. *Eur. J. Anaesthesiol.* **2013**, *30*, 55–64.
- (79) Ballantyne, J. C.; LaForge, K. S. Opioid dependence and addition during treatment of chronic pain. *Pain* **2007**, *129*, 235–255.
- (80) Goodman, A. J.; Bourdonnec, B. L.; Dolle, R. E. Mu opioid receptor antagonists: recent developments. *ChemMedChem* **2007**, *2*, 1552–1570.
- (81) National Institute on Drug Abuse DrugFacts: Nationwide Trends
<http://www.drugabuse.gov/publications/drugfacts/nationwide-trends>.
- (82) Nath, A.; Hauser, K. F.; Wojna, V.; Booze, R. M.; Maragos, W.; Prendergast, M.; Cass, W.; Turchan, J. T. Molecular basis for interactions of HIV and drugs of abuse. *JAIDS, J. Acquired Immune Defic. Syndr.* **2002**, *31*, S62–S69.

- (83) Norman, K. F.; Basso, M.; Kurmar, A.; Malow, R. Neuropsychological consequences of HIV and substance abuse: a literature review and implications for treatment and future research. *Curr. Drug Abuse Rev.* **2009**, *2*, 143–156.
- (84) Anthony, I. C.; Arango, J. C.; Stephens, B.; Simmonds, P.; Bell, J. E. The effects of illicit drugs on the HIV infected brain. *Front. Biosci.* **2008**, *13*, 1294–1307.
- (85) Noel, R. J. J.; Rivera-Amill, V.; Buch, S.; Kurmar, A. Opiates, immune system, acquired immunodeficiency syndrome, and nonhuman primate model. *J. Neurovirol.* **2008**, *14*, 279–285.
- (86) Chuang, T. K.; Killam, K. F. J.; Chuang, L. F.; Kung, H.-F.; Sheng, W. S.; Chao, C. C.; Yu, L.; Chuang, R. Y. Mu opioid receptor gene expression in immune cells. *Biochem. Biophys. Res. Commun.* **1995**, *216*, 922–930.
- (87) Chen, C.; Li, J.; Bot, G.; Szabo, I.; Rogers, T. J.; Liu-Chen, L.-Y. Heterodimerization and cross-desensitization between the mu-opioid receptor and the chemokine CCR5 receptor. *Eur. J. Pharmacol.* **2004**, *483*, 175–186.
- (88) Rogers, T. J.; Peterson, P. K. Opioid G protein-coupled receptors, signals at the crossroads of inflammation. *Trends Immunol.* **2003**, *24*, 116–121.
- (89) Rogers, T. J.; Steele, A. D.; Howard, O. M.; Oppenheim, J. J. Bidirectional heterologous desensitization of opioid and chemokine receptors. *Ann. NY Acad. Sci.* **2000**, *917*, 19–28.
- (90) Suzuki, S.; Chuang, L. F.; Yau, P.; Doi, R. H.; Chuang, R. Y. Interactions of opioid and chemokine receptors: oligomerization of mu, kappa, and delta with CCR5 on immune cells. *Exp. Cell Res.* **2002**, *280*, 192–200.
- (91) Thompson, K. A.; Cherry, C. L.; Bell, J. E.; McLean, C. A. Brain cell reservoirs of latent virus in presymptomatic HIV-infected individuals. *Am. J. Pathol.* **2011**, *179*, 1623–1629.
- (92) Peridsky, Y.; Gendelman, H. E. Mononuclear phagocyte immunity and the neuropathogenesis of HIV-1 infection. *J. Leukoc. Biol.* **2003**, *74*, 691–701.
- (93) Wiley, C. A.; Achim, C. Human immunodeficiency virus encephalitis is the pathological correlate of dementia in acquired immunodeficiency syndrome. *Ann. Neurol.* **1994**, *36*, 673–676.
- (94) Hauser, K. F.; El-Hage, N.; Steine-Martin, A.; Maragos, W. F.; Nath, A.; Peridsky, Y.; Volsky, D. J.; Knapp, P. E. HIV-1 neuropathogenesis: glial mechanisms revealed through substance abuse. *J. Neurochem.* **2007**, *100*, 567–586.
- (95) El-Hage, N.; Wu, G.; Wang, J.; Ambati, J.; Knapp, P. E.; Reed, J. L.; Bruce-Keller, A. J.; Hauser, K. F. HIV-1 Tat and opiate-induced changes in astrocytes

promote chemotaxis of microglia through the expression of MCP-1 and alternative chemokines. *Glia* **2006**, *53*, 132–146.

- (96) Combadiere, C.; Salzwedel, K.; Smith, E. D.; Tiffany, H. L.; Berger, E. A.; Murphy, P. M. Identification of CX3CR1. A chemotactic receptor for the human CX3C chemokine fractalkine and a fusion coreceptor for HIV-1. *J. Biol. Chem.* **1998**, *273*, 23799–23804.
- (97) Janecka, A.; Fichna, J.; Janecki, T. Opioid receptors and their ligands. *Curr. Top. Med. Chem.* **2004**, *4*, 1–17.
- (98) Emmerson, P. J.; Liu, M.-R.; Woods, J. H.; Medzihradsky, F. Binding affinity and selectivity of opioids at mu, delta, and kappa receptors in monkey brain membranes. *J. Pharmacol. Exp. Ther.* **1994**, *3*, 1630–1637.
- (99) Schmidhammer, H.; Burkard, W. P.; Eggstein-Aeppli, L.; Smith, C. F. Synthesis and biological evaluation of 14-alkoxymorphinans. 2. (-)-N-(cyclopropylmethyl)-4,14-dimethoxymorphinan-6-one, a selective mu opioid receptor antagonist. *J. Med. Chem.* **1989**, *32*, 418–421.
- (100) Broadbear, J. H.; Sumpter, T. L.; Burke, T. F.; Husbands, S. M.; Lewis, J. W.; Woods, J. H.; Traynor, J. R. Methocinnamox is a potent, long-lasting, and selective antagonist of morphine-mediated antinociception in the mouse: comparison with clocinnamox, beta-unaltraxamine, and beta-chlornaltraxamine. *J. Pharmacol. Exp. Ther.* **2000**, *294*, 933–940.
- (101) Kazmierski, W.; Wire, W. S.; Lui, G. K.; Knapp, R. J.; Shook, J. E.; Burks, T. F.; Yamamura, H. I.; Hruby, V. J. Design and synthesis of somatostatin analogues with topographical properties that lead to highly potent and specific mu opioid receptor antagonists with greatly reduced binding at somatostatin receptors. *J. Med. Chem.* **1988**, *31*, 2170–2177.
- (102) Ward, S. J.; Portoghese, P. S.; Takemori, A. E. Pharmacological profiles of beta-funaltrexamine (beta-FNA) and beta-chlornaltraxamine (beta-CNA) on the mouse vas deferens preparation. *Eur. J. Pharmacol.* **1982**, *80*, 377–384.
- (103) Portoghese, P. S.; Sultana, M.; Takemori, A. Design of peptidomimetic delta opioid receptor antagonists using the message-address concept. *J. Med. Chem.* **1990**, *33*, 1714–1720.
- (104) Pfeiffer, M.; Koch, T.; Schroder, H.; Laugsch, M.; Holtt, V.; Schulz, S. Heterodimerization of somatostatin and opioid receptors cross-modulates phosphorylation, internalization, and desensitization. *J. Biol. Chem.* **2002**, *277*, 19762–19772.
- (105) Bai, M. Dimerization of G-protein-coupled receptors: roles in signal transduction. *Cell. Signal.* **2004**, *16*, 175–186.

- (106) Fuxe, K.; Borroto-Escuela, D. O.; Marcellino, D.; Romero-Fernandez, W.; Frankowska, M.; Guidolin, D.; Filip, M.; Ferraro, L.; Woods, A. S.; Tarakanov, A.; Ciruela, F.; Agnati, L. F.; Tanganelli, S. GPCR heteromers and their allosteric receptor-receptor interactions. *Curr. Med. Chem.* **2012**, *19*, 356–363.
- (107) George, S. R.; O'Dowd, B. F.; Lee, S. P. G-protein-coupled receptor oligomerization and its potential for drug discovery. *Nat. Rev. Drug Disc.* **2002**, *1*, 808–820.
- (108) Herbert, T. E.; Moffett, S.; Morello, J. P.; Losiel, T. P.; Bichet, D. G.; Barret, C.; Bouvier, M. A peptide derived from a beta(2)-adrenergic receptor transmembrane domain inhibits both receptor dimerization and activation. *J. Biol. Chem.* **1996**, *271*, 16384–16392.
- (109) Pflieger, K. D. G.; Eidne, K. A. Monitoring the formation of dynamic G-protein-coupled receptor-protein complexes in living cells. *Biochem. J.* **2005**, *385*, 625–637.
- (110) Angers, S.; Salahpour, A.; Joly, E.; Hilaiet, S.; Chelsky, D.; Dennis, M.; Bouvier, M. Detection of beta 2-adrenergic receptor dimerization in living cells using bioluminescence resonance energy transfer (BRET). *Proc. Natl. Acad. Sci. USA* **2000**, *97*, 3684–3689.
- (111) Fotiadis, D.; Liang, Y.; Filipek, S.; Saperstein, D. A.; Engel, A.; Palczewski, K. Atomic-force microscopy: rhodopsin dimers in native disc membranes. *Nature* **2003**, *421*, 127–128.
- (112) Gouldson, P. R.; Higgs, C.; Smith, R. E.; Dean, M. K.; Gkoutos, G. V.; Reynolds, C. A. Dimerization and domain swapping in G-protein-coupled receptors: a computational study. *Neuropsychopharmacology* **2000**, *23*, S60–S77.
- (113) Park, J. H.; Scheerer, P.; Hofmann, K. P.; Choe, H. W.; Ernst, O. P. Crystal structure of the ligand-free G-protein-coupled receptor opsin. *Nature* **2008**, *454*, 183–187.
- (114) Wang, D.; Sun, X.; Bohn, L. M.; Sadee, W. Opioid receptor homo- and heterodimerization in living cells by quantitative bioluminescence resonance energy transfer. *Mol. Pharmacol.* **2005**, *67*, 2173–2184.
- (115) Rios, C.; Gomes, I.; Devi, L. A. Mu opioid and CB1 cannabinoid receptor interactions: reciprocal inhibition of receptor signaling and neuritogenesis. *Br. J. Pharmacol.* **2006**, *148*, 387–395.
- (116) Pfeiffer, M.; Kirscht, S.; Stumm, R.; Koch, T.; Wu, D.; Laugsch, M.; Schroder, H.; Hollt, V.; Schulz, S. Heterodimerization of substance P and mu-opioid receptors regulates receptor trafficking and resensitization. *J. Biol. Chem.* **2003**, *278*, 51630–51637.

- (117) Evans, R. M.; You, H.; Hameed, S.; Altier, C.; Mezghrani, A.; Bourinet, E.; Zamponi, G. W. Heterodimerization of ORL1 and opioid receptors and its consequences for N-type calcium channel regulation. *J. Biol. Chem.* **2010**, *285*, 1032–1040.
- (118) Jordan, B. A.; Devi, A. L. G-protein-coupled receptor heterodimerization modulates receptor function. *Nature* **1999**, *399*, 697–700.
- (119) George, S. R.; Fan, T.; Xie, Z.; Tse, R.; Tam, V.; Varghese, G.; O'Dowd, B. F. Oligomerization of mu- and delta-opioid receptors. Generation of novel functional properties. *J. Biol. Chem.* **2000**, *275*, 26128–26135.
- (120) He, L.; Fong, J.; Von Zastrow, M.; Whistler, J. L. Regulation of opioid receptor trafficking and morphine tolerance by receptor oligomerization. *Cell* **2002**, *108*, 271–282.
- (121) Portoghese, P. S. Bivalent ligands and the message-address concept in the design of selective opioid antagonists. *Trends Pharmacol. Sci.* **1989**, *10*, 230–235.
- (122) Shonberg, J.; Scammells, P. J.; Capuano, B. Design strategies for bivalent ligands targeting GPCRs. *ChemMedChem* **2011**, *6*, 963–974.
- (123) Portoghese, P. S. From models to molecules: opioid receptor dimers, bivalent ligands, and selective opioid receptor probes. *J. Med. Chem.* **2001**, *44*, 2259–2269.
- (124) Zheng, Y.; Akgun, E.; Harikumar, K. G.; Hopson, J.; Powers, M. D.; Lunzer, M. M.; Miller, L. J.; Portoghese, P. S. Induced association of mu opioid (MOP) and type 2 cholecystokinin (CCK2) receptors by novel bivalent ligands. *J. Med. Chem.* **2009**, *52*, 247–258.
- (125) Zhang, S.; Yekkirala, A.; Tang, Y.; Portoghese, P. S. A bivalent ligand (KMN-21) antagonist for mu/kappa heterodimeric opioid receptors. *Bioorg. Med. Chem. Lett.* **2009**, *19*, 6978–6980.
- (126) Daniels, D. J.; Lenard, N. R.; Etienne, C. L.; Law, P.-Y.; Roerig, S. C.; Portoghese, P. S. Opioid-induced tolerance and dependence in mice is modulated by the distance between pharmacophores in a bivalent ligand series. *Proc. Natl. Acad. Sci. U. S. A.* **2005**, *102*, 19208–19213.
- (127) Harvey, J. H.; Long, D. H.; England, P. M.; Whistler, J. L. Tuned-affinity bivalent ligands for the characterization of opioid receptor heteromers. *ACS Med. Chem. Lett.* **2012**, *3*, 640–644.
- (128) Simonin, F.; Slowe, S.; Becker, J. A.; Matthes, H. W.; Filliol, D.; Chluba, J.; Kitchen, I.; Kieffer, B. L. Analysis of [3H] bremazocine binding in single and combinatorial opioid receptor knockout mice. *Eur. J. Pharmacol.* **2001**, *414*, 189–195.

- (129) Coussens, L. M.; Werb, Z. Inflammation and cancer. *Nature* **2002**, *420*, 860–867.
- (130) Robinson, S. C.; Scott, K. A.; Wilson, J. L.; Thompson, R. G.; Proudfoot, A. E. I.; Balkwill, F. R. A chemokine receptor antagonist inhibits experimental breast cancer growth. *Cancer Res.* **2003**, *63*, 8360–8365.
- (131) Adams, J. L. Synthesis and biological evaluation of CCR5 antagonists as novel anti-prostate cancer agents, Virginia Commonwealth University, 2007, pp. 1–184.
- (132) Arnatt, C. K.; Zhang, Y. Facile synthesis of 2,3,5,6-tetrabromo-4-methyl-nitrocyclohexa-2,5-dien-1-one, a mild nitration reagent. *Tet. Lett.* **2012**, *53*, 1592–1594.
- (133) Baba, M.; Miyake, H.; Okamoto, M.; Iizawa, Y.; Okonogi, K. Establishment of a CCR5-expressing T-lymphoblastoid cell line highly susceptible to R5 HIV type 1. *AIDS Res. Hum. Retroviruses* **2000**, *16*, 935–941.
- (134) Yuan, Y.; Arnatt, C. K.; Li, G.; Haney, K. M.; Ding, D.; Jacob, J. C.; Selley, D. E.; Zhang, Y. Design and synthesis of a bivalent ligand to explore the putative heterodimerization of the mu opioid receptor and the chemokine receptor CCR5. *Org. Biomol. Chem.* **2012**, *10*, 2633–2646.
- (135) Webber, M. M.; Bello, D.; Quadar, S. Immortalized and tumorigenic adult human prostatic epithelial cell lines: characteristics and applications. Part 2. Tumorigenic cell lines. *Prostate* **1997**, *30*, 58–64.
- (136) Borenfreund, E.; Puemer, J. A. Toxicity determined in vitro by morphological alterations and neutral red absorption. *Toxicol. Lett.* **1985**, *24*, 119–124.
- (137) National Toxicology Program (NTP) Interagency Center for the Evaluation of Alternative Toxicological Methods (NICEATM) *Test method protocol for the BALB/c 3T3 neutral red uptake cytotoxicity test. A. T. f. B. C. F. a. I. V. V. S., phase III*; 2003.
- (138) Mathers, B. M.; Degenhardt, L.; Phillips, B.; Wiessing, L.; Hickman, M.; Strathdee, S. A.; Wodak, A.; Panda, S.; Tyndall, M.; Toufik, A.; Mattick, R. P. Global epidemiology of injecting drug use and HIV among people who inject drugs: a systematic review. *Lancet* **2008**, *372*, 1733–1745.
- (139) Gabuzda, D.; Wang, J. Chemokine receptors and virus entry in the central nervous system. *J. Neurovirol.* **1999**, *5*, 643–658.
- (140) Luster, A. D. Chemokines - chemotactic cytokines that mediate inflammation. *N. Engl. J. Med.* **1998**, *338*, 436–445.
- (141) Dorr, P.; Westby, M.; Dobbs, S.; Griffin, P.; Irvine, B.; Macartney, M.; Mori, G.; Rickett, G.; Smith-Burchnell, C.; Napier, C.; Webster, R.; Armour, D.; Price, D.;

- Stammen, B.; Wood, A.; Perros, M. Maraviroc (UK-427,857), a potent, orally bioavailable, and selective small-molecule inhibitor of chemokine receptor CCR5 with broad-spectrum anti-human immunodeficiency virus type 1 activity. *Antimicrob. Agents Chemother.* **2005**, *49*, 4721–4732.
- (142) Lindl, K. A.; Marks, D. R.; Kolson, D. L.; Jordan-Sciutto, K. L. HIV-Associated neurocognitive disorder: Pathogenesis and therapeutic opportunities. *J. Neuroimmune. Pharmacol.* **2010**, *5*, 294–309.
- (143) Minagar, A.; Commins, D.; Alexander, J. S.; Hoque, R.; Chiappelli, F.; Signer, E. J.; Nikbin, B.; Shapshak, P. NeuroAIDS: Characteristics and diagnosis of the neurological complications of AIDS. *Mol. Diagn. Ther.* **2008**, *12*, 25–43.
- (144) Gurwell, J. A.; Nath, A.; Sun, Q.; Zhang, J.; Martin, K. M.; Chen, Y.; Hauser, K. F. Synergistic neurotoxicity of opioids and human immunodeficiency virus-1 Tat protein in striatal neurons in vitro. *Neuroscience* **2001**, *102*, 555–563.
- (145) Zou, S.; Fitting, S.; Hahn, Y. K.; Welch, S. P.; El-Hage, N.; Hauser, K. F.; Knapp, P. E. Morphine potentiates neurodegenerative effects of HIV-1 Tat through actions at m-opioid receptor-expressing glia. *Brain* **2011**, *134*, 3613–3628.
- (146) Mahajan, S. D.; Schwartz, S. A.; Shanahan, T. C.; Chawda, R. P.; Nair, M. P. N. Morphine regulates gene expression of α - and β -chemokines and their receptors on astroglial cells via the opioid receptor. *J. Immunol.* **2002**, *169*, 3589–3599.
- (147) Szabo, I.; Chen, X. H.; Xin, L.; Adler, M. W.; Howard, O. M.; Oppenheim, J. J.; Rogers, T. J. Heterologous desensitization of opioid receptors by chemokines inhibits chemotaxis and enhances the perception of pain. *Proc. Natl. Acad. Sci. U. S. A.* **2002**, *99*, 10276–10281.
- (148) Williams, P. G.; Moore, R. E.; Paul, V. J. Isolation and structure determination of lyngbyastatin 3, a lyngbyastatin 1 homologue from the marine cyanobacterium *Lyngbya majuscula*. Determination of the configuration of the 4-amino-2,2-dimethyl-3-oxopentanoic acid unit in majusculamide C, dolastatin. *J. Nat. Prod.* **2003**, *66*, 1356–1363.
- (149) Pu, X.; Ma, D. Asymmetric total synthesis of (-)-alkaloid 223A and its 6-epimer. *J. Org. Chem.* **2003**, *68*, 4400–4405.
- (150) Davies, S. G.; Mulvaney, A. W.; Russell, A. J.; Smith, A. D. Parallel synthesis of homochiral beta-amino acids. *Tetrahedron:Asymmetry* **2007**, *18*, 1554–1566.
- (151) Zhao, G.-L.; Lin, S.; Korotvicka, A.; Deiana, L.; Kullberg, M.; Cordova, A. Asymmetric synthesis of maraviroc (UK-427,857). *Adv. Synth. Catal.* **2010**, *352*, 2291–2298.

- (152) Haycock-Lewandowski, S. J.; Wilder, A.; Ahman, J. Development of a bulk enabling route to maraviroc (UK-427,857), a CCR-5 receptor antagonist. *Org. Process Res. Dev.* **2008**, *12*, 1094–1103.
- (153) Lee, D. W.; Ha, H.-J. Selective mono-BOC protection of diamines. *Synth. Commun.* **2007**, *37*, 737–742.
- (154) Pittelkow, M.; Lewinsky, R.; Christensen, J. B. Mono carbamate protection of aliphatic diamines using alkyl phenyl carbonates. *Org. Synth.* **2007**, *84*, 209–211.
- (155) Sayre, L. M.; Portoghese, P. S. Stereospecific synthesis of 6 alpha and 6 beta-amino derivatives of naltrexone and oxymorphone. *J. Org. Chem.* **1980**, *45*, 3366–3368.
- (156) Thompson, C. M.; Wojno, H.; Greiner, E.; May, E. L.; Rice, K. C.; Selley, D. E. Activation of G-proteins by morphine and codeine congeners: insights to the relevance of O- and N-demethylated metabolites at μ - and δ -opioid receptors. *J. Pharmacol. Exp. Ther.* **2004**, *308*, 547–554.
- (157) Conklin, B. R.; Farfel, Z.; Lustig, K. D.; Julius, D.; Bourne, H. R. Substitution of three amino acids switches receptor specificity of Gq to that of Gi alpha. *Nature* **1993**, *363*, 274–276.
- (158) Martin, V. V.; Beierlein, M.; Morgan, J. L.; Rothe, A.; Gee, K. R. Novel fluo-4 analogs for fluorescent calcium measurements. *Cell Calcium* **2004**, *36*, 509–514.
- (159) Sakamoto, T.; Ushijima, H.; Okitsu, S.; Suzuki, E.; Sakai, K.; Morikawa, S.; Muller, W. E. Establishment of an HIV cell-cell fusion assay by using two genetically modified HeLa cell lines and a reporter gene. *J. Virol. Methods* **2003**, *114*, 159–166.
- (160) Lin, P.-F.; Blair, W.; Wang, T.; Spicer, T.; Gou, Q.; Zhou, N.; Gong, Y.-F.; Wang, H.-G. H.; Rose, R.; Yamanka, G.; Robinson, B.; Li, C.-B.; Fridell, R.; Deminie, C.; Demers, G.; Yang, Z.; Zadjura, L.; Meanwell, N.; Colonno, R. A small molecule HIV-1 inhibitor that targets the HIV-1 envelope and inhibits CD4 receptor binding. *Proc. Natl. Acad. Sci. USA* **2003**, *100*, 11013–11018.
- (161) Bradley, J.; Gill, J.; Bertelli, F.; Letafat, S.; Corbau, R.; Hayter, P.; Harrison, P.; Tee, A.; Keighley, W.; Perros, M.; Ciaramella, G.; Sewing, A.; Williams, C. Development and automation of a 384-well cell fusion assay to identify inhibitors of CCR5/CD4-mediated HIV virus entry. *J. Biomol. Screen.* **2004**, *9*, 516–524.
- (162) Ji, C.; Zhang, J.; Cammack, N.; Sankuratri, S. Development of a novel dual CCR5-dependent and CXCR4-dependent cell-cell fusion assay system with inducible gp160 expression. *J. Biomol. Screen.* **2006**, *11*.

- (163) Sali, A.; Blundell, T. L. Comparative protein modeling by satisfaction of spatial restraints. *J. Mol. Biol.* **1993**, *234*, 779–815.
- (164) Verdonk, M. L.; Cole, J. C.; Hartshorn, M. J.; Murray, C. W.; Taylor, R. D. Improved protein-ligand docking using GOLD. *Proteins* **2003**, *52*, 609–623.
- (165) Simpson, L. M.; Taddese, B.; Wall, I. D.; Reynolds, C. A. Bioinformatics and molecular modelling approaches to GPCR oligomerization. *Curr. Opin. Pharmacol.* **2010**, *10*, 30–37.
- (166) Gorinski, N.; Kowalsman, N.; Renner, U.; Wirth, A.; Reinartz, M. T.; Seifert, R.; Zeug, A.; Ponimaskin, E.; Niv, M. Y. Computational and experimental analysis of the transmembrane domain 4/5 dimerization interface fo the serotonin 5-HT1a receptor. *Mol. Pharmacol.* **2012**, *82*, 448–463.
- (167) Baker, N. A.; Sept, D.; Joseph, S.; Holst, M. J.; McCammon, J. A. Electrostatics of nanosystems: application to microtubules and the ribosome. *Proc. Natl. Acad. Sci. USA* **2001**, *98*, 10037–10041.
- (168) Holst, M. J.; Saied, F. Multigrid solution of the Poisson-Boltzmann equation. *J. Comp. Chem.* **1993**, *14*, 105–113.
- (169) Phillips, J. C.; Braun, R.; Wang, W.; Gumbart, J.; Tajkhorshid, E.; Villa, E.; Chipot, C.; Skeel, R. D.; Kale, L.; Schulten, K. Scalable molecular dynamics with NAMD. *J. Comp. Chem.* **2005**, *26*, 1781–1802.
- (170) Garcia-Perez, J.; Rueda, P.; Alcamí, J.; Rognan, D.; Arenzana-Seisdedos, F.; Lagane, B.; Kellenberger, E. Allosteric model of maraviroc binding to CC chemokine receptor 5 (CCR5). *J. Biol. Chem.* **2011**, *286*, 33409–33421.
- (171) Maeda, K.; Das, D.; Yin, P. D.; Tsuchiya, K.; Ogata-Aoki, H.; Nakata, H.; Norman, R. B.; Hackney, L. A.; Takaoka, Y.; Mitsuya, H. Involvement of the second extracellular loop and transmembrane residues of CCR5 in inhibitor binding and HIV-1 fusion: Insights into the mechanism of allosteric inhibition. *J. Mol. Biol.* **2008**, *381*, 956–974.
- (172) Metz, M.; Bourque, E.; Labreque, J.; Danthi, S. J.; Langille, J.; Harwig, C.; Yang, W.; Darkes, M. C.; Lau, G.; Santucci, Z.; Bridger, G. J.; Schols, D.; Fricker, S. P.; Skerlj, R. T. Prospective CCR5 small molecule antagonist compound design using a combined mutagenesis/modeling approach. *J. Am. Chem. Soc.* **2011**, *133*, 16477–16485.
- (173) Kondru, R.; Zhang, J.; Ji, C.; Mirzadegan, T.; Rotstein, D.; Sankuratri, S.; Dioszegi, M. Molecular interations of CCR5 with major classes of small-molecule anti-HIV CCR5 antagonists. *Mol. Pharmacol.* **2008**, *73*, 789–800.

- (174) Labreque, J.; Metz, M.; Lau, G.; Darkes, M. C.; Wong, R. S. Y.; Bogucki, D.; Carpenter, B.; Chen, G.; Li, T.; Nan, S.; Schols, D.; Bridger, G. J.; Fricker, S. P.; Skerlj, R. T. HIV-1 entry inhibition by small-molecule CCR5 antagonists: A combined molecular modeling and mutant study using a high-throughput assay. *Virology* **2011**, *413*, 231–243.
- (175) Larkin, M. A.; Blackshields, G.; Brown, N. P.; Chenna, R.; McGettigan, P. A.; McWilliam, H.; Valentin, F.; Wallace, I. M.; Wilm, A.; Lopez, R.; Thompson, J. D.; Gibson, T. J.; Higgins, D. G. Clustal W and Clustal X version 2.0. *Bioinformatics* **2007**, *23*, 2947–2948.
- (176) Mackerell, A. D. J.; Feig, M.; Brooks, C. L. I. Extending the treatment of backbone energetics in protein force fields: limitations of gas-phase quantum mechanics in reproducing protein conformational distributions in molecular dynamics simulations. *J. Comp. Chem.* **2004**, *25*, 1400–1415.
- (177) Brooks, B. R.; Brooks, C. L. I.; Mackerell, A. D. J.; Nilsson, L.; Petrella, R. J.; Roux, B.; Won, Y.; Archontis, G.; Bartels, C.; Boresch, S.; Caffisch, A.; Caves, L.; Cui, Q.; Dinner, A. R.; Feig, M.; Fischer, S.; Gao, J.; Hodoscek, M.; Im, W.; Kuczera, K.; Lazaridis, T.; Ma, J.; Ovchinnikov, V.; Paci, E.; Pastor, R. W.; Post, C. B.; Pu, J. Z.; Schaefer, M.; Tidor, B.; Venable, R. M.; Woodcock, H. L.; Wu, X.; Yang, W.; York, D. M.; Karplus, M. CHARMM: the biomolecular simulation program. *J. Comp. Chem.* **2009**, *30*, 1545–1614.
- (178) Humphrey, W.; Dalke, A.; Schulten, K. VMD: visual molecular dynamics. *J. Mol. Graph.* **1996**, *14*, 27–38.
- (179) Lomize, M. A.; Lomize, A. L.; Pogozheva, I. D.; Mosberg, H. I. OPM: orientations of proteins in membranes database. *Bioinformatics* **2006**, *22*, 623–625.
- (180) Zoete, V.; Cuendet, M. A.; Grosdidier, A.; Michielin, O. SwissParam, a fast force field generation tool for small organic molecules. *J. Comp. Chem.* **2011**, *32*, 2359–2368.

VITA

Christopher Kent Arnatt was born May 16, 1986 in Walpole, New Hampshire to Sylvia Arnatt, joining three older brothers. Later his family would expand to 16 when his mother married Dave Nestor, whom already had eight children, and had three additional children and adopted a child. He graduated from Fredericksburg Academy in Fredericksburg, Virginia in 2005 and went on to Hampden-Sydney College. He graduated 15th in his class, *summa cum laude*, with Honors and a bachelor of science in Chemistry from Hampden-Sydney College in 2009. In the fall of 2009 he joined the Department of Medicinal chemistry at Virginia Commonwealth University perusing his Ph.D. He holds two first author publications and is a co-author on six additional publications. He was the 2013 winner of the J.D. Smith Award, presented to the most distinguished medicinal chemistry student at VCU.